AD NUMBER

AD869619

LIMITATION CHANGES

TO:

Approved for public release; distribution is unlimited.

FROM:

Distribution authorized to U.S. Gov't. agencies and their contractors; Critical Technology; JUN 1968. Other requests shall be referred to Deputy for Development Planning, WPAFB, OH 45433. This document contains export-controlled technical data.

AUTHORITY

ASD ltr, 9 Dec 1971

Copy # 28

ASB 68-13

(20)

C15

METHOD FOR EVALUATING THE EFFECTIVENESS AND WEIGHT OF AIRCRAFT DECELERATION DEVICES

H. Greiner
J. H. Hilbig

Rohr Corporation
Chula Vista, California

TECHNICAL REPORT ASB 68-13
JUNE 1968

DEPUTY FOR DEVELOPMENT PLANNING
AERONAUTICAL SYSTEMS DIVISION
AIR FORCE SYSTEMS COMMAND
WRIGHT-PATTERSON AIR FORCE BASE, OHIO

307

DISCLAIMER NOTICE

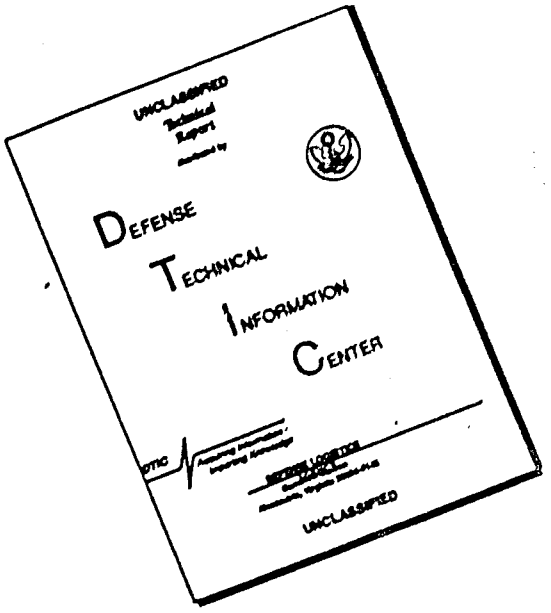

THIS DOCUMENT IS BEST QUALITY AVAILABLE. THE COPY FURNISHED TO DTIC CONTAINED A SIGNIFICANT NUMBER OF PAGES WHICH DO NOT REPRODUCE LEGIBLY.

NOTICES

When Government drawings, specifications, or other data are used for any purpose other than in connection with a definitely related Government procurement operation, the United States Government thereby incurs no responsibility nor any obligation whatsoever; and the fact that the Government may have formulated, furnished, or in any way supplied the said drawings, specifications, or any other data, is not to be regarded by implication or otherwise as in any manner licensing the holder or any other person or corporation, or conveying any rights or permission to manufacture, use, or sell any patented invention that may in any way be related thereto.

DDC release to OTC not authorized.

Copies of this report should not be returned to the Deputy for Development Planning unless return is required by security considerations, contractual obligations, or notice on a specific document.

UNCLASSIFIED

METHOD FOR EVALUATING THE EFFECTIVENESS AND WEIGHT OF AIRCRAFT DECELERATION DEVICES

H. Greiner
J. H. Hilbig

FOREWORD

This report was prepared by the Engineering Research and Development Department of Rohr Corporation of Chula Vista, California, under Contract F33615-67-C-1558. The work was administered under the direction of the Deputy for Development Planning, Wright-Patterson Air Force Base with Lt. Stephen Stumpfl acting as Project Engineer. Assisting the authors in the work were Messers. R. F. Gusky, R. J. Seaver, and N. J. Carraway.

This report covers work conducted from 15 June 1967 to 15 June 1968. The report was submitted by the Authors in May 1968.

Publication of this report does not constitute Air Force approval of the report's findings or conclusions. It is published only for the exchange and stimulation of ideas.

Fred D. Orazio Sr.

FRED D. ORAZIO, SR.
Chief, Advanced Systems Analysis Division
Deputy for Development Planning

ABSTRACT

A

This program was established in order to develop a standard and expedient method for estimating the performance and weights of deceleration devices used to decrease the landing ground roll of an aircraft. The method of approach to the problem was to obtain all data available both from flight test and theory; and to compile a step-by-step procedure for determining the weight penalties and the force increments affecting aircraft landing performance. Specifically, procedures are provided for determining airplane lift and drag, and decelerative force increments and weight penalties due to high lift devices, spoilers, wheel brakes, speed brakes, drag chutes and thrust reversers. In addition, a cursory study was made to evaluate the effectiveness of various factors affecting landing distance of three current military aircraft. The study showed that the ground roll distance was strongly influenced by touchdown speed; also that, of all the decelerating devices studied, the thrust reverser was the one most effective in reducing stopping distance. It is therefore recommended that further studies be conducted to optimize thrust reversers and devices such as deflected thrust, which reduce touchdown velocity. ( )

CONTENTS

LIST OF FIGURES

LIST OF FIGURES

LIST OF FIGURES

LIST OF FIGURES

LIST OF FIGURES

LIST OF FIGURES

LIST OF FIGURES

LIST OF FIGURES

LIST OF TABLES

NOMENCLATURE

SYMBOL	DEFINITION	UNITS
A_B	Maximum Cross-Sectional Area of the Fuselage	ft^2
A_n	Tire Footprint Area	in^2
A_{SB}	Panel Area of Aircraft Speed Brake	ft^2
AR	Total Wing Planform Aspect Ratio	
AR_{EXP}	Aspect Ratio of Exposed Wing Panels	
b	Aircraft Wing Span	ft.
b_{EXP}	Wing Span of the Exposed Wing Panels	ft.
b_d/b	Leading Edge Device Span to Wing Span Ratio	
b_F/b	Trailing Edge Flap Span to Wing Span Ratio	
$\frac{b_{F_i}}{b/2}$	Ratio of the Inboard Trailing Edge Flap Position to the Wing Semi-Span	
$\frac{b_{F_o}}{b/2}$	Ratio of the Outboard Trailing Edge Flap Position to the Wing Semi-Span	
C	Wing Chord	ft.
$\bar{C}$	Mean Aerodynamic Chord	ft.
C'	Wing Chord Length with Deflected Trailing Edge Flap	ft.
C''	Wing Chord Length with Deflected Leading Edge Device	ft.
C_1	Correction Factor	
C_1, C_2	Taper Ratio Correction Factors for Maximum Wing Lift	
C'/C	Ratio of Airfoil Chord with Deflected Trailing Edge Flap to Undeflected Airfoil Chord.	
C_D	Drag Coefficient	
$C_{D_{min}}$	Minimum Drag Coefficient	

NOMENCLATURE

SYMBOL	DEFINITION	UNITS
C_{D_o}	Minimum Drag Coefficient	
$C_{D_{TD}}$	Drag Coefficient at Touchdown	
$\Delta C_{D_{DC}}$	Increment of Minimum Drag Coefficient Due to Drag Chute Deployment.	
ΔC_{D_i}	Induced Drag Coefficient	
$\Delta C_{D_{i_{flap}}}$	Increment of Wing Induced Drag Coefficient Due to Flap Deflection.	
$\Delta C_{D_{LG}}$	Increment of Minimum Drag Coefficient Due to Landing Gear	
$\Delta C_{D_{Min}}$	Increment of Wing Minimum Drag Coefficient	
$\Delta C_{D_{SB}}$	Increment of Minimum Drag Due to Speed Brake Deflection	
$\Delta C_{D_{SP}}$	Increment of Minimum Drag Due to Spoiler Deflection	
$\Delta C_{D_{TR}}$	Increment of Minimum Drag Due to Thrust Reverser Door Deployment.	
$\Delta C_{d_{flap}}$	Increment of Section Profile Drag Coefficient Due to Flap Deflection.	
$\Delta C_{d_{o_c}}$	Increment of Minimum Drag Due to Drag Chute Deployment Based on Drag Chute Canopy Area.	
C_d/C	Ratio of Leading Edge Device Chord to Undeflected Airfoil Chord.	
C_d/C''	Ratio of Leading Edge Device Chord to Deflected Airfoil Chord.	
ΔC_{D_δ}	Increment of Drag Due to BLC Flap Deployment.	
C_{EXP}	Wing Chord at Wing-Fuselage Intersection	ft.
C_F	Flap Chord Length	ft.
C_{F_I}	Trailing Edge Flap Inboard Edge Flap Chord Length	ft.

NOMENCLATURE

SYMBOL	DEFINITION	UNITS
C_{F_o}	Trailing Edge Flap Outboard Edge Flap Chord Length.	ft.
C_{F_1}	Double-Slotted Flap - Flap 1 Chord Length, Measured from Flap 1 Leading Edge to Airfoil Trailing Edge.	ft.
C_{F_2}	Double-Slotted Flap - Flap 2 Chord Length	ft.
C_F/C	Ratio of Flap Chord to Undeflected Airfoil Chord.	
C_F/C'	Ratio of Flap Chord to Deflected Airfoil Chord.	
C_f	Skin-Friction Coefficient	
C_L	Wing Lift Coefficient	
$C_{L_{DES}}$	Design Wing Lift Coefficient	
$C_{L_{D_i}}$	Lift Coefficient Used in Determining Drag Due-To-Lift.	
$C_{L_{i_H}}$	Variation of Lift Coefficient with i_H	/deg.
$C_{L_{MAX}}$	Wing Maximum Lift Coefficient	
C_{L_K}	Lift Coefficient where C_{D_o} Occurs	
$C_{L_{TD}}$	Wing Lift Coefficient at Touchdown	
C_{L_α}	Variation of Wing Lift Coefficient with Angle-of-Attack	/deg.
$C_{L_{\alpha_{EXP}}}$	Variation of Exposed Wing Lift Coefficient with Angle-of-Attack.	/deg.
$C_{L_{\alpha_{TOT}}}$	Variation of Aircraft Lift Coefficient with Angle-of-Attack.	/deg.
$C_{L_{\alpha_W}}$	Variation of Wing Lift Coefficient with Angle-of-Attack.	/deg.

NOMENCLATURE

SYMBOL	DEFINITION	UNITS
$C_{L_{\alpha_{WB}}}$	Variation of Wing-Body Lift Coefficient with Angle-of-Attack.	/deg.
$(C_{L_{\alpha}})_{\delta}$	Lift Curve Slope of the Wing at Flap Deflection δ	/deg.
$C_{L_{\delta_e}}$	Variation of Lift Coefficient with δ_e	/deg.
$C_{L_{\delta_F}}$	Variation of Lift Coefficient with δ_F	/deg.
C_{L_T} Crit.	Wing Circulation Lift Coefficient Corresponding to C_{μ} Crit.	
ΔC_L	Increase in Wing Lift Coefficient in the Linear C_{L_α} Range Due to Deflected Flap.	
$\Delta C_{L_{MAX}}$	Incremental Maximum Lift Coefficient.	
$(\Delta C_{L_T})_{\delta_B}$	Increment in Wing Circulation Lift Coefficient Due to Blowing Flap Deflection.	
$(\Delta C_{L_T})_{\delta_S}$	Increment in Wing Circulation Lift Coefficient Due to Suction Flap Deflection.	
C_ℓ	Airfoil Section Lift Coefficient	
C_ℓ'	Reference Airfoil Section Lift Coefficient	
C_{ℓ_i}	Airfoil Section Design Lift Coefficient	
$C_{\ell_{MAX}}$	Airfoil Section Maximum Lift Coefficient	
C_{ℓ_R}	Blowing Jet Reaction Section Lift Coefficient	
C_{ℓ_α}	Section Lift Curve Slope; $\partial C_\ell / \partial \alpha$	/deg.
$(C_{\ell_\alpha})_{\delta}$	Lift Curve Slope of the Flapped Airfoil Section at Flap Deflection δ.	/deg.

NOMENCLATURE

SYMBOL	DEFINITION	UNITS
C_{ℓ_Γ}	Section Circulation Lift Coefficient	
$(C_{\ell_\Gamma})_{PF}$	Potential Flow Section Circulation Lift Coefficient	
ΔC_ℓ	Increase in Section Lift Coefficient in the Linear C_{ℓ_α} Range Due to Deflected Flap.	
$\Delta C'_\ell$	Increase in Section Lift Coefficient Due to Deflected Flap.	
$\Delta C_{\ell_{max}}$	Increment of Maximum Airfoil Section Lift Coefficient	
ΔC_{ℓ_S}	Increment of Section Lift Coefficient Due to Suction.	
ΔC_{ℓ_α}	Incremental Change in Section Lift Curve Slope.	/deg.
$(\Delta C_{\ell_\Gamma})_{\delta_B}$	Incremental Change in Section Circulation Lift Coefficient Due To Blowing Flap Deflection.	
$(\Delta C_{\ell_\Gamma})_{\delta_S}$	Incremental Change in Section Circulation Lift Coefficient Due to Suction Flap Deflection.	
C_{m_o}	Pitching Moment Coefficient @ $C_L = 0$	
$C_{m_{C_L}}$	Variation of Pitching Moment Coefficient with C_L	
$C_{m_{i_H}}$	Variation of Pitching Moment Coefficient with i_H	
$C_{m_{\delta_e}}$	Variation of Pitching Moment Coefficient with δ_e	
$C_{m_{\delta_F}}$	Variation of Pitching Moment Coefficient with δ_F	
C_{PR}	Plume Shape Factor.	
C_p	Base Pressure Coefficient.	

NOMENCLATURE

SYMBOL	DEFINITION	UNITS
C_{Q_S}	Suction Air Flow Coefficient	
C_R	Wing Root Chord Length	ft.
C_T	Wing Tip Chord Length	ft.
C_μ	Blowing Jet Momentum Coefficient	
$C_{\mu_{Crit.}}$	Critical Blowing Jet Momentum Coe ficient	
D	Drag = $C_D qS$	lbs
D_C	Drag Chute Canopy Diameter	ft.
D_{RF}	Thrust Reverser Door Overall Diameter at Engine Flange	in.
D_f	Rim Flange Diameter	in.
D_o	Tire Outside Diameter	in.
ΔD_{chute}	Incremental Drag of Drag Chute	lbs.
d	Fuselage Maximum Diameter	ft.
d	Tire Radial Deflection (Difference Between Loaded and Unloaded Section Heights)	in.
d/b	Maximum Fuselage Diameter to Wing Span Ratio	
E	Flap Chord to Section Chord Ratio	
FA/FÓ	Plain Flap Aspect Ratio Correction Factor	
F_g	Gross Thrust	lbs.
FH	Free Height (Unloaded Section Height above the Top of the Rim Flange)	in.
F_{MG}	Vertical Reaction Force on the Main Landing Gear	lbs.
FN	Net Thrust at Approach Speed	lbs.
F_{NW}	Vertical Reaction Force on the Nose Gear	lbs.
F_v	Vertical Force On Tire	lbs.
f_e	Equivalent Parasite Area	ft^2
g	Gravitational Force = 32.2 ft/sec^2	

NOMENCLATURE

SYMBOL	DEFINITION	UNITS
GW	Gross Weight	lb.
h_s	Deflected Spoiler Height	ft.
I_F	Interference Factor of Trailing Edge Flaps	
i_T	Thrust Line Incidence Angle	deg.
K	Empirical Constant for Wing Section Angle-of-Zero-Lift.	
K'	Flap Span Correction Factor	
$K_{B_{(W)}}$	Ratio of the Body Lift in the Presence of the Wing to the Wing Alone Lift.	
K_b	Flap Span Correction Factor.	
K_D	Sweep Angle Correction Factor	
K.E.	Kinetic Energy Design Factor	
KIAS	Knots Indicated Air Speed	Knots
K_N	Ratio of the Fuselage Nose Lift to the Wing-Alone Lift	
K_S	Suction Flow Constant	
$K_{W_{(B)}}$	Ratio of the Wing Lift in the Presence of the Body to the Wing Alone Lift	
k	Equivalent Sand Roughness Height	in.
k_1	Portion of the (GW-L) Term Supported by the Main Landing Gear (Static)	
k_1, k_2	Plain Flap Correction Factor for Section Maximum Lift	
k_1, k_2, k_3	Flap Maximum Lift Correction Factors	
L	Thrust Reverser Door Overall Length	in.
L	Aircraft Lift = $C_L qS$	lbs.
ℓ	Length	ft.

NOMENCLATURE

SYMBOL	DEFINITION	UNITS
ℓ_b	Fuselage Length	ft.
$\ell_{fuselage}$	Fuselage Length	ft.
$\ell_{x_{c.g.}}$	Horizontal Distance from Nose Gear to Aircraft Center-of-Gravity	ft.
$\ell_{x_{mg}}$	Horizontal Distance from Nose Gear to Aircraft Main Landing Gear	ft.
$\ell_{z_{c.g.}}$	Vertical Distance from Ground to Aircraft Center-of-Gravity	ft.
$\ell_{z_{T.L.}}$	Vertical Distance from Ground to Aircraft Thrust Line.	ft.
M	Mach Number	
M_{aero}	Aerodynamic Pitching Moment	ft-lbs.
N	Number of Wheelswith Brakes	
NPR	Nozzle Pressure Ratio	
P_n	Net Bearing Pressure	lb/in^2
Q	BLC Flow Quantity	$ft^3/sec.$
q	Dynamic Pressure = $\frac{1}{2} \rho V^2$	lbs/ft^2
R	Pitch Control Reaction Force	lbs.
R_n, RN	Reynold's Number	
RCR	Runway Condition Reading	
$(R/S)_{TD}$	Rate of Sink at Runway Contact	ft/sec.
S	Area	ft^2
S_B	Wing Area Affected by Trailing Edge Blowing Flap	ft^2
S_{chute}	Canopy Area of Deployed Drag Chute	ft^2
S_d	Wing Area Affected by Leading Edge Device	ft^2
S_{EXP}	Exposed Wing Area	ft^2

NOMENCLATURE

SYMBOL	DEFINITION	UNITS
S_F	Wing Area Affected by Trailing Edge Flap	ft^2
S_{REF}	Aircraft Reference Area	ft^2
S_S	Wing Area Affected by Trailing Edge Suction Flap	ft^2
S_{SP}	Wing Area Affected by Spoiler	ft^2
S_{TOT}	Total Wing Planform Area	ft^2
S_{TR}	Base Area of Deployed Thrust Reverser Doors	ft^2
s	Blowing or Suction Slot Width	ft
T	Engine Thrust	lbs
T_R	Reversed Thrust	lbs
TR	Wing Planform Taper Ratio	
TR_{EXP}	Taper Ratio of Exposed Wing Panel	
t	Airfoil Thickness	ft
t/C	Wing Section Maximum Thickness to Wing Chord Ratio	ft
V	Velocity	knots
V_{APP}	Approach Velocity	knots
V_{CO}	Thrust Reverser Cutoff Velocity	knots
V_J	Blowing Jet Velocity	ft/sec.
V_{TD}	Velocity at Runway Contact (touchdown)	knots
$\dot{V}$	Time Rate of Change in Aircraft Velocity	ft/sec^2
W	Aircraft Weight	lbs
W	Thrust Plume Leading Edge Shape Parameter	ft
W_E	Aircraft Empty Weight	lbs.
$\dot{W}_J$	Blowing Jet Mass Flow Rate	lb/sec.
X	Thrust Plume Leading Edge Shape Parameter	ft
x	Airfoil Section Chord Location	ft

NOMENCLATURE

SYMBOL	DEFINITION	UNITS
x_s	Chordwise Spoiler Location	ft
$x_{t_{MAX}}/C$	Position of Maximum Section Thickness to Wing Chord Ratio.	
Δx_R	Distance R is Located from C.G. Measured Along ℓ	ft.
Δx_T	Distance T is Located from C.G. Measured Along ℓ	ft.
Y	Thrust Plume Leading Edge Shape Parameter	ft
y	Airfoil Section Thickness Corresponding to x	ft
Δy	Airfoil Section Leading Edge Sharpness Parameter	
ΔZ_{cg}	Distance C.G. is Located from Centerline Measured Vertical	ft
α	Angle of Attack	deg.
$\alpha_{C_{L_{MAX}}}$	Angle of Attack for Maximum Wing Lift	deg.
α_s	Angle of Attack at Touchdown	deg.
α_i	Design Airfoil Section Angle-of-Attack	deg.
α_o	Angle of Attack at Zero-Lift	deg.
α^*	Angle of Attack where C_{ℓ_α} Becomes Non-Linear	deg.
$(\alpha_\delta)_{C_L}$	Rate of Change of Wing Zero-Lift Angle-of-Attack with Flap Deflection.	
$(\alpha_\delta)_{C_\ell}$	Rate of Change of Airfoil Section Zero-Lift Angle-of-Attack with Flap Deflection	
$\Delta\alpha$	Change in Angle-of-Attack	deg.
$\Delta\alpha_{C_{L_{MAX}}}$	Incremental Angle-of-Attack for Maximum Wing Lift	deg.
$\Delta\alpha_o$	Incremental Angle-of-Attack for Zero-Lift	deg.

NOMENCLATURE

SYMBOL	DEFINITION	UNITS
$\Delta\alpha_{SP}$	Change in Zero-Lift Angle-of-Attack Due to Spoiler Deflection	deg.
β	Characteristic Angle	deg.
Γ	Circulation	$ft^2/sec.$
γ	Flight Path Angle	deg.
$\Delta_1, \Delta_2, \Delta_3$	Induced Drag Coefficient Correction Factors	
δ	Deflection Angle	deg.
δ_d	Leading Edge Device Deflection Angle	deg.
δ_e	Elevator Deflection Angle	deg.
δ_F	Trailing Edge Flap Deflection Angle	deg.
δ_{F_1}	Double-Slotted Flap Deflection Angle (Flap 1)	deg.
δ_{F_2}	Double-Slotted Flap Deflection Angle - Flap 2 Measured from Flap 1 Chord Line to Flap 2 Chord Line	deg.
δ_J	Blowing Jet Deflection Angle	deg.
δ_{SB}	Speed Brake Deflection Angle	deg.
δ_{SP}	Spoiler Deflection Angle	deg.
δ_T	Thrust Deflection Angle	deg.
η	Thrust Reverser Effectiveness	
η_o	Spanwise Location of Outboard Flap Edge (% of Semi-Span)	
η_i	Spanwise Location of Inboard Flap Edge (% of Semi-Span)	
$\Lambda_{C/4}$	Sweep Angle of the Quarter Chord Line	deg.
Λ_{LE}	Leading Edge Sweep Angle	deg.
λ	Wing Taper Ratio	
λ_B	Blowing Flap Lift Factor	
$\lambda_{B_{Crit.}}$	Critical Blowing Flap Lift Factor	

NOMENCLATURE

SYMBOL	DEFINITION	UNITS
$\lambda_1, \lambda_2, \lambda_3$	Plain Flapped Wing Correction Factor	
$(\lambda_1 \lambda_2)_{\text{Flap 1}}$	Double-Slotted Flap Lift Correction Factor, Flap 1	
$(\lambda_1 \lambda_{22})_{\text{Flap 2}}$	Double-Slotted Flap Lift Correction Factor, Flap 2	
λ_3	Flap Span Correction Factor	
μ_{avg}	Average Braking Friction Coefficient	
μ_B	Braking Friction Coefficient	
μ_{max}	Maximum Braking Friction Coefficient	
μ_R	Rolling Friction Coefficient	
$\mu_{req.}$	Required Braking Friction Coefficient	
π	Pi = 3.14159	
ρ	Air Density	lb/ft^3
σ	Standard Deviation	
ϕ_{TE}	Wing Section Trailing Edge Included Angle	deg.
X	BLC Trailing Edge Flap Factor	

SECTION I

INTRODUCTION

The objective of this report is to provide a method of analysis that will facilitate the evaluation of the effectiveness of deceleration devices upon the landing ground roll of aircraft.

In limited-warfare situations, aircraft must operate out of small advanced airfields which may be close to enemy held territory so that approach and take-off paths are subject to hostile ground fire. In addition, terrain features often limit the length of runway available. The requirements for steep approach path and short landing distance are incompatible with the basic design of modern high-speed jet aircraft; therefore a variety of devices are used to change lift, drag and braking characteristics.

There are many methods currently in use to determine the touchdown speed and ground roll of an aircraft. Some are mathematical methods based entirely on theory and others are largely empirical, relying almost entirely on test data. In many cases the results of these methods do not agree nor, in many cases, do they lend themselves to rapid, ordered methods of solution.

Since accurate evaluation of the landing characteristics of competing aircraft designs is currently of great importance the Deputy for Development Planning generated a Proposal Request (PR number SES-7-3537) to provide a methodology to satisfy the aforementioned requirement. As successful bidder, the Rohr Corporation has conducted a one-year study of landing deceleration devices and has compiled the present handbook.

To initiate the study an extensive literature survey was conducted and data collected from manufacturers with regard to all types of deceleration devices and aircraft performance during landing. On the basis of the data and various existing theoretical approaches, simplified yet rigorous methods were established for computing touchdown velocity and the forces affecting deceleration during landing ground roll. In addition, methods were formulated for prediction of weight penalties associated with the pertinent devices. These methods for determining the deceleration forces and weights are presented in the form of charts and graphs, and where appropriate, step by step procedures. A sample calculation is provided in Section II to illustrate the use of the handbook for determining touchdown velocity, decelerative force increments and weight penalties.

Because of the low velocities uaually involved during landing ground roll, the airplane drag is usually small compared with the other

deceleration forces. As a result, inaccuracies in computing drag were regarded as tolerable, and for certain of the increments of drag, methods are employed that result in first-order answers. In this regard, the aircraft is assumed to consist of wing-body combinations with a high lift device(s) and an appropriate deceleration device(s).

The deceleration devices given consideration are wheel brakes, speed brakes, spoilers, drag chutes and thrust reversers. Wheel brake effectiveness is considered in conjunction with a number of runway surface conditions and tire types and sizes.

The high lift devices given consideration include plain, split, slotted and Fowler trailing edge flaps, and leading edge slots and slats. In addition, methods are suggested to account for boundary layer control where suction or blowing is applied at the nose of the trailing edge flap.

SECTION II

AIRCRAFT FORCES AND USE OF HANDBOOK

1. GENERAL

It is the purpose of this handbook to provide an analytical means for determining the forces exerted on an aircraft during the landing ground roll. As will be shown later, the forces and their order of significance are:

1. Touchdown Speed (a function of $C_{L_{TD}}$)
2. Reverse Thrust (when applicable)
3. Wheel Braking
4. Drag
5. Lift

In addition, for evaluation purposes, a means is provided to determine the weight of the components of the airplane that produce the forces.

2. FORCE ANALYSIS

Before proceeding with the force and weights handbook, a preliminary study was made to determine the significance of the various decelerating devices. This was accomplished by means of a computerized landing stopping distance equation. The sensitivity of each device (or force) was evaluated.

Calculations were made for the F-4, F-5, and B-52H aircraft. The five factors mentioned above were parametrically varied.

A nominal, or base, condition (i) was established for each aircraft. This was selected on the basis of each manufacturer's data and recommended landing procedure. Where it was not specified, an engineering estimate was made. Variations of the values of the parameters from this base condition were then completed with the results shown in Figures 2-1 through 2-3.

These curves are all similar for the aircraft analyzed. As shown, when the slope of the curve is small, the effect on the landing stopping distance is large. The results also indicated the significance of each device with the order of importance indicated in the first paragraph:

As a further explanation of the sensitivity charts, the following example is given.

If it were required to reduce the landing stopping distance of an F-5 by 40% from the nominal case, it could be accomplished as follows:

1. By increasing the drag by a factor of 5.8 (approximately the value of the drag chute), or
2. Increasing the braking efficiency by a factor of 1.8. This could probably be obtainable with an anti-skid device, $\mu_{req} = 1.8 \times .3 = .54$, or
3. Using a thrust reverser having 50% efficiency ($\eta = -.5$) and a cut-off velocity of 40 knots, or
4. By a reduction in touchdown velocity by about 20%.

(In all of the calculations it was assumed that the deceleration device was effective at the time of touchdown, $t = 0$).

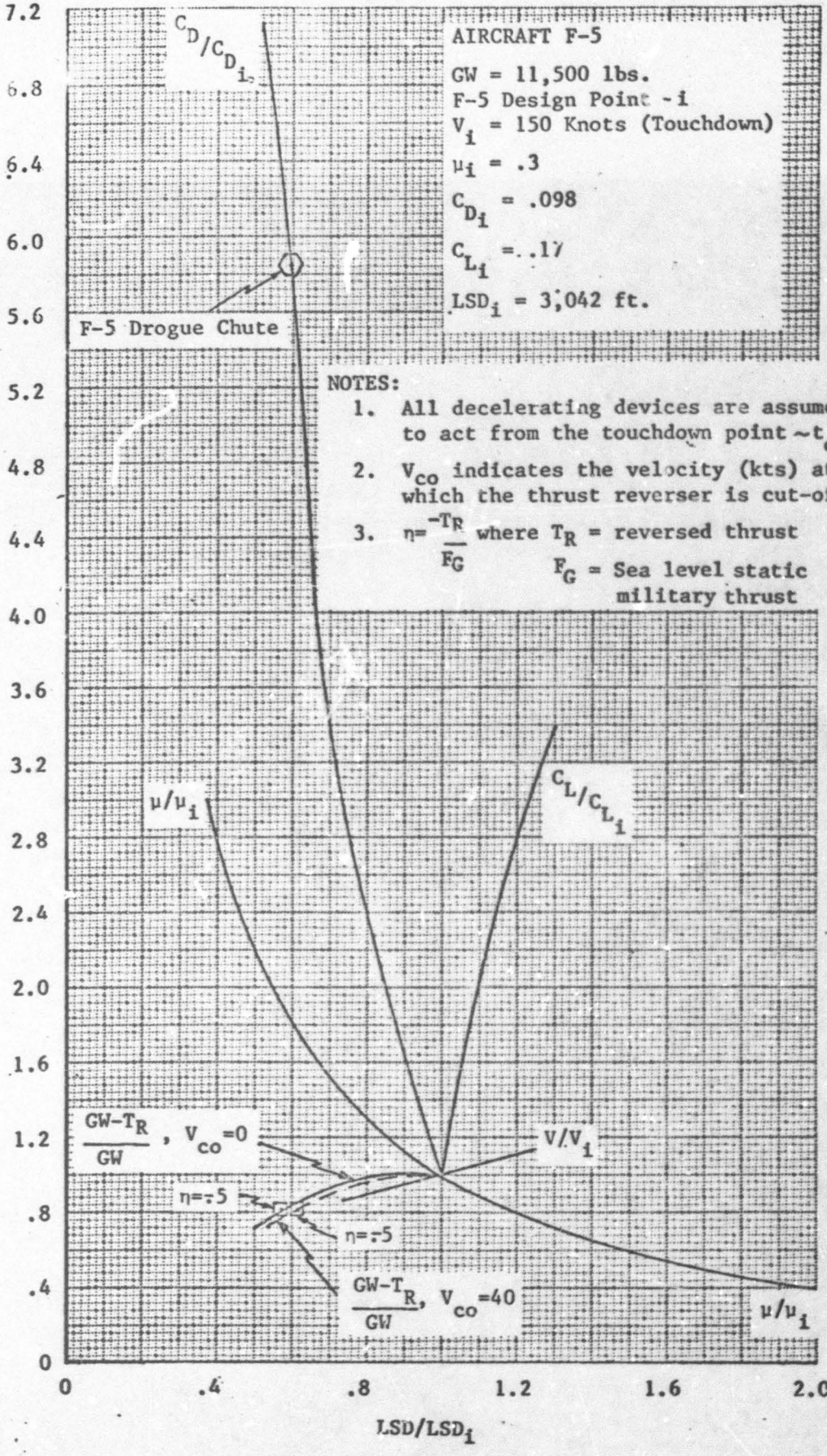

FIGURE 2-1 : Sensitivity of F-5 Landing Distance to Effectiveness of the Various Factors Affecting Landing Distance.

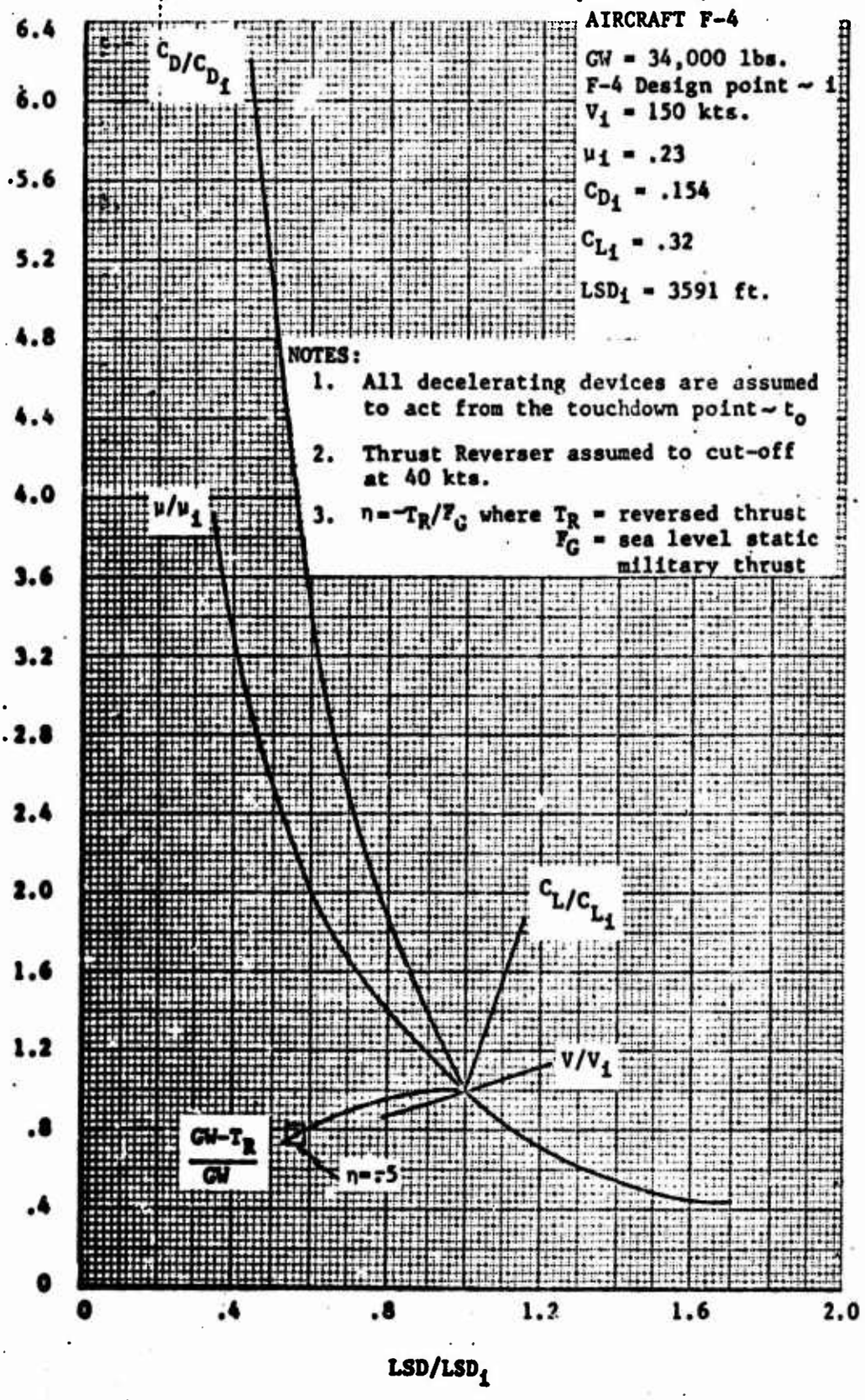

FIGURE 2-2 : Sensitivity of F-4 Landing Distance to Effectiveness of Various Factors Affecting Landing Distance.

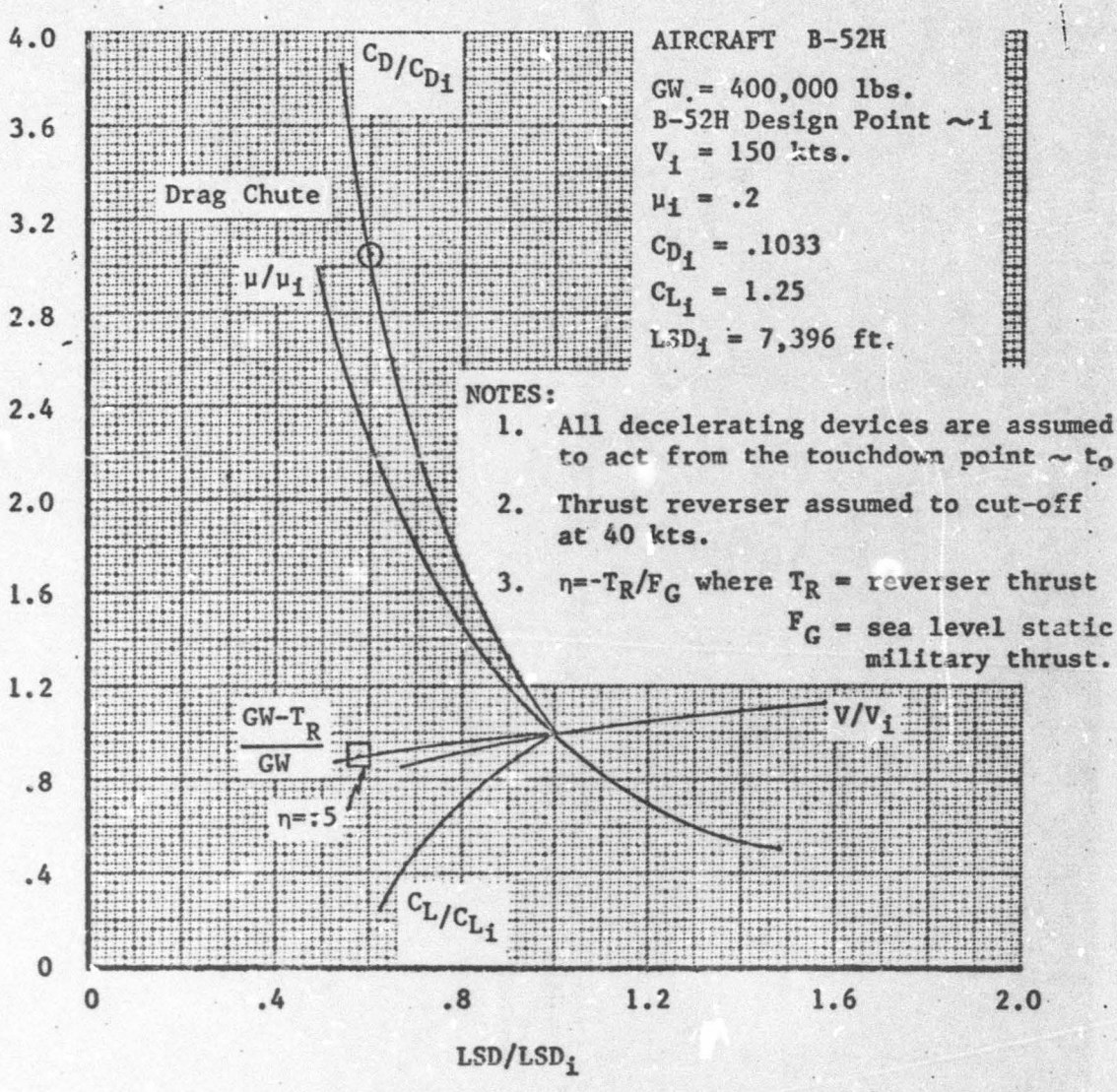

FIGURE 2-3 : Sensitivity of B-52H Landing Distance to Effectiveness of the Various Factors Affecting Landing Distance.

The above results were obtained by solving the standard one-dimensional equation of motion:

$$\frac{GW}{g}\dot{V} = T - D - (\text{Braking Force}) \qquad \text{(II-1)}$$

where

T is the aircraft thrust (forward or reverse)

D is the aircraft drag

$(\text{Braking Force}) = \mu_B k_1 (GW-L) + \mu_R (1 - k_1) (GW-L)$

where μ_B is the braking coefficient (a constant)

μ_R is the rolling coefficient (a constant)

GW is the weight of the aircraft

L is the lift of the aircraft

k_1 is the portion of (GW-L) supported by the main landing gear (static)

During this study, it became evident that a more accurate method should be applied. (Since this study was only concerned with the forces themselves and not the solution of the landing stopping distance, the recommended equations with no results are presented). The complete equations of motion which describe the forces and moments acting on the aircraft are as follows:

$$\Sigma\text{Forces Vertical} = 0 = GW - F_{mg} - F_{nw} - L \qquad \text{(II-2)}$$

$$\Sigma\text{Forces Horizontal} = 0 = \frac{GW}{g}\dot{V} + T - D - \mu_B F_{mg} - \mu_R F_{nw} \qquad \text{(II-3)}$$

$$\Sigma\text{Moments about the nose wheel} = 0 = \ell_{x_{c.g.}} (GW-L) + M_{aero} + D\ell_{z_{c.g.}} - T\ell_{z_{T.L.}} - F_{mg}\ell_{x_{mg}} - \frac{GW}{g}\dot{V}\ell_{z_{c.g.}} \qquad \text{(II-4)}$$

Figure 2-4 shows the forces diagrammatically.

where GW = Aircraft Gross Weight

F_{mg} = Vertical reaction force on the main landing gear

F_{ng} = Vertical reaction force on the nose gear

L = Aircraft lift = $C_L qS$

g = Gravitational force = 32.2 Ft/Sec^2

$\dot{V}$ = Rate of change of aircraft velocity

T = Thrust (+ Forward, - Reverse)

D = Aircraft drag = $C_D qS$

μ_B = Braking coefficient μ_B = f (F_{mg}, tire description, runway description, anti-skid device)

μ_R = Rolling Coefficient

M_{aero} = Aerodynamic pitching moment

$\ell_{z_{c.g.}}$ = Vertical distance from nose gear to aircraft c.g.

$\ell_{x_{c.g.}}$ = Horizontal distance from nose gear to aircraft c.g.

$\ell_{z_{T.L.}}$ = Vertical distance from nose gear to aircraft thrust line.

$\ell_{x_{mg}}$ = Horizontal distance from nose gear to aircraft main landing gear.

Rewriting the moment equation (II-4) as follows:

$$F_{mg} = \frac{1}{\ell_{x_{mg}}} \left(M_{aero} + \ell_{x_{c.g.}} (GW-L) + D\ell_{z_{c.g.}} - T\ell_{z_{T.L.}} - \frac{GW}{g} \dot{V} \ell_{z_{c.g.}} \right) \quad \text{(II-5)}$$

It can easily be seen that the braking force ($\mu_B \cdot F_{mg}$) is not solely a function of the GW and L. Using the above equation accounts for the unloading of the main landing gear due to deceleration.

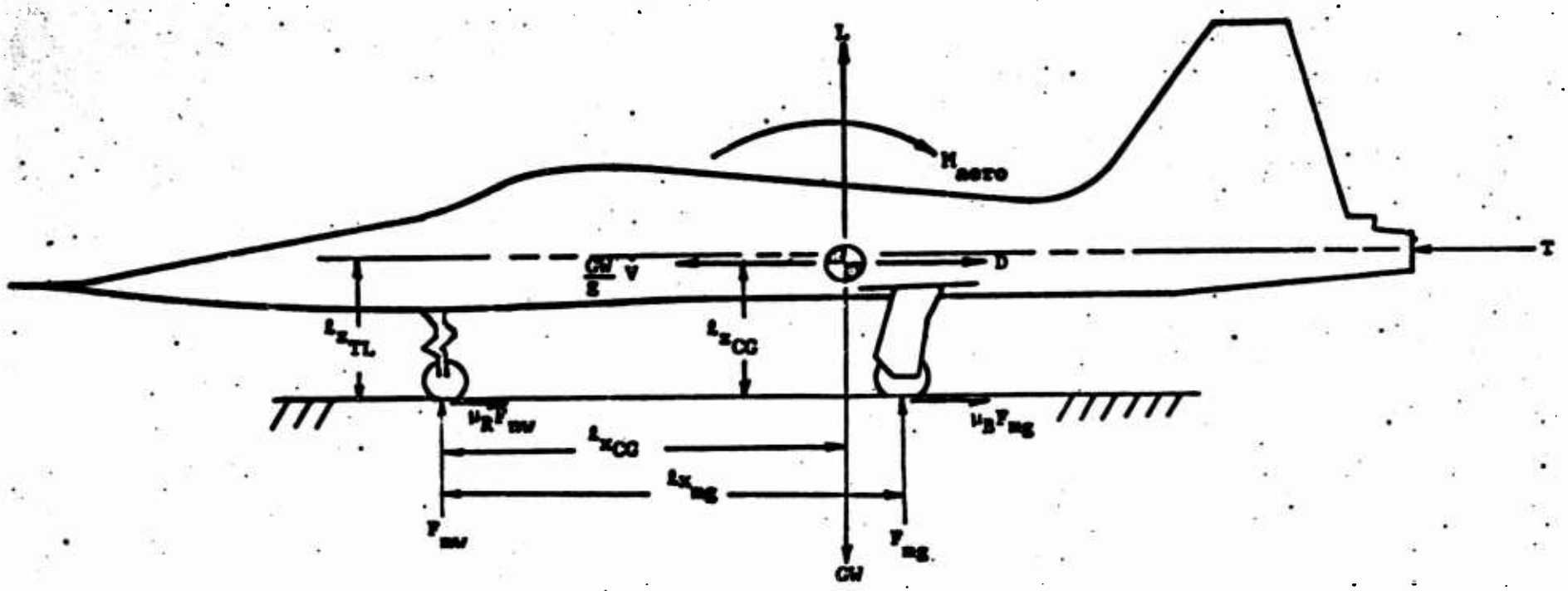

FIGURE 2-4: Force and Moment Vector Diagram for Ground Roll Analysis.

3. USE OF HANDBOOK

The use of this handbook is predicated on the fact that a good physical description of the aircraft is available.

By going through each section it is then possible to obtain the coefficients necessary to solve the landing stopping distance equations. These coefficients are (in general terms):

η	Thrust Factor (negative for reversed thrust)
μ_R	Rolling Coefficient
μ_B	Braking Coefficient
C_L	Lift Coefficient
C_D	Drag Coefficient

Also, the weights section permits an evaluation of each aircraft component contributing to the coefficients. Each section is self-contained, i.e., reference to other sections is not required to obtain an answer.

The general procedure for each item considered is

1. Obtain a good physical description
2. Determine the initial conditions
3. Enter the appropriate section

A detailed sample problem follows.

4. SAMPLE CALCULATION

The sample calculation will use the Northrop F-5A aircraft as the example. The lift and drag characteristics at the touchdown velocity are calculated using the methods of Section III. The braking and rolling coefficients are calculated in Section IV. Due to lack of data, representative, generalized values of the Section V data are given. Weight increments of the various devices considered are calculated by Section VI methods.

Some of the physical characteristics of the F-5 have been modified in this calculation in order to facilitate the purpose of the sample calculation, namely, to illustrate the use of the handbook. The physical characteristics are listed below. In addition, various assumptions are made as noted at appropriate places within the calculations.

A. COMPUTATION OF THE LIFT, DRAG, AND TOUCHDOWN VELOCITY FOR AN AIRCRAFT IN THE LANDING CONFIGURATION.

1. Step 1 - Aircraft Data

The list of the required data is given by forms provided in Section III-5A. These have been filled out with the chosen data and are listed below.

2. Step 2 - Airfoil Section Characteristics

a. From Table III-1, for NACA Section 65-006 (assume section characteristics of 65A-004.8 are equivalent to Section 65-006)

1. α_o = 0.0 degrees
2. C_{ℓ_α} = .105 per degree (6.02 per radian)
3. $C_{\ell_{max}}$ = .92

b. For NACA-Type sections calculate:

1. $\alpha_o = K(\alpha_i - 9.12)C_{\ell_i}$

where C_{ℓ_i} = 0.00 (airfoil section designation)

α_i = 0.0 degrees (Table III-2, NACA 6-Series, C_{ℓ_i} = 0.0)

K = 0.74 for NACA 6-digit series

α_o = 0.0 degrees

2. $C_{\ell_\alpha} = 2\pi + 4.7\left(\frac{t}{C}\right)[1 + .00375\phi_{TE}]$

where $\frac{t}{C}$ = .048 (airfoil section data-input)

ϕ_{TE} = 5.65 degrees (Figure 3-4h)

C_{ℓ_α} = 6.76 per radian (= .114 per degree)

DATA ACQUISITION LIST

I. Basic Wing Data

1. Airfoil Data

a. Type Section	65A-004.8 Modified	
b. t/c	.048	
c. ϕ_{TE}	6.0	degs.
d. $(X_{tMAX})/C$	.40	

2. Planform Data

a. S_{TOT}	170.0	$ft.^2$
b. S_{EXP}	120.9	$ft.^2$
c. $\Lambda_{LE}, \Lambda_{C/4}$	32.0 , 26.0	degs.
d. AR	3.750	
e. AR_{EXP}	3.12	
f. TR	.2	
g. TR_{EXP}	.246	
h. $\bar{c}$	7.73	ft.

II. Fuselage Data

a. A_B	12	$ft.^2$
b. S_{WET}	750	$ft.^2$
c. d	5.8	ft.
d. b	25.25	ft.

e. d/b .230

f. ℓ_B 45.0 ft.

III. High Lift Device

1. Trailing Edge Flap *

a. Type Single Slotted

b. c_f/c .260

c. c_f/c' .260

d. c'/c 1.000

e. δ_f 45.0 degs.

f. b_f/b .270

g. b_{fi}/b .231

h. b_{fo}/b .50

i. S_f 54.0 $ft.^2$

2. Leading Edge Device

a. Type Flap

b. c_d/c or c_d/c'' .15

c. c''/c 1.00

d. δ_d 30 degs.

e. b_d/b .58

f. S_d 84.0 $ft.^2$

IV. Miscellaneous Data

a. α_g	9	degs.
b. W	12000	lbs.
c. W_e	7900	lbs.
d. F_N	0	lbs.

*NOTE: FOR DOUBLE-SLOTTED FLAPS THE FOLLOWING DATA IS REQUIRED

$c_f/c' = c_{FLAP_{TOTAL}}/c'$ _____

$c_{FLAP\,2}/c'$ _____

$\delta_f = \delta_{FLAP\,1}$ _____

$\delta_{FLAP\,2}$ _____

3. $C_{\ell_{max}} = (C_{\ell_{max}})_{base} + \sum_{M=1}^{M=4} \Delta_M C_{\ell_{max}}$

where $(C_{\ell_{max}})_{base}$ = .80 (Figure 3-7, for Δy = .93 from Figure 3-6)

$\Delta_1 C_{\ell_{max}}$ = 0.00 (Figure 3-8b, Δy = .93, % camber =0.5, $x_{t_{MAX}}$ = .40)

$\Delta_2 C_{\ell_{max}}$ = 0.19 (Figure 3-9, Δy = .93, t_{MAX} = .40)

$\Delta_3 C_{\ell_{max}}$ = -0.125 (Figure 3-10, Δy = .93, RN_w = 1.2×10^6 (V = 250 ft/sec.) - extrapolated from available curves in Figure 3-10)

$\Delta_4 C_{\ell_{max}}$ = 0 (Figure 3-11, assume no NACA standard roughness)

hence, $C_{\ell_{max}}$ = .86 (Summing $(C_{\ell_{max}})_{base}$ and $\Delta C_{\ell_{max}}$ values)

3. <u>Step 3 - Wing Alone Characteristics</u>

a. α_o = 0.0 degrees (use value from Step 2, part a.)

b. $$C_{L_{\alpha_W}} = \frac{2\pi AR}{2 + \left\{ \frac{4\pi^2 AR^2}{C_{\ell_\alpha}^2} \left[1 + \left(\tan\Lambda_{LE} - \frac{2}{AR} \left(\frac{1-TR}{1+TR} \right) \right)^2 \right] + 4 \right\}^{1/2}}$$

where C_{ℓ_α} = 6.02 per radian (use value from Step 2, part a.)

AR = 3.75

TR = .2

Λ_{LE} = 32.0 degrees

Hence, C_{L_α} = 3.63 per radian (= .063 per degree)

c. Determination of High or Low Aspect Ratio:

$$\frac{4}{(C_1 + 1)\text{Cos}\Lambda_{LE}} = 3.18$$

where C_1 = .48 (Figure 3-12, TR = .2)

$\text{Cos}\Lambda_{LE}$ = .850

Use High-Aspect Ratio methods:

$$C_{L_{MAX}} = C_{\ell_{max}} \left(\frac{C_{L_{MAX}}}{C_{\ell_{max}}}\right)$$

where $C_{\ell_{max}}$ = .92 (use value from Step 2, part a.)

$$\frac{C_{L_{MAX}}}{C_{\ell_{max}}} = 1.04 \text{ (Figure 3-13, } \Lambda_{LE} = 32°, \Delta y = .93)$$

Hence, $C_{L_{MAX}}$ = .96

$$\alpha_{C_{L_{MAX}}} = \frac{C_{L_{MAX}}}{C_{L_\alpha}} + \alpha_o + \Delta\alpha_{C_{L_{MAX}}}$$

where $C_{L_{MAX}}$ = .96

C_{L_α} = .063 per degree

α_o = 0.0 degrees

$\Delta\alpha_{C_{L_{MAX}}}$ = 5.45° (Figure 3-14, Λ_{LE} = 32°, Δy = .93)

Hence, $\alpha_{C_{L_{MAX}}}$ = 20.7 degrees

4. Step 4 - Fuselage Effects on Lift

a. α_o = 0.0 degrees

b. $$C_{L_{\alpha_{WB}}} = \left[K_N + K_{B(W)} + K_{W(B)}\right] C_{L_{\alpha_{EXP}}} \frac{S_{EXP}}{S_{REF}}$$

where K_N = 2.0 per radian (based on body frontal area)

= 2.0 $\left(\frac{12}{170}\right)$ = .141 (based on reference area)

$K_{W(B)}$ = 1.19 (Figure 3-20, $\frac{d}{b}$ = .230)

$K_{B(W)}$ = 0.345 (Figure 3-20, $\frac{d}{b}$ = .230)

$C_{L_{\alpha_{EXP}}}$ - Use exposed area aspect ratio and taper ratio and calculate C_{L_α} as in Step 3b.

$AR = AR_{EXP} = 3.12$

$TR = TR_{EXP} = .246$

Hence, $C_{L_{\alpha_{EXP}}}$ = 3.31 per radian (= .058 per degree)

$S_{EXP} = 120.9\ ft^2$

$S_{REF} = S_{TOT} = 170\ ft^2$

Hence, $C_{L_{\alpha_{WB}}}$ = 3.94 per radian (= .069 per degree)

The final value for the aircraft is then:

$$C_{L_{\alpha_{TOT}}} = (C_{L_{\alpha_W}} + C_{L_{\alpha_{WB}}}) / 2.$$

= 3.79 per radian (= .066 per degree)

e. $$C_{L_{MAX_{WB}}} = \left[\frac{C_{L_{MAX_{WB}}}}{C_{L_{MAX_W}}}\right] C_{L_{MAX_W}}$$

where $C_{L_{MAX_W}}$ = .96 (from Step 3c.)

$$\left[\frac{C_{L_{MAX_{WB}}}}{C_{L_{MAX_W}}}\right] = .93 \text{ (Figure 3-21, } \frac{d}{b} = .230,$$

$(C_2 + 1)AR\ Tan\Lambda_{LE} = 3.72,$

$C_2 = .90$, Figure 3-16, TR=.246)

Hence, $C_{L_{MAX_{WB}}} = .89$

$$\alpha_{C_{L_{MAX_{WB}}}} = \left[\frac{\alpha_{C_{L_{MAX_{WB}}}}}{\alpha_{C_{L_{MAX_W}}}}\right] \alpha_{C_{L_{MAX_W}}}$$

where $\alpha_{C_{L_{MAX_W}}} = 20.7$ degrees

$$\left[\frac{\alpha_{C_{L_{MAX_{WB}}}}}{\alpha_{C_{L_{MAX_W}}}}\right] = .87 \quad \text{(Figure 3-22, } \frac{d}{b} = .230,$$

$(C_2 + 1)AR\ Tan\Lambda_{LE} = 3.72)$

Hence, $\alpha_{C_{L_{MAX_{WB}}}} = 18.0$ degrees

5. Step 5 - High Lift Devices - Trailing Edge Flaps

Single Slotted Flap

Flap chord to wing chord ratio, $C_{F/C} = .260$

Deflection angle, $\delta_F = 45°$

Flap Span, $b_{F/b} = .270$

Inboard flap edge location, $b_{F_{i/b}} = .231$

Outboard flap edge location, $b_{F_{o/b}} = .501$

Wing area affected by flap deflection, $S_F = 54\ ft^2$.

For a single slotted part-span flap, Section 3 of Step 5 applies:

a. $\Delta C_\ell = .96$ (Figure 3-34, $\delta_F = 45°$, $C_{F/C} = .260$)

b. $\Delta C_L = \Delta C_\ell \left(\frac{C_{L_\alpha}}{C_{\ell_\alpha}}\right) \left[\frac{(\alpha_\delta)_{C_L}}{(\alpha_\delta)_{C_\ell}}\right] K_b$

where $\Delta C_\ell = .96$ (part 5a above)

$\left(\frac{C_{L_\alpha}}{C_{\ell_\alpha}}\right) = .63$ ($C_{L_\alpha} = 3.79$ (part 4b), $C_{\ell_\alpha} = 6.02$ (part 2a))

$\left[\frac{(\alpha_\delta)_{C_L}}{(\alpha_\delta)_{C_\ell}}\right] = 1.36$ (Figure 3-32, AR = 3.12,

$(\alpha_\delta)_{C_\ell} = -\frac{(C_{\ell_\delta})_\alpha}{(C_{\ell_\alpha})_\delta} = \left(\frac{\Delta C_\ell}{\delta_F}\right)\left(\frac{2\pi}{C_{\ell_\alpha}}\right) = -.212$)

$K_b = .385$ (Figure 3-33, $\frac{b_F}{b} = .27$, $TR_{EXP} = .246$)

Hence, $\Delta C_L = .317$

c. $C_{L_\alpha} = 3.79$ per radian ($= C_{L_{\alpha_{WB}}}$)

d. $\Delta\alpha_o = \frac{\Delta C_L}{C_{L_\alpha}} (C_1)$

where $\Delta C_L = .317$ (Step 5-3b.)

$C_{L_\alpha} = 3.79$ per radian

$C_1 = 1.2$ for AR < 4

Hence, $\Delta\alpha_o = -5.75°$

e. $\Delta C_{\ell_{max}} = k_1 k_2 k_3 (C_{\ell_{max}})_{base}$

where $(\Delta C_{\ell_{max}})_{base} = 1.003$ (Figure 3-27, $\frac{t}{C} = .048$, Curve C)

$k_1 = 1.015$ (Figure 3-28, $C_{F/C} = .260$)

$k_2 = 1.000$ (Figure 3-29, $\delta_f = 45°$)

$k_3 = 1.000$ (Figure 3-30, $\delta_f = 45°$)

Hence, $\Delta C_{\ell_{max}} = 1.02$

f. $\Delta C_{L_{MAX}} = \Delta C_{\ell_{max}} \frac{S_F}{S_{REF}} (1 - .08 \cos^2 \Lambda_{C/4}) \cos^{3/4} \Lambda_{C/4}$

where $\Delta C_{\ell_{max}} = 1.02$ as above

$S_F = 54$ ft^2 (given data)

$S_{REF} = 170$ ft^2

$\Lambda_{C/4} = 24°$

Hence, $\Delta C_{L_{MAX}} = .283$

g. $\Delta\alpha_{C_{L_{MAX}}} = -.5 \frac{\Delta C_{L_{MAX}}}{C_{L_\alpha}}$ for AR < 4.

where $\Delta C_{L_{MAX}} = .283$ (Step 5f.)

$C_{L_\alpha} = 3.79$ per radian (Step 4b.)

Hence, $\Delta\alpha_{C_{L_{MAX}}} = -2.1°$

and $\alpha_{C_{L_{MAX}}} = 15.9°$

6. <u>Step 6 - High Lift Devices - Leading Edge</u>

Leading Edge Plain Flap

Leading Edge flap chord to wing chord, $C_{d/C} = .15$

Deflection angle, $\delta_d = 30°$

Leading Edge flap span ratio, $b_{d/b} = .58$

Wing area influenced by deflected leading edge flap, $S_d = 84.0$ ft^2.

a. $\Delta C_\ell = C_{\ell_\alpha} \frac{\Delta\alpha}{\delta} \delta$

where C_{ℓ_α} = 6.02 per radian (Step 2.a)

$\frac{\Delta\alpha}{\delta}$ = .27 (Figure 3.40, $C_{d/C}$ = .15)

δ = 30 degrees

Hence, ΔC_ℓ = .85

b. $\Delta C_L = \Delta C_\ell \left(\frac{C_{L_\alpha}}{C_{\ell_\alpha}}\right) \left[\frac{(\alpha_\delta)_{C_L}}{(\alpha_\delta)_{C_\ell}}\right] K_b$

where ΔC_ℓ = .85

$\left(\frac{C_{L_\alpha}}{C_{\ell_\alpha}}\right)$ = .63 (See Step 5c)

$\left[\frac{(\alpha_\delta)_{C_L}}{(\alpha_\delta)_{C_\ell}}\right]$ = 1.27 (Figure 3-32, AR = 3.12, $(\alpha_\delta)_{C_\ell}$ = -.284,

$= \frac{(C_{\ell_\delta})_\alpha}{(C_{\ell_\alpha})_\delta} = \left(\frac{\Delta C_\ell}{\delta_d}\right)\left(\frac{2\pi}{C_{\ell_\alpha}}\right)$)

K_b = .73 (Figure 3-33, $b_{d/b}$ = .58, λ = .246)

Hence, ΔC_L = .50

c. $C_{L_\alpha} = C_{L_{\alpha_{WB}}}$ = 3.79 per radian

d. $\Delta\alpha_o = \frac{\Delta C_L}{C_{L_\alpha}}$ (.2)

where ΔC_L = .50

C_{L_α} = 3.79 per radian

Hence, $\Delta\alpha_o$ = 1.5 degrees

e. $\Delta C_{\ell_{max}} = \left(\frac{\Delta C_{\ell_{max}}}{\delta_d}\right) \delta_d$

where $\left(\frac{\Delta C_{\ell_{max}}}{\delta_d}\right)$ = .0253 (Figure 3-41; $C_{d/C}$ = .15)

δ_d = 15°

Hence, $\Delta C_{\ell_{max}}$ = .38

f. $\Delta C_{L_{MAX}} = \Delta C_{\ell_{max}} \frac{S_d}{S_{REF}} (1 - .08 \cos^2\Lambda_{C/4}) \cos^{3/4}\Lambda_{C/4}$

where $\Delta C_{\ell_{max}}$ = .38

S_d = 84.0 ft^2 (given data)

S_{REF} = 170 ft^2.

$\Lambda_{C/4}$ = 24.0 degrees

Hence, $\Delta C_{L_{MAX}}$ = .164

g. $\Delta\alpha_{C_{L_{MAX}}} = + \frac{\Delta C_{L_{MAX}}}{C_{L_\alpha}}$

where $\Delta C_{L_{MAX}}$ = .164

C_{L_α} = 3.79 per radian

Hence, $\Delta\alpha_{C_{L_{MAX}}}$ = 2.5 degrees

7. Step 7 - Landing Lift Characteristics

For a wing with a single slotted trailing edge flap (δ_F=45°) and a plain leading edge flap (δ_d = 30°), the following lift characteristics were calculated:

a. $\alpha_o = \alpha_{o_{clean}} + \Delta\alpha_{o_F} + \Delta\alpha_{o_d}$

where α_o - wing with deflected flaps/devices angle of zero lift

$\alpha_{o_{clean}}$ = 0.0° - angle-of-zero-lift for wing without deflected flaps or devices = 0°

$\Delta\alpha_{o_F}$ = -5.75° - increment of zero-lift- angle-of-attack for wing with deflected T.E. flap

$\Delta\alpha_{o_d}$ = + 1.5° - increment of zero-lift angle-of-attack for wing with deflected leading edge flap

Hence, α_o = -4.25°

b. $C_{L_\alpha} = C_{L_{\alpha_{WB_F}}}$

where $C_{L_{\alpha_{WB_F}}}$ = 3.79 per radian (Step 5c.)

c. $C_{L_{MAX}} = C_{L_{MAX_{\delta=0}}} + \Delta C_{L_{MAX_F}} + \Delta C_{L_{MAX_d}}$

where $C_{L_{MAX_{\delta=0}}}$ = .89 ($C_{L_{MAX_{WB}}}$ - Step 4c) - maximum lift coefficient for wing-body combination with undeflected flaps/devices.

$\Delta C_{L_{MAX_F}}$ = .283 (Step 5f - T.E. Flaps) - increment of maximum lift coefficient for trailing edge single slotted flap.

$\Delta C_{L_{MAX_d}}$ = .164 (Step 5f - L.E. Flaps) - increment of maximum lift coefficient for leading edge plain flap.

Hence, $C_{L_{MAX}}$ = 1.34

d. $\alpha_{C_{L_{MAX}}} = \alpha_{C_{L_{MAX_{WB}}}} + \Delta\alpha_{C_{L_{MAX_F}}} + \Delta\alpha_{C_{L_{MAX_d}}}$

where $\alpha_{C_{L_{MAX_{WB}}}}$ = 18.0° (Step 4c.)

$\Delta\alpha_{C_{L_{MAX_F}}}$ = -2.1° (Step 5g - T.E Flaps)

$\Delta\alpha_{C_{L_{MAX_d}}}$ = 2.5° (Step 5g - L.E. Flaps)

Hence, $\alpha_{C_{L_{MAX}}}$ = 18.4°

e. $C_L = C_{L_\alpha} (\alpha - \alpha_o)$

Therefore for α = 9°, C_L = .878, using previously calculated values of C_{L_α} and α_o, and assuming a linear lift curve from α_o to α = 9°,

and for α = 0°, C_L = .281

8. Step 8 - Touchdown Speed

The touchdown velocity is:

$$V_{TD} = \left[\frac{W - F_N \sin (\alpha_g - \gamma)}{.00119\, C_{L_{TD}}\, S_{REF}} \right]^{1/2}$$

where W = 12,000 lb.

F_N = 0 lb.

α_g = 9°

γ = -2°

$C_{L_{TD}}$ = .878 (step 7e)

S_{REF} = 170 ft^2.

Therefore V_{TD} = 260 ft/sec. = 154.6 knots

9. Step 9 - Aircraft Minimum Drag (No High Lift Devices)

a. Landing gear drag - The assumed wing reference area is 170 ft^2. The empirical method b. therefore applies:

$$\Delta C_{D_{LG}} = \left[.275 \left(\frac{W_E}{S_{REF}} \right) - 6 \right] \left(\frac{1}{S_{REF}} \right)$$

where W_E = 7,900 lb.

S_{REF} = 170 ft^2

therefore $\Delta C_{D_{LG}}$ = .0377

b. The Reynold's number of the wing and fuselage (standard sea level conditions) are:

$$RN_{Wing} = .00636\ V_{TD}\ MAC \times 10^5$$

where V_{TD} = 260 ft/sec.

MAC = 7.73 ft.

$$RN_{fuselage} = .00636\ V_{TD}\ \ell_{fuselage} \times 10^5$$

where V_{TD} = 260 ft/sec.

$\ell_{fuselage}$ = 45.0 ft.

Therefore $RN_{Wing} = 1.28 \times 10^6$

$RN_{fuselage} = 7.43 \times 10^6$

c. The minimum wing and tail drag is:

$$\Delta C_{D_{min_{W+T}}} = 1.4 \left[2 C_f \left(1 + 2\, t/C + 100\, (t/C)^4\right)\right]$$

where 1.4 - factor accounts for the tail surfaces

$C_f = .0044$ (Figure 3-43 for $RN_{Wing} = 1.28 \times 10^6$,

$(\ell/k = 3.7 \times 10^5$, $\ell = 93.0$ inches (MAC), $k = .25 \times 10^{-3}$,

smooth paint surface))

$$\frac{t}{c} = .048$$

Hence, $\Delta C_{D_{min}}$ wing $= .0135$

d. Minimum fuselage drag is:

$$\Delta C_{D_{min}} \text{ fuselage} = 1.02 C_f \left[1 + \frac{1.5}{(\ell_{b/d})^{1.5}} + \frac{7}{(\ell_{b/d})^3}\right] \frac{S_{wet}}{S_{REF}}$$

where $C_f = .0032$ (Figure 3-43, $RN_{fuselage} = 7.43 \times 10^6$,

$\ell_{b/k}$ 21.5×10^5, $\ell_B = 540$ inches,

$k = .25 \times 10^{-3}$ smooth paint surface)

$\ell_{b/d} = 7.77$ ($\ell_b = 45.0$ ft., $d = 5.8$ ft.)

$S_{wet} = 750$ ft^2

$S_{REF} = 170$ ft^2

Therefore, $\Delta C_{D_{min}}$ fuselage $= .0156$

e. The total minimum drag coefficient is therefore

$$C_{D_{min}} = \Delta C_{D_{min}}{}_{wing} + \Delta C_{D_{min}}{}_{fuselage} + \Delta C_{D_{LG}}$$

where $\Delta C_{D_{min}}{}_{wing} = .0135$

$\Delta C_{D_{min}}{}_{fuselage} = .0156$

$\Delta C_{D_{LG}} = .0377$

and $C_{D_{min}} = .0668$

10. Step 10 - Drag Due To Lift - Clean Wing

$$\Delta C_{D_i} = \frac{C_{L_{D_i}}{}^2}{\pi (AR)} (1 + \Delta_1 \Delta_2) + K_D \Delta_3$$

where $C_{L_{D_i}} = C_{L_{TD}} - C_{L_{DES}} = .778$ ($C_{L_{TD}} = .878$, $C_{L_{DES}} = .10$)

$AR = 3.75$

$\Delta_1 = .014$ (Figure 3-44, TR = .20, AR = 3.75)

$\Delta_2 = 1.19$ (Figure 3-45, $\Lambda_{C/4} = 24°$, AR = 3.75)

$K_D = 1.00$ (Figure 3-47, $\Lambda_{LE} = 32°$)

$\Delta_3 = 0.010$ (Figure 3-46a, $\frac{\text{Tan}\alpha_g}{\text{Tan}\alpha_{C_{L_{MAX}}}} = .49$ ($\alpha_g = 9°$, $\alpha_{C_{L_{MAX}}} = 18.0°$),

$$J = .3(C_1 + 1)AR \cos\Lambda_{LE} \left\{ (C_1 + 1)(C_2 + 1) - \left[\frac{(C_2 + 1)AR \tan\Lambda_{LE}}{7} \right]^2 \right\}$$

where C_1 = .48, C_2 = .52, AR = 3.75,

Λ_{LE} = 32°, resulting in J = 2.81)

Hence, ΔC_{D_i} = .062

11. Step 11 - Drag Of High Lift Devices

a. Trailing Edge Flaps

1. Minimum drag coefficient of a single slotted flap is:

$$\Delta C_{D_{\substack{min \\ flap}}} = \Delta C_{d_{flap}} K_b I_F$$

where $\Delta C_{d_{flap}}$ = .082, (Figure 3-48b $c_{F/C}$ = .260, δ_F = 45°)

K_b = .385 (Figure 3-33, $b_{F/b}$ = .27, λ = .246)

I_F = (1. + .00667 δ_F) = 1.3 (δ_F = 45°) for AR < 4.0

Hence, $\Delta C_{D_{\substack{min \\ flap}}}$ = .041

2. The drag due to lift of a flap is:

$$\Delta C_{D_{i_{flap}}} = K' \frac{(\Delta C_L)^2}{\pi AR}$$

where K' = 1.32 (Figure 3-49a - 3-49c AR = 3.75,

$\eta_o = b_{F_o/b/2}$=.50, η_i = .231; extrapolate

from the three point curve obtained to

AR = 3.75)

ΔC_L = .317 (Step 6b.)

AR = 3.75

Hence, $\Delta C_{D_{i_{flap}}}$ = .0113

b. Leading edge devices

For a leading edge flap

$$\Delta C_{D_{min}}{}_{device} = (1 - \cos\delta_d) \frac{b_d}{b} \frac{C_d}{C} \frac{S_d}{S_{REF}}$$

where $\delta_d = 30°$

$b_{d/b} = .58$

$C_{d/C} = .15$

$S_d = 84\ ft^2$

$S_{REF} = 170\ ft^2$

and $\Delta C_{D_{min}} = .00577$

Assume $\Delta C_{D_i}{}_{device} = 0$

12. Step 12 - Drag Of Additional Drag Devices

For this sample calculation it is assumed that the aircraft utilizes a speed brake and a drag chute as deceleration devices during the landing ground roll. The minimum drag increments of these devices are calculated below:

a. Spoilers - Assuming no spoilers are used on the aircraft,

$\Delta C_{D_{SP}} = 0.0$

b. Speed Brake - The Speed Brake has a panel area of 6.42 ft^2, and a maximum deflection of 45°. By equation (III-50):

$$\Delta C_{D_{SB}} = 1.13 \sin\delta_{SB} \frac{A_{SB}}{S_{REF}}$$

where $\sin\delta_{SB} = .707$

$A_{SB} = 6.42\ ft^2$

$S_{REF} = 170\ ft^2$

Therefore $\Delta C_{D_{SB}} = .0302$

c. Drag Chute - The aircraft utilizes a 15-foot diameter ring-slot type parachute as a deceleration device during the landing ground roll. The calculation method for drag chute minimum drag coefficient is:

$$\Delta C_{D_{DC}} = \Delta C_{D_{o_c}} \frac{S_{chute}}{S_{REF}}$$

where $S_{chute} = 176.5\ ft^2$ $(= \frac{\pi}{4} D_c^2$, where $D_c = 15$ feet)

and assuming a value of

$$\Delta C_{D_{o_c}} = 0.55 \text{ (Reference 11 - design)}$$

(based on the parachute canopy area), the drag chute drag coefficient can be calculated based on airplane reference area, S_{REF}, as:

$$\Delta C_{D_{DC}} = 0.572$$

d. Thrust Reverser Door Deployment: For the aircraft equipped with thrust reversers, the base drag coefficient of the thrust reverser doors when fully deployed is:

$$\Delta C_{D_{TR}} = 0.5 \frac{S_{TR}}{S_{REF}}$$

where the average base pressure coefficient is -0.5

$S_{TR} = 6\ ft^2$ total base area of the fully deployed thrust reverser doors

$S_{REF} = 170\ ft^2$

Therefore, $\Delta C_{D_{TR}} = 0.0175$

13. Step 13 - Total Drag Coefficient

Summing the drag terms calculated in Steps 9 through 12, the total aircraft drag coefficient at touchdown is calculated:

$$C_{D_{TD}} = \underbrace{C_{D_{min}}}_{\text{Step 9}} + \underbrace{\Delta C_{D_i}}_{\text{Step 10}} + \underbrace{\left[\Delta C_{D_{i_{flap}}} + \Delta C_{D_{min_{flap}}} + \Delta C_{D_{min_{device}}}\right]}_{\text{Step 11}} + \underbrace{(\Delta C_{D_{min}})_{DD}}_{\text{Step 12}}$$

where $C_{D_{min}} = .0668$

$\Delta C_{D_i} = .0620$

$\Delta C_{D_{i_{flap}}} = .0113$

$\Delta C_{D_{min_{flap}}} = .0410$

$\Delta C_{D_{min_{device}}} = .0058$

$(\Delta C_{D_{min}})_{DD} = 0.00$ (at touchdown)

Therefore, $C_{D_{TD}} = .1869$ at $\alpha_g = 9°$

Similarly, $C_D = .1378$ at $\alpha_g = 0°$

} No spoilers, speed brakes, drag chutes or thrust reversers.

B. WHEEL BRAKING

1. Given data

Same aircraft as in Section II, Subsection A.

GW = 13,500 lb.

No anti-skid system

V = 100 knots

Tire: Type VIII 22 x 8.5-11

Assume .8 GW on main gear

Dry, Wet and icy runways

2. Solution

a. Dry Runway

1. To find the tire footprint area (Subsection 6) the values of D_o, W, and D_f are found in Table IV-4:

$D_o = 22.00$
$W = 8.50$ } Type VIII, 22 x 8.5-11
$D_f = 12.75$

2. Using equation (VI-19) for type VIII tires, the net footprint area, A_n, is calculated:

$$A_n = .404(D_o + D_f)\sqrt{(D_oW) - .16(D_o - D_f)[(D_o+W) - .16(D_o-D_f)]}$$

$$= 44.1 \text{ in}^2/\text{tire}$$

3. For a non-anti-skid system, the μ_{avg} is calculated using equation (IV-12) in Subsection 3:

$$\mu_{avg} = f(V)(.837 - 0.00099 \frac{F_{mg}}{A_n})$$

where, $F_{mg} = .8(GW) = 10{,}800$ lb.

$A_n = 88.2$ in^2 (Two tires)

$f(V) = C_1 + C_2V + C_3V^2 + C_4V^3 + C_5V^4$

where, $C_1 = 1.0$

$C_2 = -.24492 \times 10^{-1}$

$C_3 = .3368 \times 10^{-3}$

$C_4 = -.20098 \times 10^{-5}$

$C_5 = .42539 \times 10^{-8}$

For V = 100 knots, f(V) = .334

Hence, $\mu_{avg} = .238$ for dry runways

Assume $\mu_R = .025$ for dry runways

b. Wet Runway

For the wet runway, the procedure outlined in Subsection 4, paragraph B and Equation (VI-15) is used:

$$\mu_{B_{wet}} = \mu_{avg} \quad f(\text{tread},V)$$

where μ_{avg} = .238 (from dry runway calculation - no anti-skid system)

$$f(\text{tread},V) = C_1 + C_2V + C_3V^2 + C_4V^3 + C_5V^4$$

where, $C_1 = 1.0$

$C_2 = -.11943 \times 10^{-1}$

$C_3 = .75657 \times 10^{-}$ Tread design - ribs

$C_4 = .14953 \times 10^{-6}$

$C_5 = -.590157 \times 10^{-10}$

for V = 100 knots, f(tread,V) = .407

Hence, $\mu_{B_{wet}}$ = .097

c. Ice and Snow-Covered Runways

The procedure for analyzing the braking coefficient for ice and snow-covered runways is outlined in Subsection 4, paragraph A.

1. An appropriate value of μ_{max} is obtained from Table IV-2:

   μ_{max} = 0.18

2. For a non-anti-skid brake system:

   $$\mu_{avg} = 0.9 \frac{\mu_{skid}}{\mu_{max}} (\mu_{max})_{anti\text{-}skid}$$

   where $\frac{\mu_{skid}}{\mu_{max}}$ = f(V) from Eq. IV- 11 = .334 (V=100 kts)

   $(\mu_{max})_{anti\text{-}skid}$ = .18 from above part 1.

   Hence, μ_{avg} = .054

C. THRUST

For the Sample Calculation, it is assumed that the aircraft is equipped with a barrel mounted target-type thrust reverser. From this section, the following generalized statements can be made, since sufficient information on the installation and performance of the reverser is unavailable:

Reverser Effectiveness: $\eta = -.60$ (For aft fuselage mounted engines with inlets far forward)

Cutoff Velocity: $V_{co} = 20$ Knots

Plume Shape: This is dependent upon aircraft speed and engine nozzle pressure ratio. For a general example of how to use the chart provided, see Subsection 7.

D. WEIGHT PENALTY-EVALUATION

1. Trailing Edge Flaps (Single-Slotted)

$$W = 5.17\ (S)^{.94} \qquad \text{(VI-1)}$$

where S = Flap planform area = 19.0 ft^2

W = 85 lb.

2. Leading Edge Flaps

$$W = 4.65\ (S)^{1.05} \qquad \text{(VI-3)}$$

where S = Device planform area = 12.30 ft^2

W = 65 lb.

3. Boundary Layer Control: No BLC Incorporated; W = 0.0 lb

4. Spoilers: No Spoilers Incorporated; W = 0.0 lb.

5. Drag Chute (Ring Slot)

$$W_{RING} = 1.15(D_C)^{1.43} \qquad \text{(VI-6)}$$

where D_C = 15 feet (canopy diameter)

W_{RING} = 55 lb.

6. Wheel Brakes and Systems

$$W_{BS} = N\,(2.2\,[.000380\,(KE)^{3/4}]^{1/2} + [.000380\,(KE)^{3/4}]) \qquad \text{(VI-7)}$$

where N = Number of Tires With Brakes (= 2 tires)

KE = Kinetic Energy Design Factor
(Assume = 10^7 ft/lb)

W_{BS} = 161 lbs.

7. Thrust Reversers (Deflecting Engine Primary Gases)

$$W = .111D_{EF} \quad \text{(L and } D_{EF} \text{ in inches)} \qquad \text{(VI-9)}$$

where L = Overall Thrust Reverser Door Length,
(Assume = 24 inches)

D_{EF} = Overall Diameter At Engine Flange,
(Assume D_{EF} = 18 inches)

Therefore, W = 47.5 lb per door, 95 lb. per reverser and 190 lb. per aircraft.

8. Speed Brakes

$$W = .0185S\,(KIAS) \qquad \text{(VI-10)}$$

where S = 6.24 ft^2

KIAS = Knots Indicated Airspeed,
(Assume KIAS = 200 Knots Maximum Limit For Deployment of Speed Brakes)

Therefore, W = 23 lbs.

E. DECELERATION FORCES DURING LANDING GROUND ROLL

1. General

Using equations (II-1) through (II-4), the following expression for total deceleration force may be derived:

$$\text{Deceleration Force} = \frac{GW}{g}\dot{V} =$$

$$\left[T - D - \mu_R (GW - L) - \frac{(\mu_B - \mu_R)}{\ell_{x_{mg}}}\left(M_{aero} + \ell_{x_{cg}}(GW - L)\right.\right.$$

$$\left.\left. -T\ell_{z_{T.L.}} + D\ell_{z_{cg}}\right)\right] \Bigg/ \left[-1 + (\mu_R - \mu_B)\frac{\ell_{z_{cg}}}{\ell_{x_{mg}}}\right]$$

For this sample problem, the following calculations of total deceleration force were made:

Case 1. At touchdown ($V = V_{TD}$, $\alpha_g = 9°$), no thrust reversal; speed brakes, drag chute not deployed.

Case 2. During landing ground roll ($V = 100$ kts, $\alpha_g = 0°$), with speed brakes, drag chute deployed; no thrust reverser installation.

Case 3. During landing ground roll ($V = 100$ kts, $\alpha_g = 0°$), with thrust reverser installation fully deployed; no speed brake or drag chute installation.

The following aircraft geometric constants are used in each case:

Base Gross Weight, GW = 12000 lb. (includes leading edge and trailing edge flaps, wheel brakes and systems)

$\ell_{x_{mg}}$ = 20.0 feet

$\ell_{x_{cg}}$ = 17.7 feet

$\ell_{z_{cg}}$ = 4.2 feet

$\ell_{z_{TL}}$ = 4.5 feet

2. Case 1 (V = 154.6 knots, α_s = 9°)

For Case 1, the following values are used:

GW = 12000 lb. (Base Weight)

T = 0 (Net Thrust)

C_D = .187 (Section III)

C_L = .878 (Section III)

V_{TD} = 154.6 Kts. (Section III)

M_{aero} = 0 (No data available)

$q = \frac{1}{2} \rho V^2 = 80.5$ lb/ft^2

S_{REF} = 170 ft^2

D = 2560 lb. (Drag = $C_D q S_{REF}$)

L = 12000 lb ($L = C_L q S_{REF}$)

μ_R = .025 (Section IV)

μ_B = .238 (Section IV - Dry Runway)

Inserting these values in the equation above results in:

$$\frac{GW}{g} \dot{V} = 2560 \text{ lb.}$$

3. Case 2. ($V = 100$ knots, $\alpha_g = 0°$)

For Case 2, the following values are used:

$T = 0$ (Net Thrust)

$C_D = .740$ (Section III - Basic aircraft + speed brake + drag chute)

$C_L = .281$ (Section III, $\alpha_g = 0°$)

$V = 100$ Knots

$M_{aero} = 0$ (No data available)

$q = 33.6$ lb/ft^2

$S_{REF} = 170$ ft^2

$D = 4230$ lb ($D = C_D q S_{TOT}$)

$L = 1605$ lb ($L = C_L q S_{TOT}$)

$\mu_R = .025$ (Section IV)

$\mu_B = .238$ (Section IV - Dry Runway)

$GW = 12078$ lb. (Base weight + drag chute and speed brake)

Inserting these values in the total deceleration force equation results in:

$$\frac{GW}{g}\dot{V} = 6322 \text{ lb.}$$

4. Case 3. ($V = 100$ knots, $\alpha_g = 0°$)

For Case 3, the following values are used:

$T = nF_G$ - Ram Drag

where $F_G = 4770$ lb (at $V = 100$ knots)

Ram Drag $= 410$ lb (at $V = 100$ knots, $\dot{W}_A = 78$ lb/sec)

$n = -.60$ (Section V)

$T = -3270$ lb

$C_D = .1553$ (Section III, $\alpha_g = 0°$ Basic airplane + thrust reverser door)

$C_L = .281$ (Section III, $\alpha_g = 0°$)

$GW = 12167$ lb. (Base weight + thrust reverser less speed brakes)

$$V = 100 \text{ kts.}$$

$$M_{aero} = 0 \text{ (No data available)}$$

$$q = 33.6 \text{ lb/ft}^2$$

$$S_{REF} = 170 \text{ ft}^2$$

$$D = 885 \text{ lb.}$$

$$L = 1605 \text{ lb.}$$

$$\mu_R = .025 \text{ (Section IV)}$$

$$\mu_B = .238 \text{ (Section IV - Dry Runway)}$$

Inserting these values in the total deceleration force equation results in:

$$\frac{GW}{g} \dot{V} = 6368 \text{ lb.}$$

5. Summary

From the calculations in cases 2 and 3 above, it is evident that the subject aircraft equipped with thrust reversers ($n = -.60$) has a deceleration force slightly greater than the deceleration force of the subject aircraft equipped with a 15 foot diameter ring-slot drag chute, at a ground speed of 100 knots. Solving for $\dot{V}$, the aircraft deceleration can be determined; the deceleration integrated with respect to time results in the aircraft velocity, which in turn can be integrated with respect to time to determine the landing ground roll distance from touchdown to runway exit. This evaluation is outside the scope of this handbook, but digital computer programs can be written to facilitate a landing ground roll calculation of the nature described above.

SECTION III

COMPUTATION OF THE LIFT, DRAG, AND TOUCHDOWN VELOCITY FOR AN AIRCRAFT IN THE LANDING CONFIGURATION.

1. GENERAL

Based on the sensitivity study discussed in Section II, the most important factor that determines the landing stopping distance (LSD) is the touchdown velocity (V_{TD}), see Figure 3-1. The touchdown velocity is the speed at which the airplane first comes into contact with the runway during a landing maneuver. For example, in the extreme case of vertical landing ($V_{TD} = 0$), LSD is zero.

From classical aerodynamics the equation for lift is:

$$L = C_{L_{TD}} \cdot q \cdot S_{REF} \qquad \text{(III-1)}$$

and at the instant before touchdown,

$$W = L \cos \gamma + T \sin (\alpha + i_T - \gamma) + D \sin\gamma \qquad \text{(III-2)}$$

for $\gamma \leq 4°$ this can be approximated by

$$W = L + T \sin (\alpha + i_T - \gamma)$$

and solving for the touchdown speed in knots for a sea level standard day.

$$V_{TD} = \left\{ \left(\frac{W - T \sin (\alpha + i_T - \gamma)}{S_{REF}} \right) / (.0034\, C_{L_{TD}}) \right\}^{1/2} \qquad \text{(III-3)}$$

If a description of the airplane is given then the weight (W), wing area (S), and thrust level (T) are easily determined. The angle-of-attack (α) and (γ) flight path angle are normally given. However

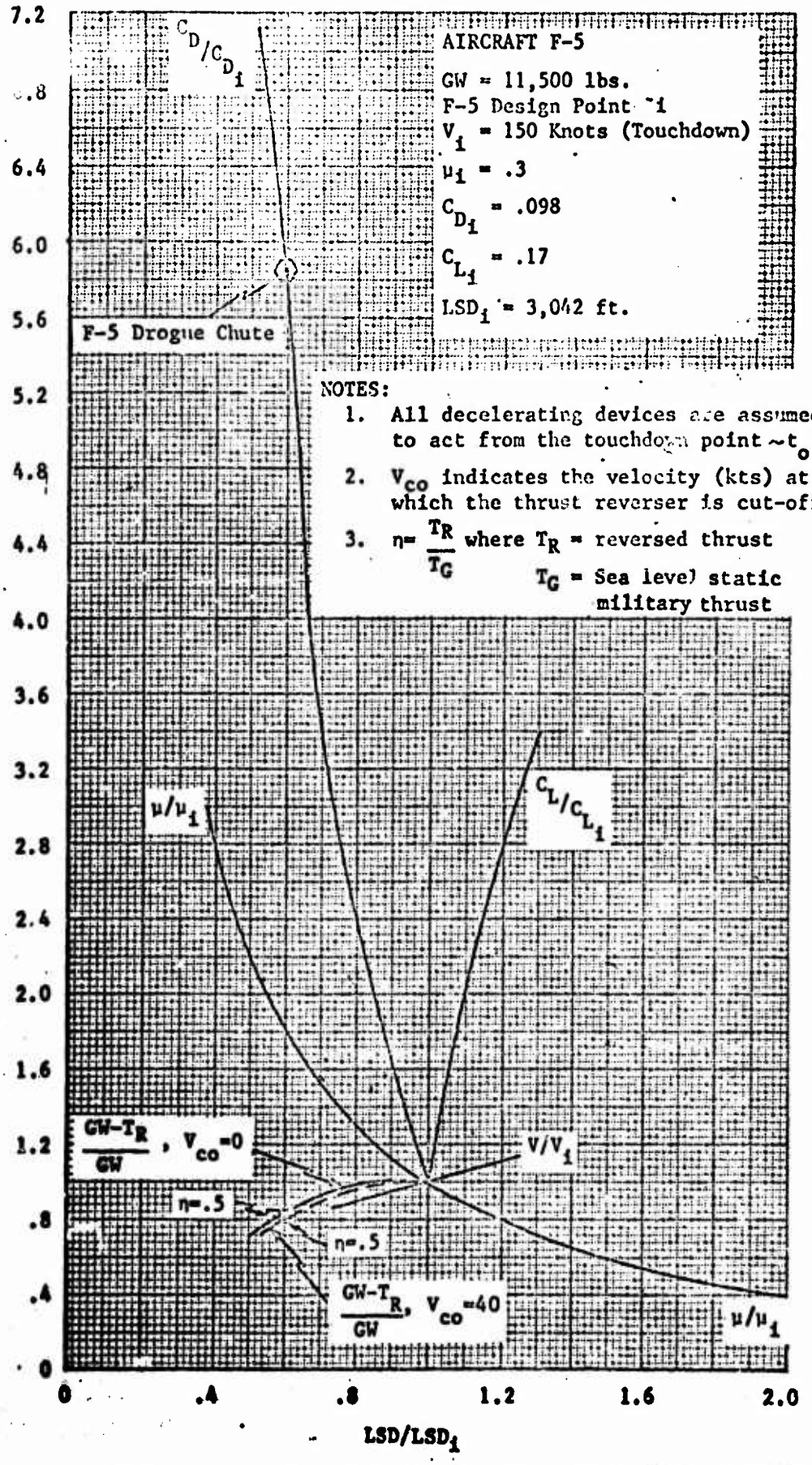

FIGURE 3-1 : Sensitivity of F-5 Landing Distance to Effectiveness of the Various Factors Affecting Landing Distance.

$C_{L_{TD}}$ is not easily obtained if only geometrical information is known.

A method of determining $C_{L_{TD}}$ from geometrical information is presented by Subsection 5-G.

Once $C_{L_{TD}}$ is known, (and therefore V_{TD} is known) one must be able to compute the aerodynamic drag of the airplane in order to:

1. Be able to determine the effect of drag on the LSD.
2. Determine the rate of sink at runway contact. Many current aircraft use neither a flare technique nor a power off approach.

$$R/S_{TD_{(FPS)}} = 1.689\ V_{APP_{(KNOTS)}} \cdot \text{Sin}\ \gamma$$

$$\text{where Sin}\ \gamma = \frac{D-T\ [\text{Cos}\ (\alpha + i_T)]}{W-T\ [\text{Sin}\ (\alpha + i_T)]}$$

Again thrust (T) and weight (W) are known for a given airplane. The drag is given by:

$$D = C_D \cdot q \cdot S_{REF} \qquad \text{(III-4)}$$

and for a sea level standard day

$$D = .0034\ (V_{APP})^2 \cdot S_{RFF} \cdot C_D$$

The procedure for obtaining C_D will be given in Subsections 5-I through 5-M.

It is the intent of this report to show how $C_{L_{TD}}$ and C_D can be obtained for any conventional aircraft in the landing configuration. This handbook and the computer program (Reference 1) were developed for this purpose. This handbook provides the necessary data and

procedures with which to perform hand calculations. Comparisons with actual aircraft data are included.

2. SCOPE

Studies of aircraft landing performance have shown that there are 7 parameters to be considered when computing the landing stopping distance. These are:

1. Weight
2. Thrust (Idle or Reverse)
3. Wheel Braking
4. Aerodynamic Pitching Moment
5. Aerodynamic Lift
6. Aerodynamic Drag
7. Touchdown Velocity

It is the purpose of this section to provide an engineer with a tool with which he can readily determine:

1. Aerodynamic Lift
2. Aerodynamic Drag
3. Touchdown Velocity

The only required knowledge of the airplane is:

1. Detailed Geometry
2. Weight
3. Thrust

3. METHODS VALIDATION

A. PREFACE

To determine if the methodology and procedures used were valid,

comparisons were made with several manufacturer's low speed aerodynamic data. The amount of data available was limited. Comparisons were completed for the following aircraft in the landing configuration (gear down, flaps extended):

1. Boeing B-52H
2. Douglas A-4C
3. McDonnell F-4
4. Northrop F-5
5. Republic F-105

The comparison plots (Figures 3-2a through 3-2u) show the calculated points (by computer program) and the manufacturer's data. The following information was compared:

1.	α_o	angle-of-attack at zero lift
2.	C_{L_α}	lift curve slope
3.	$C_{L_{MAX}}$	maximum lift coefficient
4.	$\alpha_{C_{L_{MAX}}}$	angle-of-attack for maximum lift
5.	C_D	minimum drag coefficient
6.	$C_{D_{TD}}$	total drag coefficient corresponding to the lift coefficient at touchdown

B. DISCUSSION

A discussion of the differences will be made in two parts. The first part (1) gives general reasons that are common to all aircraft. The second part (2) discusses each aircraft.

1. General Reasons

One particular problem for evaluation was that the aircraft manufacturer's data usually showed both the L.E. and T.E. devices deflected simultaneously. This prevented determining their independent and interdependent effects.

a. Lift Characteristics (α_o, $C_{L_{MAX}}$, $\alpha_{C_{L_{MAX}}}$, C_{L_α})

In highly-swept-wings, the angles-of-attack required to obtain the maximum lift coefficient are only of academic

interest. These high angles (> 20°) are normally larger than the airplane ground clearance angle. For this reason most manufacturer's arbitrarily cut off the data above some given angle-of-attack ($\alpha \approx 20°$). Therefore, actual comparisons of $\alpha_{C_{L_{MAX}}}$ and $C_{L_{MAX}}$ were not always available.

b. Drag Characteristics (C_{D_o}, $C_{D_{TD}}$)

There were several unknown factors that contributed to some differences in the drag comparisons. They were

1. Landing Gear Drag - Since no accurate methods for computing landing gear drag were uncovered during the literature search, an empirical method was developed. This was based on several aircraft manufacturer's data. The results are shown in Figure 3-42 and Step 9 of the Computation Methods Subsection 5. Some manufacturer's data show $\Delta C_{D_{LG}}$ to be a function of C_L, some do not.

2. Airfoil Information - Most aircraft use some type of NACA section-modified. Accurate descriptions of these modifications were unavailable. A principal unknown was the design lift coefficient which could effect the drag-due-to-lift characteristics.

3. Trim Drag - Some aircraft manufacturer's data did not provide sufficient detail to determine the effects of trim drag. The methods used did not compute trim drag. Comparison at lift may therefore be questionable if in the actual case trim drag is significant.

c. Touchdown Characteristics ($C_{L_{TD}}$, V_{TD})

There are two significant factors (and one minor factor) influencing the touchdown characteristics:

1. α_g - Angle-of-Attack at Touchdown - This is a function of pilot's visibility, aircraft geometry, and glideslope. Only an estimate of the aircraft ground clearance angle was available and therefore was used as the only criteria.

2. F_N - Power Used During a Landing - No power information was available and so zero power was used.

3. γ - The Flight Path Angle at Touchdown - The Flight Path Angle at touchdown is of some significance. Currently, military fighter-type aircraft do not use a flare technique for touchdown and so there is some effect of power and available ground clearance angle.

2. Discussion of the Particular Airplane

a. B-52H - Comparison of the B-52H estimated data with manufacturer's data is presented by Figures 3-2a, b and c. The B-52H lift characteristics are significantly affected by the aircraft fuel load and wing flexibility characteristics. The methods described in this handbook do not attempt to account for wing flexibility.

The flaps on the B-52H are divided into four sections on the wing. These effects cannot be calculated since the handbook determines flap effects for two-section flaps.

The landing gear drag, as obtained from Boeing, shows a decrease in $\Delta C_{D_{LG}}$ with increasing C_L.

The design lift coefficient for the wing was unknown and so a $C_{L_{DES}} = .1$ was assumed.

b. A-4 - Comparison of the A-4 estimated data with manufacturer's data is presented by Figures 3-2d, e and f. Landing gear drag data for the A-4 was unavailable. Trim drag data was also unknown. Detailed slat geometry was unavailable and so approximations to the amount of extension of the chord were made. The term "slats automatic" means that as the angle-of-attack is increased the slat extension increases: $C_{L_{DES}}$ assumed = 0.

c. F-4 - Comparison of the F-4 estimated data with manufacturer's data is presented by Figures 3-2g, h and i. The F-4 manufacturer's data was arbitrarily cut-off at $\alpha = 20°$.

The data presented for $\delta_F = 60°$ also included BLC effects. The remaining data had no BLC effects. The nomenclature for the L.E. flap (30°/60°/60°) indicates the flap was constructed in 3 sections with the inboard section deflected only 30°. $C_{L_{DES}}$ assumed = 0.

The F-4 $\Delta C_{D_{LG}}$ decreased with increasing C_L.

d. F-5 - Comparison of the F-5 estimated data with manufacturer's data is presented in Figures 3-2j through 3-2r. Accurate landing gear drag data was unavailable. The term (23°/18°) for the leading edge flap indicates the flap is constructed and deflected in two parts. T.E. flap translation was unknown (if it exists). $C_{L_{DES}}$ assumed = 0.

e. F-105 - Comparison of the F-105 estimated data with manufacturer's data is presented in Figures 3-2s, t and u. Very limited aerodynamic data was available. Trim and separate T.E. and L.E. device effects were unknown.

The $\Delta C_{D_{LG}}$ showed an increase with increasing C_L. The maximum lift data was arbitrarily cut-off at $\alpha = 20°$.

Accurate geometry data was unknown.

3. Closing Comments - If an accurate evaluation of an aircraft's landing characteristics is to be made by use of this method it is imperative that accurate detailed geometry is available. For evaluation of the touchdown conditions, angle-of-attack and rate-of-sink (flight path angle) limitations must be known.

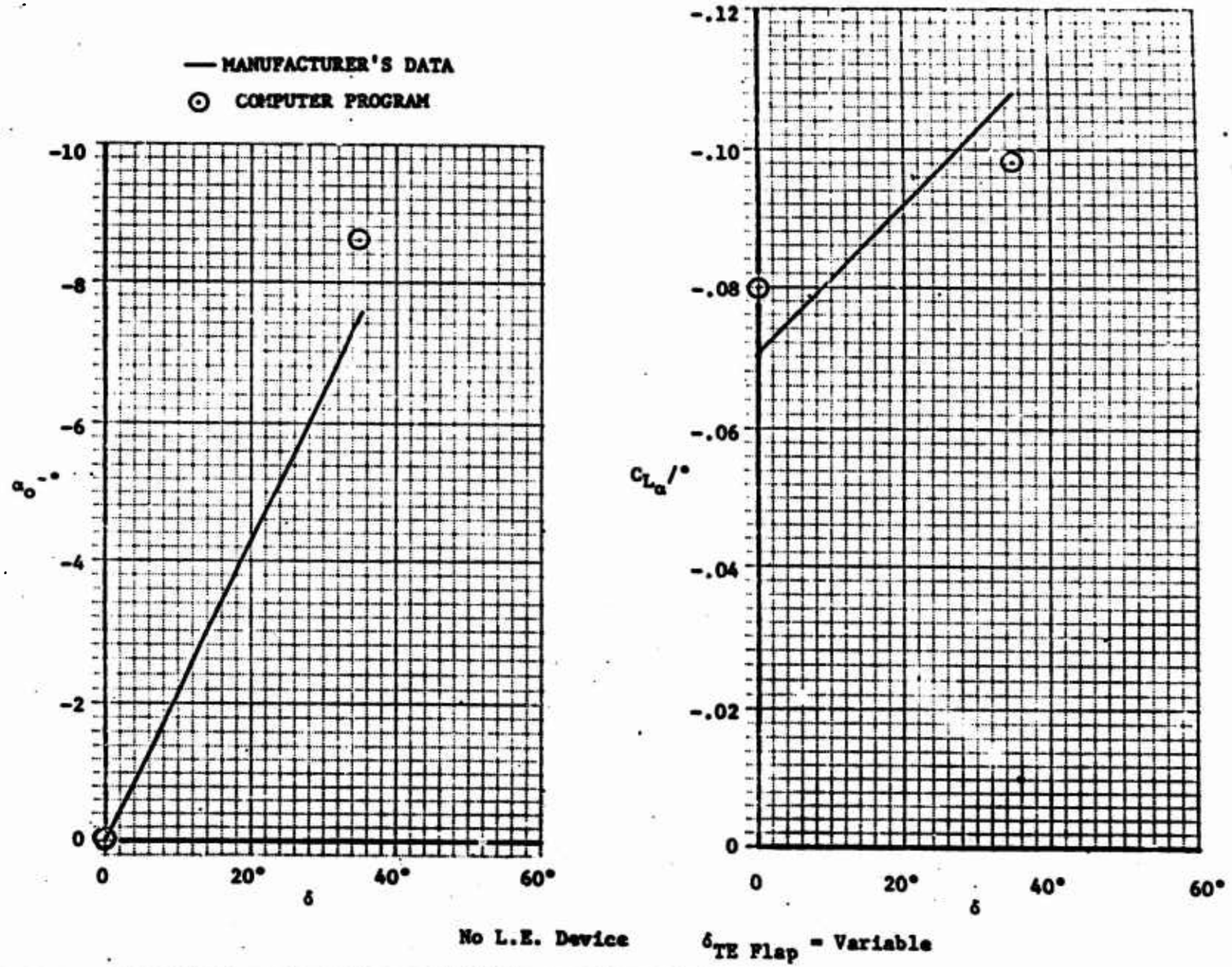

No L.E. Device $\delta_{TE\ Flap}$ = Variable

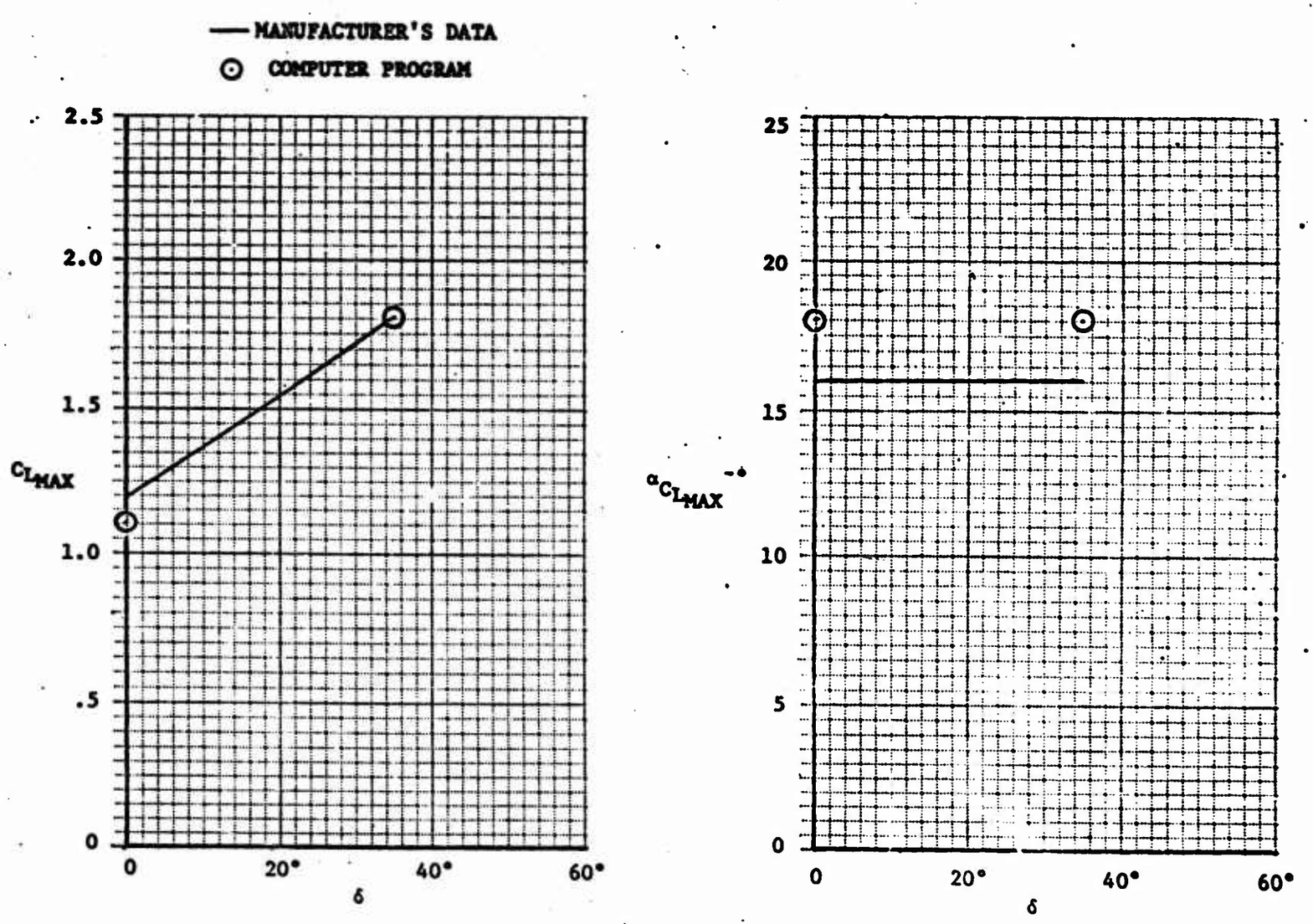

No L.E. Device $\delta_{TE\ Flap}$ = Variable

FIGURE 3-2b: Comparison of B-52H $C_{L_{MAX}}$ and $\alpha_{C_{L_{MAX}}}$ Predictions with Manufacturer's Data

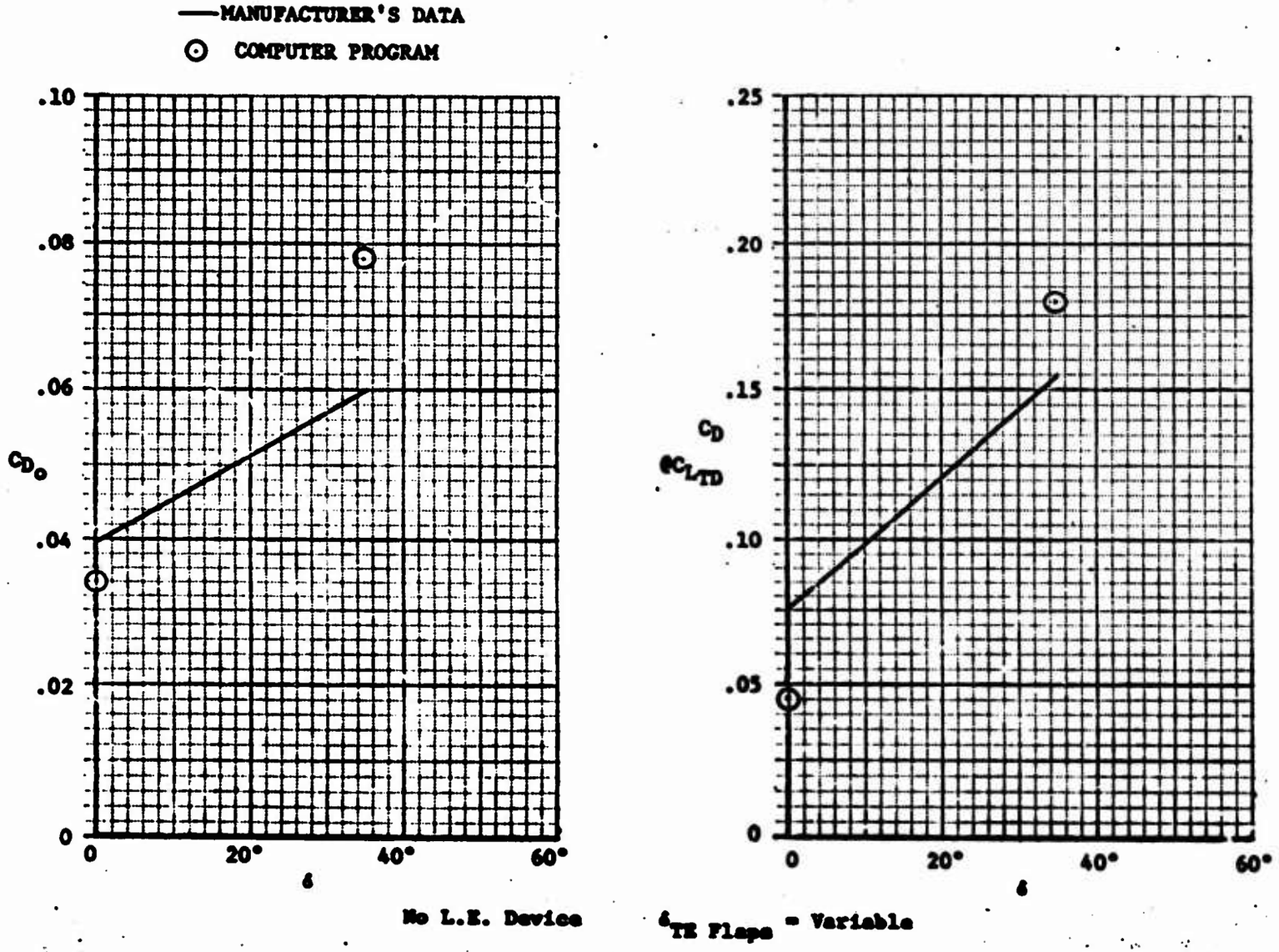

FIGURE 3-2c: Comparison of B-52H C_{D_o} and $C_{D_{@C_{L_{TD}}}}$ Predictions with Manufacturer's Data

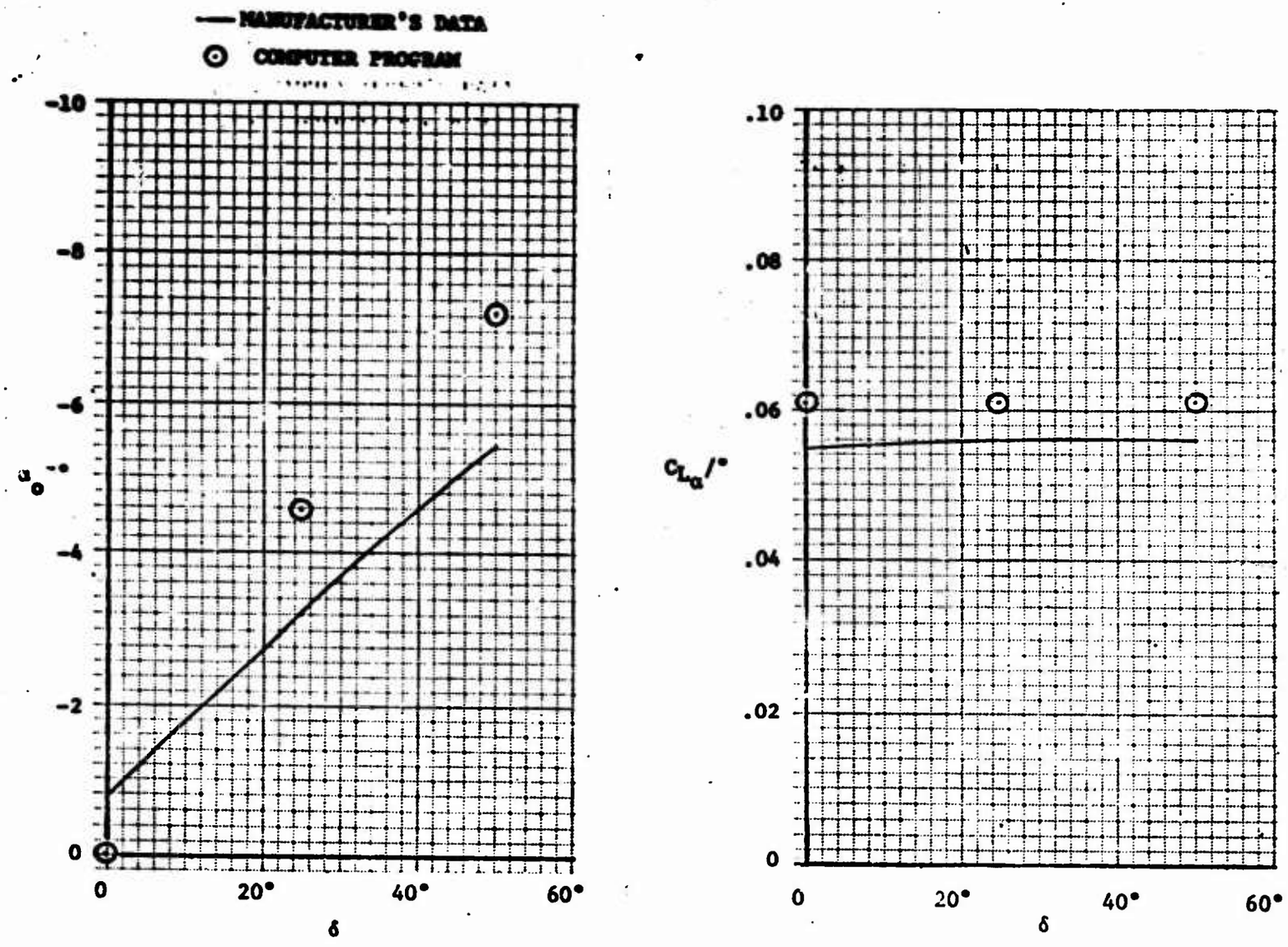

$\delta_{LE\ Slats}$ = Automatic $\delta_{TE\ Flaps}$ = Variable

FIGURE 3-2d: Comparison of A-4 α_o and C_{L_α} Predictions with Manufacturer's Data

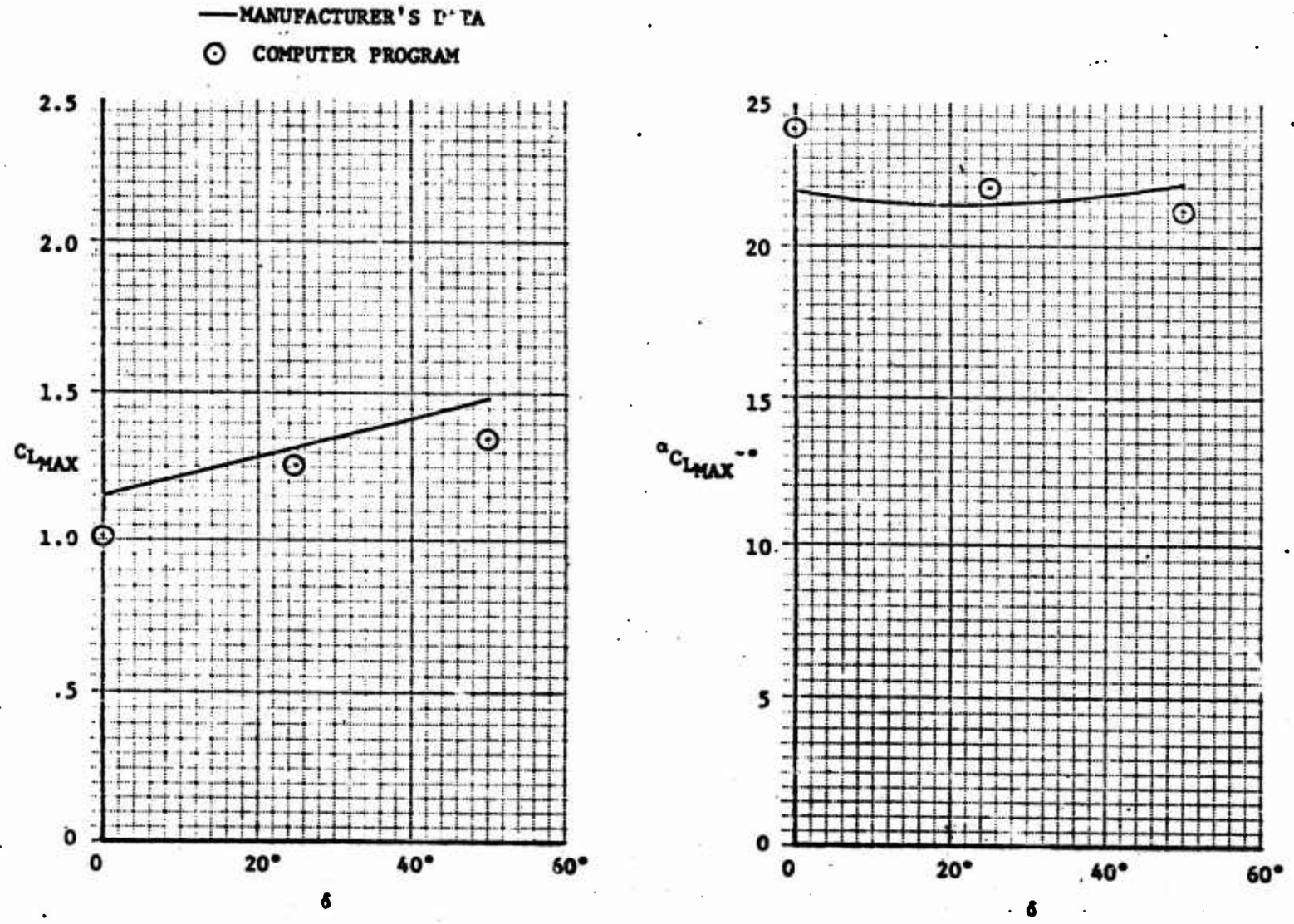

FIGURE 3-2e: Comparison of A-4 $C_{L_{MAX}}$ and $\alpha_{C_{L_{MAX}}}$ Predictions with Manufacturer's Data

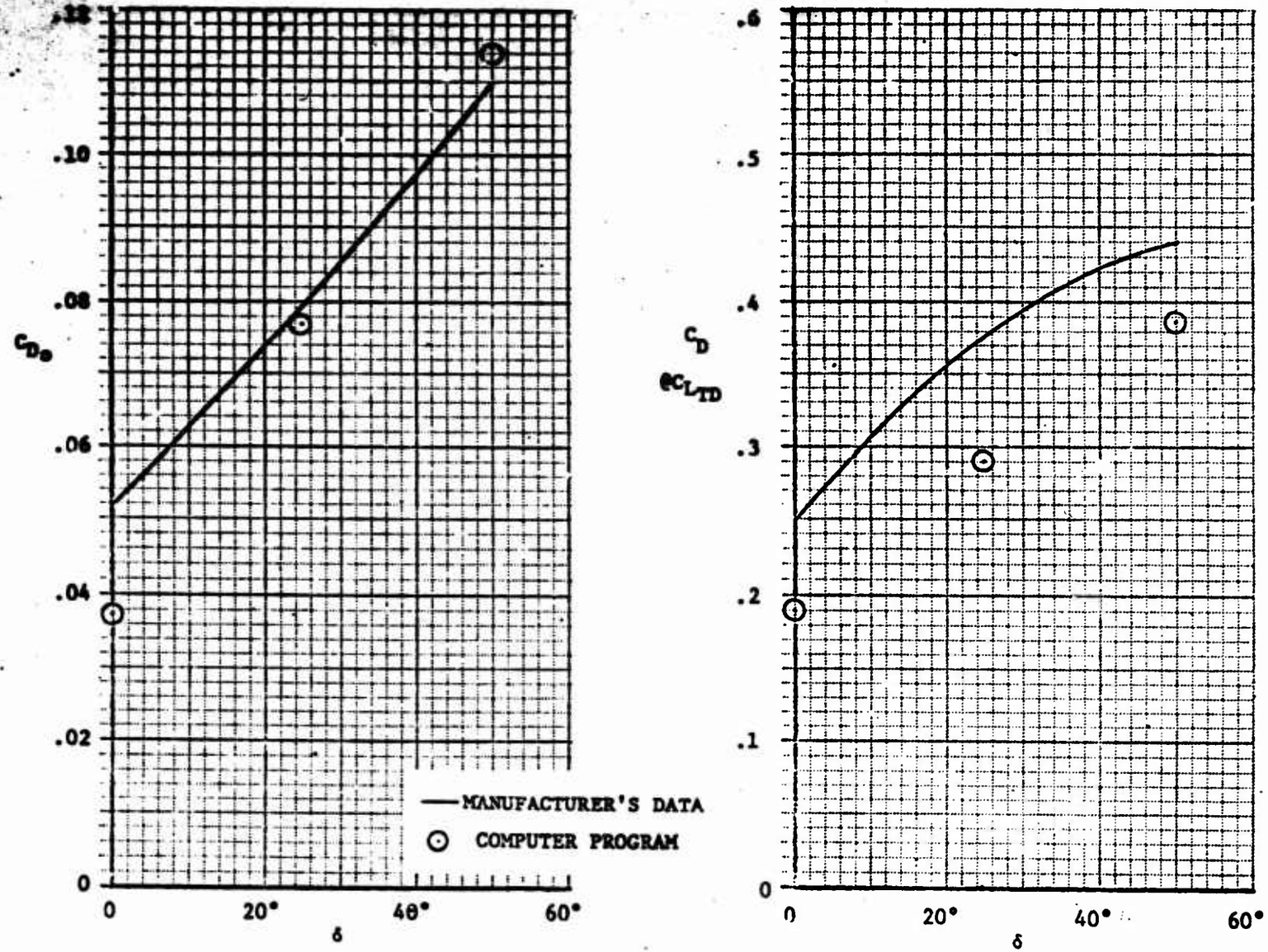

$\delta_{LE\ Slats}$ = Automatic $\delta_{TE\ Flaps}$ = Variable

FIGURE 3-2f: Comparison of A-4 C_{D_o} and $C_{D@C_{L_{TD}}}$ Predictions with Manufacturer's Data

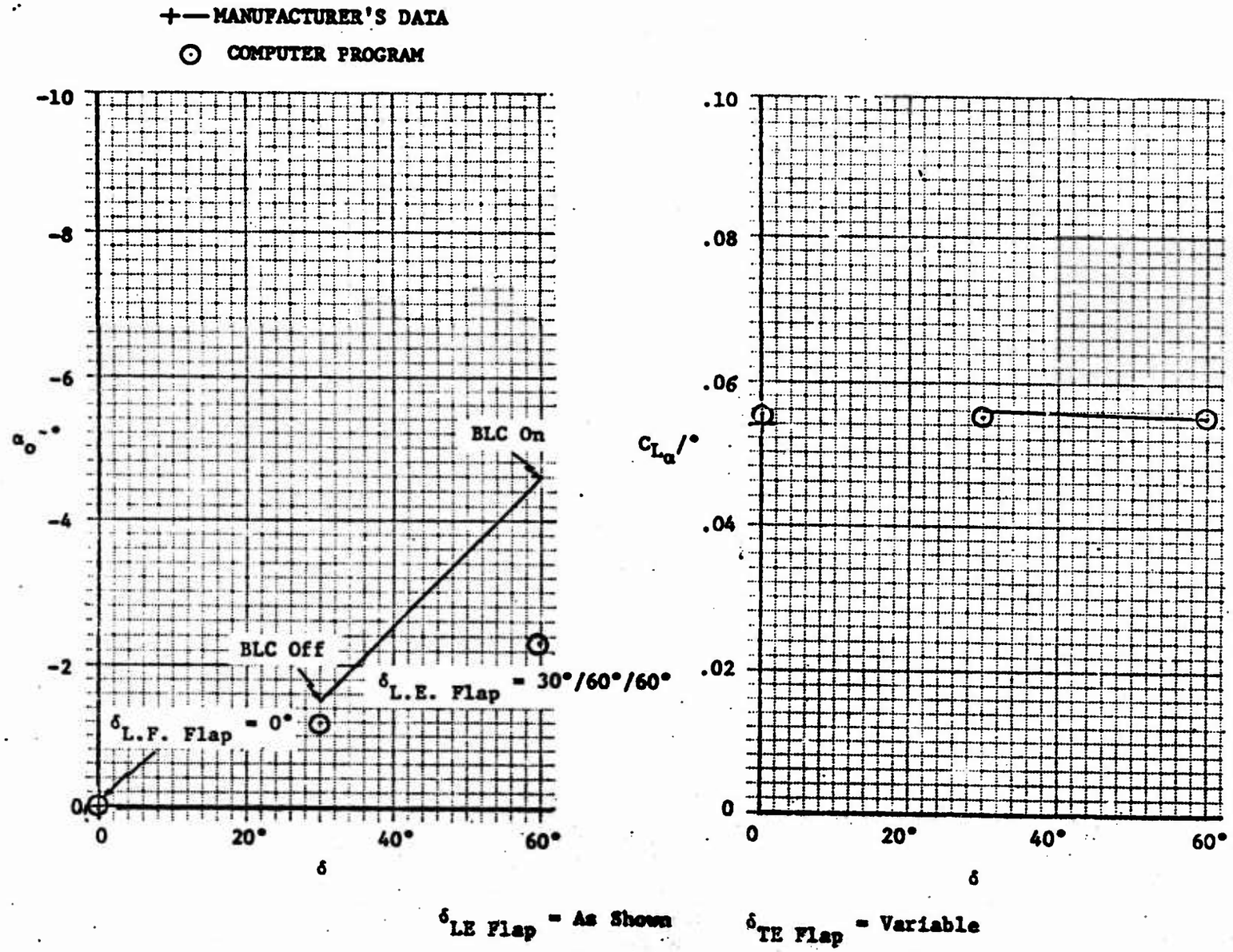

FIGURE 3-2g: Comparison of F-4 α_o and C_{L_α} Predictions with Manufacturer's Data

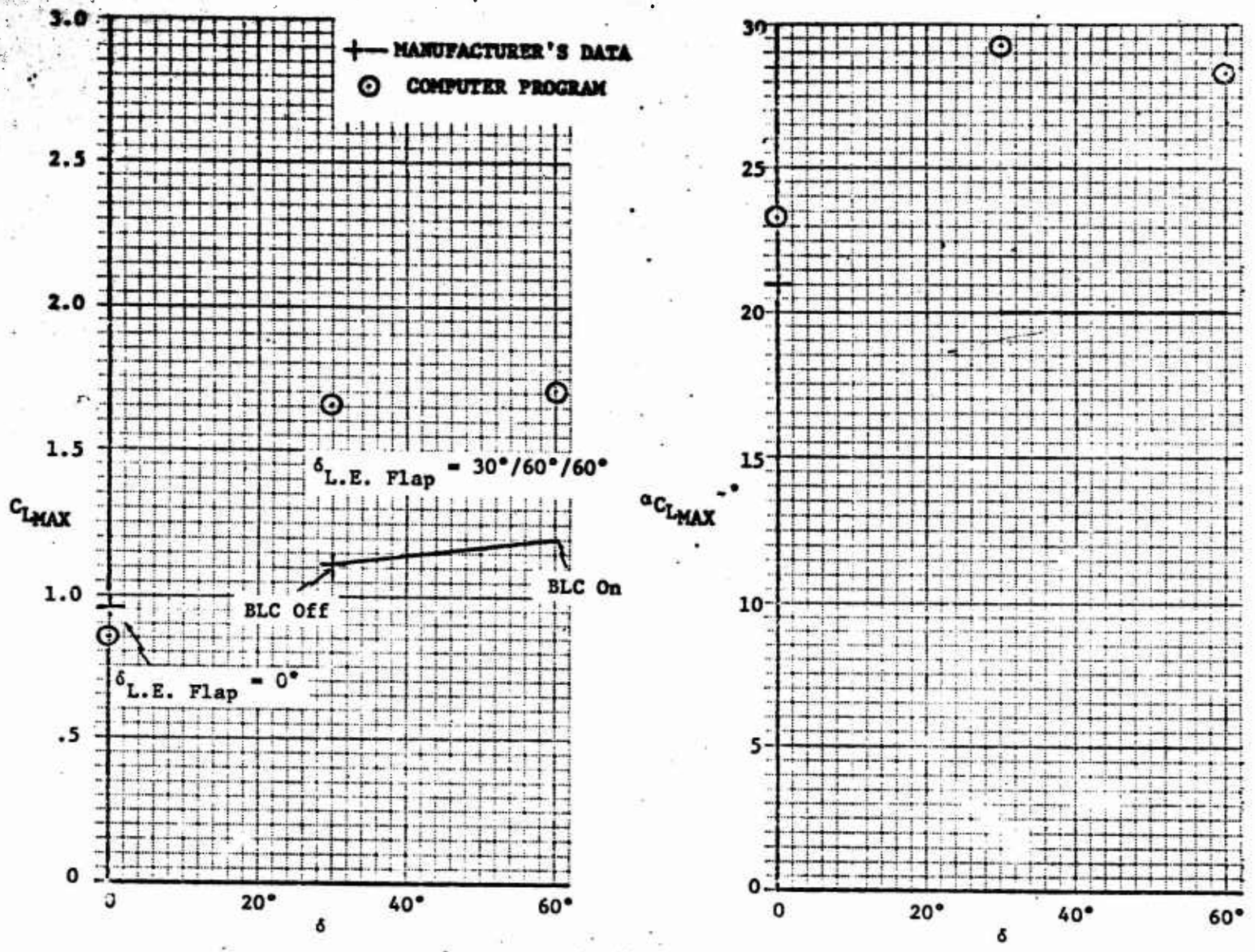

$\delta_{LE\ Flap}$ = As Shown $\delta_{TE\ Flap}$ = Variable

FIGURE 3-2h: Comparison of F-4 $C_{L_{MAX}}$ and $\alpha_{C_{L_{MAX}}}$ Predictions with Manufacturer's Data

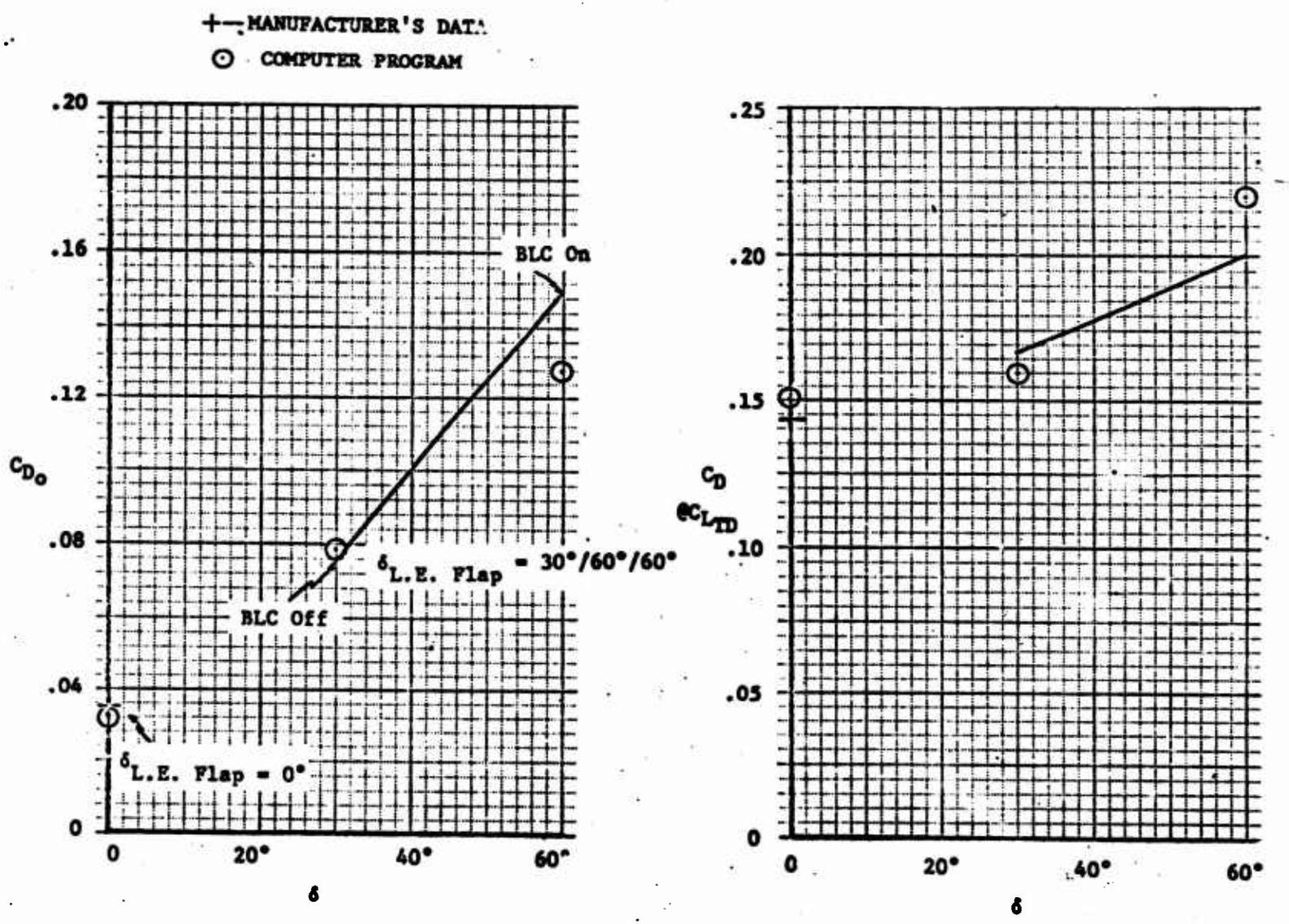

FIGURE 3-21: Comparison of F-4 C_{D_o} and $C_{D@C_{L_{TD}}}$ Predictions with Manufacturer's Data

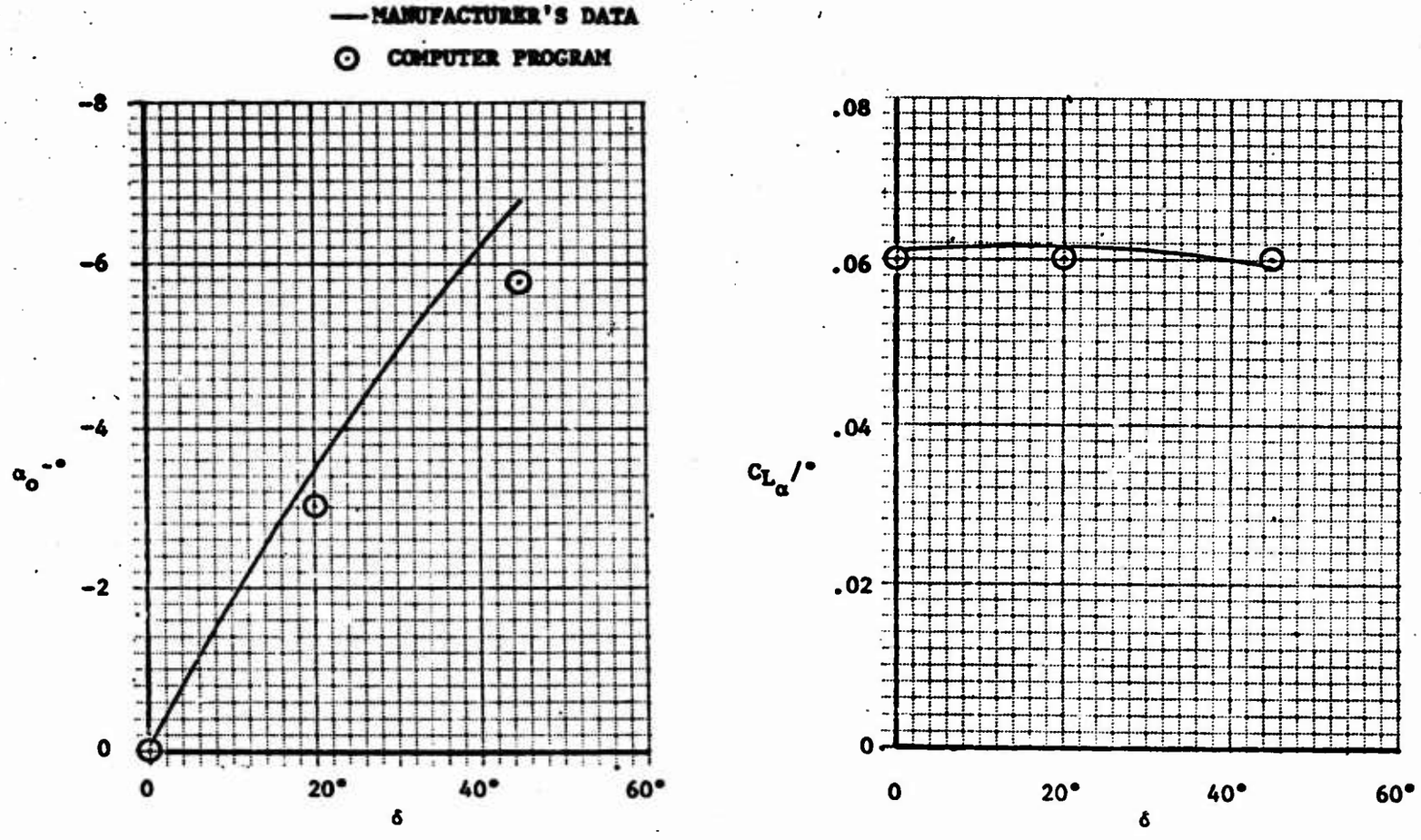

$\delta_{LE\ Flap} = 0°$ $\delta_{TE\ Flap} = Variable$

FIGURE 3-2j: Comparison of F-5 α_o and C_{L_α} Predictions with Manufacturer's Data

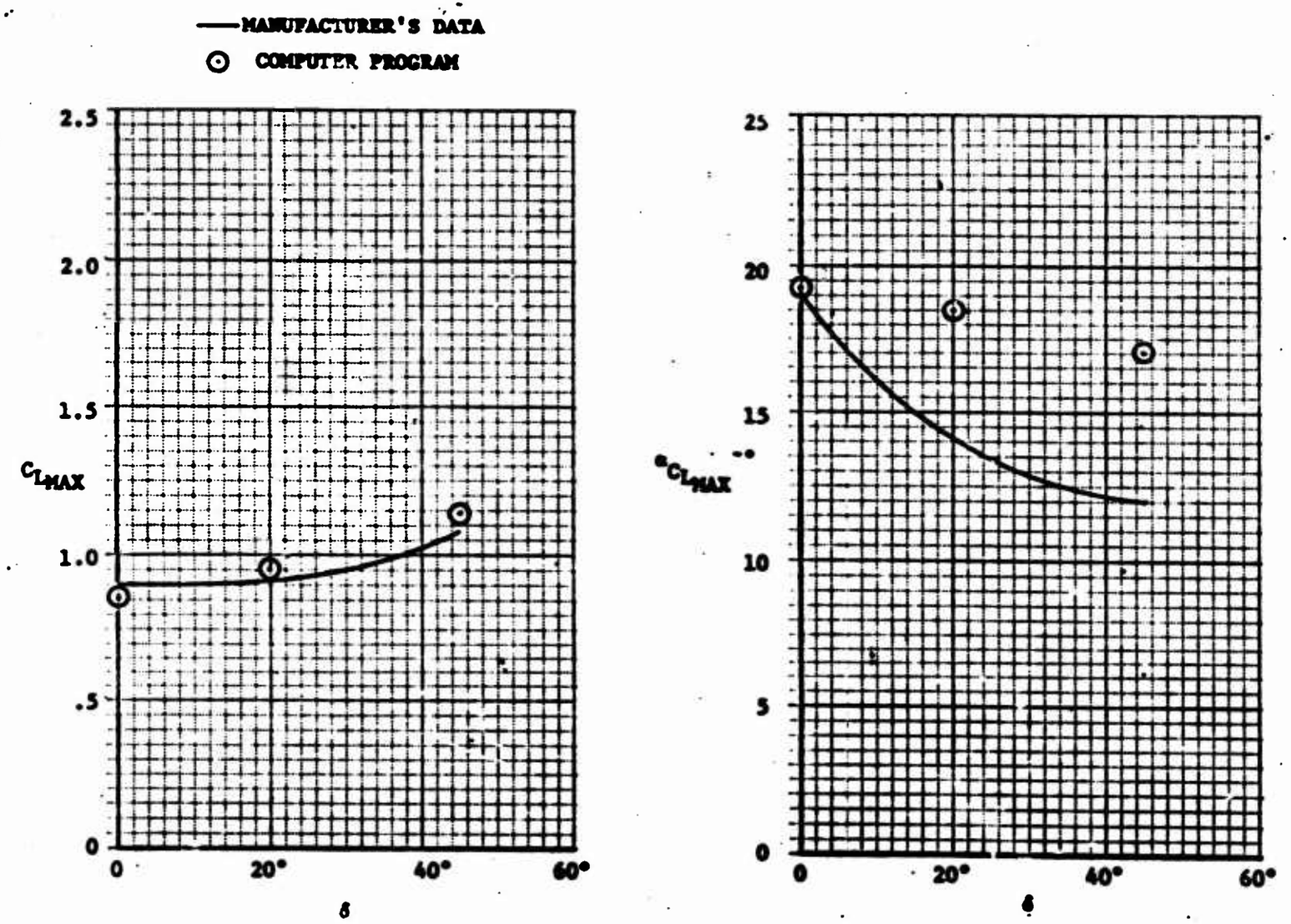

$\delta_{LE\ Flap} = 0°$ $\delta_{TE\ Flap}$ = Variable

FIGURE 3-2k: Comparison of F-5 $C_{L_{MAX}}$ and $\alpha_{C_{L_{MAX}}}$ Predictions with Manufacturer's Data

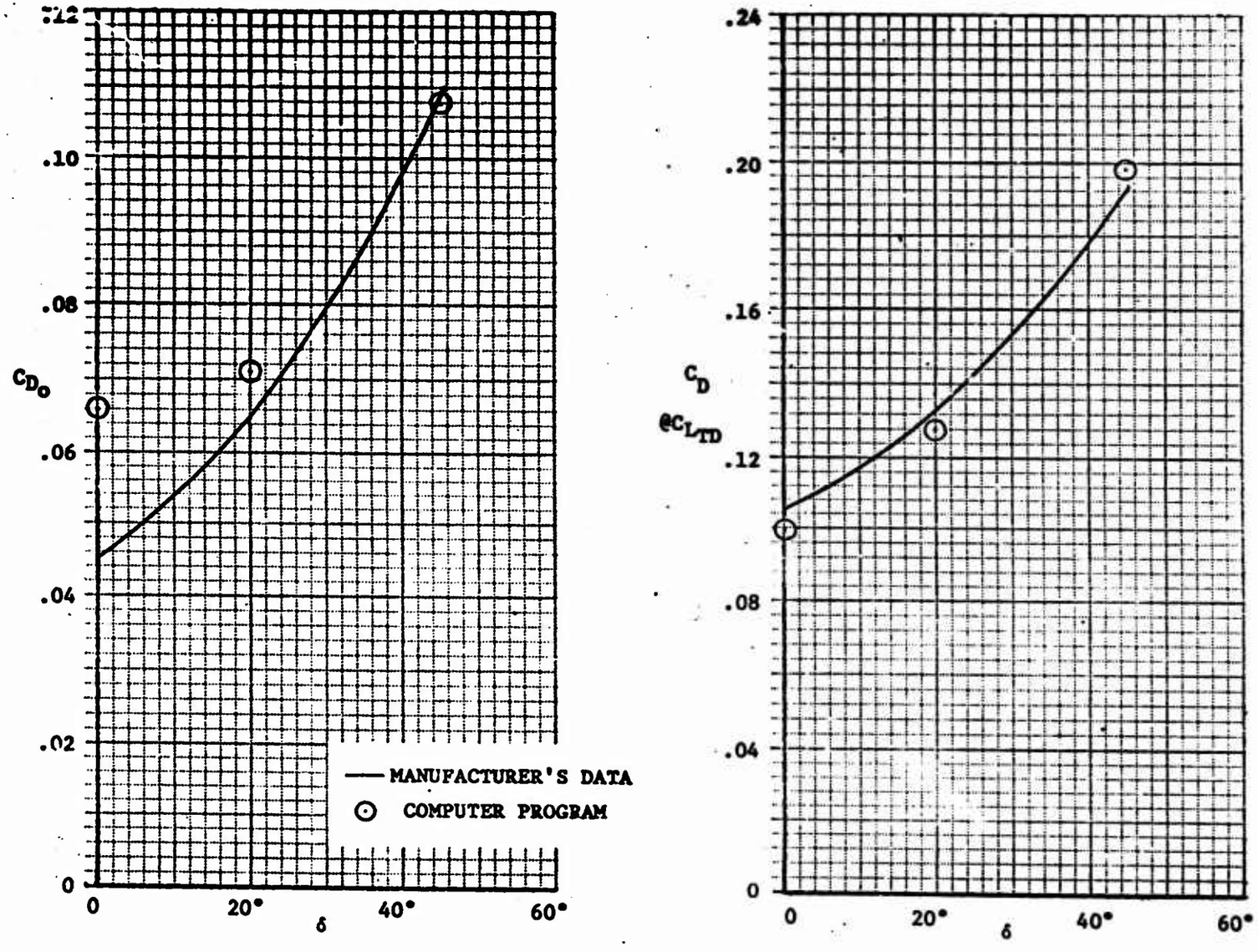

$\delta_{LE\ Flap} = 0$ $\delta_{TE\ Flap} = Variable$

FIGURE 3-21: Comparison of F-5 C_{D_o} and $C_{D@C_{L_{TD}}}$ Predictions with Manufacturer's Data

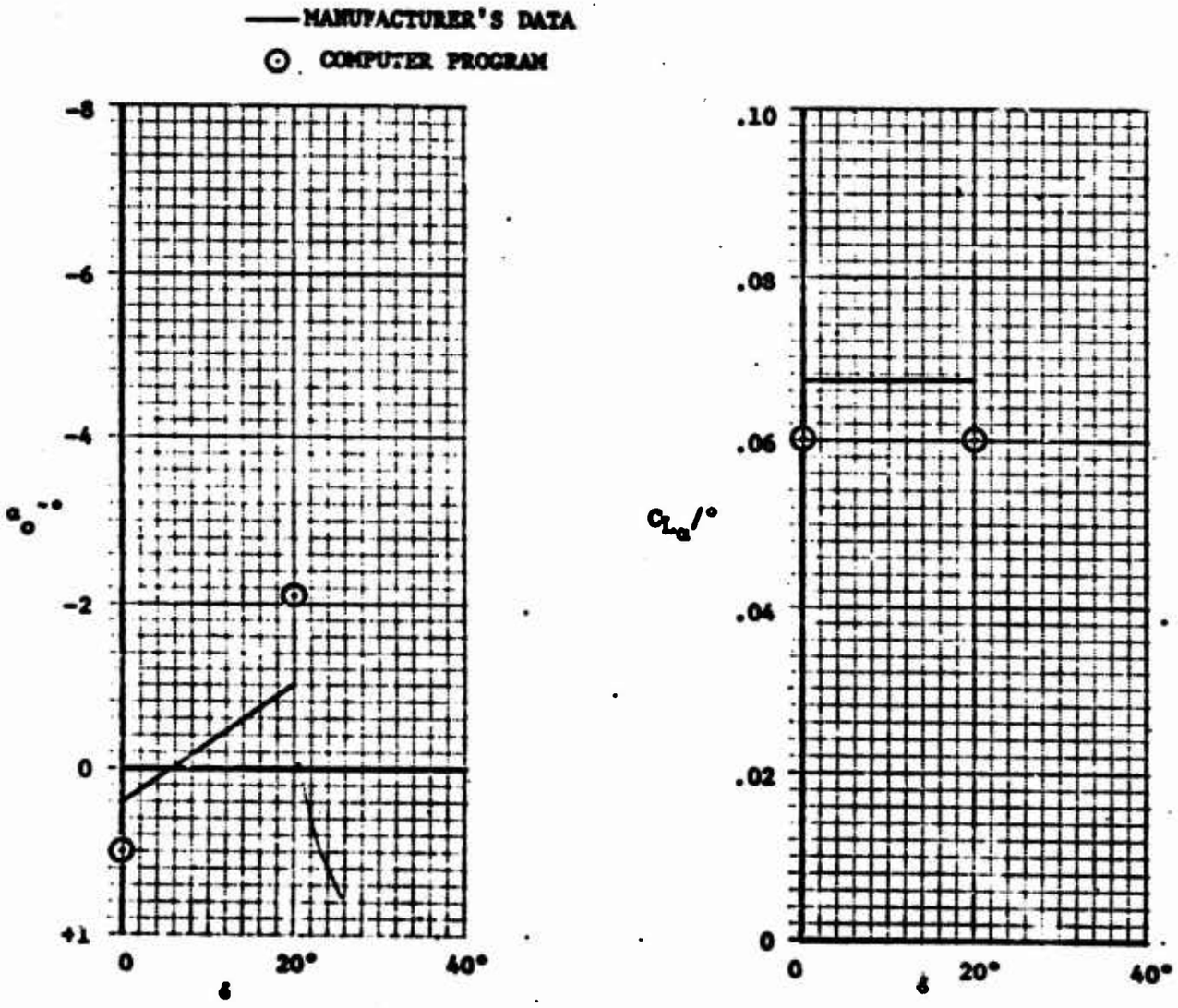

FIGURE 3-2a: Comparison of F-5 α_o and C_{L_α} Predictions with Manufacturer's Data

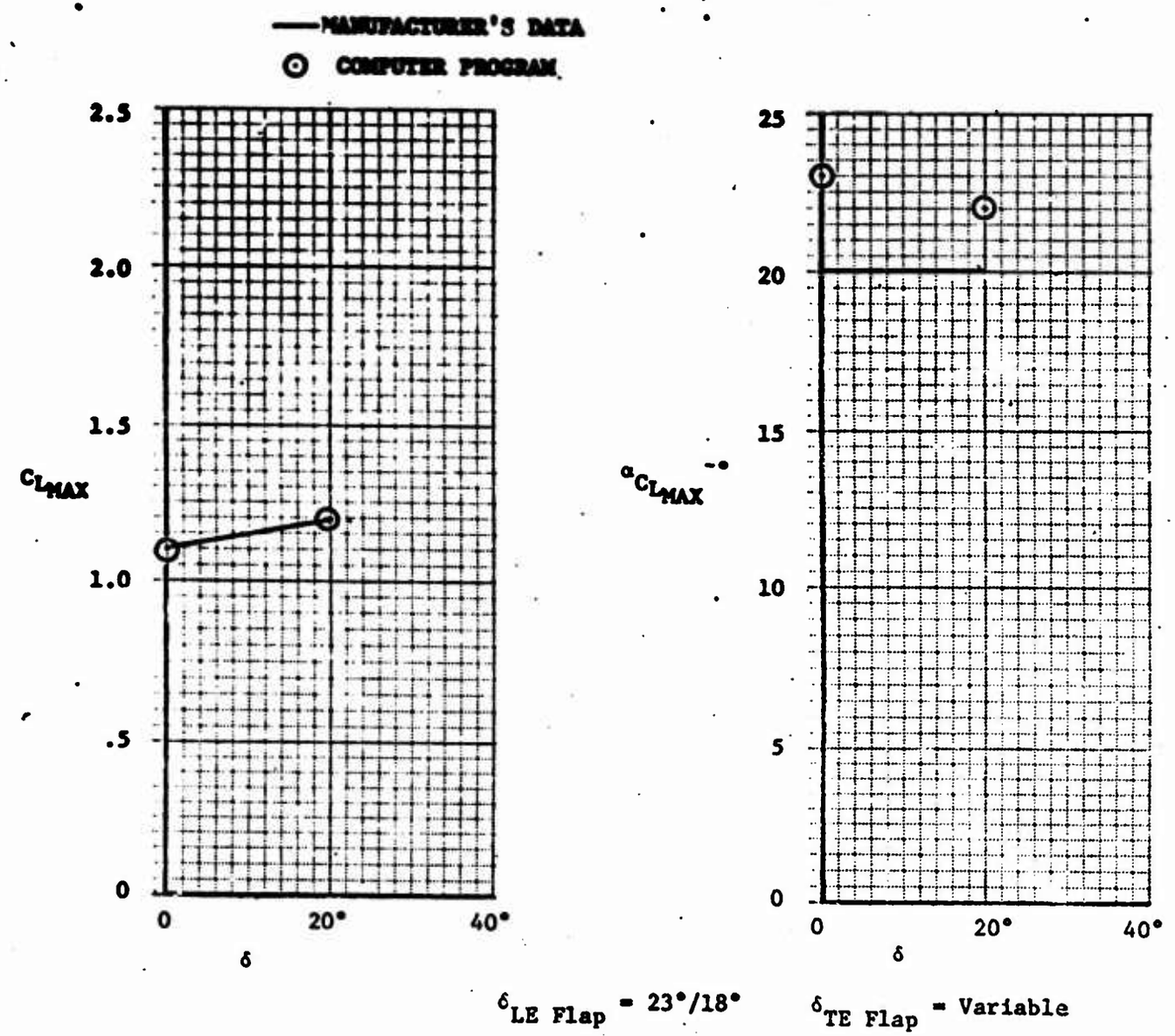

FIGURE 3-2n: Comparison of F-5 $C_{L_{MAX}}$ and $\alpha C_{L_{MAX}}$ Predictions with Manufacturer's Data

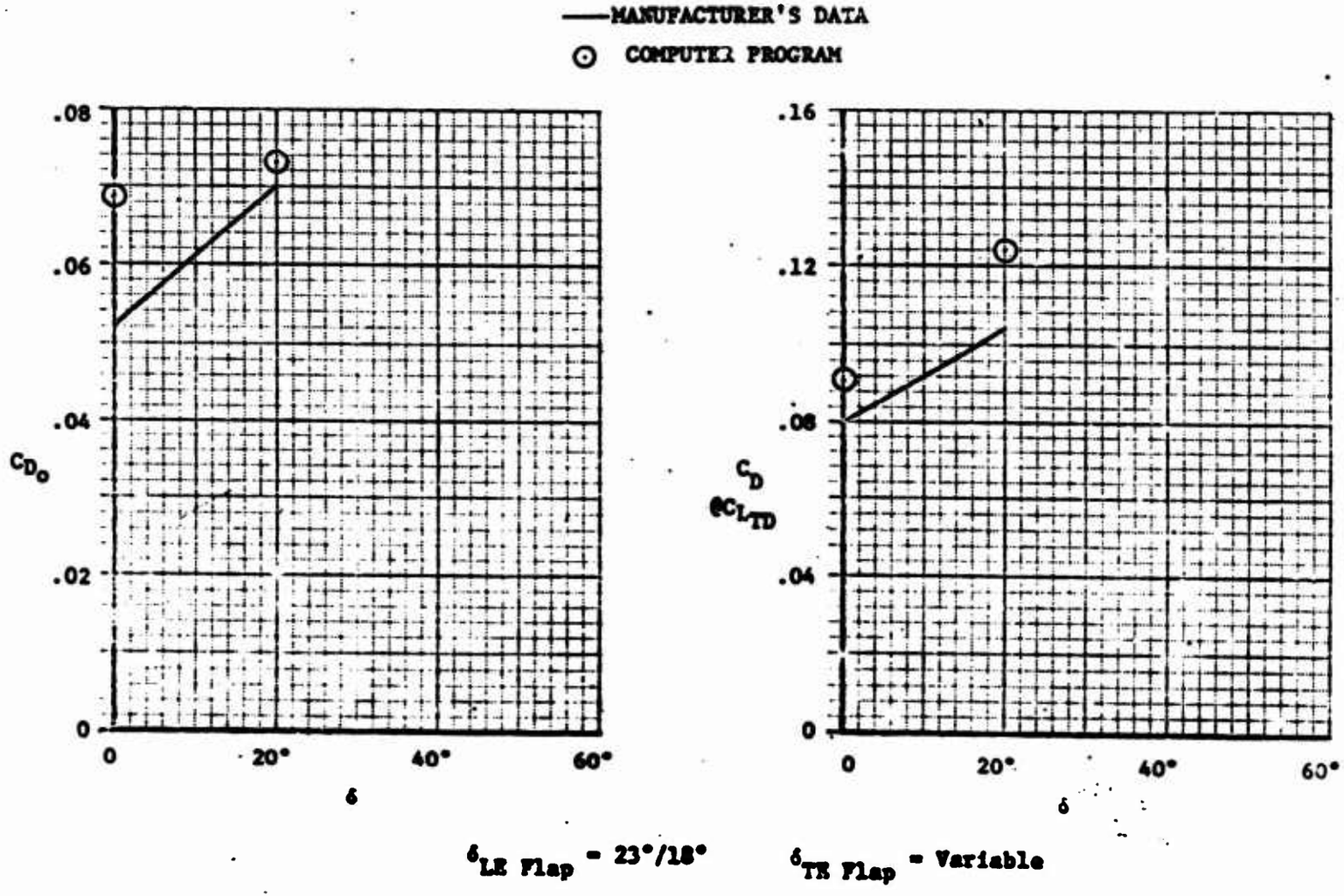

FIGURE 3-2o: Comparison of F-5 C_{D_o} and $C_{D_{@C_{L_{TD}}}}$ Predictions with Manufacturer's Data

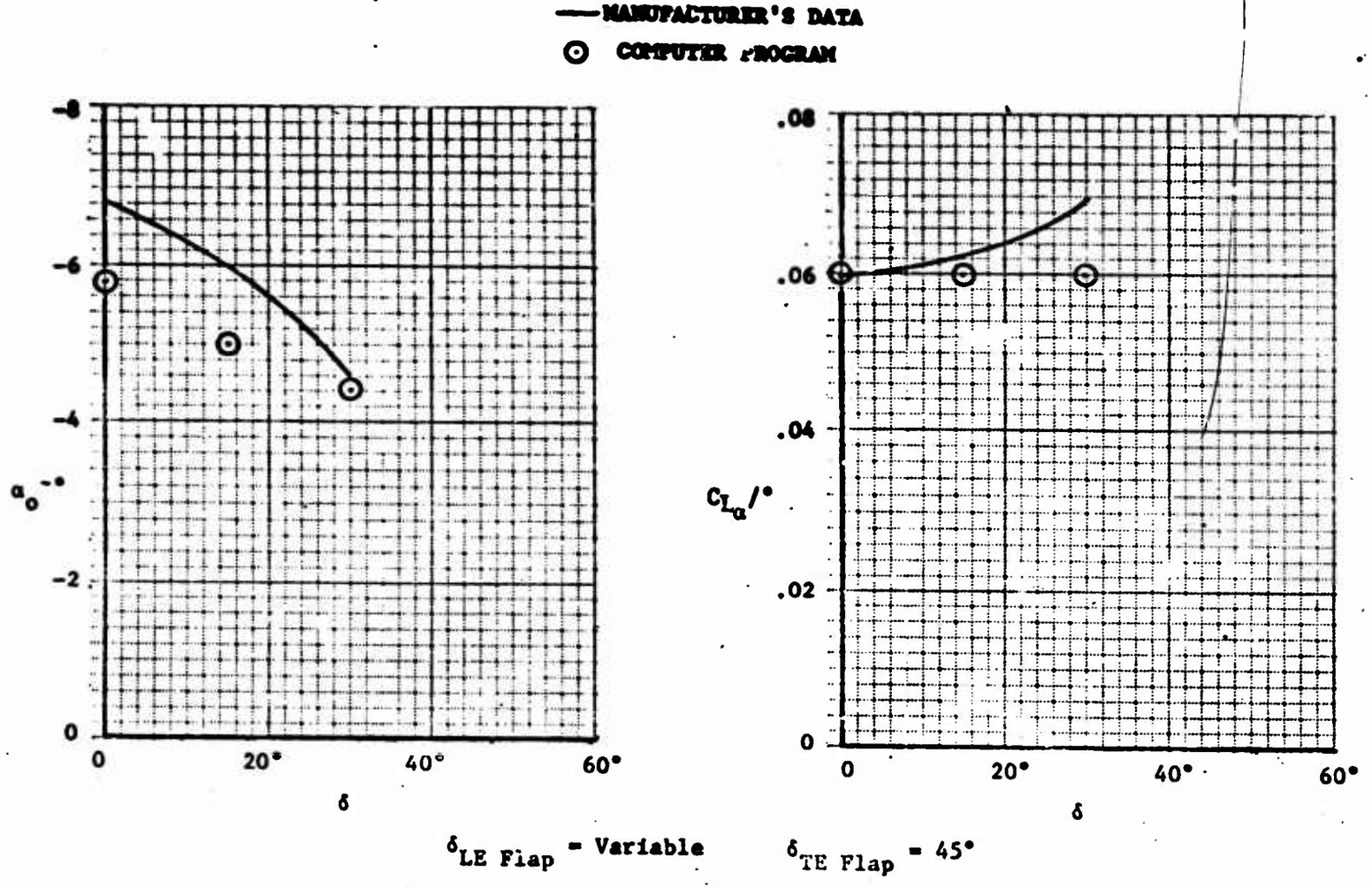

FIGURE 3-2p: Comparison of F-5 α_o and C_{L_α} Predictions with Manufacturer's Data

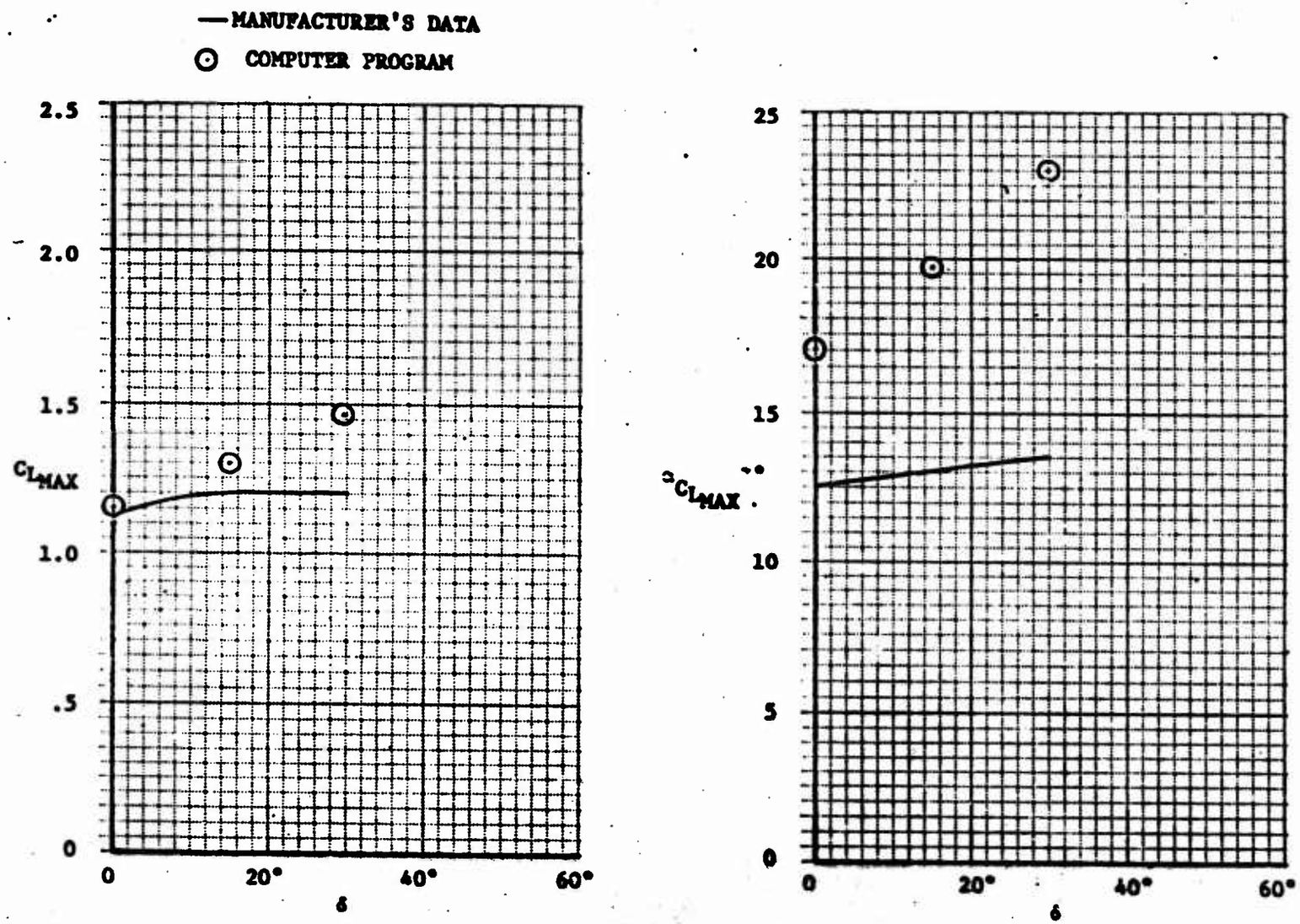

FIGURE 3-2q: Comparison of F-5 $C_{L_{MAX}}$ and $^{a}C_{L_{MAX}}$ Predictions with Manufacturer's Data

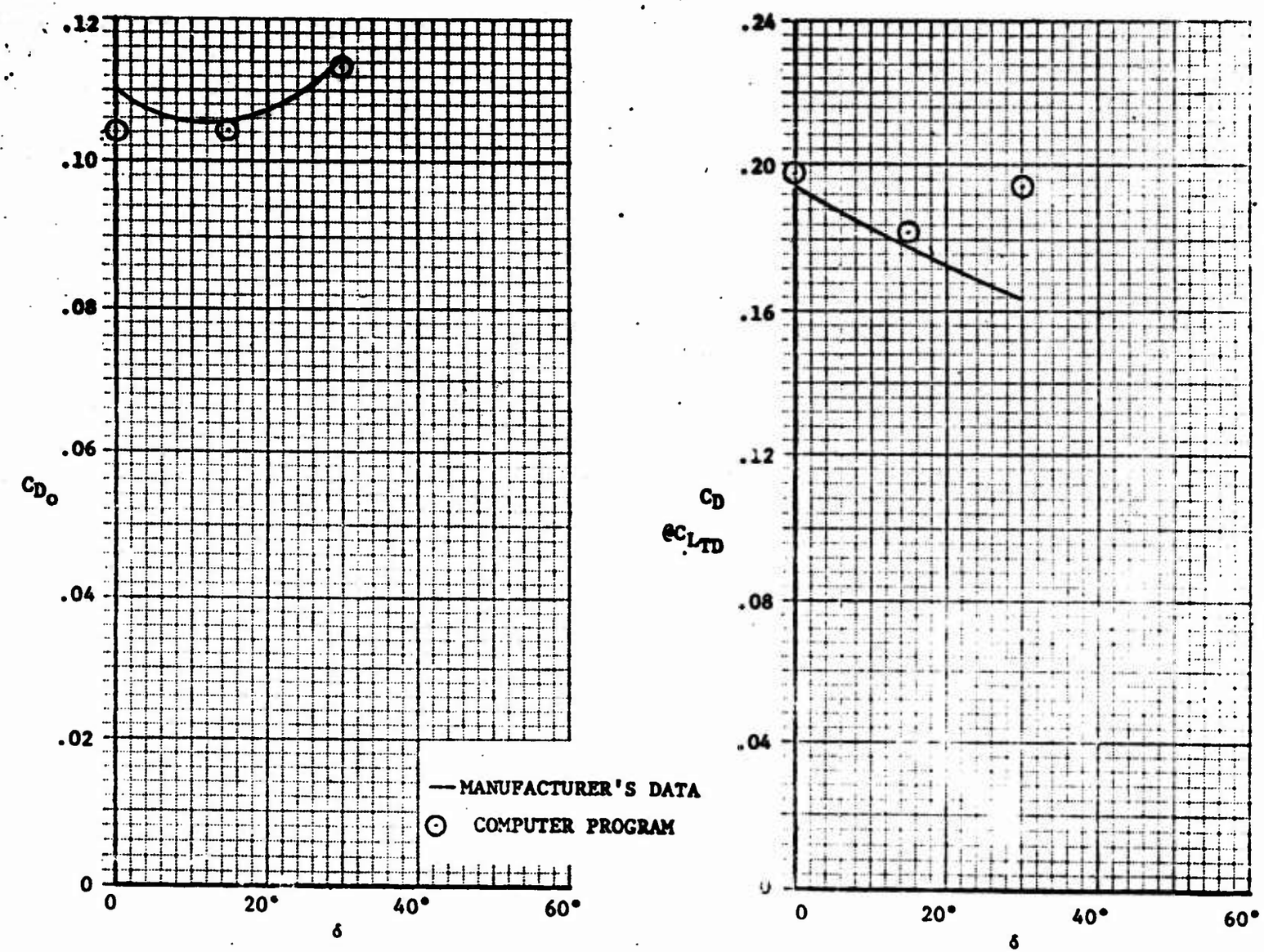

$\delta_{LE\ Flap}$ = Variable $\delta_{TE\ Flap}$ = 45°

FIGURE 3-2r: Comparison C_{D_o} and $C_{D@C_{L_{TD}}}$ Predictions with Manufacturer's Data

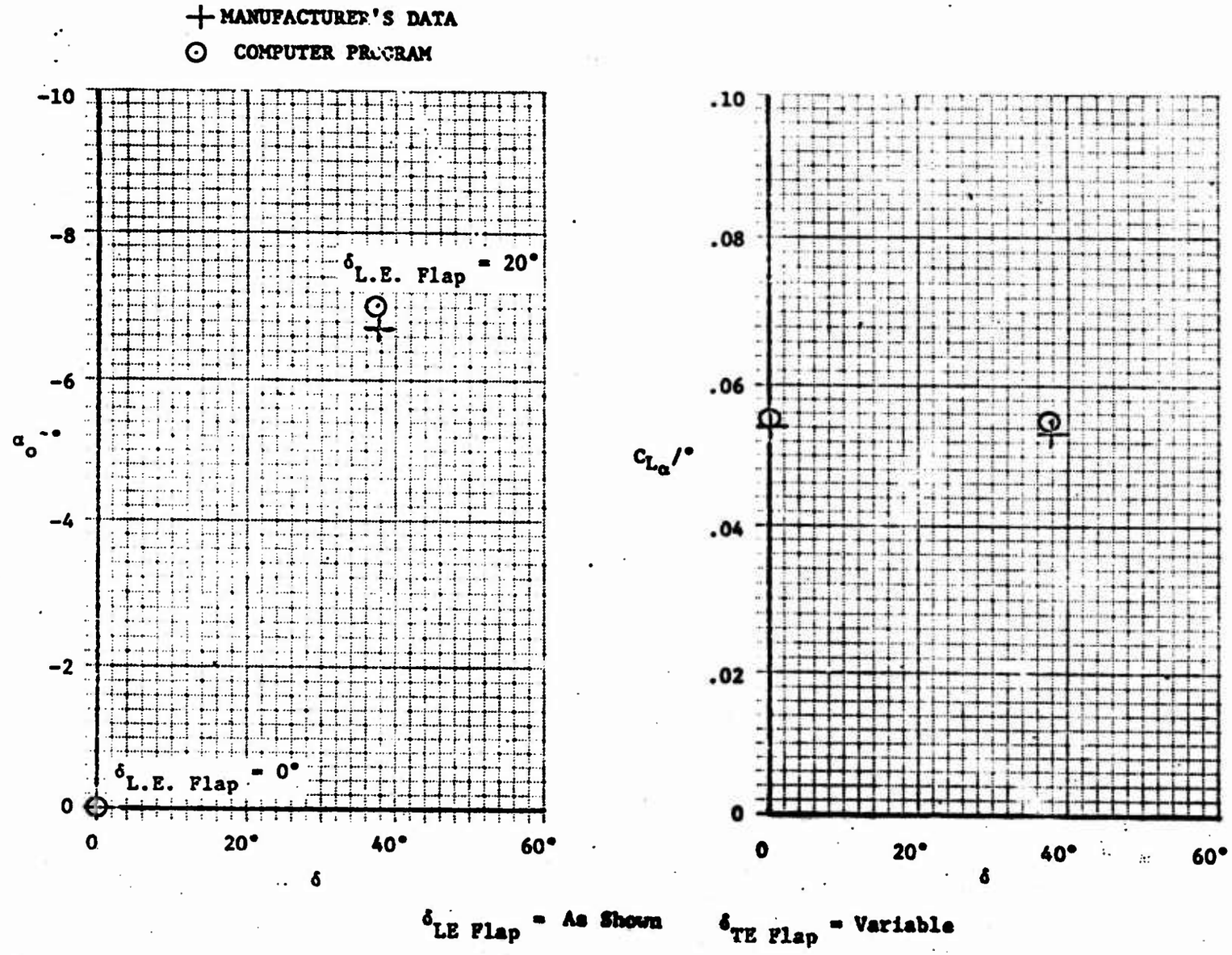

FIGURE 3-2s: Comparison of F-105 α_o and C_{L_α} Predictions with Manufacturer's Data

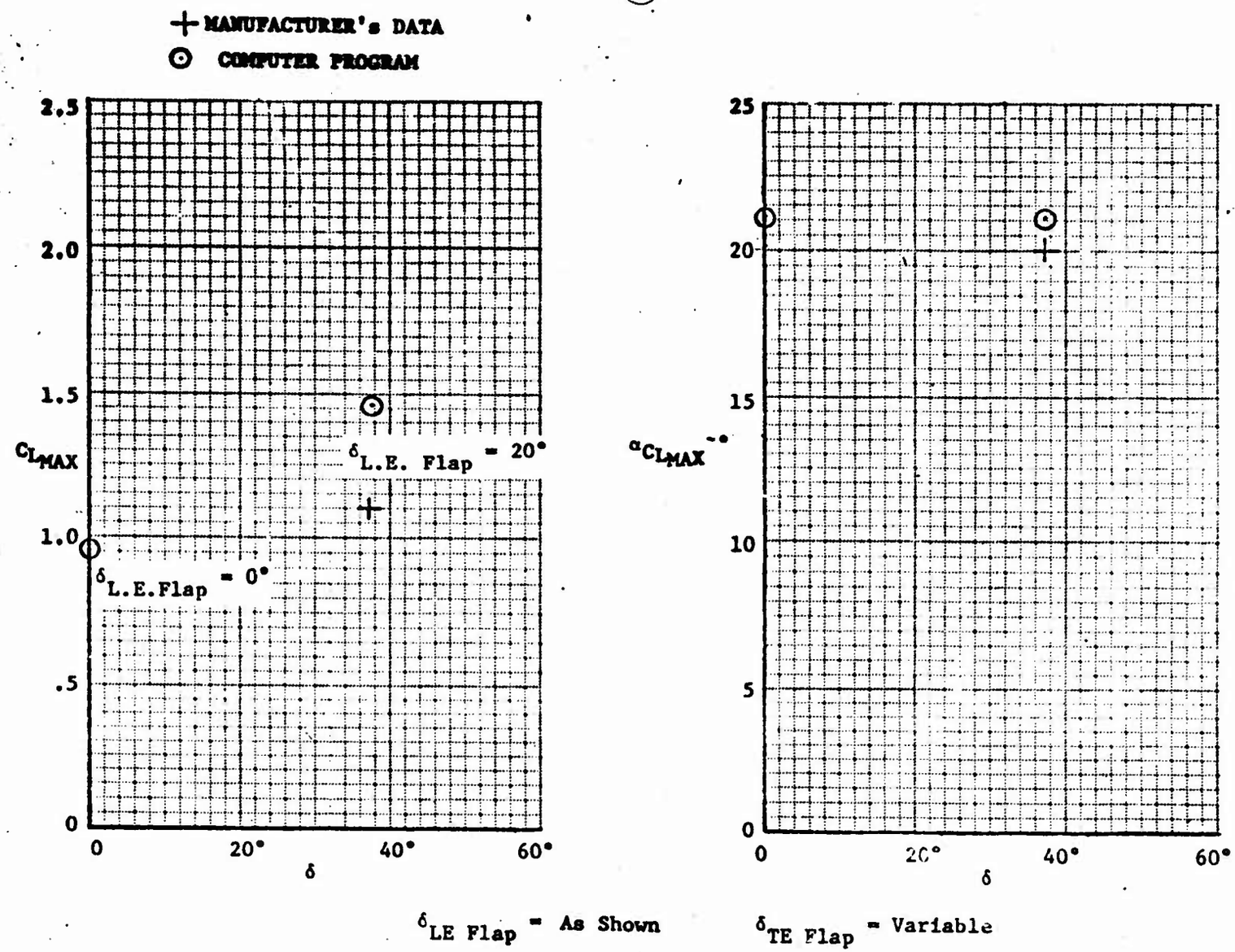

FIGURE 3-2t: Comparison of F-105 $C_{L_{MAX}}$ and $\alpha_{C_{L_{MAX}}}$ Predictions with Manufacturer's Data

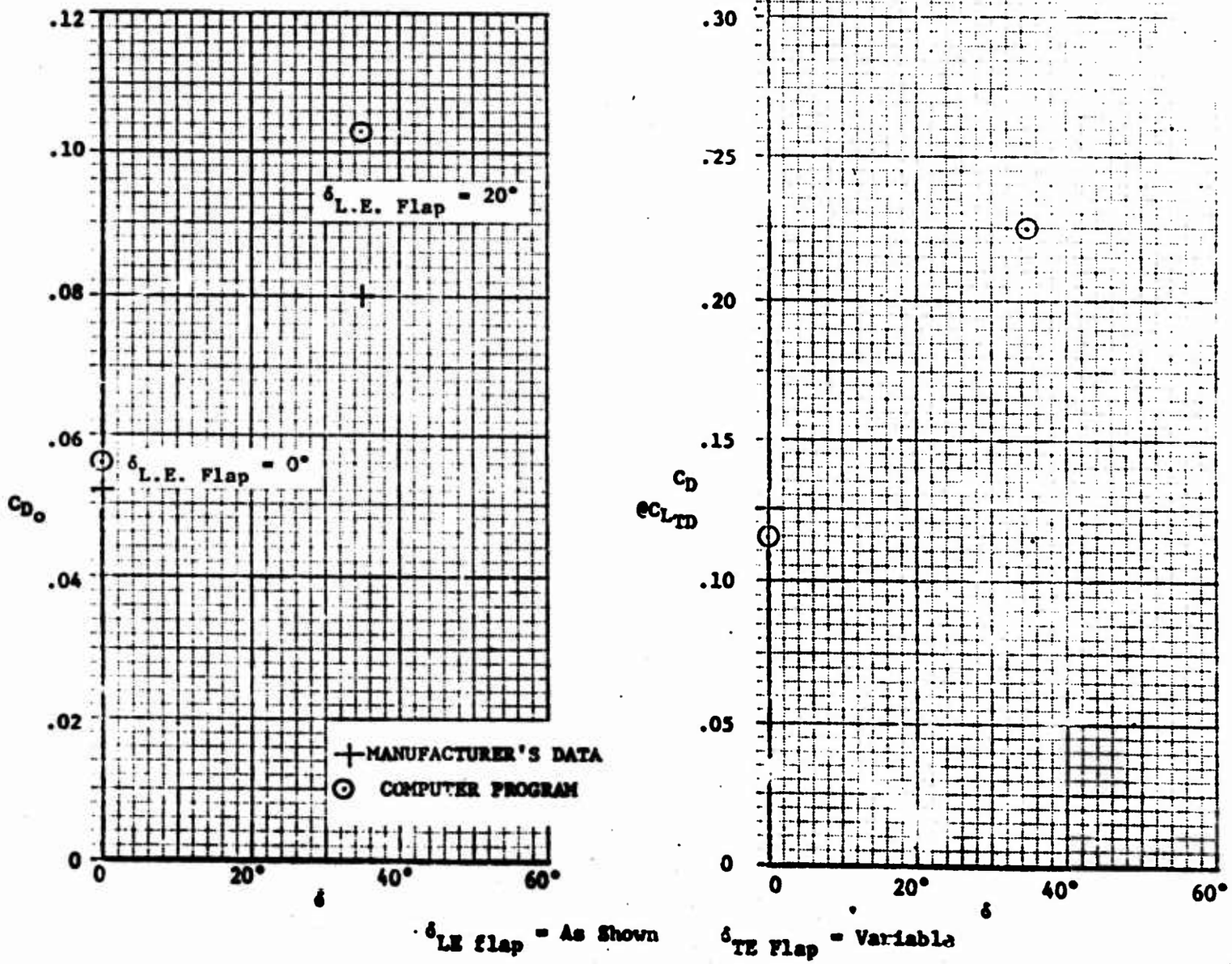

FIGURE 3-2u: Comparison of F-105 C_{D_o} and $C_{D@C_{L_{TD}}}$ Predictions with Manufacturer's Data

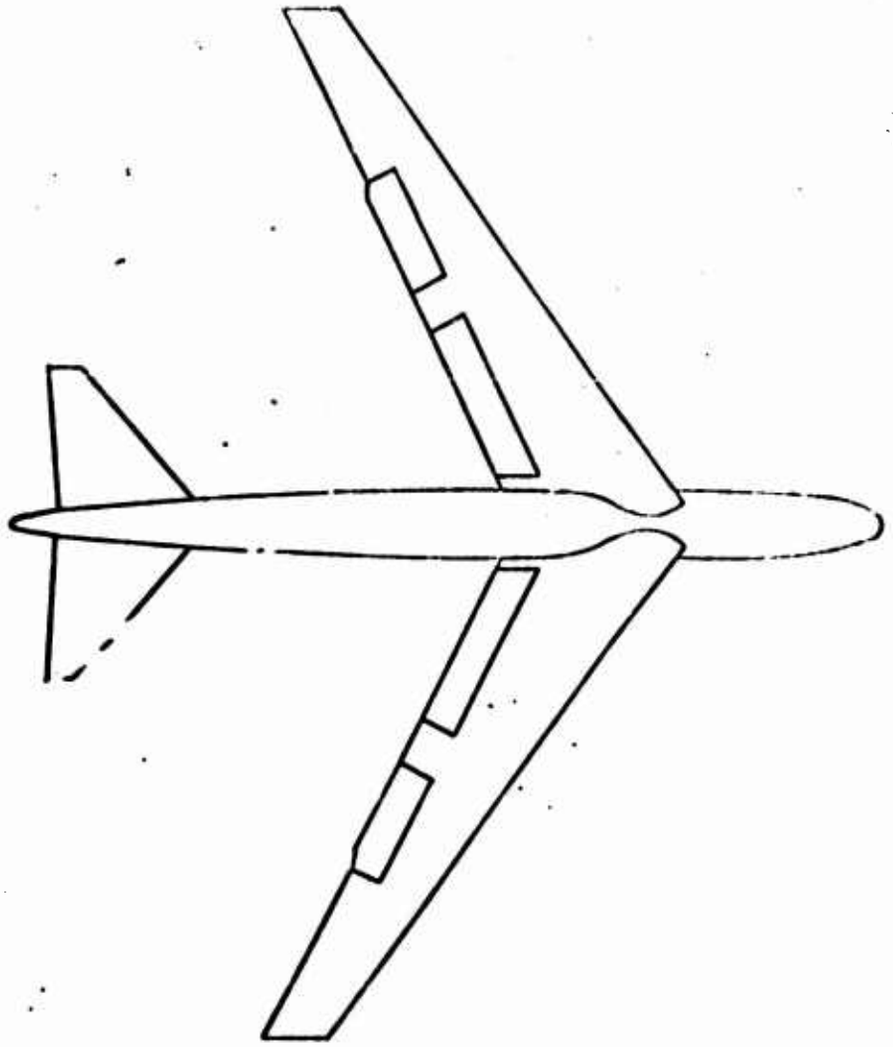

FIGURE 3-3a: B-52H Planform

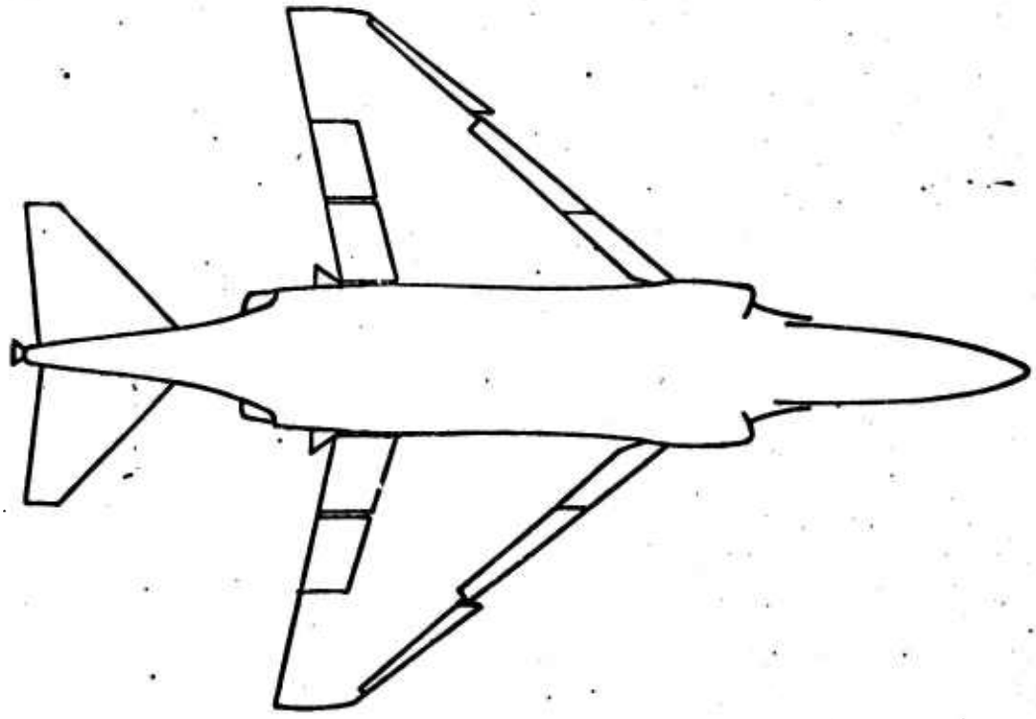

FIGURE 3-3b: F-4 Planform

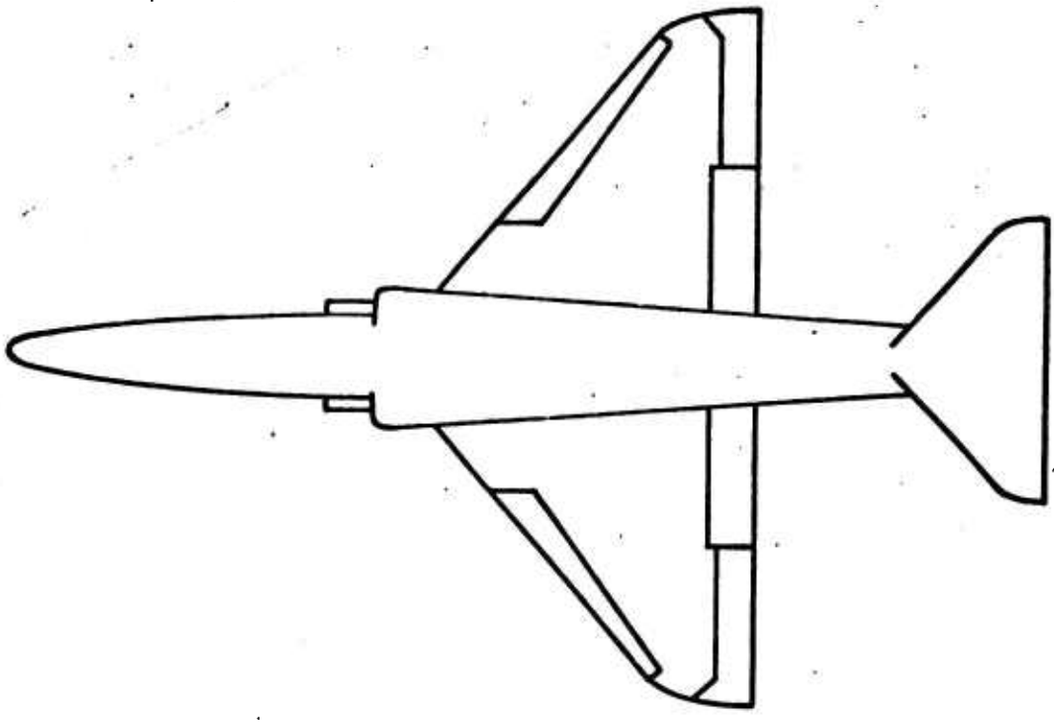

FIGURE 3-3c: A-4C Planform

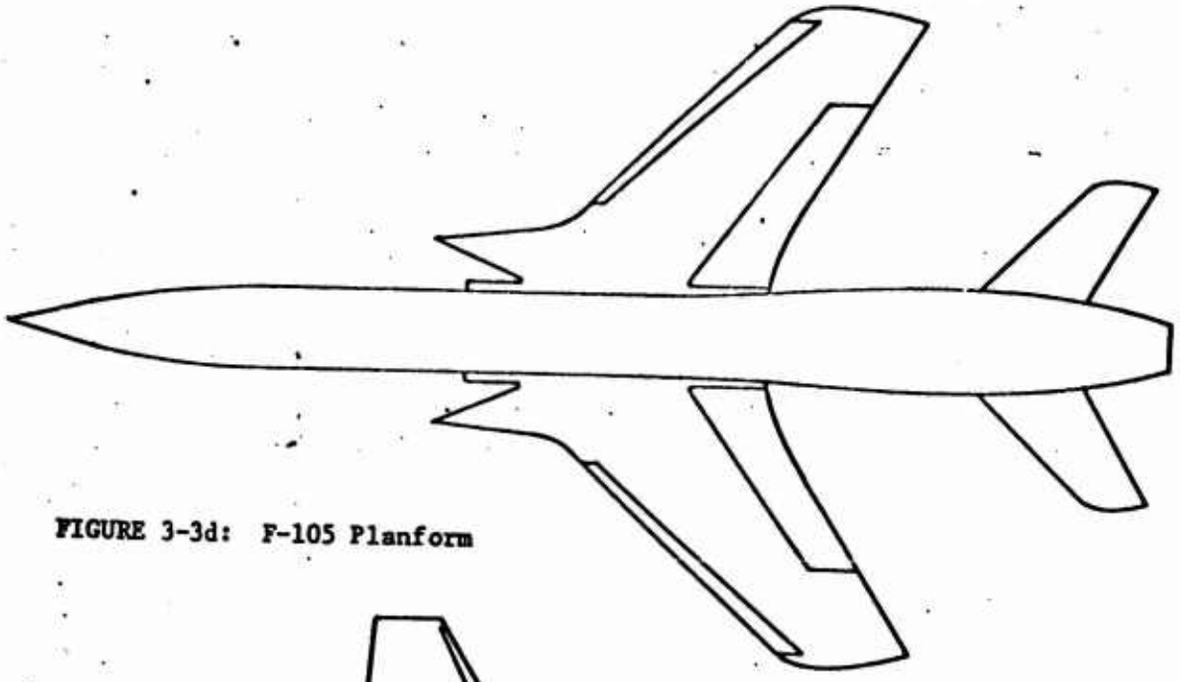

FIGURE 3-3d: F-105 Planform

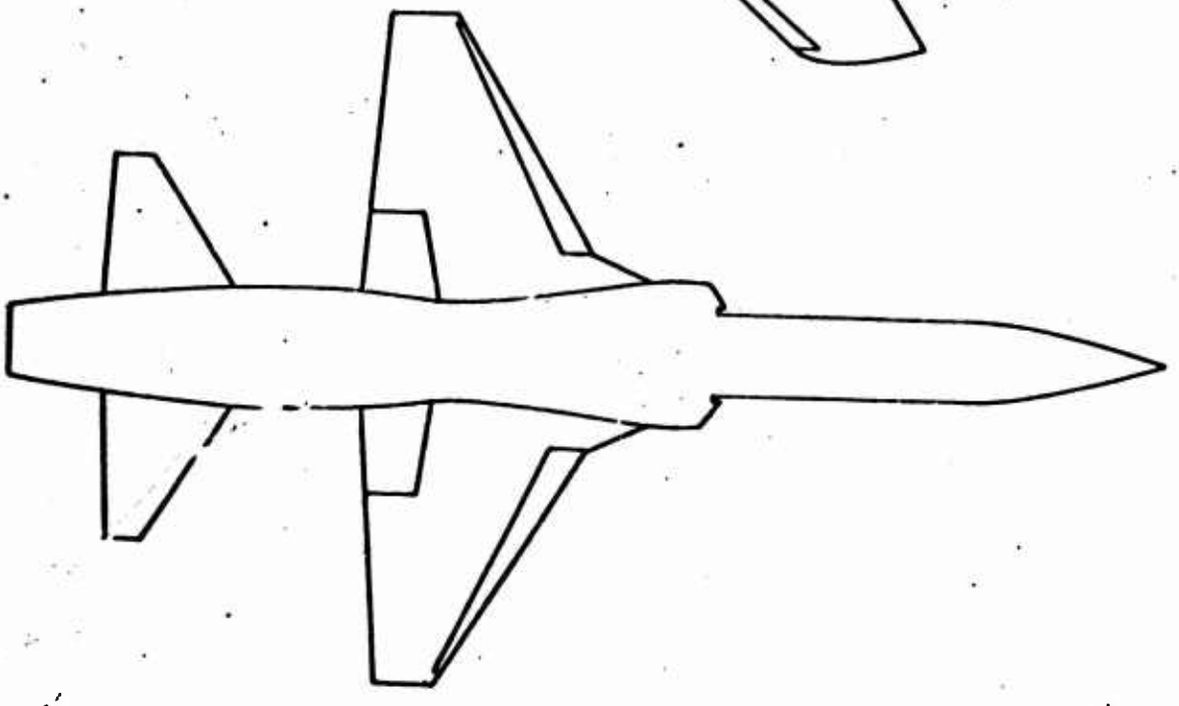

FIGURE 3-3e: F-5 Planform

4. GENERAL DESCRIPTION OF COMPUTATION METHODS

A. PREFACE

The following paragraphs describe the methods and procedures that were used to compute a conventional aircraft's low speed C_L and C_D. The study was based primarily on the USAF DATCOM (Reference 2) and supplemented with data from ARC R & M 2622 (Reference 3). In addition, some empirical functions have been included. These empirical functions are based on data obtained from real-aircraft. (References 4 through 9).

Basically the methods:

1. Use existing methodology to determine a logic and basis for computing C_L and C_D.
2. Modify the existing empirical methods, so that good results are obtained based on several real-aircraft data.

The procedures involved are based on certain observations. In the low-speed flight regime the wing with its high-lift devices generates most of the C_L and C_D. For moderate angles-of-attack body influence is minor unless the body width is large compared to the wing span. The vertical tail has no effect on C_L and only a minor effect on C_D. The effect of the horizontal tail is argumentative, considering that:

a. For large aspect ratio swept wing configurations (bombers, transports, etc.) the horizontal tail has only a minor effect on C_L and C_D.

b. For conventional fighter type aircraft with normal tail arm and horizontal tail area less than .3 wing area, the effect is small. Trim drag is not high and the reduction in C_L due to trim compensates the increase in C_L due to lifting surface area increase.

c. For pure delta wing aircraft the "horizontal tail" is included in the wing.

d. Unique designs where large tail areas and short tail arms have appreciable effects are not considered within the scope of this study.

Because of the low velocities usually involved during landing ground roll calculations, the airplane drag is usually small compared with the other decelerating forces employed. Therefore, except in extreme cases, inaccuracies in computing drag are tolerable. To obtain the first order answers required for the analysis included herein, the aircraft is considered to consist of wing-body combinations with high lift devices. Effects of dihedral, twist, and spanwise variation in airfoil section and thickness are neglected.

B. QUALIFICATIONS

There are a few requirements for the type of wing geometries that can be calculated. They are:

1. The wing must have constant section type and thickness ratio.
2. No dihedral.
3. No twist.
4. Leading and trailing edges must be straight lines.

Approximations for wings that contain the above geometry can usually be made.

C. HIGH LIFT DEVICES

The types of high lift devices that were considered for the computer program were those that could be compared with actual operating aircraft. They were

Trailing Edge Flaps:

Plain
Split
Single-slotted
Double-slotted
Fowler

Leading Edge Devices

Flap

Slat

For high lift devices not considered in the above list representative values for aerodynamic characteristics are given in the handbook section. Boundary-Layer-Control (BLC) data on existing aircraft was non-existent except for one isolated case.

D. COMPUTATION PROCEDURE

The computation procedure employed in the determination of C_L and C_D will:

1. Determine the necessary geometric parameters, such as wing area, flap deflection, mean aerodynamic chord, etc.;
2. Determine the wing airfoil section characteristics by using either Table III-1 or the empirical relationships of pages 85 and 91 ;
3. Compute the wing alone lift characteristics;
4. Compute the effect of the fuselage on the lift characteristics;
5. After selection of the type of trailing edge flap, compute its increment to the lift characteristics;
6. If a leading edge device is used, compute its increment to the lift characteristics;
7. Determine the angle-of-attack at touchdown and compute the corresponding lift coefficient;
8. Determine the touchdown velocity and Reynold's numbers;
9. Compute wing and wing-body zero-lift drag;
10. Determine the flaps-up drag due to lift;
11. Determine the flap-down increment to zero-lift drag and drag due-to-lift;
12. Sum all the above contributions for total lift and drag coefficients.

E. RESULTS

The results of the computation consists of:

1. Lift Characteristics - No High Lift Device

   α_o Angle of Attack at Zero Lift

   C_{L_α} Lift Curve Slope

   $C_{L_{MAX}}$ Maximum Lift Coefficient

   $\alpha_{C_{L_{MAX}}}$ Angle of Attack for Maximum Lift

2. Lift Characteristics - With High Lift Device

   Same as above plus:
   Lift increment due to device @ $\alpha = 0$
   Lift increment due to device @ $C_{L_{MAX}}$

3. Drag Characteristics

   C_{D_o} Zero lift drag coefficient

   C_{D_i} Induced drag at $C_{L_{TD}}$

   $C_{L_{@V_{TD}}}$ Lift coefficient @ V_{TD}

   V_{TD} Touchdown velocity

   C_D Total drag coefficient @ $C_{L_{TD}}$

5. DATA COMPUTATIONS - MANUAL (Equations, Methods, Procedures, Tables and Graphs.)

A. STEP 1.- AIRCRAFT DATA

Before beginning any computation (either by computer or by hand) the physical data described on pages 81 through 86 are required. To facilitate the gathering of this information, an aircraft "Data Acquisition List" has been provided (see pages 83 to 85). Graphical descriptions of this geometry is given in Figures 3-4a through 3-4h.

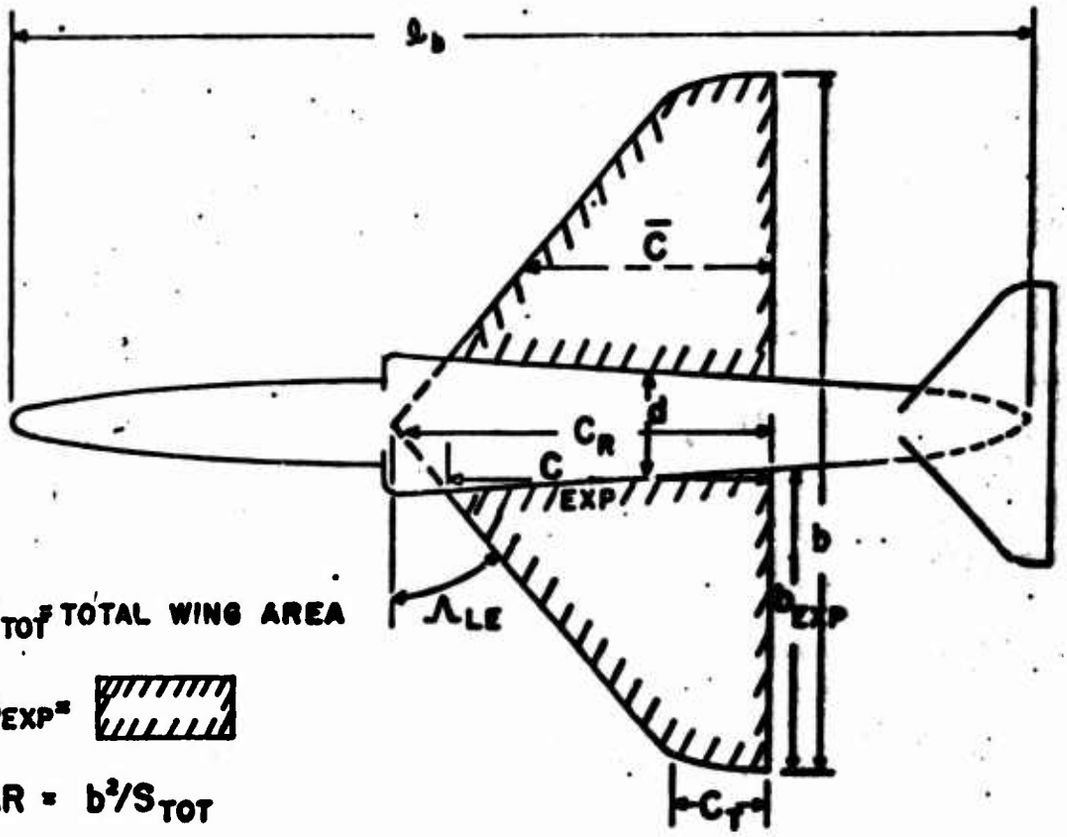

S_{TOT} = TOTAL WING AREA

S_{EXP} =

$AR = b^2/S_{TOT}$

$AR_{EXP} = b_{EXP}^2/S_{EXP}$

$TR = C_T/C_R$

$TR_{EXP} = C_T/C_{EXP}$

λ/b

FIGURE 3-4a Wing Nomenclature

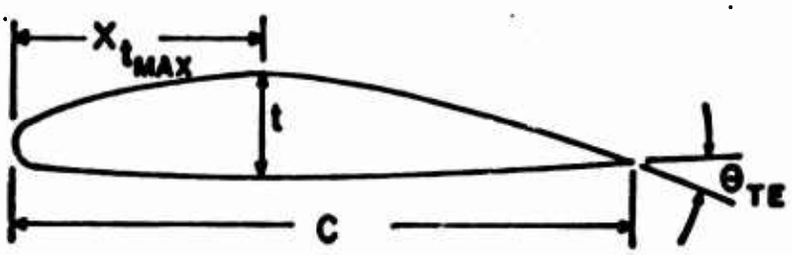

FIGURE 3-4b Section Nomenclature

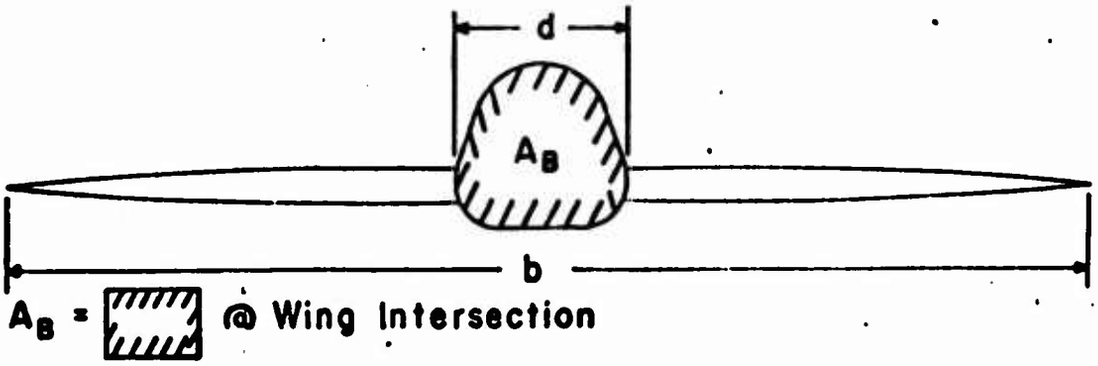

FIGURE 3-4c Wing & Fuselage Nomenclature

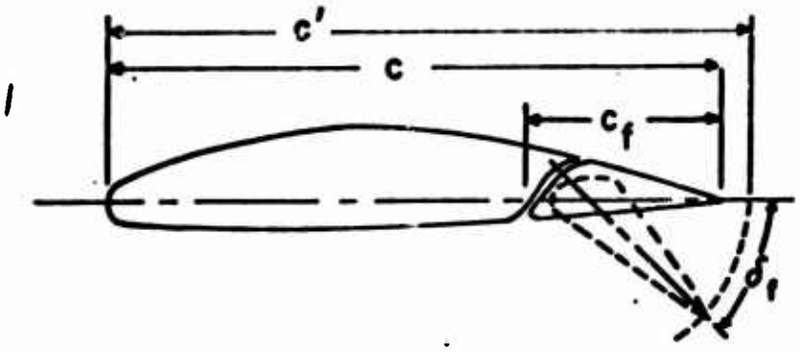

FIGURE 3-4d Trailing Edge Flap Nomenclature

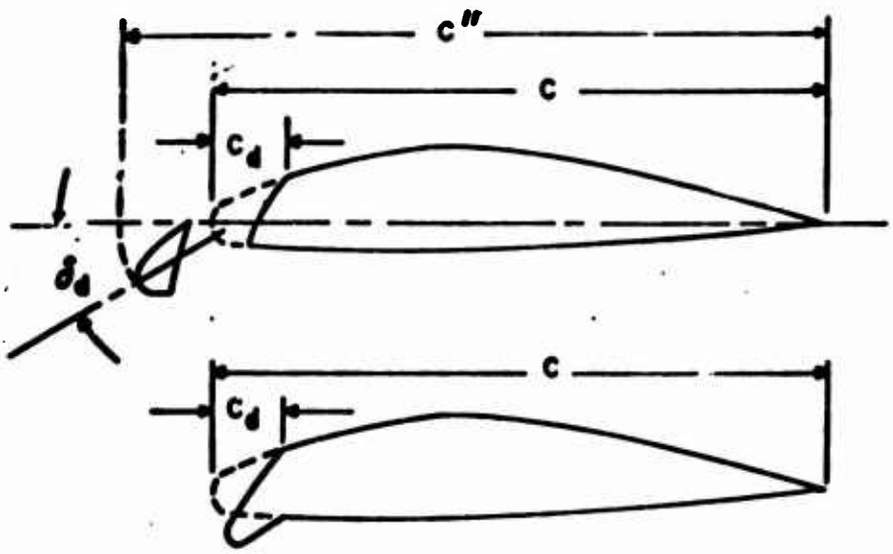

FIGURE 3-4e Leading Edge Device Nomenclature

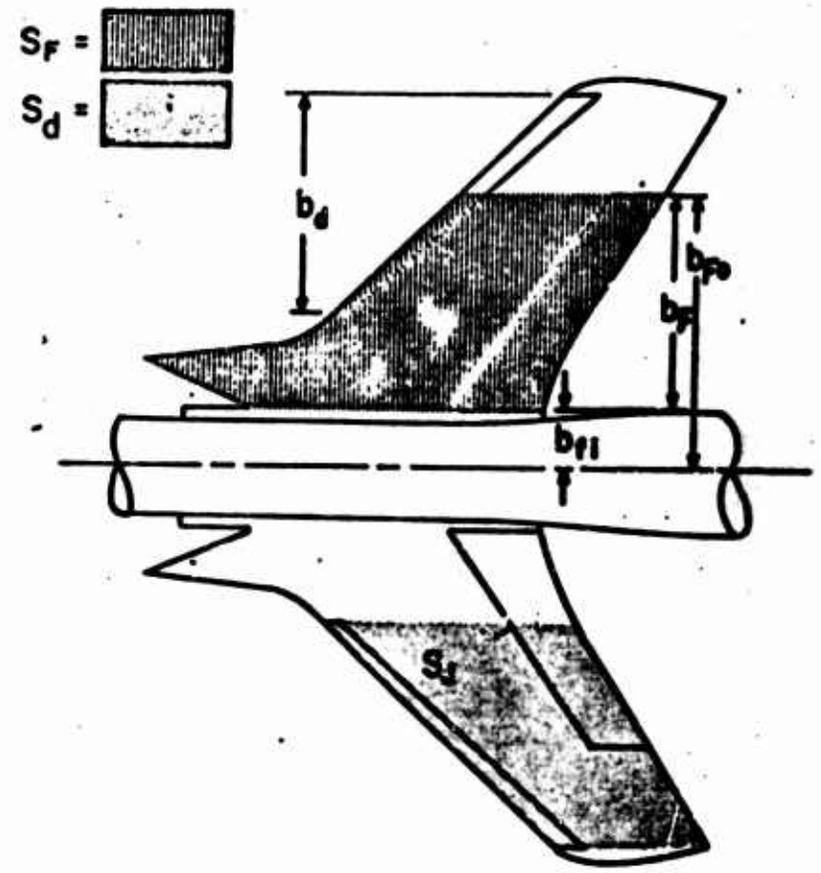

FIGURE 3-4f Flap Area Definitions

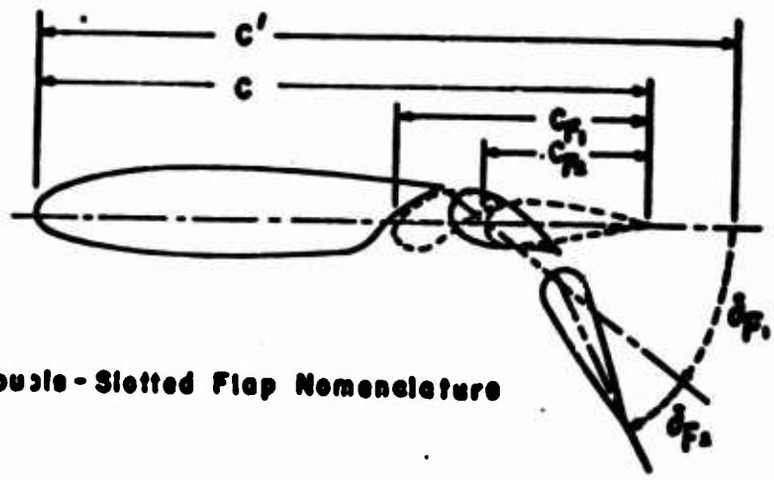

FIGURE 3-4g Double-Slotted Flap Nomenclature

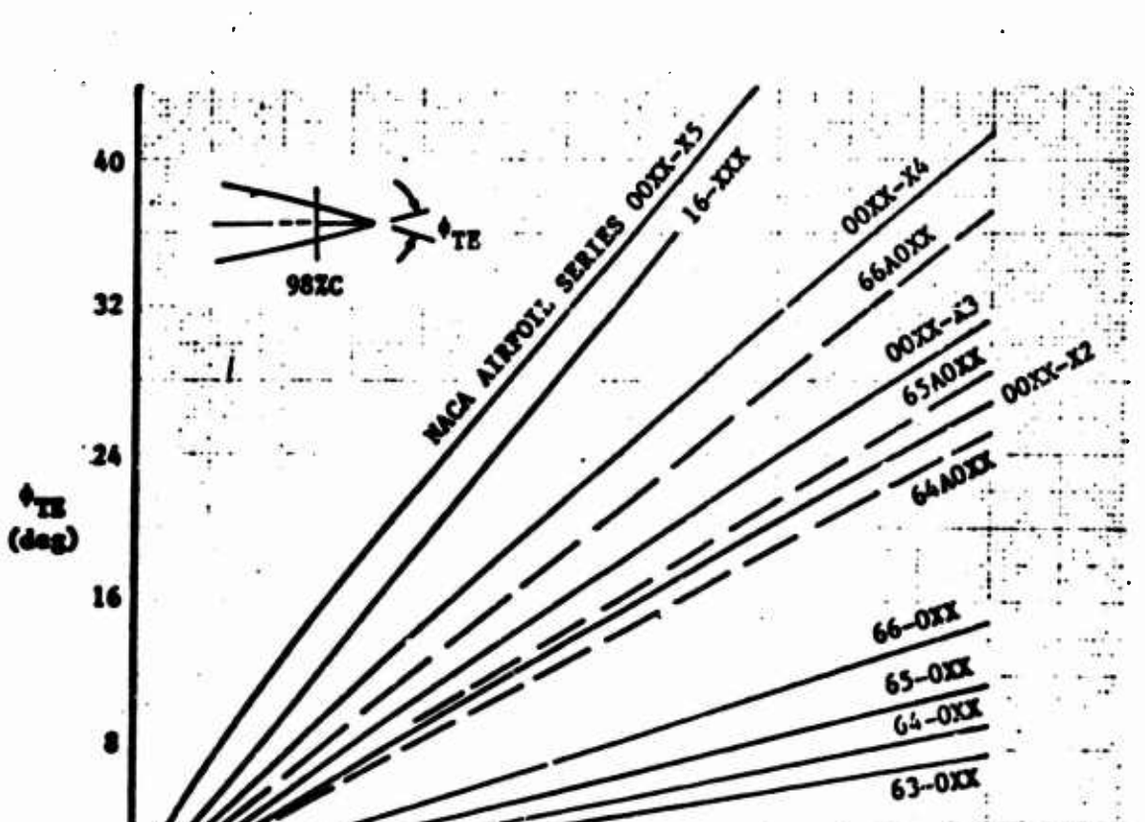

FIGURE 3-4h Variation of Trailing-Edge Angle with Airfoil Thickness Ratio.

1. Input Data Requirements

Whether the computer program is used or hand calculations are to be made the following geometrical data must be known (See Figures 3-4a through 3-4h for explanations):

Variable	Description	Units
	AIRFOIL SECTION CHARACTERISTICS	
	Airfoil Section Designation	Integer
t/C	Maximum Thickness Ratio	-
ϕ_{TE}	Trailing Edge Included Angle	Degs.
$X_{MAX/C}$	Position of Max Thickness Along Chord	-
	WING PLANFORM CHARACTERISTICS	
S_{TOT}	Wing Area - Total Planform	Ft^2
S_{EXP}	Wing Area - Exposed Panels	Ft^2
Λ_{LE}	Leading Edge Sweep Angle	Degs.
AR	Aspect Ratio - Total Planform	-
AR_{EXP}	Aspect Ratio - Exposed Panels	-
TR	Taper Ratio - Total Planform	-
TR_{EXP}	Taper Ratio - Exposed Panels	-
	FUSELAGE CHARACTERISTICS	
d/b	Max. Fuselage Diameter to Wing Span Ratio	-
A_B	Max. Cross Section Area of Fuselage	Ft^2
	TRAILING EDGE FLAP CHARACTERISTICS	
	Flap Type	Integer
C_F/C	Ratio of Flap Chord to Undeflected Airfoil Chord	-
C_F/C'	Ratio of Flap Chord to Deflected Airfoil Chord	-
C'/C	Ratio of Deflected to Undeflected Airfoil Chord	-
δ_F	Flap Deflection Angle	Degs.

Variable	Description	Units
b_F/b	Flap Span to Wing Span Ratio	-
S_F	Area of Wing Effected by Flap	Ft^2

LEADING EDGE DEVICE CHARACTERISTICS

	Device Type	Integer
$C_d/C, C_d/C''$	Ratio of Device Chord to Airfoil Chord (Deflected or Undeflected)	-
C''/C	Ratio of Deflected to Undeflected Airfoil Chord	-
δ_d	Device Deflection Angle	Degs.
b_d/b	Flap Span to Wing Span Ratio	-
S_d	Area of Wing Effected by Leading Edge Device	Ft^2

An additional input requirement is the airfoil section aerodynamic characteristics. Since most aircraft use some form of an NACA airfoil section, the section characteristics are easily obtained from TableIII-1. If the section used cannot be approximated from this table then the procedures shown on pages 85 and 91 can be used.

The preceding data is sufficient if only the lift characteristics are to be calculated.

If the lift characteristics at touchdown, the touchdown velocity, and the drag characteristics are desired, then the following information must be obtained:

Variable	Description	Units
α_g	Wing Angle-of-attack at touchdown	Degs.
W	Aircraft Weight	Lbs.
W_E	Aircraft Empty Weight	Lbs.
ℓ_b	Fuselage Length	Ft.
d	Fuselage Width at Wing	Ft.

DATA ACQUISITION LIST

I. Basic Wing Data

1. Airfoil Data

a. Type Section _____

b. t/c _____

c. ϕ_{TE} _____ degs.

d. $(X_{t_{MAX}})/C$ _____

2. Planform Data

a. S_{TOT} _____ $ft.^2$

b. S_{EXP} _____ $ft.^2$

c. $\Lambda_{LE}, \Lambda_{C/4}$ _____ degs.

d. AR _____

e. AR_{EXP} _____

f. TR _____

g. TR_{EXP} _____

h. $\bar{c}$ _____ ft.

II. Fuselage Data

a. A_B _____ $ft.^2$

b. S_B _____ $ft.^2$

c. d _____ ft.

d. b _____ ft.

e. d/b _____

f. ℓ_B _____ ft.

III. High Lift Device

1. Trailing Edge Flap

a. Type _____

b. c_f/c _____

c. c_f/c' _____

d. c'/c _____

e. δ_f _____ degs.

f. b_f/b _____

g. b_{f_1}/b _____

h. b_{f_2}/b _____

i. S_f _____ ft.^{2}

2. Leading Edge Device

a. Type _____

b. c_d/c or c_d/c'' _____

c. c''/c _____

d. δ_d _____ degs.

e. b_d/b _____

f. S_d _____ ft.^{2}

IV. Miscellaneous Data

a. α_g _____ degs.

b. W _____ lbs.

c. W_e _____ lbs.

d. F_N _____ lbs.

* NOTE: FOR DOUBLE-SLOTTED FLAPS THE FOLLOWING DATA IS REQUIRED

$c_f/c' = c_{FLAP_{TOTAL}}/c'$ _____

$c_{FLAP\,2}/c'$ _____

$\delta_f = \delta_{FLAP\,1}$ _____

$\delta_{FLAP\,2}$ _____

Variable	Description	Units
S_{Wet}	Fuselage Wetted Area	Ft^2
$\bar{C}$	Mean Aerodynamic Chord	Ft.
$\frac{b_{F_i}}{b/2}$	Ratio of Flap Edge Inboard Position to Wing Semispan	-
$\frac{b_{F_o}}{b/2}$	Ratio of Flap Edge Outboard Position to Wing Semispan	-
F_N	Net Thrust at Approach Speed	Lbs.

B. STEP 2 - AIRFOIL SECTION CHARACTERISTICS

1. If an NACA airfoil section is used, a good approximation can be obtained from the following table (Table III-1). The section data required is:

α_o - Angle-of-attack at zero lift - Degs.

C_{l_α} - Lift curve slope - per Degs.

$C_{l_{max}}$ - Maximum lift coefficient

2. If some other type section is used for which no experimental values are available, then an approximation using Glauert's equation gives

$$\alpha_o = \int_0^1 \frac{1}{\pi \left(1-\frac{x}{C}\right)\sqrt{\frac{x}{C}\left(1-\frac{x}{C}\right)}} \frac{y}{C}\, dx \quad \text{- Radians}$$

where x is the airfoil section chord location
y is the thickness corresponding to x
C is the airfoil section chord

also for NACA type sections

$$\alpha_o = K (\alpha_i - 9.12)\, C_{l_i} \quad \text{- Degs.}$$

where C_{l_i} is the design lift coefficient, from Table III-2.

α_i is the design angle-of-attack, from Table III-2.

and K = 0.93 for NACA 4-digit series
1.08 for NACA 5-digit series
0.74 for NACA 6-digit series

TABLE III - 1

EXPERIMENTAL AIRFOIL SECTION DATA

(α^* angle of attack where C_{ℓ_α} becomes nonlinear)

Airfoil	α_o (deg)	C_{ℓ_α} (per deg)	$\alpha_{C_{\ell_{max}}}$ (deg)	$C_{\ell_{max}}$	α^* (deg)
0006	0	.108	9.0	.92	9.0
0009	0	.109	13.4	1.32	11.4
1408	0.8	.109	14.0	1.35	10.0
1410	-1.0	.108	14.3	1.50	11.0
1412	-1.1	.108	15.2	1.58	12.0
2412	-2.0	.105	16.8	1.68	9.5
2415	-2.0	.106	16.4	1.63	10.0
2418	-2.3	.103	14.0	1.47	10.0
2421	-1.8	.103	16.0	1.47	8.0
2424	-1.8	.098	16.0	1.29	8.4
4412	-3.8	.105	14.0	1.67	7.5
4415	-4.3	.105	15.0	1.64	8.0
4418	-3.8	.105	14.0	1.53	7.2
4421	-3.8	.103	16.0	1.47	6.0
4424	-3.8	.100	16.0	1.38	4.8
23012	-1.4	.107	18.0	1.79	12.0
23015	-1.0	.107	18.0	1.72	10.0
23018	-1.2	.104	16.0	1.60	11.8
23021	-1.2	.103	15.0	1.50	10.3
23024	-0.8	.097	15.0	1.40	9.7
63-006	0	.112	10.0	.87	7.7
-009	0	.111	11.0	1.15	10.7
63-206	-1.9	.112	10.5	1.06	6.0
-209	-1.4	.110	12.0	1.4	10.8
-210	-1.2	.113	14.5	1.56	9.6
63_1-012	0	.116	14.0	1.45	12.8
-212	-2.0	.114	14.5	1.63	11.4
-412	-2.8	.117	15.0	1.77	9.6
63_2-015	0	.117	14.5	1.47	11.0
-215	-1.0	.116	15.0	1.60	8.8
-415	-2.8	.118	15.0	1.68	10.0
-615	-3.6	.117	15.0	1.67	8.6

TABLE III - 1 (Continued)

Airfoil	α_o (deg)	C_{ℓ_α} (per deg)	$\alpha_{C_{\ell_{max}}}$ (deg)	$C_{\ell_{max}}$	α^* (deg)
63_3-018	0	.118	15.5	1.54	11.2
-218	-1.4	.118	14.5	1.85	8.0
-418	-2.7	.118	16.0	1.57	7.0
-618	-3.8	.118	16.0	1.59	4.2
63_4-021	0	.118	17.0	1.38	9.0
-221	-1.5	.118	15.0	1.44	9.2
-421	-2.8	.120	16.0	1.48	6.7
63,4-420	-2.2	.109	14.0	1.42	7.6
63,4-420 a = .3	-2.4	.111	16.0	1.35	6.0
63(420)-422	-3.2	.112	14.0	1.36	6.0
63(420)-517	-3.0	.108	15.0	1.60	8.0
64-006	0	.109	9.0	.8	7.2
-009	0	.110	11.0	1.17	10.0
64-108	0	.110	10.0	1.1	10.0
-110	-1.0	.110	13.0	1.4	10.0
64-206	-1.0	.110	12.0	1.03	8.0
-208	-1.2	.113	10.5	1.23	8.8
-209	-1.5	.107	13.0	1.40	8.9
-210	-1.6	.110	14.0	1.45	10.8
64_1-012	0	.111	14.5	1.45	11.0
-112	-0.8	.113	14.0	1.50	12.2
-212	-1.3	.113	15.0	1.55	11.0
-412	-2.6	.112	15.0	1.67	8.0
64_2-015	0	.112	15.0	1.48	13.0
-215	-1.6	.112	15.0	1.57	10.0
-415	-2.8	.115	15.0	1.65	8.0
64_3-018	0	.111	17.0	1.50	12.0
-218	-1.3	.115	16.0	1.53	10.0
-418	-2.9	.116	14.0	1.57	8.0
-618	-3.8	.116	16.0	1.58	5.6
64_4-021	0	.110	14.0	1.30	10.3
-221	-1.2	.117	13.0	1.32	6.8
-421	-2.8	.120	13.0	1.42	6.4

TABLE III - 1 (Continued)

Airfoil	α_o (deg)	C_{ℓ_α} (per deg)	$\alpha_{C_{\ell_{max}}}$ (deg)	$C_{\ell_{max}}$	α^* (deg)
65-006	0	.105	12.0	.92	7.6
-009	0	.107	11.0	1.08	9.8
65-206	-1.6	.105	12.0	1.03	6.0
-209	-1.2	.106	12.0	1.30	10.0
-210	-1.6	.108	13.0	1.40	9.6
65-410	-2.5	.112	14.0	1.52	8.0
65_1-012	0	.110	14.0	1.36	10.0
-212	-1.0	.108	14.0	1.47	9.4
-212 a = .6	-1.4	.108	14.0	1.50	9.6
-412	-3.0	.111	15.5	1.66	10.5
65_2-015	0	.111	15.0	1.42	11.2
-215	-1.2	.112	15.5	1.53	10.0
-415	-2.6	.111	16.0	1.61	8.7
-415 a = .5	-2.6	.111	20.0	1.60	7.0
65(215)-114	-0.7	.112	15.0	1.44	10.5
65(216)-415 a = .5	-3.0	.106	18.0	1.60	6.0
65,3-018	0	.100	17.0	1.44	10.0
-418 a = .8	-3.0	.112	20.0	1.58	4.4
-618	-4.0	.110	20.0	1.60	4.9
65_3-018	0	.100	16.0	1.37	10.0
-218	-1.2	.100	18.0	1.48	8.8
-418	-2.4	.110	18.0	1.54	4.9
-418 a = .5	-2.8	.115	18.0	1.50	6.0
-618	-4.0	.113	18.0	1.64	5.2
-618 a = .5	-4.2	.104	20.0	1.51	5.3
65_4-021	0	.112	18.5	1.40	7.4
-221	-1.3	.115	20.5	1.46	6.0
-421	-2.8	.116	22.0	1.56	5.0
-421 a = .5	-2.8	.116	20.0	1.43	5.6
65(421)-420	-2.4	.116	20.0	1.52	4.7
66-006	0	.100	9.0	.80	6.5
-009	0	.103	10.0	1.05	10.0

TABLE III - 1 (Continued)

Airfoil	α_o (deg)	C_{ℓ_α} (per deg)	$\alpha_{C_{\ell_{max}}}$ (deg)	$C_{\ell_{max}}$	α^* (deg)
66-206	-1.6	.108	10.5	1.00	7.0
-209	-1.0	.107	11.0	1.17	9.0
-210	-1.3	.110	11.0	1.27	10.0
66_1-012	0	.106	14.0	1.25	11.2
-212	-1.2	.102	15.0	1.46	11.6
66_2-015	0	.105	15.5	1.35	12.0
-215	-1.3	.106	16.0	1.50	11.4
-415	-2.6	.106	17.0	1.60	10.0
66(215)-016	0	.105	14.0	1.33	10.0
-216	-2.0	.114	16.0	1.55	8.8
-216 a = .6	-1.2	.100	16.0	1.46	7.0
-416	-2.6	.100	18.0	1.60	4.0
63A010	0	.105	18.0	1.20	10.0
63A210	-1.5	.103	14.0	1.43	10.0
64A010	0	.110	12.0	1.23	10.0
64A210	-1.5	.105	8.0	1.44	10.0
64A410	-3.0	.100	15.0	1.61	10.0
64_1A212	-2.0	.100	14.0	1.54	11.0
64_2A215	-2.0	.095	15.0	1.50	12.0

TABLE III-2

THEORETICAL LOW SPEED AERODYNAMIC CHARACTERTISTICS
OF VARIOUS AIRFOIL MEAN LINES**

MEAN LINE	C_{ℓ_i}	α_i (deg)	$C_{m_{C/4}}$ at C_{ℓ_i}	REMARKS
Four-Digit Series				
62	0.9	2.81	-0.113	For other NACA four-digit mean lines, multiply the corresponding 6-percent camber* C_{ℓ_i}, α_i and $C_{m_{C/4}}$ by the ratio of the camber designators, i.e. (2/6), (3/6), (4/6), (5/6).
63	0.8	1.60	-0.134	
64	0.76	0.74	-0.157	
65	0.75	0	-0.187	
66	0.76	-0.74	-0.222	
67	0.80	-1.60	-0.266	
Five-Digit Series				
210	0.30	2.09	-0.006	For other NACA five-digit mean lines, multiply the corresponding C_{ℓ_i}, α_i and $C_{m_{C/4}}$ by the ratio of camber designators, i.e., (3/2), (4/2), (5/2), (6/2).
220	0.30	1.86	-0.010	
230	0.30	1.65	-0.014	
240	0.30	1.45	-0.019	
250	0.30	1.26	-0.026	
6-Series				
a=0	1.0	4.56	-0.088	For NACA 6-series airfoils, multiply the corresponding mean line C_{ℓ_i} α_i and $C_{m_{C/4}}$ by the ratio of design lift coefficients.
0.1	1.0	4.43	-0.086	
0.2	1.0	4.17	-0.094	
0.3	1.0	3.84	-0.106	
0.4	1.0	3.46	-0.121	
0.5	1.0	3.04	-0.139	
0.6	1.0	2.58	-0.158	
0.7	1.0	2.09	-0.179	
0.8	1.0	1.54	-0.202	
0.9	1.0	0.90	-0.225	
1.0	1.0	0	-0.250	

* "Corresponding" cambers are those for which the chordwise position of maximum camber is the same.

** Lift coefficient is based on airfoil chord.

For C_{ℓ_α} the following equation can be used

$$C_{\ell_\alpha} = 2\pi + 4.7 \left(\frac{t}{C}\right) \left[1 + .00375 \quad \phi_{TE}\right] \quad \text{(per r.d.)}$$

A reduction in C_{ℓ_α} due to surface roughness can be obtained from Figure 3-5.

To obtain $C_{\ell_{max}}$ the next expression may be used

$$C_{\ell_{max}} = C_{\ell_{max_{(base)}}} f(\Delta y) + \sum_{M=1}^{M=4} \Delta_M C_{\ell_{max}} f(\Delta y)$$

where $f(\Delta y)$ - an airfoil profile factor, defined at 6%C, which can either be computed or obtained from Figure 3-6 .

$C_{\ell_{max_{(base)}}}$ - A base max lift coefficient, Figure 3-7.

$\Delta_1 C_{\ell_{max}}$ - Effect of airfoil camber & location, Figure 3-8a and 3-8b.

$\Delta_2 C_{\ell_{max}}$ - Effect of airfoil thickness, Figure 3-9.

$\Delta_3 C_{\ell_{max}}$ - Effect of Reynold's number, Figure 3-10.

$\Delta_4 C_{\ell_{max}}$ - Effect of surface roughness, Figure 3-11.

C. STEP 3 - WING ALONE CHARACTERISTICS

1. α_o The wing alone angle-of-attack for zero lift is equal to the airfoil section α_o for the restrictions placed on the aircraft geometries that are to be considered.

2. C_{L_α} A good estimation of the wing-alone lift curve slope can be obtained from the following expression.

$$C_{L_\alpha} = \frac{2\pi \, AR}{2 + \left\{ \frac{4\pi^2 AR^2}{C_{\ell_\alpha}^2} \left[1 + \left(\tan \Lambda_{LE} - \frac{2}{AR} \frac{1-TR}{1+TR} \right)^2 \right] + 4 \right\}^{\frac{1}{2}}} \qquad \text{(III-5)}$$

3. $C_{L_{MAX}}$ The maximum lift coefficient is largely dependent on aspect ratio. For purposes of this method, AR selection is based on the following relationship:

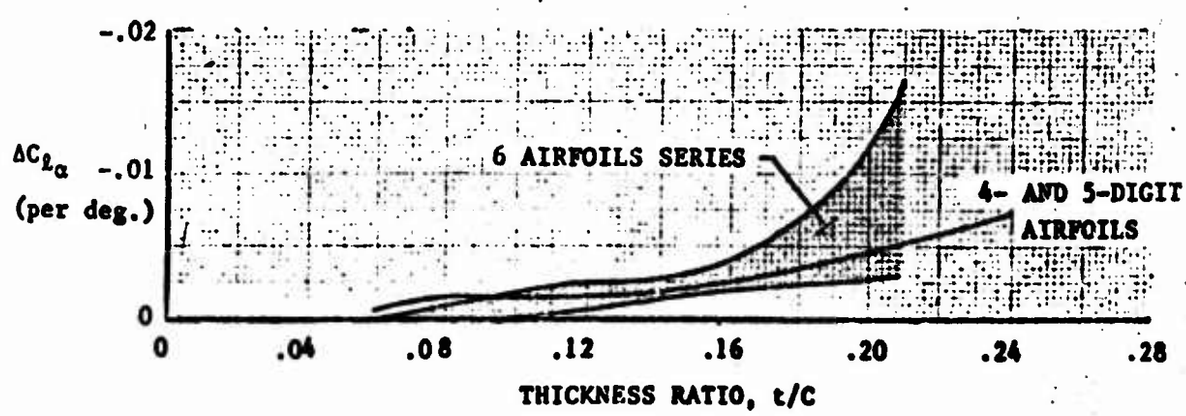

FIGURE 3-5: Effect of NACA Roughness on Section Lift-Curve Slope.

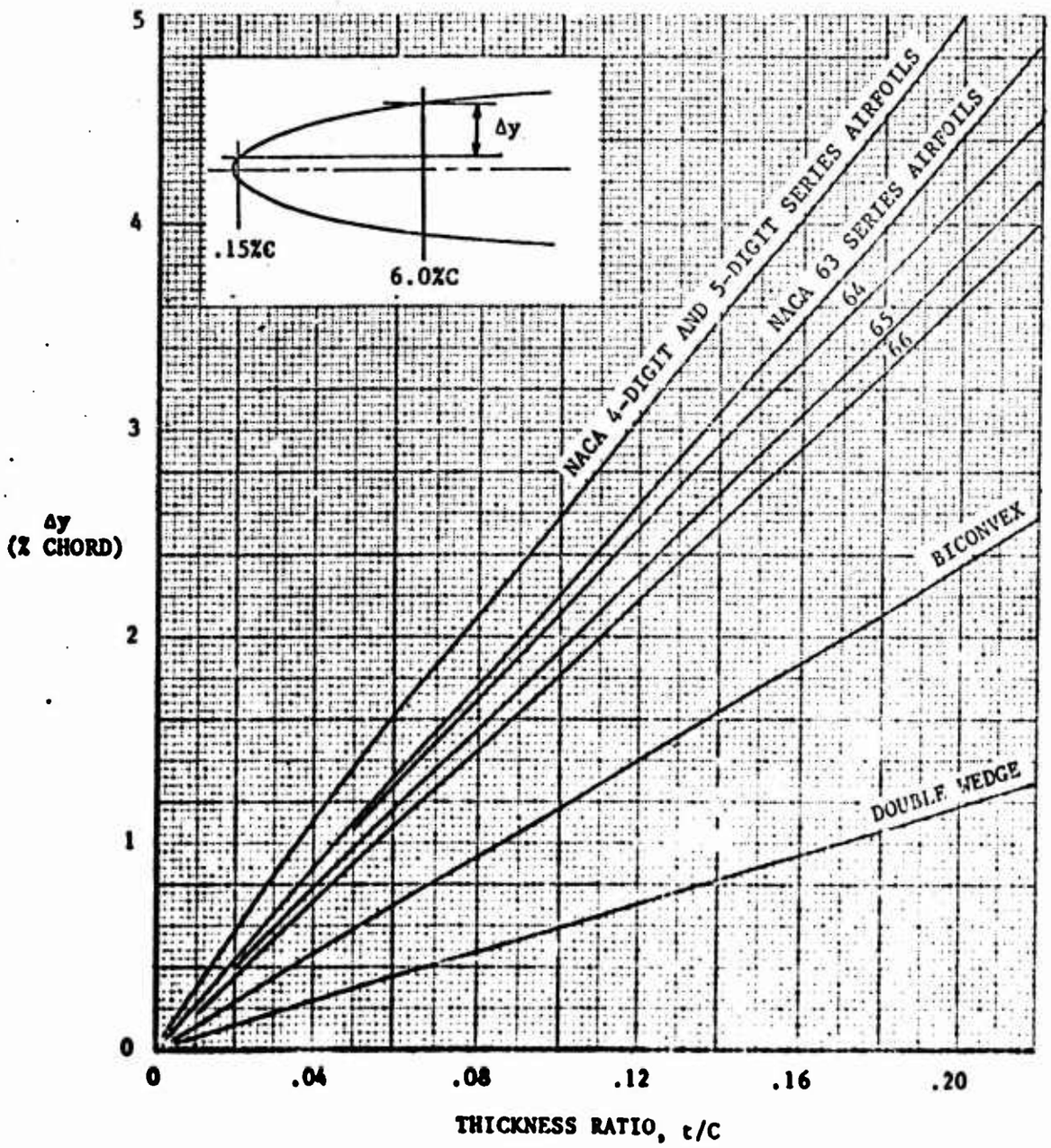

FIGURE 3-6: Variation of Leading-Edge Sharpness Parameter with Airfoil Thickness Ratio.

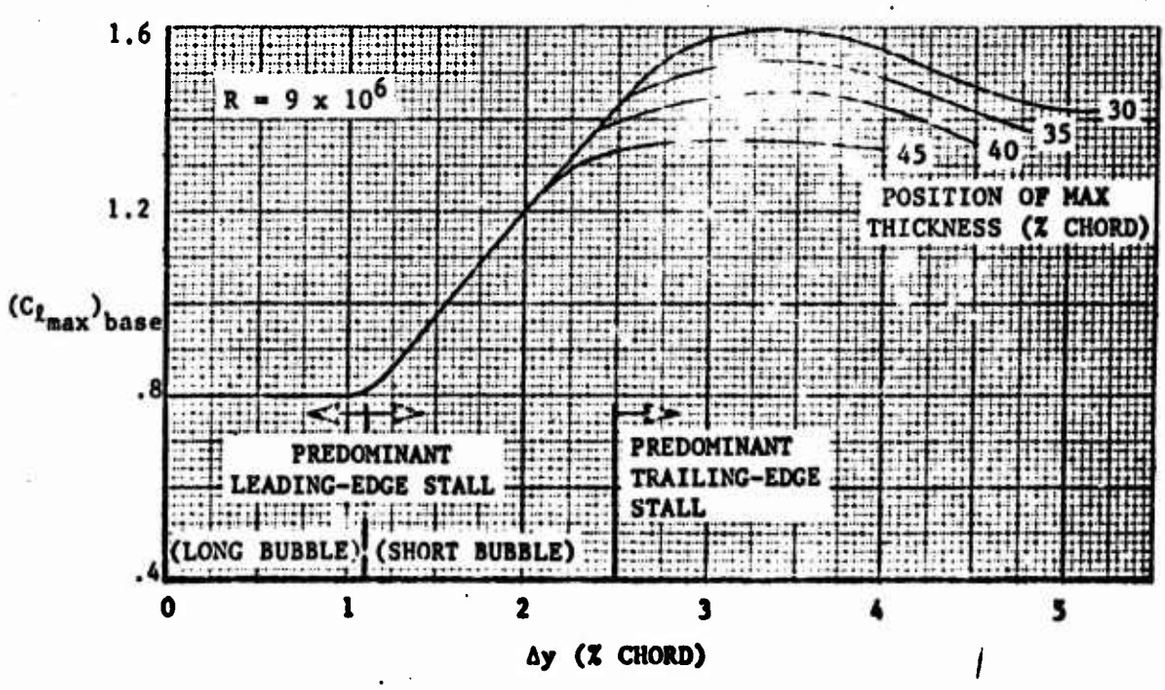

FIGURE 3-7: Airfoil Section Maximum Lift Coefficient of Uncambered Airfoils.

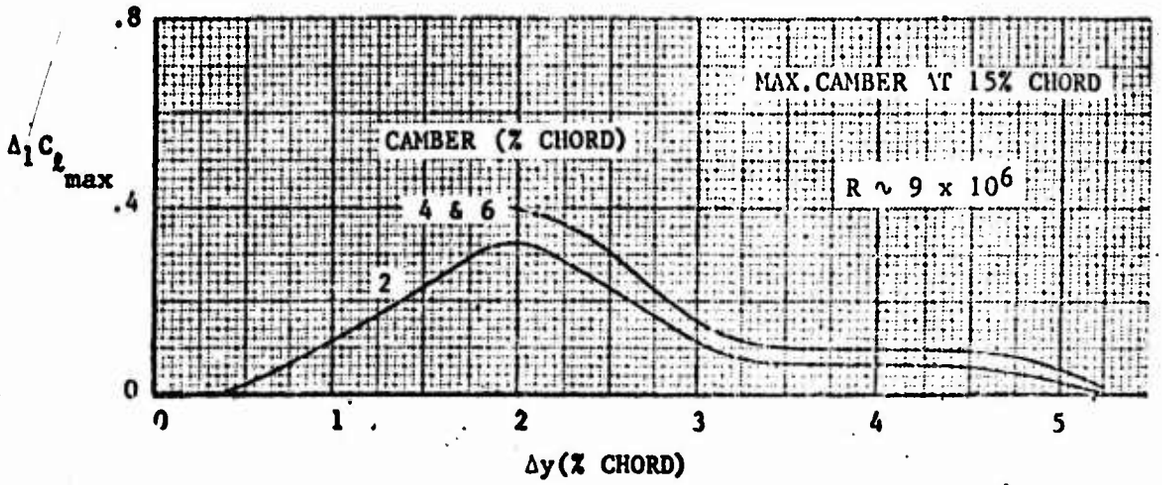

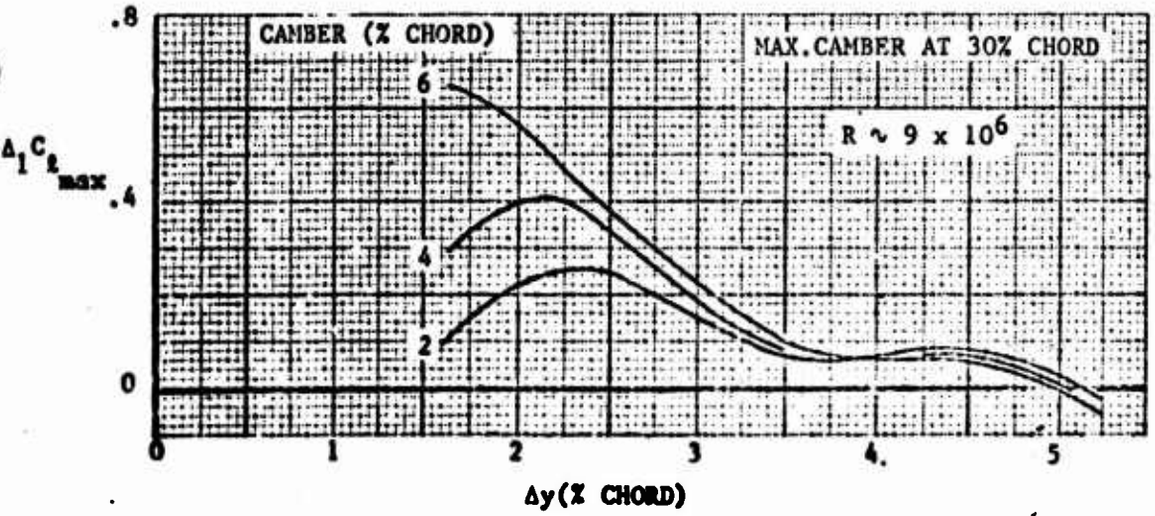

FIGURE3-8a: Effect of Airfoil Camber Location and Amount on Section Maximum Lift.

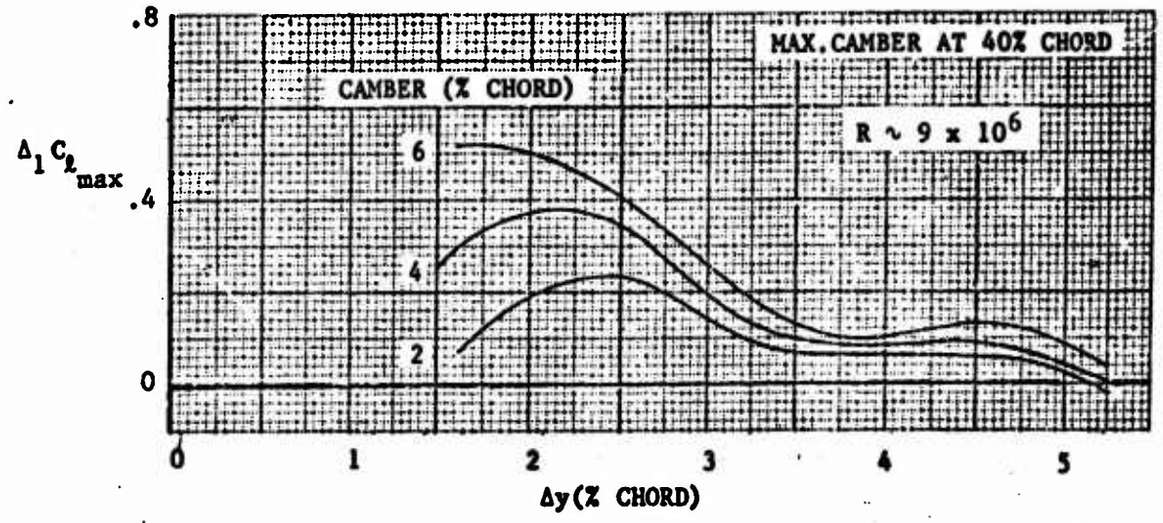

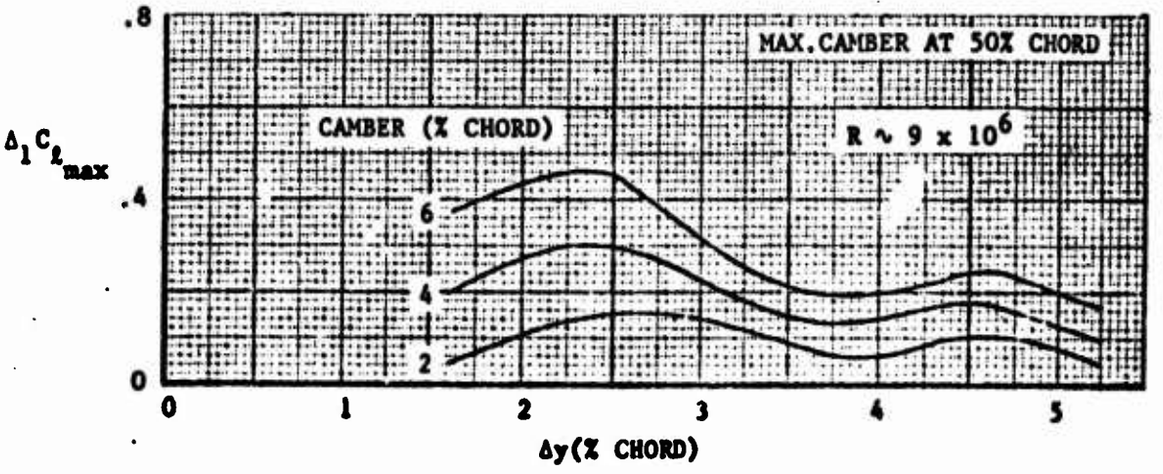

FIGURE 3-8b: Effect of Airfoil Camber Location and Amount on Section Maximum Lift.

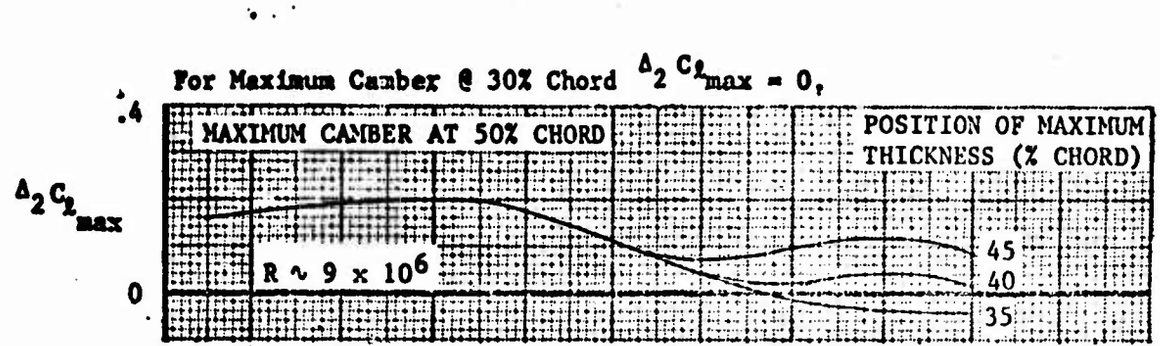

FIGURE 3-9: Effect of Position of Maximum Thickness on Section Maximum Lift.

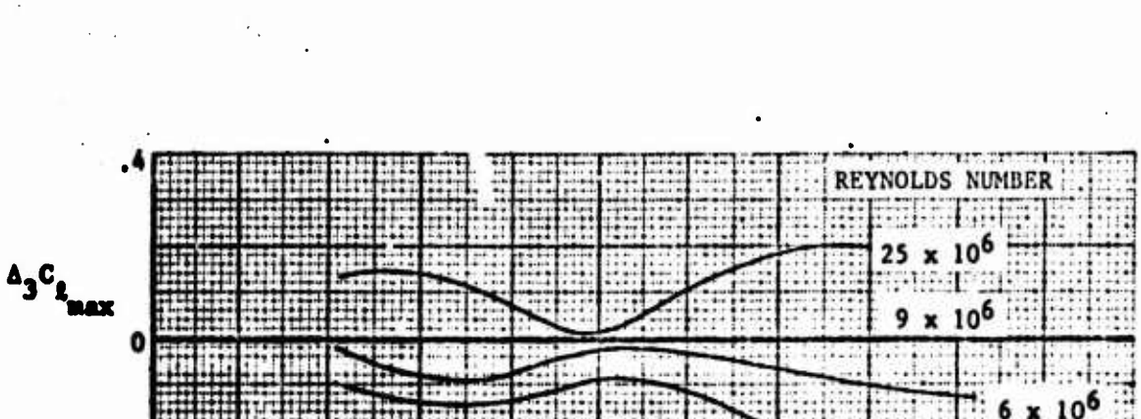

FIGURE 3-10: Effect of Reynolds Number on Section Maximum Lift.

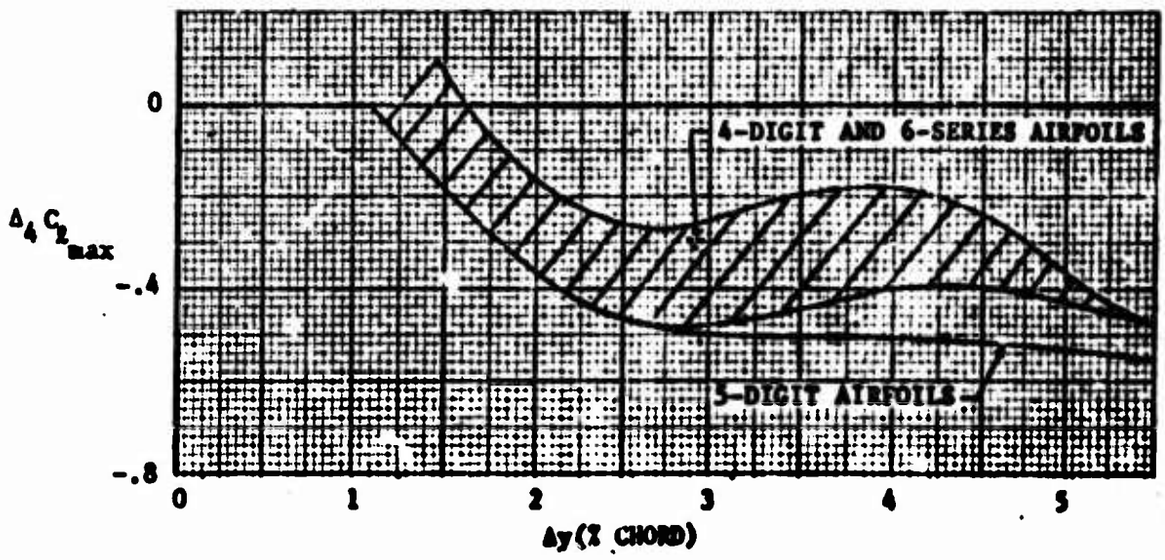

FIGURE 3-11: Effect of NACA Standard Roughness on Section Maximum Lift.

High AR $\quad AR > \dfrac{4}{(C_1 + 1)\ \text{Cos}\ \Lambda_{LE}}$

Low AR $\quad AR < \dfrac{3}{(C_1 + 1)\ \text{Cos}\ \Lambda_{LE}}$

where the value of $C_1 = f\ (TR)$ can be obtained from Figure 3-12. Either relationship may be used when AR lies between the two functions.

HIGH AR

For the case of the High AR wing $C_{L_{MAX}}$ is determined from the expression

$$C_{L_{MAX}} = \left(\frac{C_{L_{MAX}}}{C_{\ell_{max}}}\right) C_{\ell_{max}}$$

$$\alpha_{C_{L_{MAX}}} = \frac{C_{L_{MAX}}}{C_{L_\alpha}} + \alpha_o + \Delta\alpha_{C_{L_{MAX}}}$$

The function $\dfrac{C_{L_{MAX}}}{C_{\ell_{max}}} = f\ (\Lambda_{LE}, \Delta y)$ and comes from Figure 3-13.

$C_{\ell_{max}}$ comes from Step 2

α_o comes from Step 2

$\Delta\alpha_{C_{L_{MAX}}} = f\ (\Lambda_{LE}, \Delta y)$ and comes from Figure 3-14.

LOW AR

To compute the low AR maximum lift coefficient

$$C_{L_{MAX}} = (C_{L_{MAX\ base}}) + \Delta C_{L_{MAX}}$$

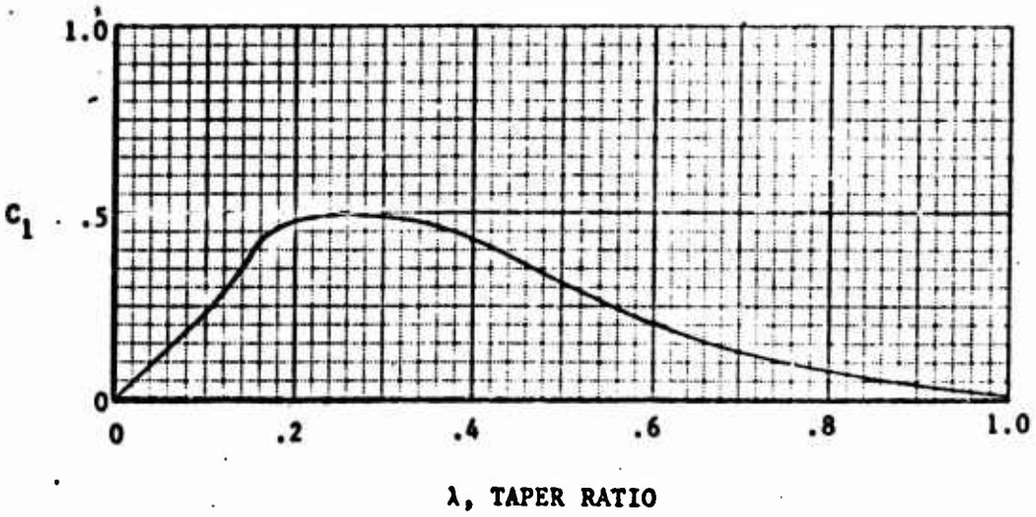

FIGURE 3-12: Taper Ratio Correction Factor

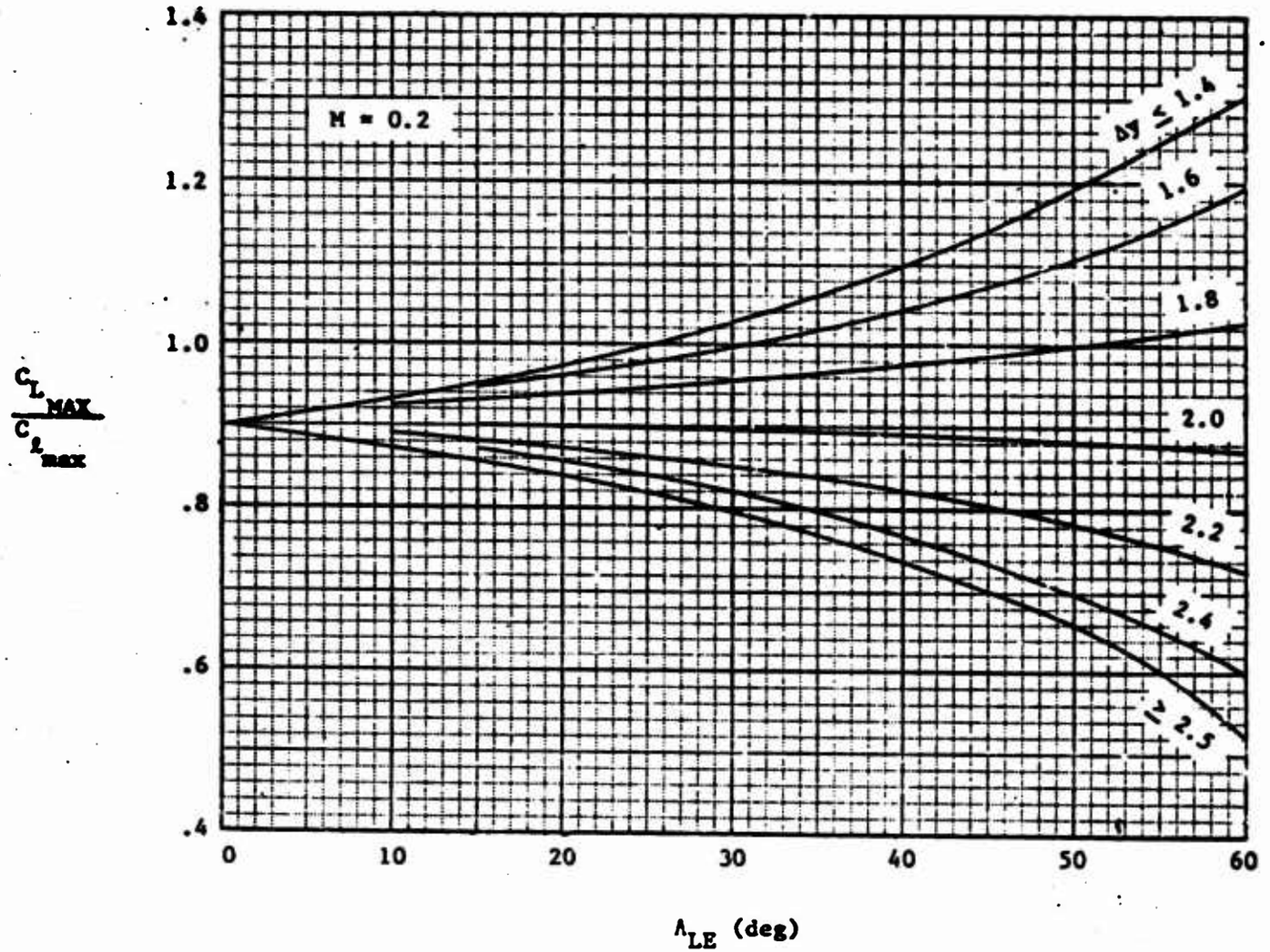

FIGURE 3-13: Subsonic Maximum Lift of High-Aspect-Ratio Wings.

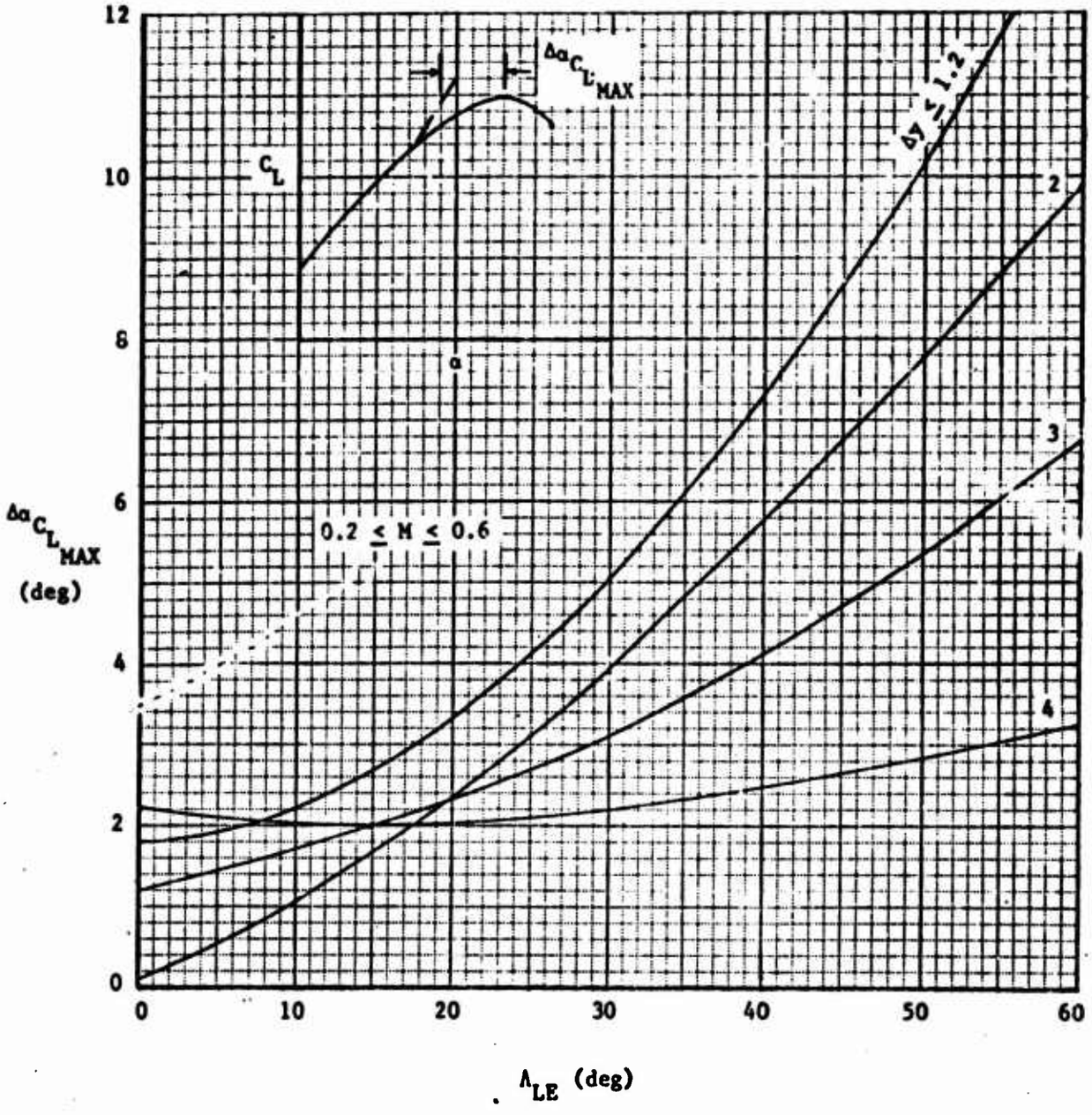

FIGURE3-14: Angle-of-Attack Increment for Subsonic Maximum Lift of High-Aspect-Ratio Wings.

$$\alpha_{C_{L_{MAX}}} = (\alpha_{C_{L_{MAX\ base}}}) + \Delta\alpha_{C_{L_{MAX}}}$$

The value

$$(C_{L_{MAX\ base}}) = f\left[(C_1 + 1)\ AR\ \text{Cos}\ \Lambda_{LE},\ \Delta y \right]$$

and is obtained from Figure 3-15a or 3-15b, depending on the position of maximum thickness. The value

$$\Delta C_{L_{MAX}} = f\left[(C_2 + 1)\ AR\ \tan\ \Lambda_{LE} \right]$$

where C_2 comes from Figure 3-16 and then $\Delta C_{L_{MAX}}$ from Figure 3-17.

$$(\alpha_{C_{L_{MAX\ base}}}) = f\left[(C_1 + 1) AR\ \text{Cos}\ \Lambda_{LE} \right]$$

and is shown in Figure 3-18.

$$\Delta\alpha_{C_{L_{MAX}}} = f\left[(C_2 + 1) AR\ \tan\ \Lambda_{LE} \right]$$

and comes from Figure 3-19.

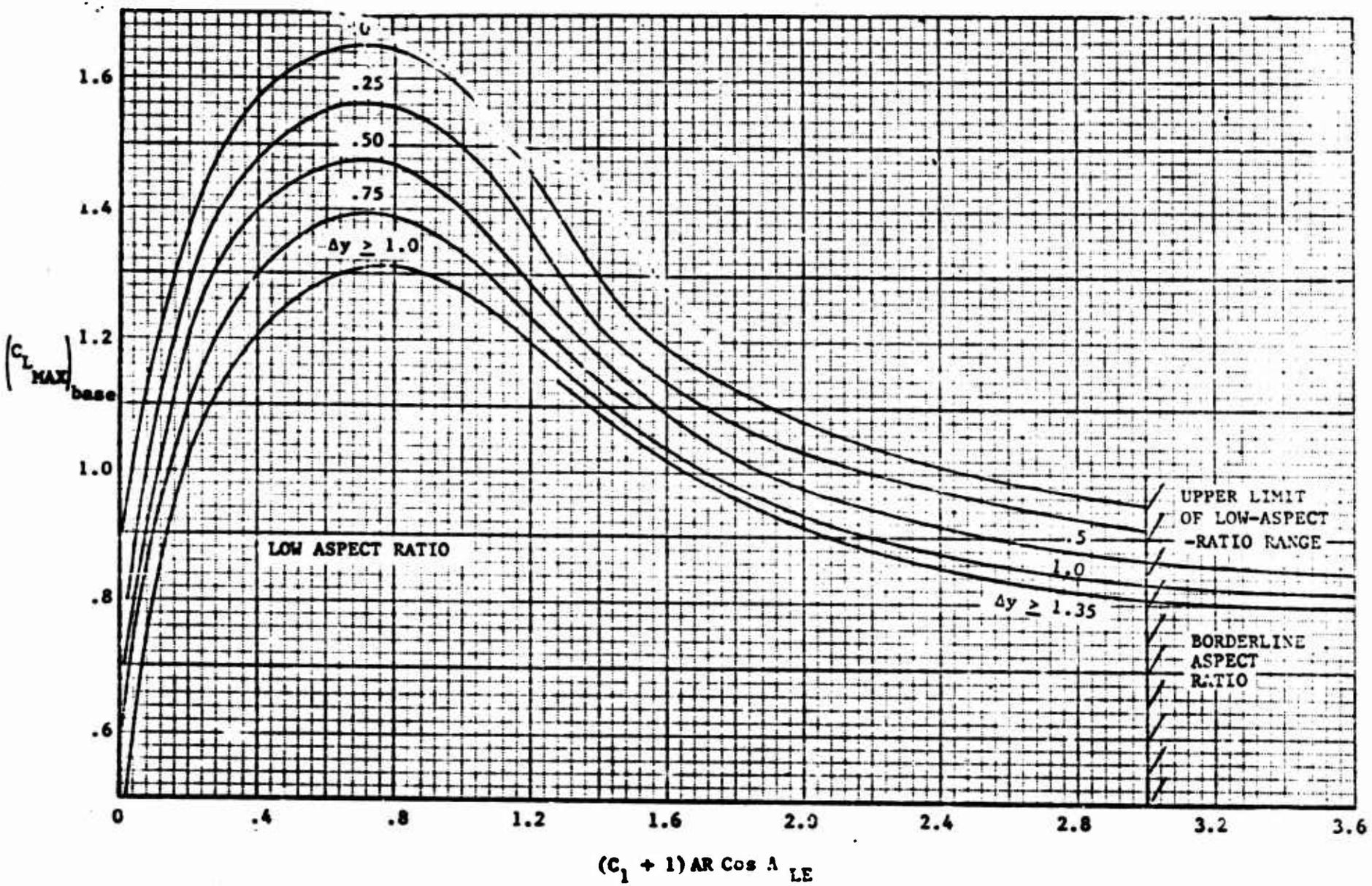

FIGURE 3-15a Subsonic Maximum Lift of Wings with Position of Max Thickness at or Forward of 35 Percent Chord.

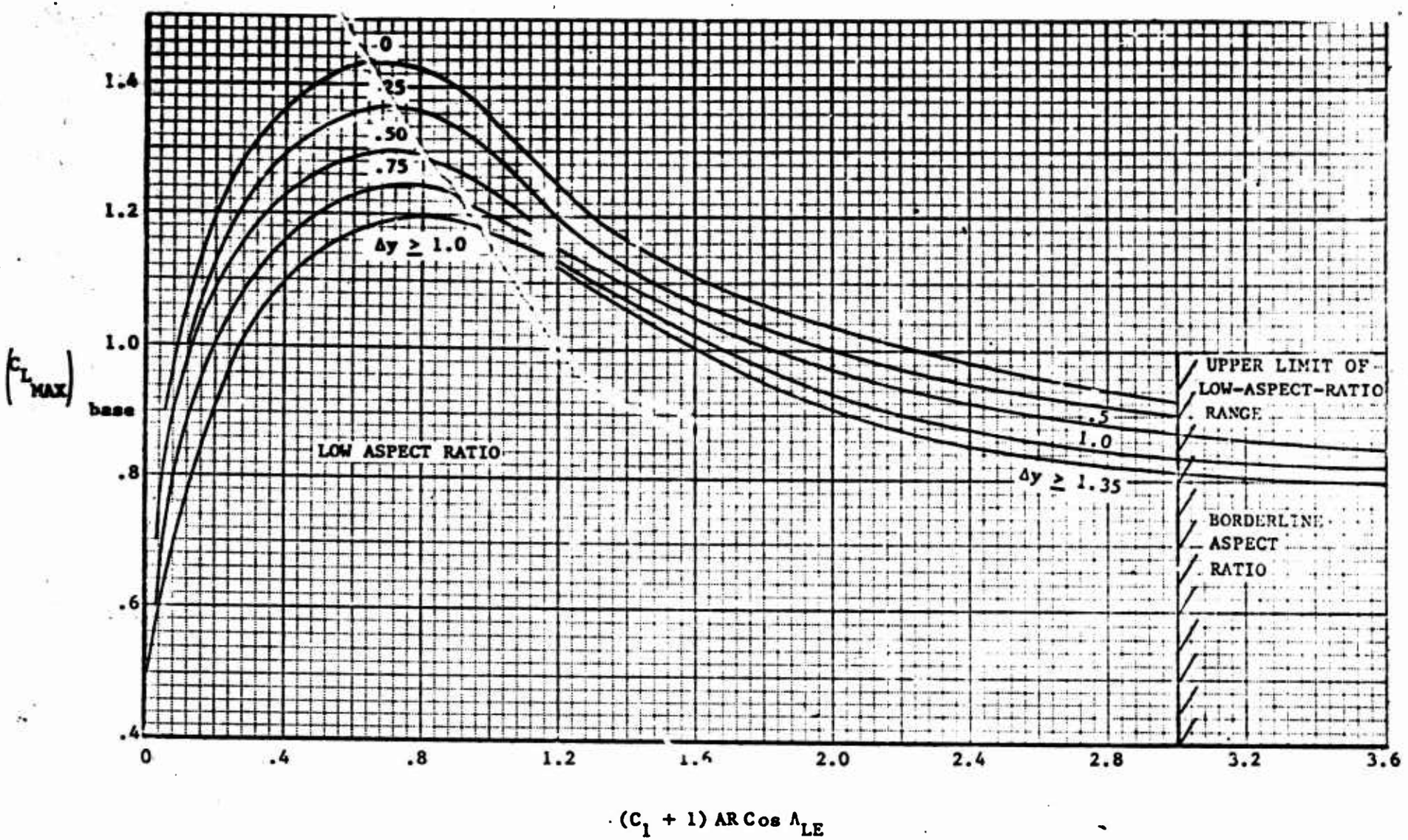

FIGURE 3-15b Subsonic Maximum Lift of Wings with Position of Max Thickness Between 35 & 50 Percent Chord.

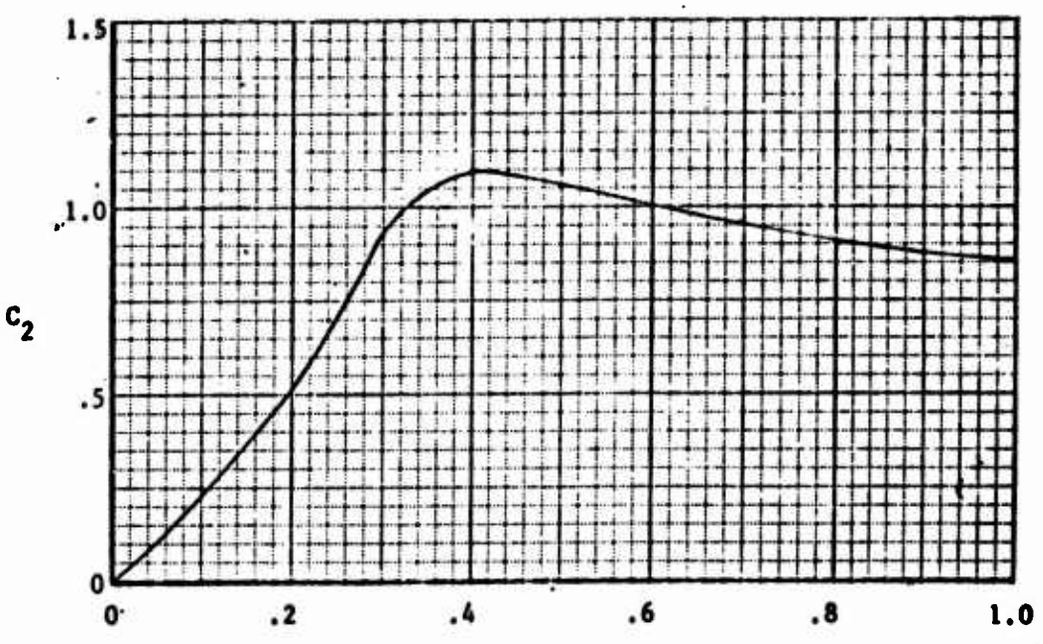

FIGURE 3-16: Taper Ratio Correction Factor

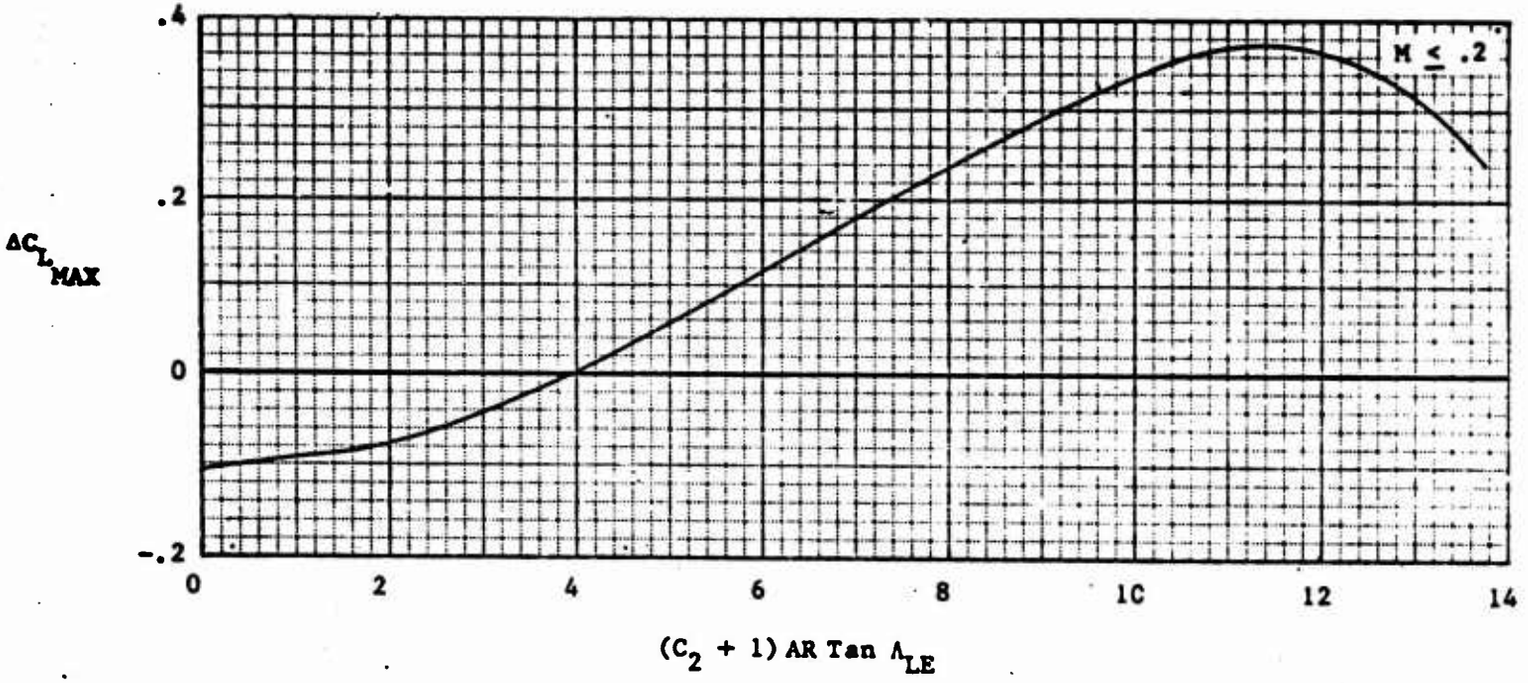

FIGURE3-17: Subsonic Maximum-Lift Increment for Low-Aspect-Ratio Wings

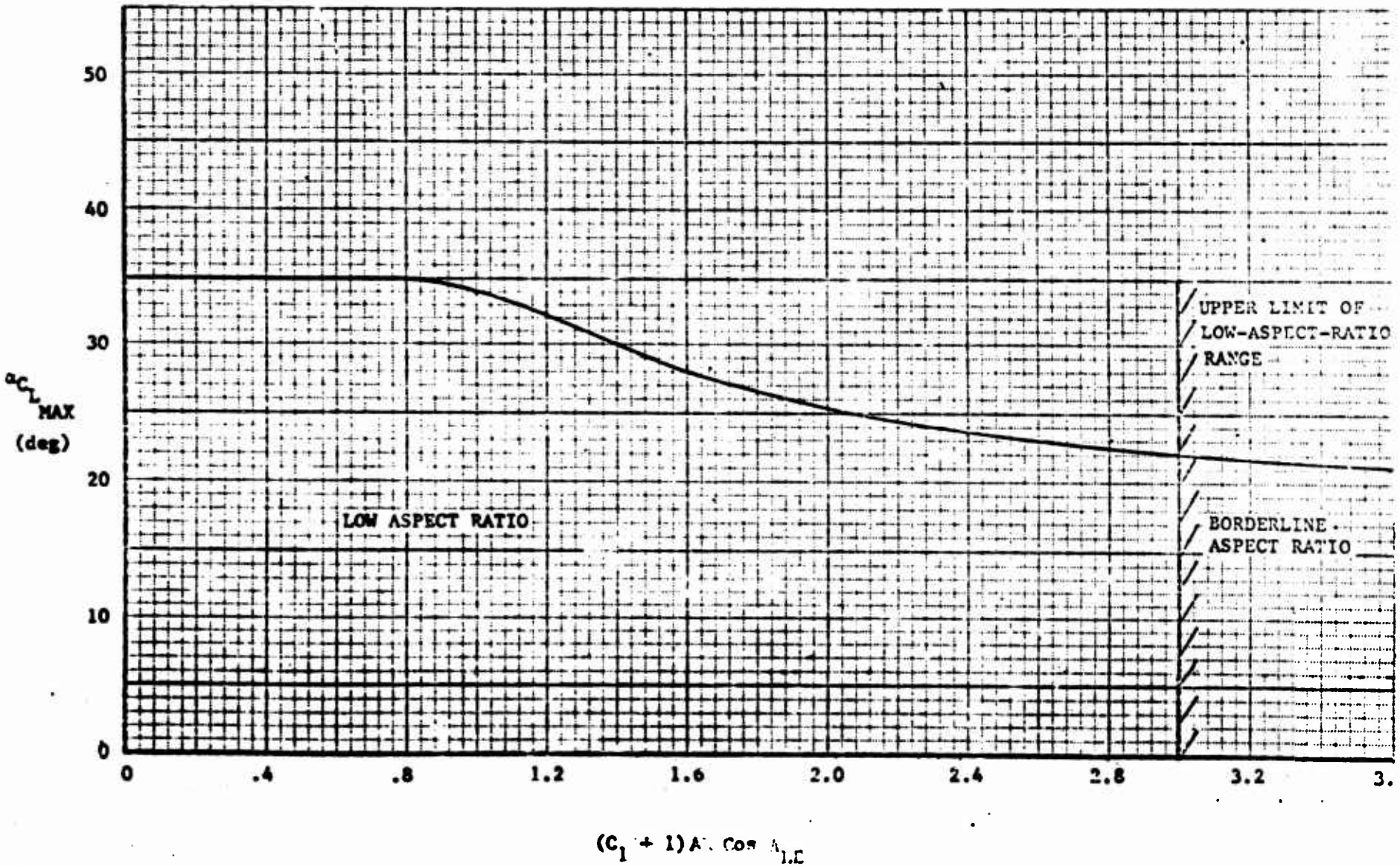

FIGURE 3-28 Angle of Attack for Subsonic Maximum Lift of Low-Aspect-Ratio Wings

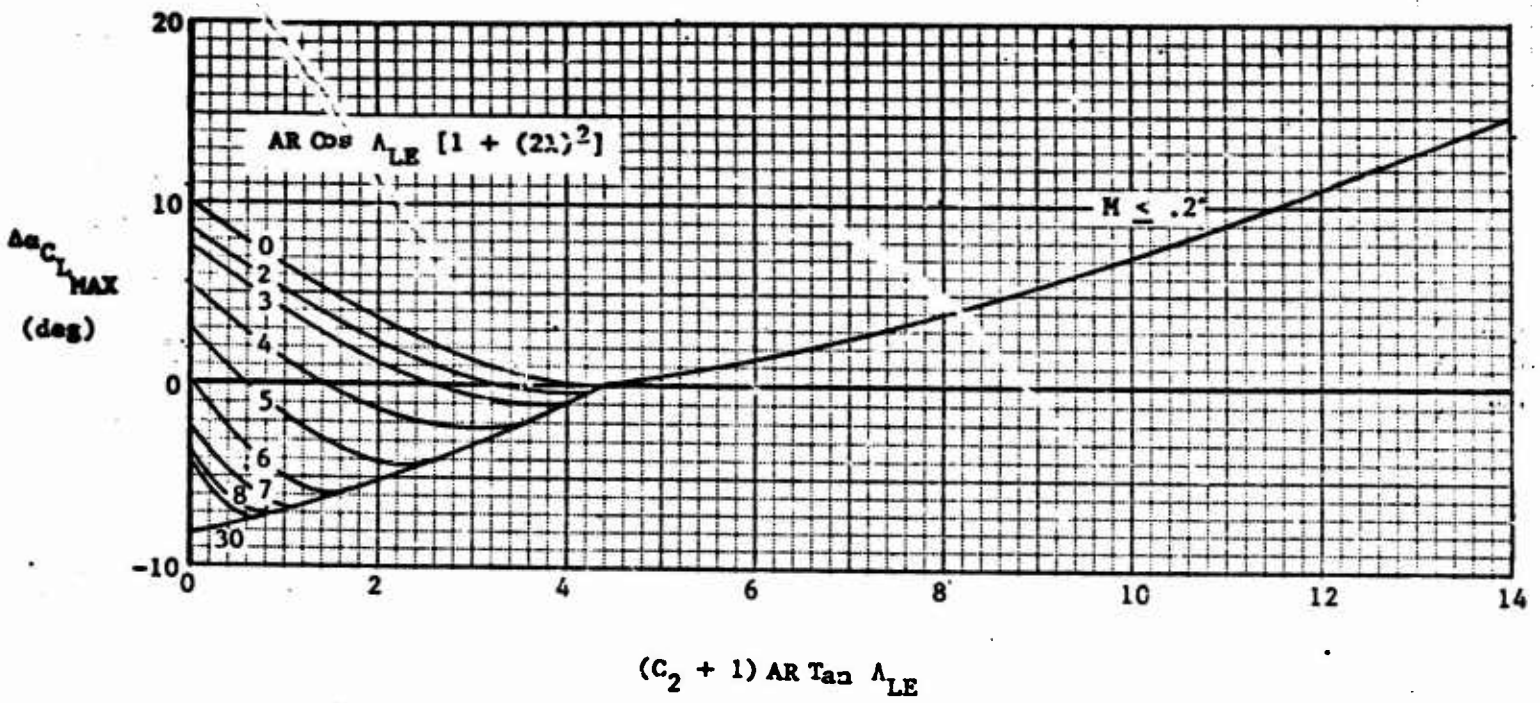

FIGURE 3-19 Angle-of-Attack Increment for Subsonic Maximum Lift of Low-Aspect-Ratio Wings

D. STEP 4 - FUSELAGE EFFECTS ON LIFT

1. α_o Assume no change in α_o due to the fuselage.

2. C_{L_α} The effect of the fuselage on the lift is considered to be composed of three (3) parts:

   a. Fuselage Nose - K_N

   b. Wing lift in presence of fuselage - $K_{W_{(B)}}$

   c. Lift on fuselage due to wing - $K_{B_{(W)}}$

Such that,

$$C_{L_{\alpha_{WB}}} = \left[K_N + K_{W_{(B)}} + K_{B_{(W)}} \right] C_{L_{\alpha_{EXP}}} \frac{S_{EXP}}{S_{REF}} \qquad \text{(III-6)}$$

K_N = 2 per radian based on body frontal area (A_B)

$K_{W_{(B)}}$ and $K_{B_{(W)}}$ from Figure 3-20.

$C_{L_{\alpha_{EXP}}}$ is the exposed lift curve slope computed by the same equation as Step 3b using exposed planform geometry.

S_{EXP} and S_{REF} are the exposed planform and aircraft reference areas respectively.

From empirical analysis of data for existing aircraft, the final value is given as

$$C_{L_{\alpha_{TOT}}} = (C_{L_{\alpha_W}} + C_{L_{\alpha_{WB}}}) / 2 \qquad \text{(III-7)}$$

where $C_{L_{\alpha_W}}$ was obtained in Step 3b.

3. $C_{L_{MAX}}$ The wing-fuselage maximum lift coefficient can be obtained from the following equations:

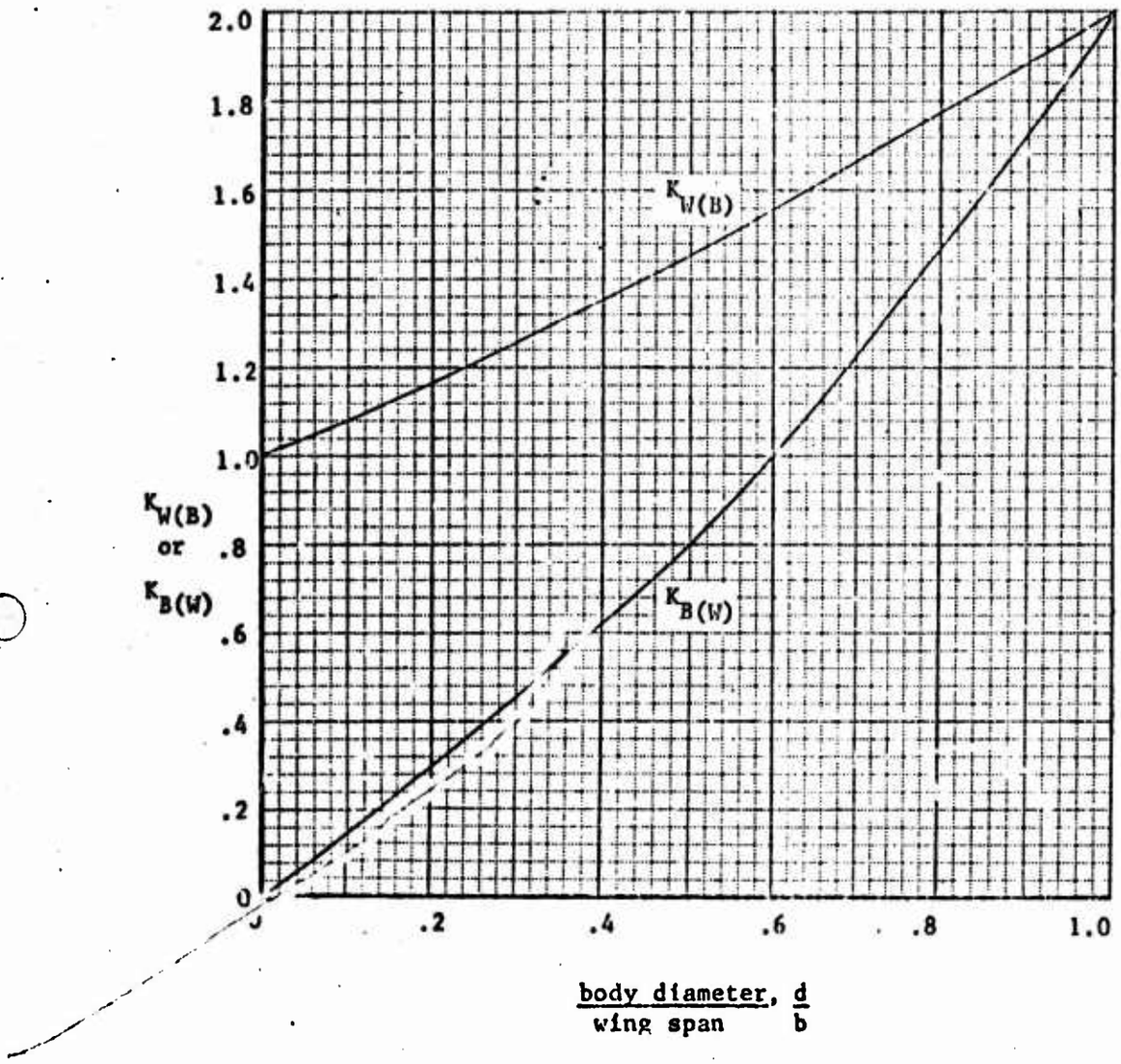

FIGURE 3-20 Lift Ratios $K_{W(B)}$ and $K_{B(W)}$ - Slender-Body-Theory-Fixed Incidence - All Speeds.

$$C_{L_{MAX(WB)}} = \frac{(C_{L_{MAX\ WB}})}{(C_{L_{MAX}})_W} \quad (C_{L_{MAX\ W}}) \qquad \text{(III-8)}$$

where the ratio $(C_{L_{MAX\ WB}}) \Big/ (C_{L_{MAX\ W}})$ can be obtained from Figure 3-21 and is a function

$f\ [\ d/b,\ (C_2 + 1)\ AR\ Tan\ A_{LE}\ ]$

$(C_{L_{MAX\ W}})$ comes from Step 3c.

To compute the angle-of-attack for maximum lift

$$(\alpha_{C_{L_{MAX\ WB}}}) = \frac{(\alpha_{C_{L_{MAX\ WB}}})}{(\alpha_{C_{L_{MAX}}})_W} \quad (\alpha_{C_{L_{MAX\ W}}}) \qquad \text{(III-9)}$$

where the ratio $\dfrac{(\alpha_{C_{L_{MAX\ WB}}})}{(\alpha_{C_{L_{MAX}}})}$ is given in Figure 3-22 and $(\alpha_{C_{L_{MAX\ W}}})$ comes from Step 3c.

E. STEP 5 - HIGH LIFT DEVICES - TRAILING EDGE FLAPS

This section determines the changes in the lift characteristics due to the use of a trailing edge flap. Five types of flaps are considered:

1. Plain
2. Split
3. Single slotted
4. Double slotted
5. Fowler

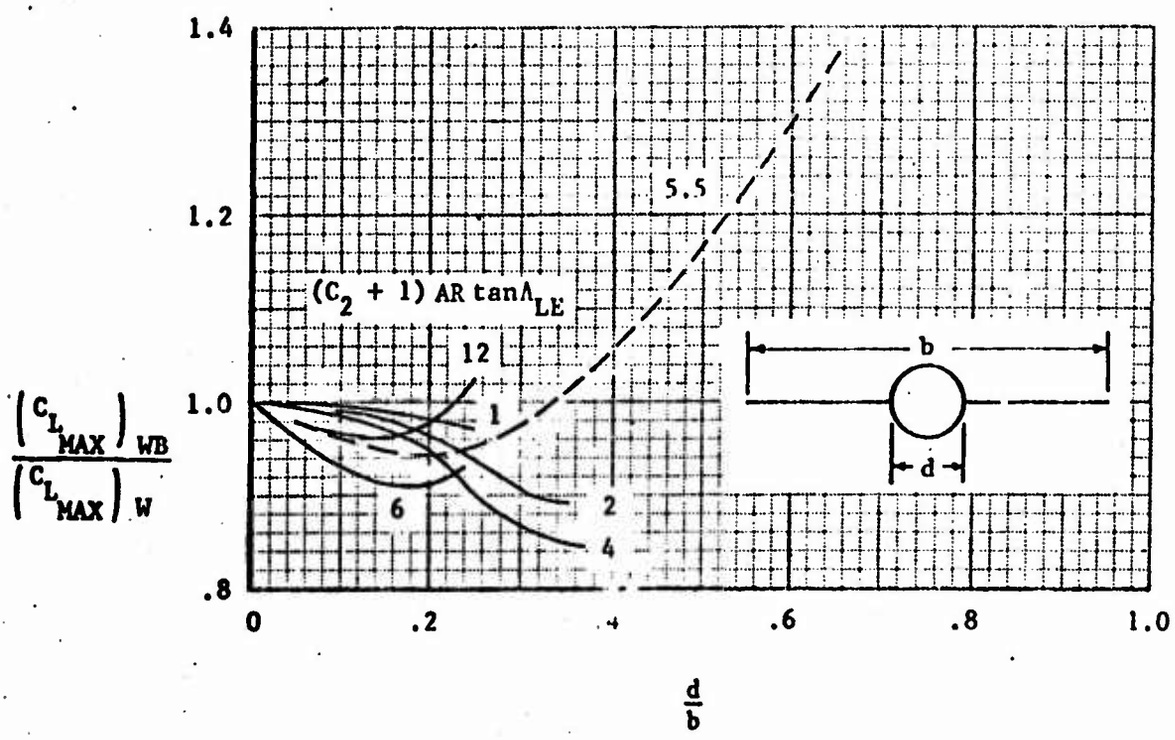

FIGURE 3-[illegible] Wing-Body Maximum Lift Coefficient.

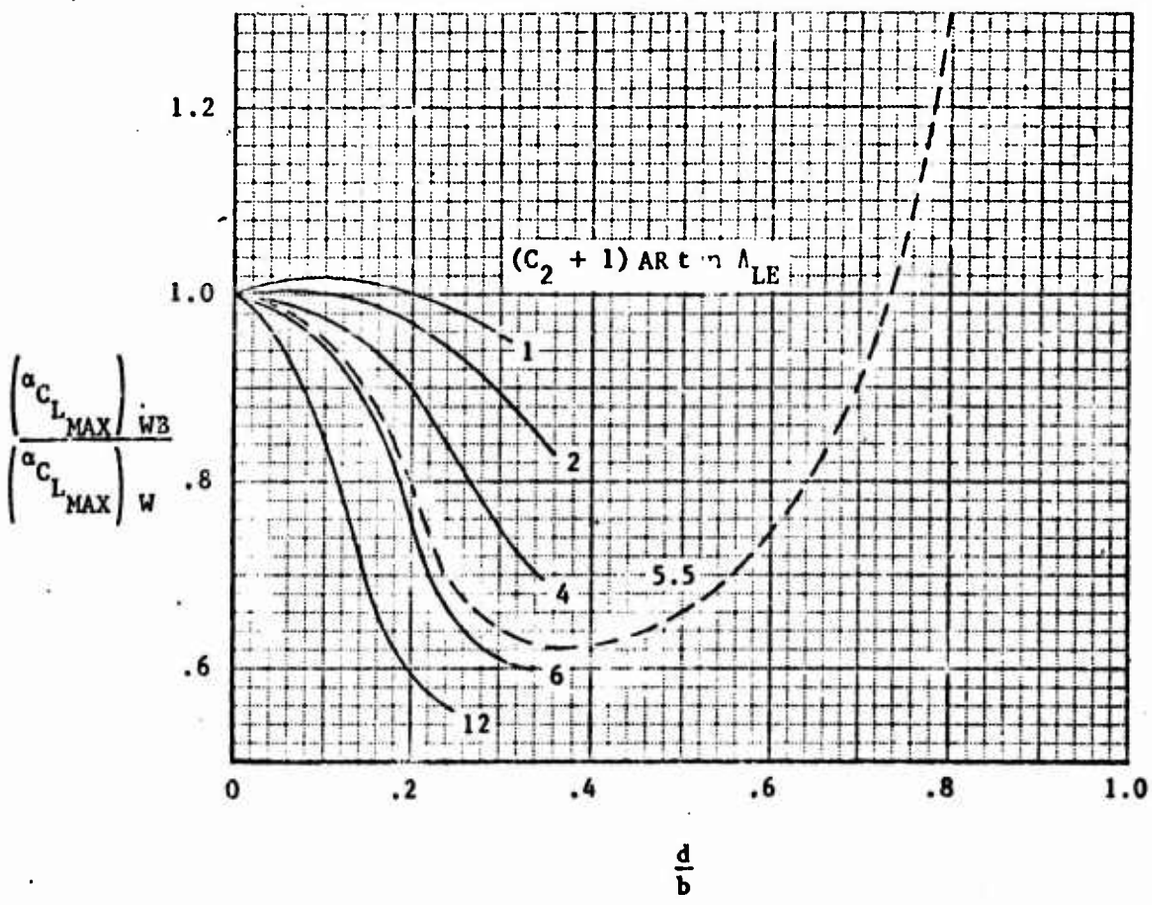

FIGURE 3-22 Wing-Body Angle-of-Attack for Maximum Lift.

The general procedure is to

1. First determine the changes to section characteristics.
2. Then account for planform effects.

The methods presented are those that give the best agreement with real-aircraft data. Therefore, some empirical constants and procedures will be used.

The nomenclature that will be used in all the cases is defined below.

ΔC_ℓ - increase in section lift coefficient in the linear C_{ℓ_α} range due to flap.

ΔC_L - Increase in wing lift coefficient in the linear C_{L_α} range due to flap.

$(C_{\ell_\alpha})_\delta$ - lift curve slope of the flapped airfoil section at flap deflection δ.

$(C_{L_\alpha})_\delta$ - lift curve slope of the wing with the flap deflection δ.

$\Delta C_{\ell_{max}}$ - increase in section maximum lift coefficient due to flap deflection δ.

$\Delta\alpha_o$ - change in zero-lift angle-of-attack due to deflecting the flap.

$\Delta\alpha_{C_{L_{MAX}}}$ - change in wing angle of attack for maximum lift coefficient due to flap deflection δ.

The various types of flaps and their effects will be discussed on the following pages.

1. Plain Flap

The procedure for computing the plain flap ΔC_L is unique from the others.

a. ΔC_L, wing lift increment is computed directly from

$$\Delta C_L = \lambda_1\lambda_2\lambda_3 \, (FA/F6) \qquad \text{(III-10)}$$

where FA/F6 = F (AR) Figure 3-23

$\lambda_1 = \lambda_1 (C_{F/C})$ Figure 3-24

$\lambda_2 = \lambda_2 (\delta_F)$ Figure 3-25

$\lambda_3 = \lambda_3 (b_{F/b})$ Figure 3-26

b. C_{L_α} for flap deflected is the same as the clean wing C_{L_α}

c. $\Delta\alpha_o$ the change in the zero lift angle-of-attack, is obtained from the relation.

$$\Delta\alpha_o = \frac{\Delta C_L}{C_{L_\alpha}} \quad (C_1) \qquad \text{(III-11)}$$

where $C_1 = 1.$ for AR > 4

$C_1 = 1.2$ for AR < 4

d. $\Delta C_{\ell_{max}}$ - The increase in section maximum lift coefficient is obtained from

$$\Delta C_{\ell_{max}} = k_1 k_2 (\Delta C_{\ell_{max\ base}})$$

where $(\Delta C_{\ell_{max}})_{base}$ - is the reference increment obtained from Figure 3-27, curve D and a function of the airfoil thickness t/ C.

k_1 - is a function of $C_{F/C}$ correcting for the base value of $C_{F/C} = .25$ (Figure 3-28).

k_2 - is a deflection correction factor accounting for the base value for a plain flap of $\delta_F = 60^o$ (Figure 3-29).

e. The wing increase in $C_{L_{MAX}}$ can now be computed from

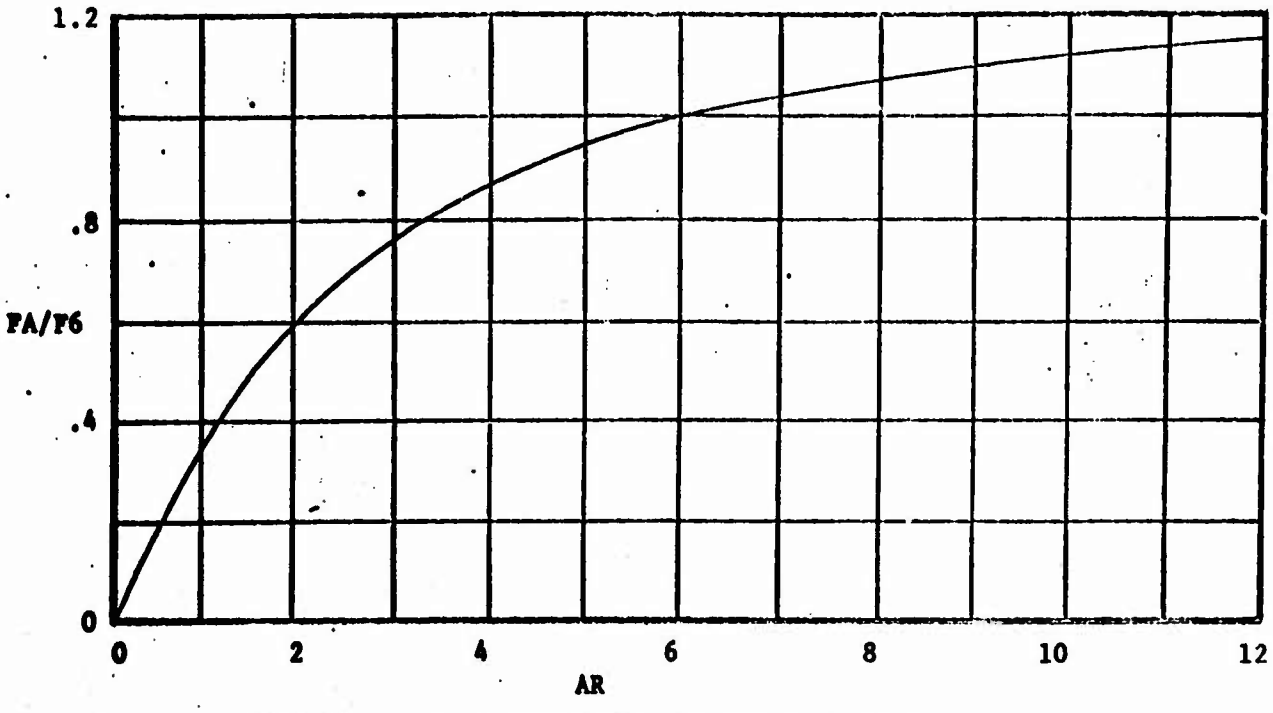

FIGURE 3-23: Aspect Ratio Correccion Factor.

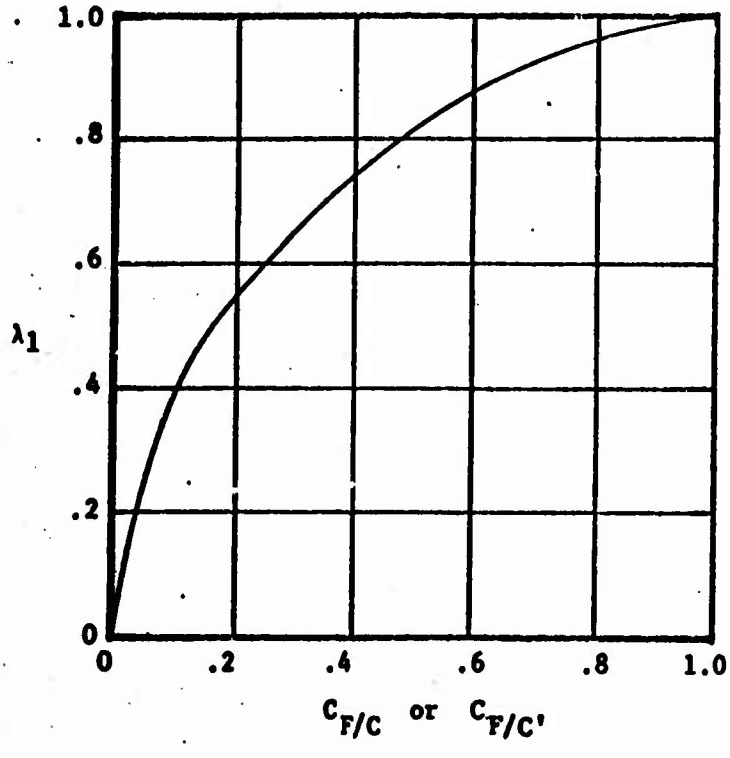

FIGURE 3-24: Flap Chord Correction Factor.

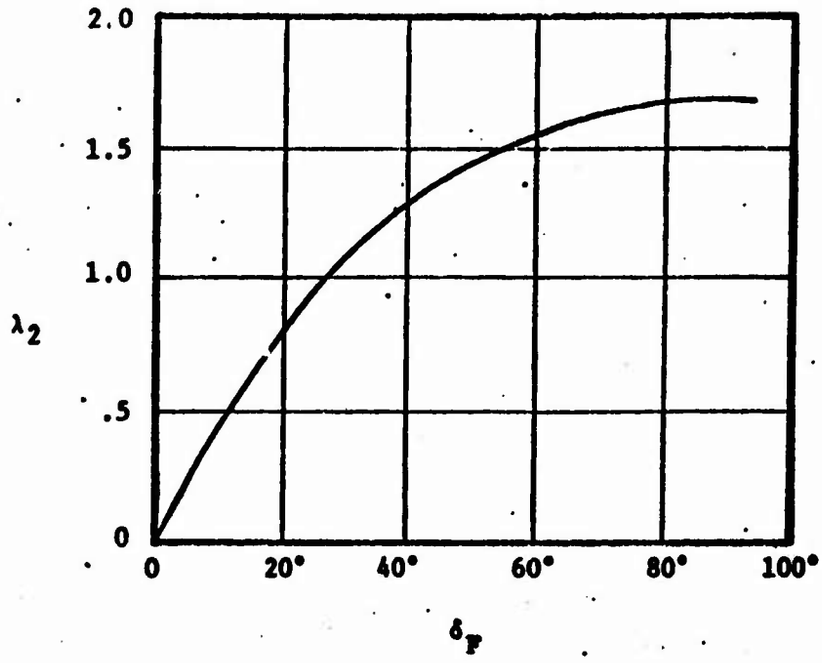

FIGURE 3-25: Flap Deflection Correction Factor - Plain Flap

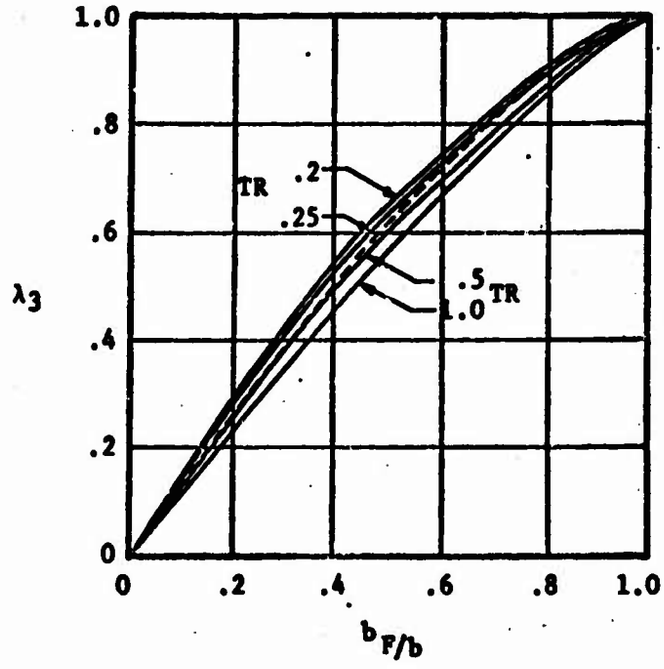

FIGURE 3-26: Flap Span Correction Factor.

$$\Delta C'_{L_{MAX}} = \Delta C_{\ell_{MAX}} \frac{S_F}{S_{REF}} (1 - .08 \cos^2 \Lambda_{C/4}) \cos^{3/4} \Lambda_{C/4} \qquad \text{(III-12)}$$

where $\Delta C_{\ell_{max}}$ comes from part d

S_F is the wing area affected by the flap

S_{REF} is the wing reference area

$$\Lambda_{C/4} = \text{Tan}^{-1} \left[\text{Tan} \Lambda_{LE} - \frac{(1 - TR)}{(1 + TR)AR)} \right]$$

f. $\Delta\alpha_{C_{L_{MAX}}}$ - The change in the angle-of-attack for maximum lift can be obtained as follows:

$$\text{for } AR < 4, \ \Delta\alpha_{C_{L_{MAX}}} = -.5 \left(\frac{\Delta C_{L_{MAX}}}{C_{L_\alpha}} \right)$$

$$AR > 4, \ \Delta\alpha_{C_{L_{MAX}}} = 0$$

2. Split Flap

The section lift characteristics for the split flap are obtained as follows:

a. $\Delta C_\ell = K (\Delta C_\ell)_{C_{F/C}}$

where $(\Delta C_\ell)_{C_{F/C}} = f(\delta_F, t/C)$ based on $C_{F/C} = .2$ and can be obtained from Figure 3-30.

K is obtained from Figure 3-31 and corrects for $C_{F/C}$ other than .2

b. $\Delta C_{\ell_{max}} = k_1 k_2 (\Delta C_{\ell_{max\ base}})$

this method is the same as for the plain flap but is briefly repeated

$(\Delta C_{\ell_{max\ base}})$ Figure 3-27

k_1 Figure 3-28

k_2 Figure 3-29

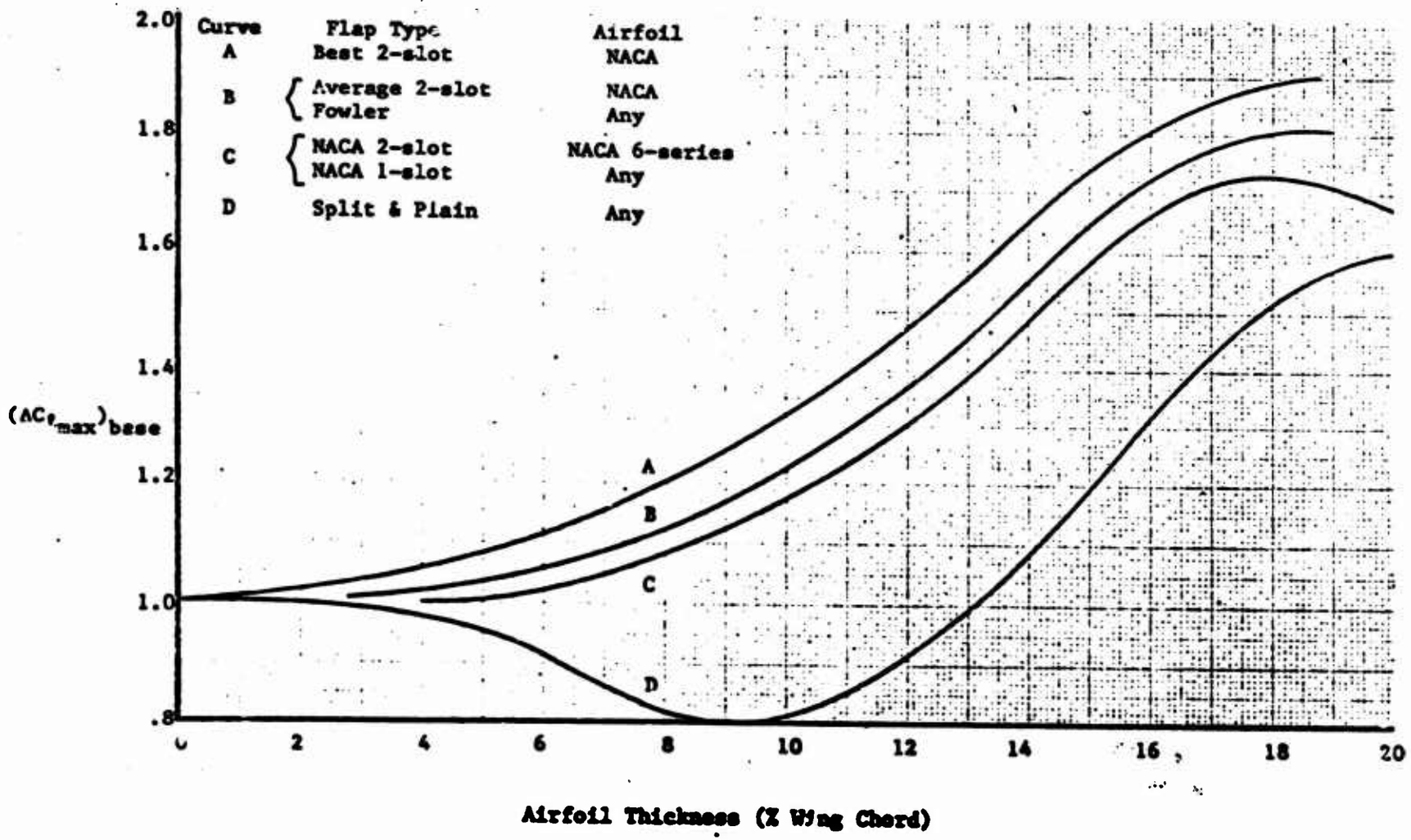

FIGURE 3-27 Maximum-Lift Increments for 25%-Chord Flaps at Reference Flap Angle.

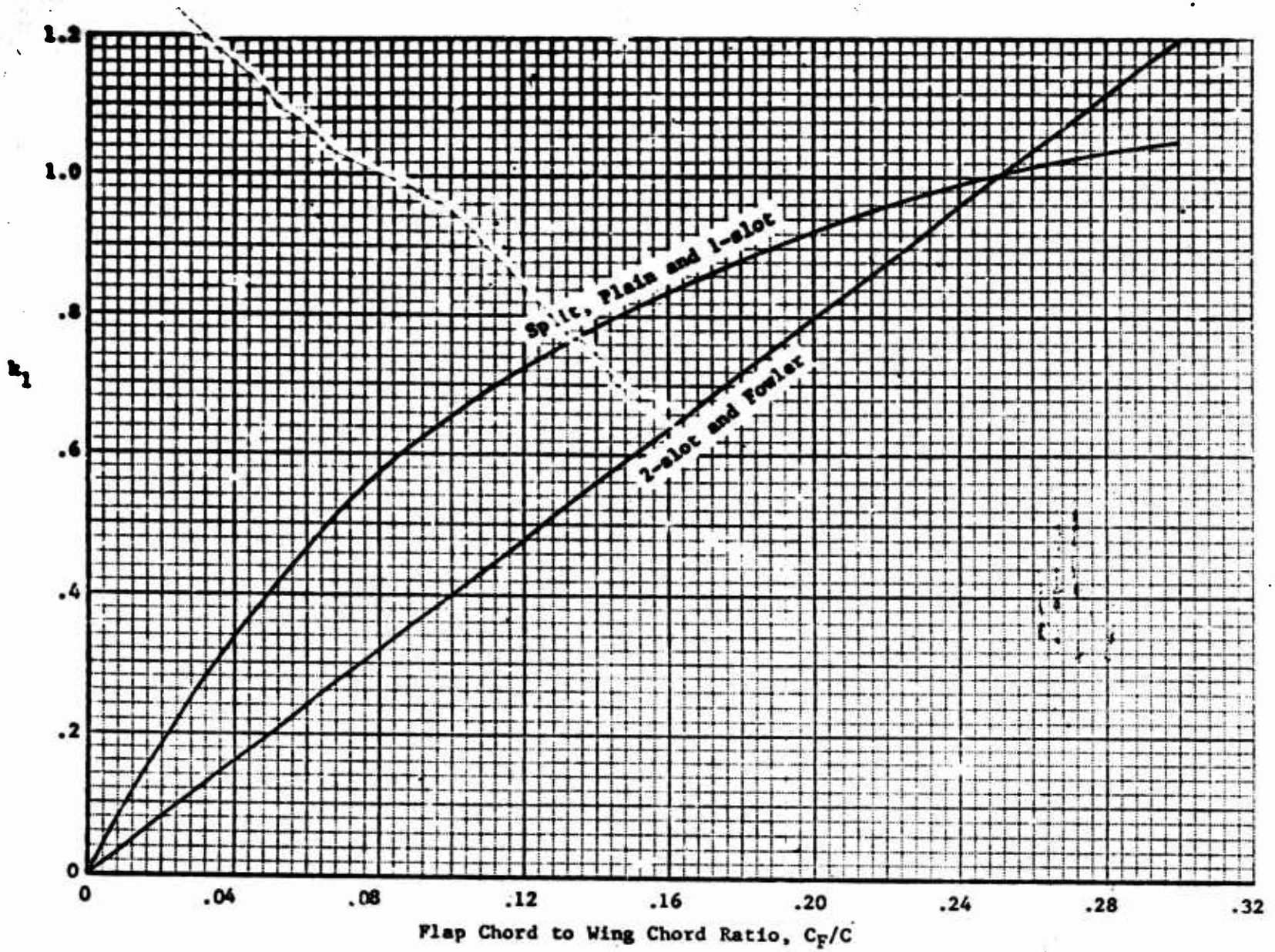

FIGURE 3-28 Flap Chord Correction Factor.

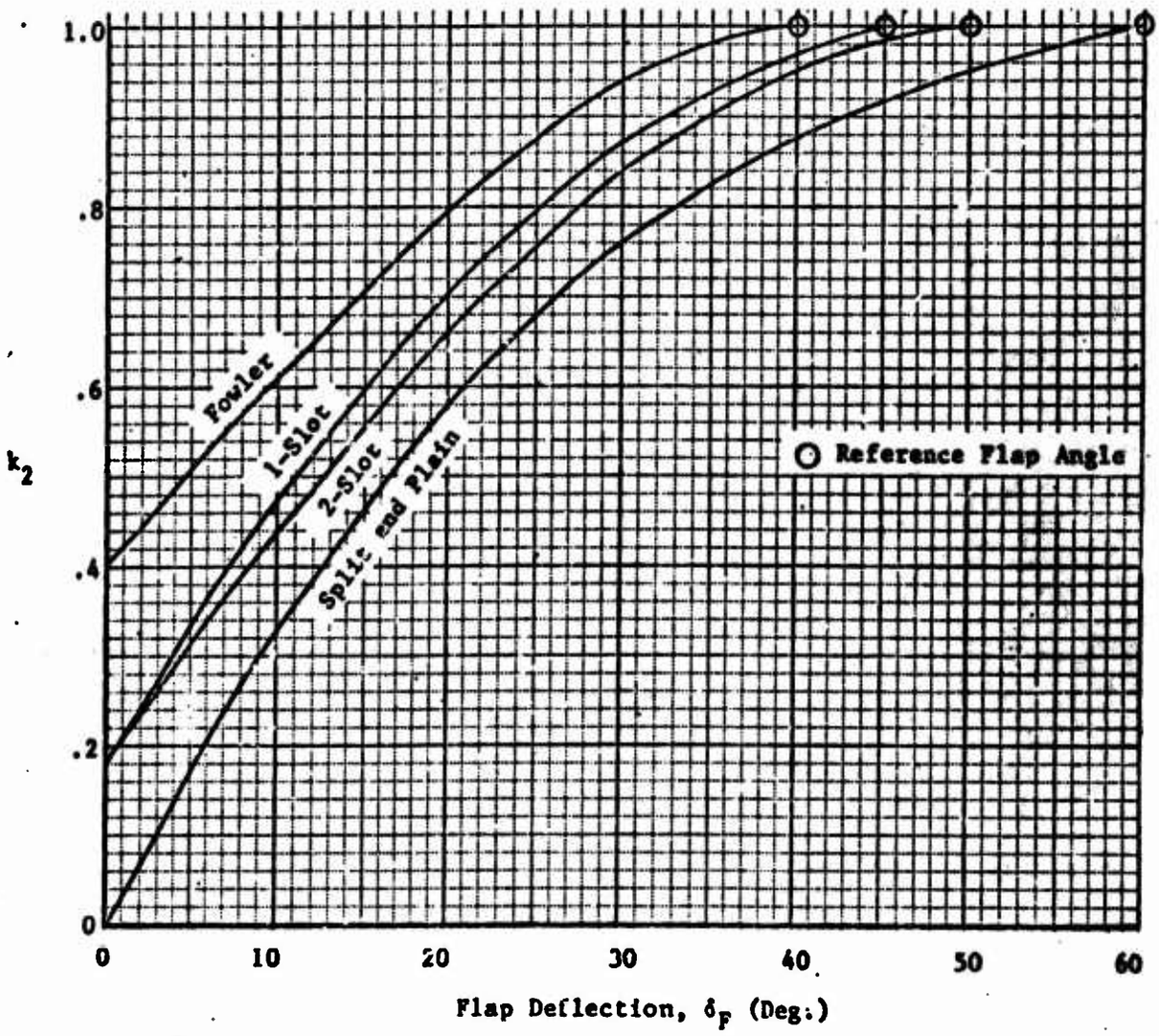

FIGURE 3-29 Flap Angle Correction Factor.

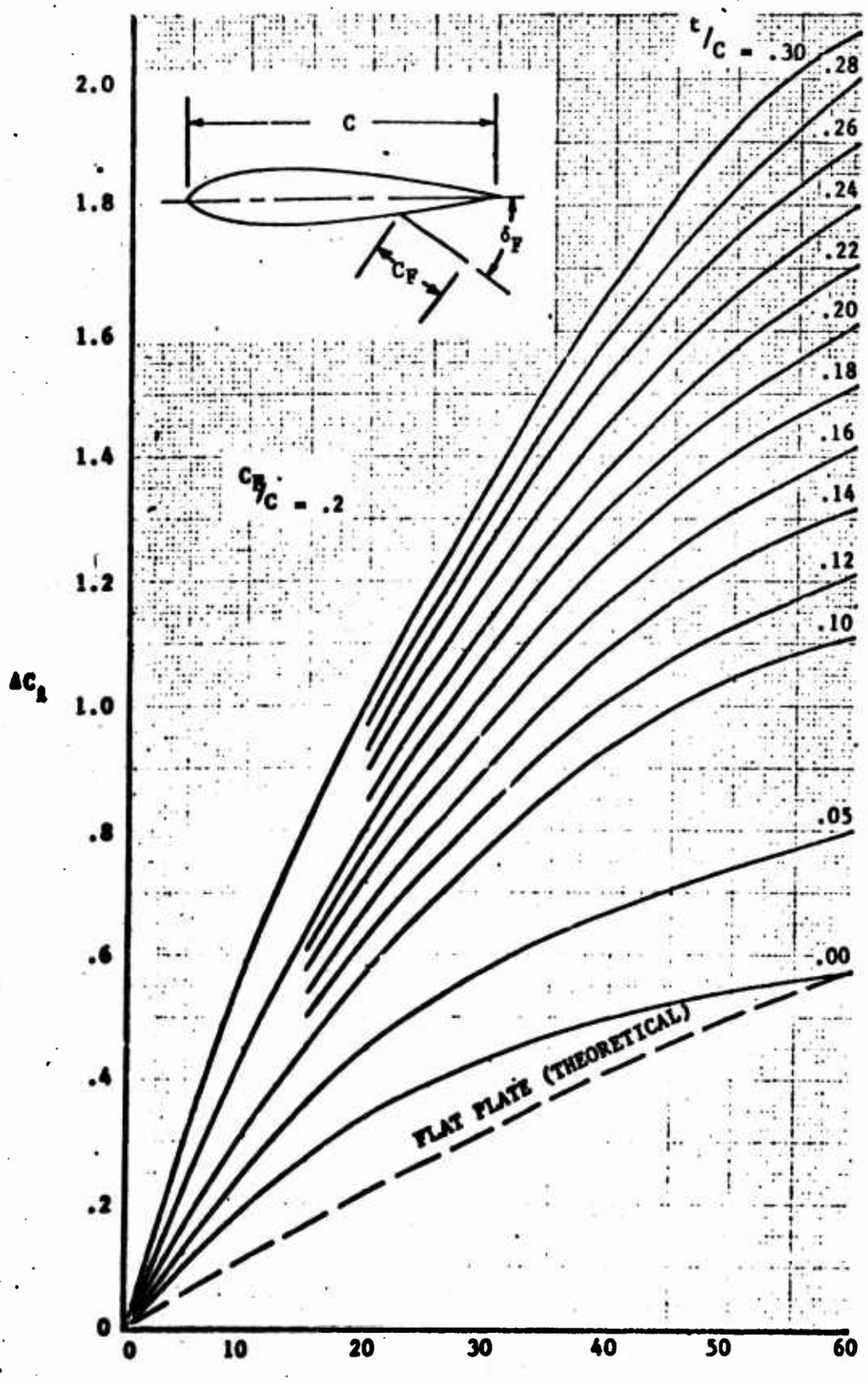

FIGURE 3-30 Lift-Coefficient Increment for 20%-Chord Split Flaps.

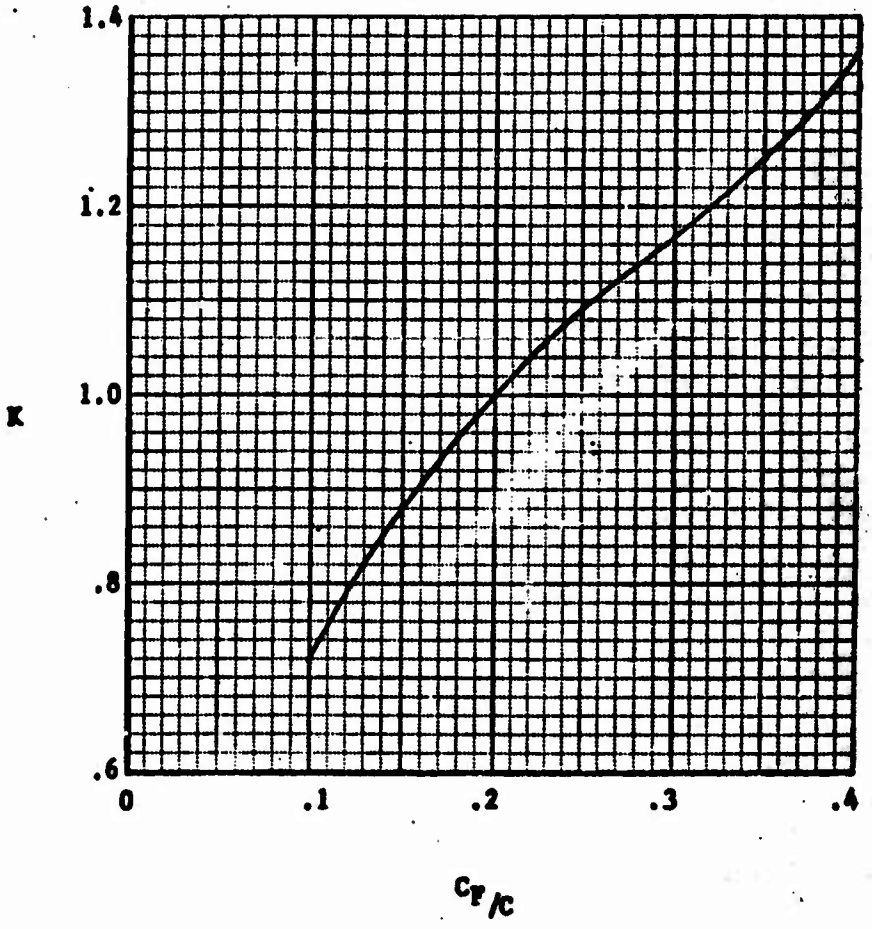

FIGURE 3-31 Correction Factor for Chord Ratio of Split Flaps.

c. The wing increments can now be computed from

$$\Delta C_L = \Delta C_\ell \left(\frac{C_{L_\alpha}}{C_{\ell_\alpha}}\right)\left[\frac{(\alpha_\delta)_{C_L}}{(\alpha_\delta)_{C_\ell}}\right] K_b \qquad \text{(III-13)}$$

where ΔC_ℓ is obtained from part (a)

$\frac{C_{L_\alpha}}{C_{\ell_\alpha}}$ is the ratio of the clean wing lift curve slope to the clean section lift curve slope.

$\left[\frac{(\alpha_\delta)_{C_L}}{(\alpha_\delta)_{C_\ell}}\right]$ is obtained from Figure 3-32

where $(\alpha_\delta)_{C_\ell} = -\frac{(C_{\ell_\delta})_\alpha}{(C_{\ell_\alpha})_\delta}$

and $(C_{\ell_\delta})_\alpha = \frac{\Delta C_\ell \text{(from part (a))}}{\delta_F \text{ (flap deflection)}}$

$(C_{\ell_\alpha})_\delta$ is the flapped section lift curve slope which for a split flap = C_{ℓ_α}

K_b is a span factor correction which is obtained from Figure 3-33.

d. C_{L_α} is the same as the clean wing-fuselage lift curve slope.

e. $\Delta\alpha_o$ The change in angle-of-attack at zero-lift is obtained from

$$\Delta\alpha_o = \frac{\Delta C_L}{C_{L_\alpha}} (C_1) \qquad \text{(III-14)}$$

where $C_1 = 1.$ for AR > 4

$C_1 = 1.2$ for AR < 4

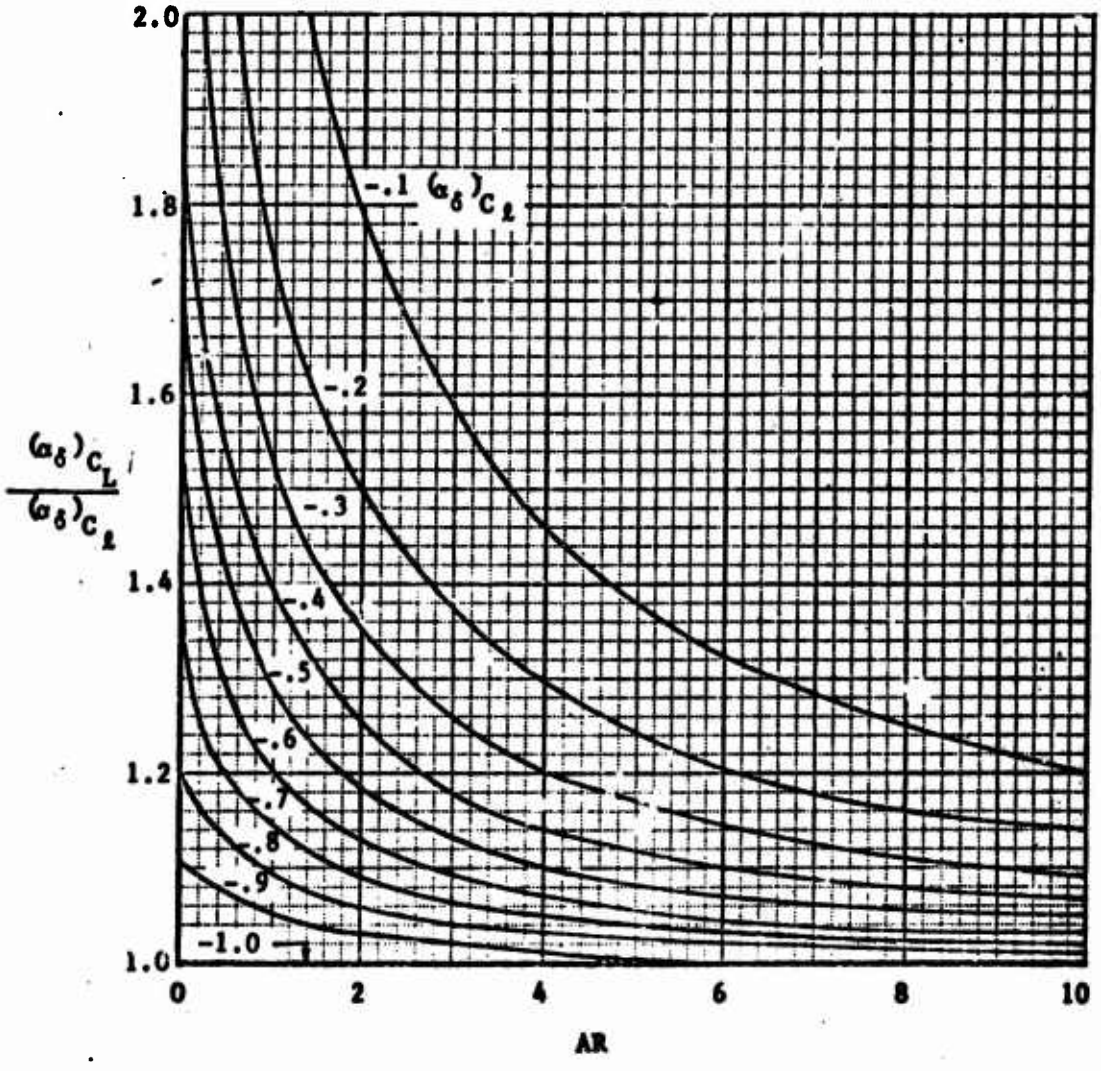

FIGURE 3-32 Flap Chord Factor.

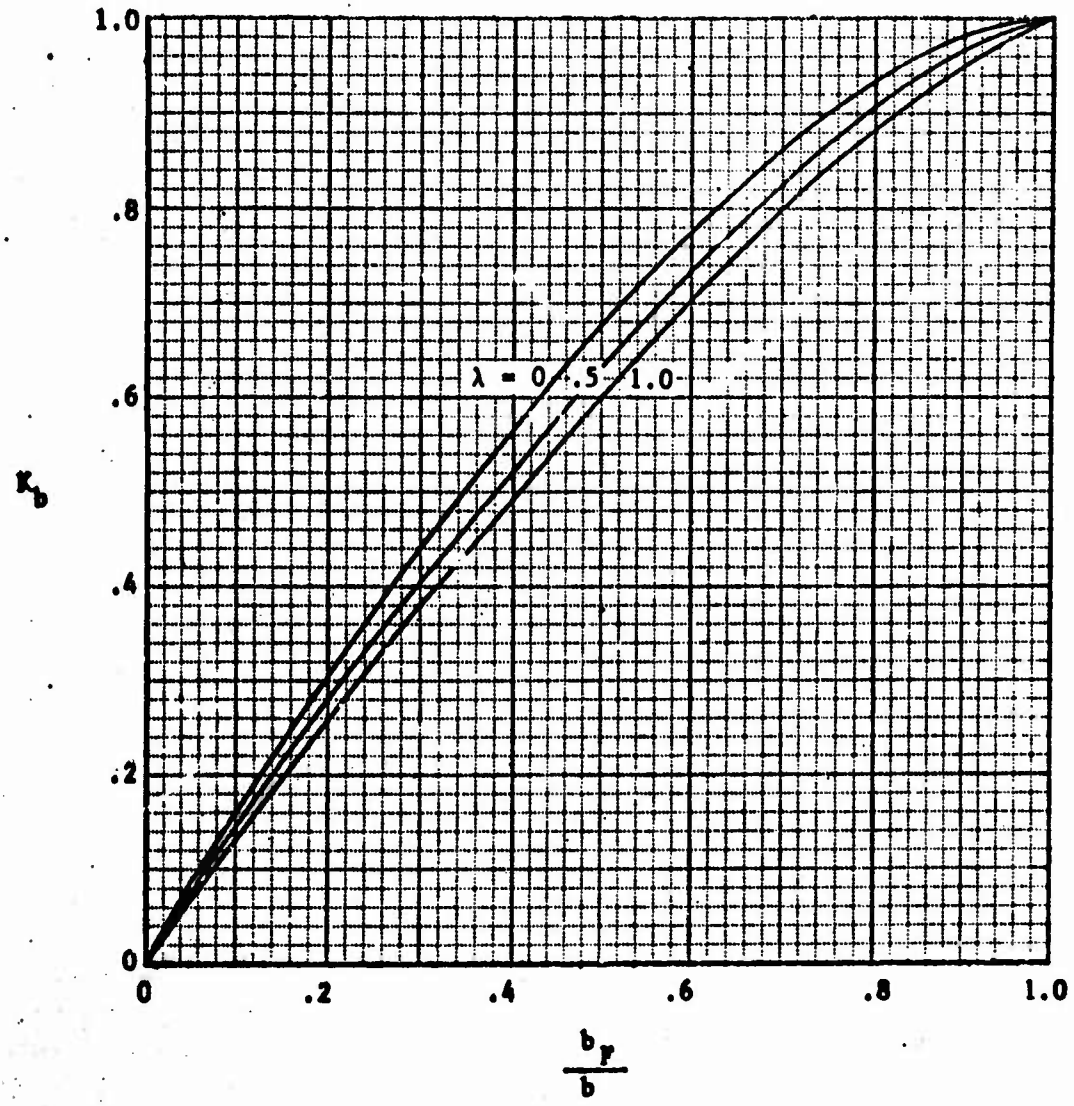

FIGURE 3-33 Span Factor for Inboard Flaps.

f. $\Delta C_{L_{MAX}} = \Delta C_{\ell_{max}} \frac{S_F}{S_{REF}} (1 - .08 \cos^2 \Lambda_{C/4}) \cos^{3/4} \Lambda_{C/4}$ (III-15)

where $\Delta C_{\ell_{max}}$ comes from part b.

S_F is the wing area affected by the flap

S_{REF} is the wing reference area

$\Lambda_{C/4} = \text{Tan}^{-1} \left[\text{Tan } \Lambda_{LE} - \frac{(1 - TR)}{(1 + TR)\ AR} \right]$

g. $\Delta\alpha_{C_{L_{MAX}}}$ - The change in the angle-of-attack for maximum lift can be obtained as follows:

for $AR < 4$ $\Delta\alpha_{C_{L_{MAX}}} = -.5 \left(\frac{\Delta C_{L_{MAX}}}{C_{L_\alpha}} \right)$

$AR > 4$ $\Delta\alpha_{C_{L_{MAX}}} = 0$

3. <u>Single Slotted Flaps</u>

For the purposes of this study a single-slotted flap is considered to have a fixed-hinge position (non-translating)

a. ΔC_ℓ the section lift increment is

$\Delta C_\ell = f \ (\delta_F, C_{F/C})$

from Figure 3-34.

b. ΔC_L the wing lift increment is

$\Delta C_L = \Delta C_\ell \ \frac{C_{L_\alpha}}{C_{\ell_\alpha}} \left[\frac{(\alpha_\delta)_{C_L}}{(\alpha_\delta)_{C_\ell}} \right] K_b$ (III-16)

The details of this are described in the split flap Section 3, but is briefly repeated here

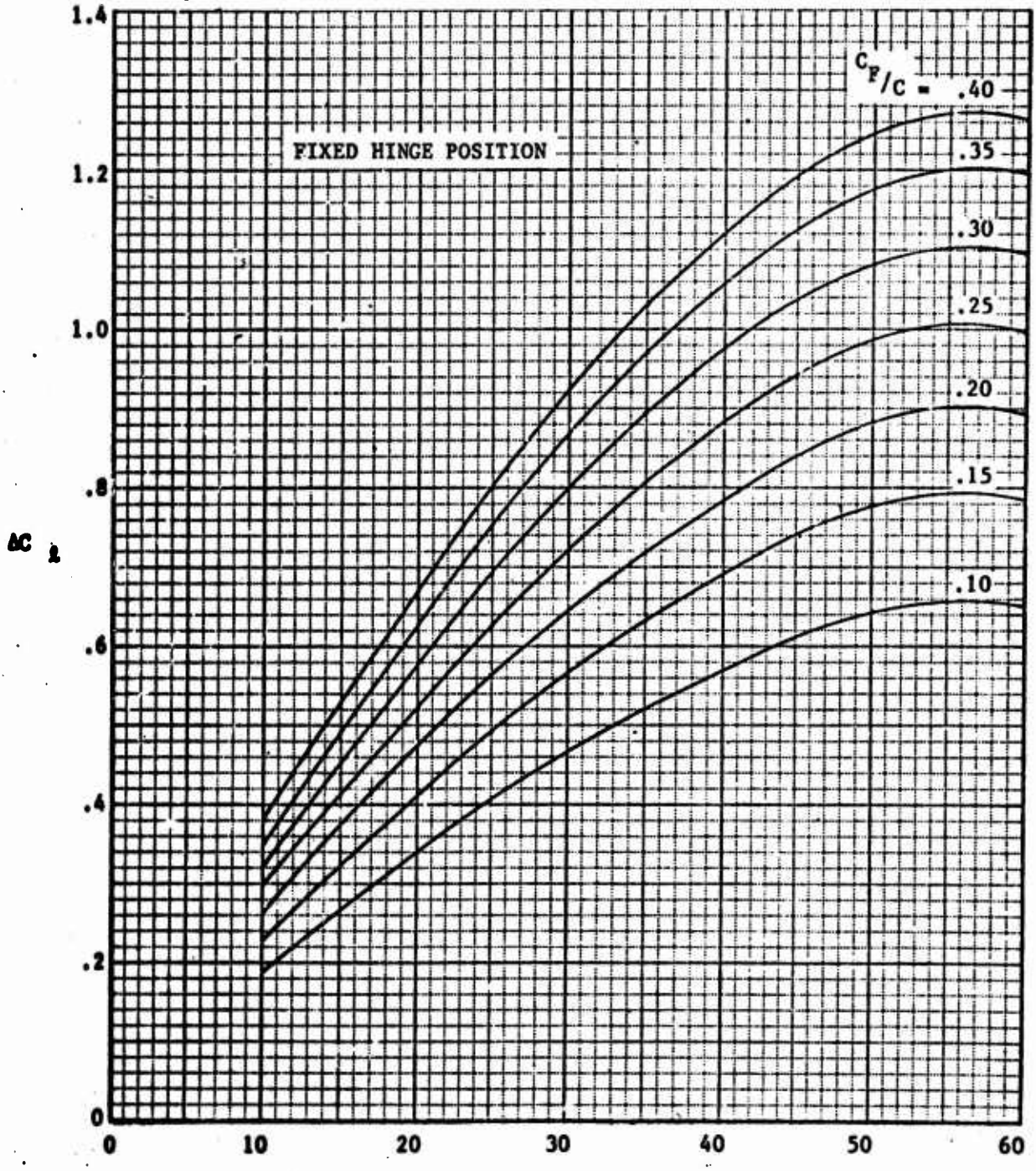

FIGURE 3-34 Lift-Coefficient Increments for Single Slotted Flaps.

$\frac{C_{L_\alpha}}{C_{\ell_\alpha}}$ ratio of the wing to section lift curve slope.

$\left[\frac{(\alpha_\delta)_{C_L}}{(\alpha_\delta)_{C_\ell}}\right]$ from Figure 3-32

K_b from Figure 3-33

c. C_{L_α} for the flap deflected is the same as the clean wing C_{L_α}

d. $\Delta\alpha_o$ The change in angle-of-attack at zero-lift is obtained from

$$\Delta\alpha_o = \frac{\Delta C_L}{C_{L_\alpha}} (C_1) \qquad \text{(III-17)}$$

where $C_1 = 1.$ for $AR > 4$

$C_1 = 1.2$ for $AR < 4$

e. $\Delta C_{\ell_{max}}$ is the increase in the section maximum lift coefficient and as described previously

$$\Delta C_{\ell_{max}} = k_1 k_2 k_3 (\Delta C_{\ell_{max\ base}})$$

$(\Delta C_{\ell_{max\ base}})$ Figure 3-27

k_1 Figure 3-28

k_2 Figure 3-29

k_3 is an angle correction factor obtained from Figure 3-35.

f. The total wing increment in lift can be computed from

$$\Delta C_{L_{MAX}} = \Delta C_{\ell_{max}} \frac{S_F}{S_{REF}} (1 - .08 \cos^2 \Lambda_{C/4}) \cos^{3/4} \Lambda_{C/4} \qquad \text{(III-18)}$$

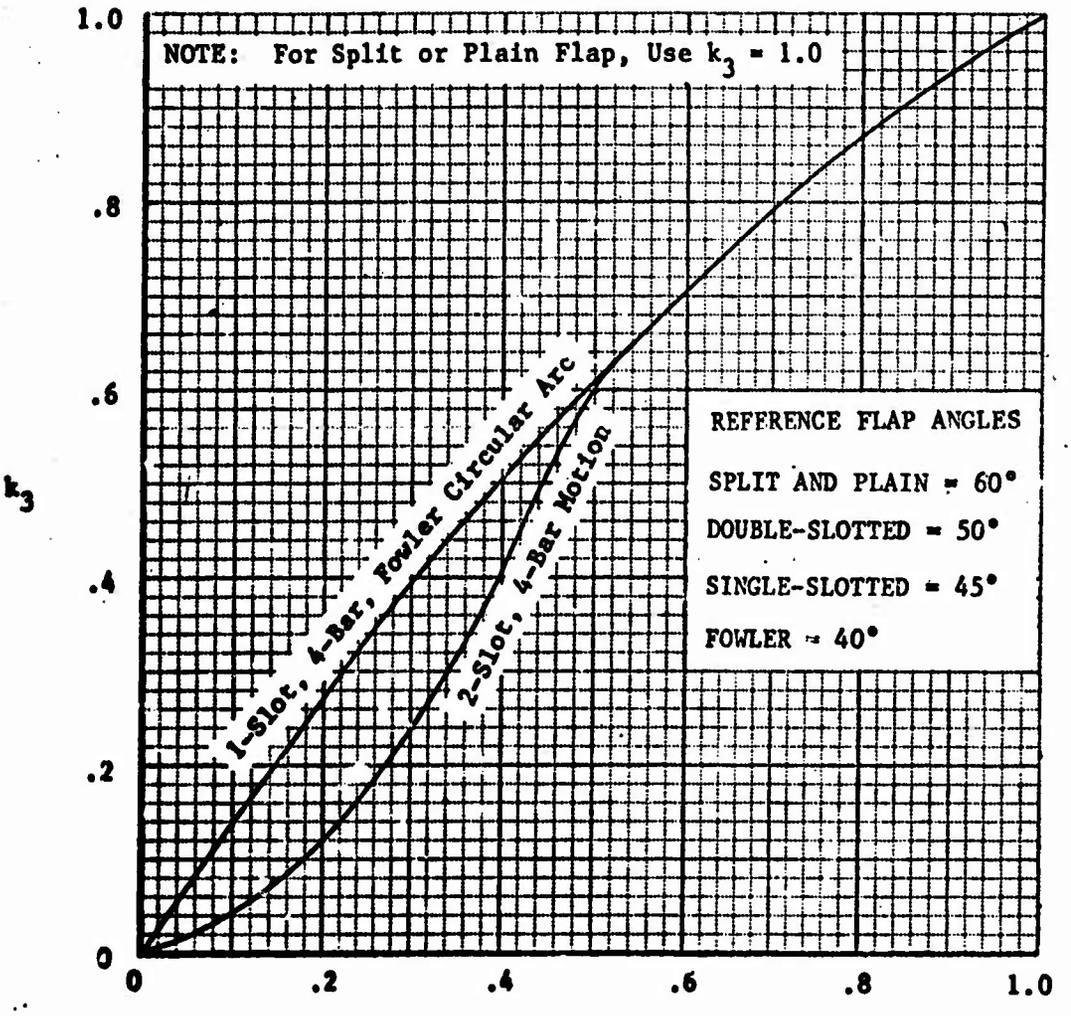

FIGURE 3-33: Flap Motion Correction Factor.

where $\Delta C_{\ell_{max}}$ comes from part e.

S_F is the wing area affected by the flap

S_{REF} is the wing reference area,

$$\Lambda_{C/4} = \text{Tan}^{-1}\left[\text{Tan}\,\Lambda_{LE} - \frac{(1 - TR)}{(1 + TR)AR}\right]$$

g. $\Delta\alpha_{C_{L_{MAX}}}$ - The change in the angle-of-attack for maximum lift can be obtained as follows:

$$\text{for AR} < 4 \quad \Delta\alpha_{C_{L_{MAX}}} = -.5\,\frac{\Delta C_{L_{MAX}}}{C_{L_\alpha}}$$

$$\text{AR} > 4 \quad \Delta\alpha_{C_{L_{MAX}}} = 0$$

4. Double Slotted Flap

The procedure for obtaining the lift characteristics of a double slotted flap is as follows:

a. The wing lift increment ΔC_L is computed directly from

$$\Delta C_L = \left[(\lambda_1\,\lambda_2)_{\text{Flap 1}} + (\lambda_1\,\lambda_{22})_{\text{Flap 2}}\right]\lambda_3\,(FA/F6) \qquad \text{(III-19)}$$

where $(\lambda_1\,\lambda_2)_{\text{Flap 1}}$ is the increment based on the total flap chord and the deflection of the first flap and is obtained from Figures 3-24 and 3-36.

$(\lambda_1 \cdot \lambda_{22})_{\text{Flap 2}}$ is the increment based on the second (and largest) flap chord and its deflection and is obtained from Figures 3-24 and 3-37.

λ_3 from Figure 3-26

FA/F6 from Figure 3-23

b. C_{L_α} - For any type of flap where a translation of the flap chord occurs the lift curve slope can be obtained from

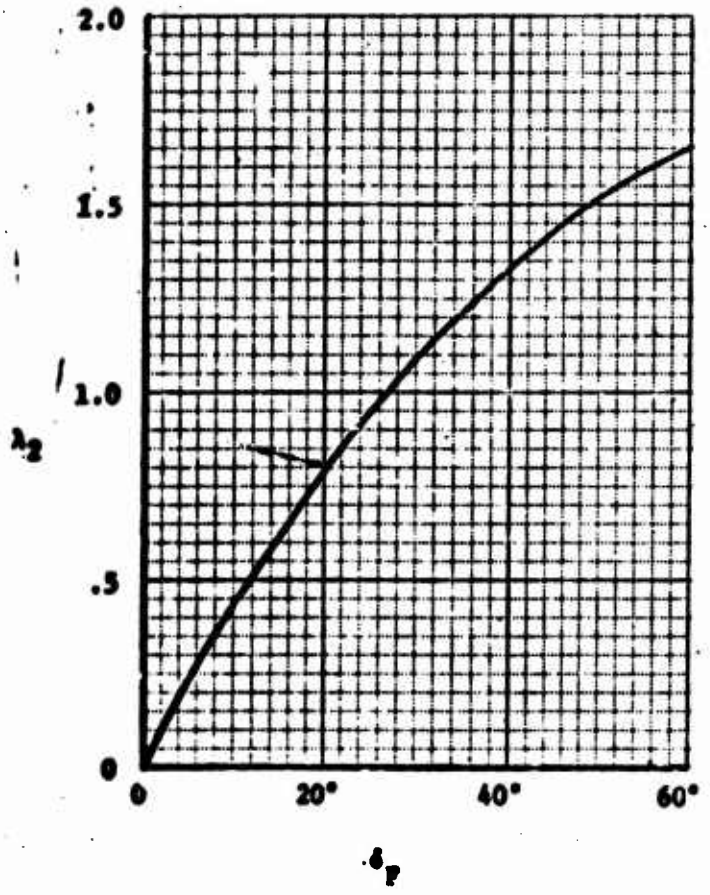

FIGURE 3-36: Flap Deflection Correction Factor - Double Slotted (1st Flap)

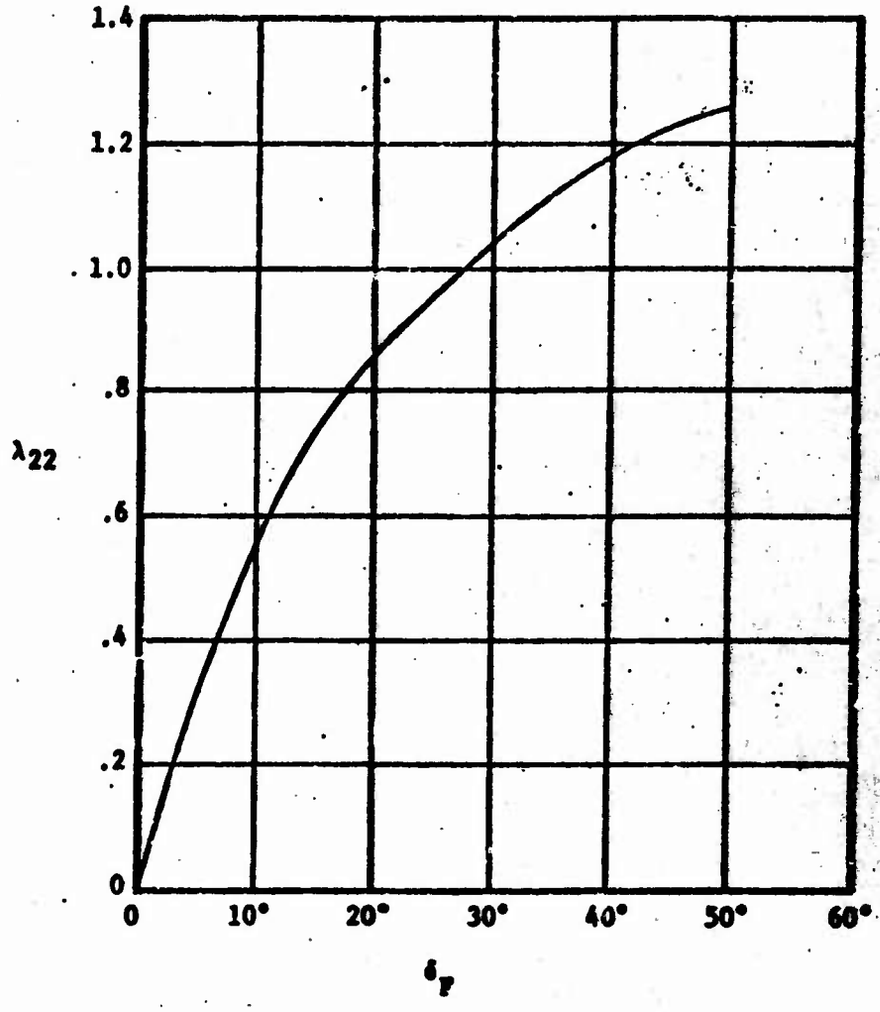

FIGURE 3-37: Flap Deflection Correction Factor- Double Slotted (2nd Flap)

$$C_{L_\alpha} = (C_{L_{\alpha\,\delta}}) - \left[\left(\frac{C'}{C} - 1\right)\frac{S_F}{S_{REF}} + 1\right](C_{L_{\alpha\,\delta=0}}) \qquad \text{(III-20)}$$

c. $\Delta\alpha_o$ The change in angle-of-attack at zero-lift is obtained from

$$\Delta\alpha_o = \frac{\Delta C_L}{C_{L_\alpha}}\frac{C'}{C}(C_1)$$

where C_1 = 1. for Ak > 4

C_1 = 1.2 for AR < 4

C'/C is the deflected to undeflected wing chord ratio.

d. $\Delta C_{\ell_{max}}$ is the increase in the section maximum lift coefficient and as described previously

$$\Delta C_{\ell_{max}} = k_1\, k_2\, k_3\, (\Delta C_{\ell_{max\ base}})$$

$(\Delta C_{\ell_{max\ base}})$ Figure 3-27

k_1 Figure 3-28

k_2 Figure 3-29

k_3 is an angle correction factor obtained from Figure 3-35.

e. The total wing increment in lift can be computed from

$$\Delta C_{L_{MAX}} = \Delta C_{\ell_{max}}\frac{S_F}{S_{TOT}}(1 - .08\,\mathrm{Cos}^2\,\Lambda_{C/4})\,\mathrm{Cos}^{3/4}\Lambda_{C/4} \qquad \text{(III-21)}$$

where $\Delta C_{\ell_{max}}$ comes from part (d)

S_F is the wing area affected by the flap

S_{REF} is the wing reference area

$$\Lambda_{C/4} = \mathrm{Tan}^{-1}\left[\mathrm{Tan}\,\Lambda_{LE} - \frac{(1 - TR)}{(1 + TR)AR}\right]$$

f. $\Delta\alpha_{C_{L_{MAX}}}$ - The change in the angle-of-attack for maximum lift can be obtained as follows:

for AR < 4 $\quad \Delta\alpha_{C_{L_{MAX}}} = -.5 \left(\frac{\Delta C_{L_{MAX}}}{C_{L_\alpha}}\right)$

AR > 4 $\quad \Delta\alpha_{C_{L_{MAX}}} = 0$

5. Fowler Flap

For the purpose of this study a Fowler Flap is considered to be a single-slotted flap, that when extended is in an optimum position.

a. ΔC_ℓ, the section lift increment is computed from

$$\Delta C_\ell = \frac{\Delta C_\ell}{\Delta C'_\ell} \Delta C'_\ell$$

where $\Delta C'_\ell$ comes from Figure 3-38

and $\frac{\Delta C_\ell}{\Delta C'_\ell}$ is obtained from Figure 3-39

and is a function of $(C'/C, C_{\ell/\Delta C'_\ell})$.

1. C'/C is the ratio of airfoil chord with flap extended to airfoil chord with flap retracted.

2. $C_{\ell/\Delta C'_\ell}$; C_ℓ is the airfoil section (no flaps) lift coefficient at $\alpha = 10^\circ$ and $\Delta C'_\ell$ comes from Figure 3-38

b. ΔC_L the wing lift increment is

$$\Delta C_L = \Delta C_\ell \frac{C_{L_\alpha}}{C_{\ell_\alpha}} \left[\frac{(\alpha_\delta)_{C_L}}{(\alpha_\delta)_{C_\ell}}\right] K_b . \qquad \text{(III-22)}$$

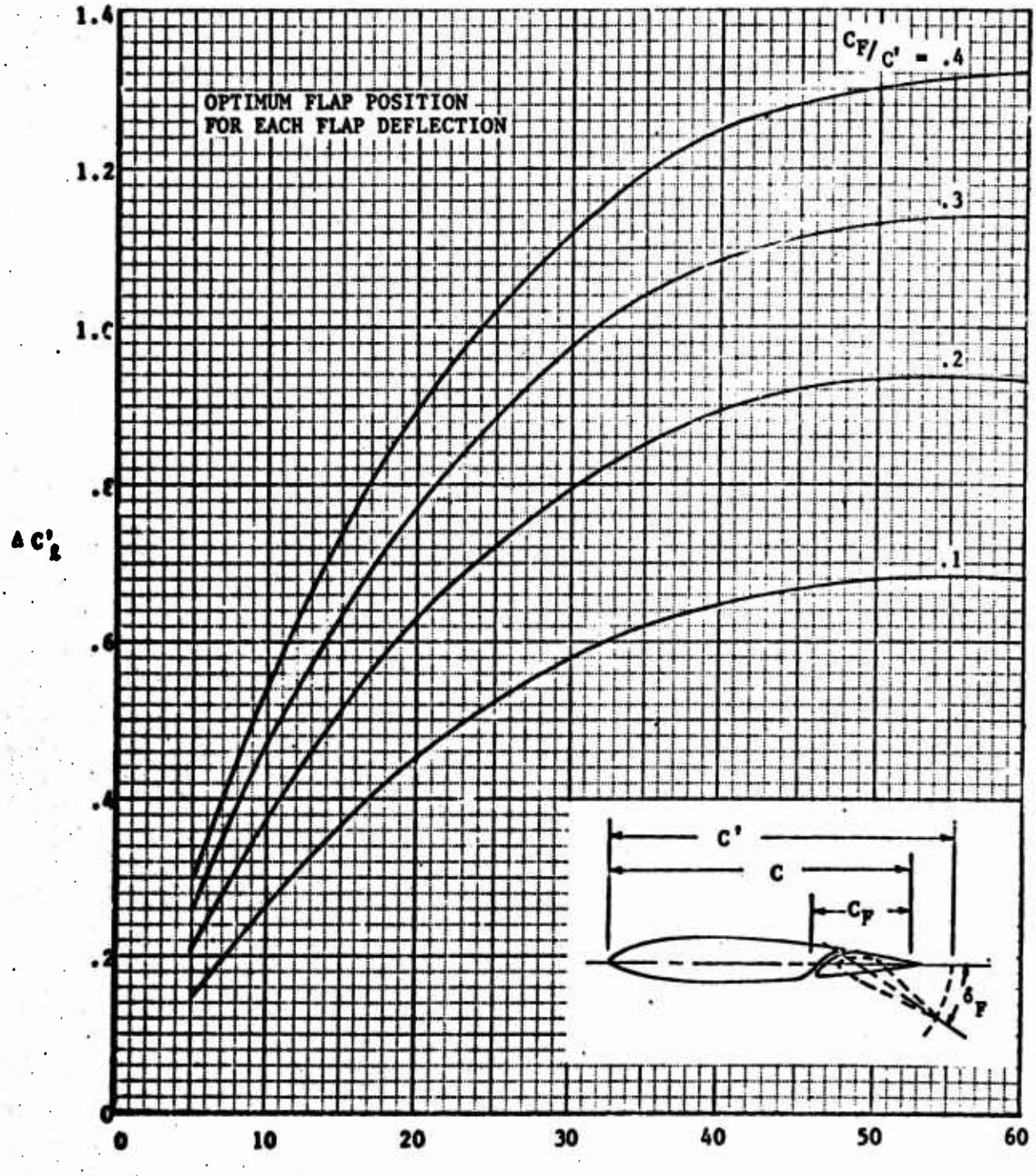

FIGURE 3-38 Lift-Coefficient Increments for Fowler Flaps.

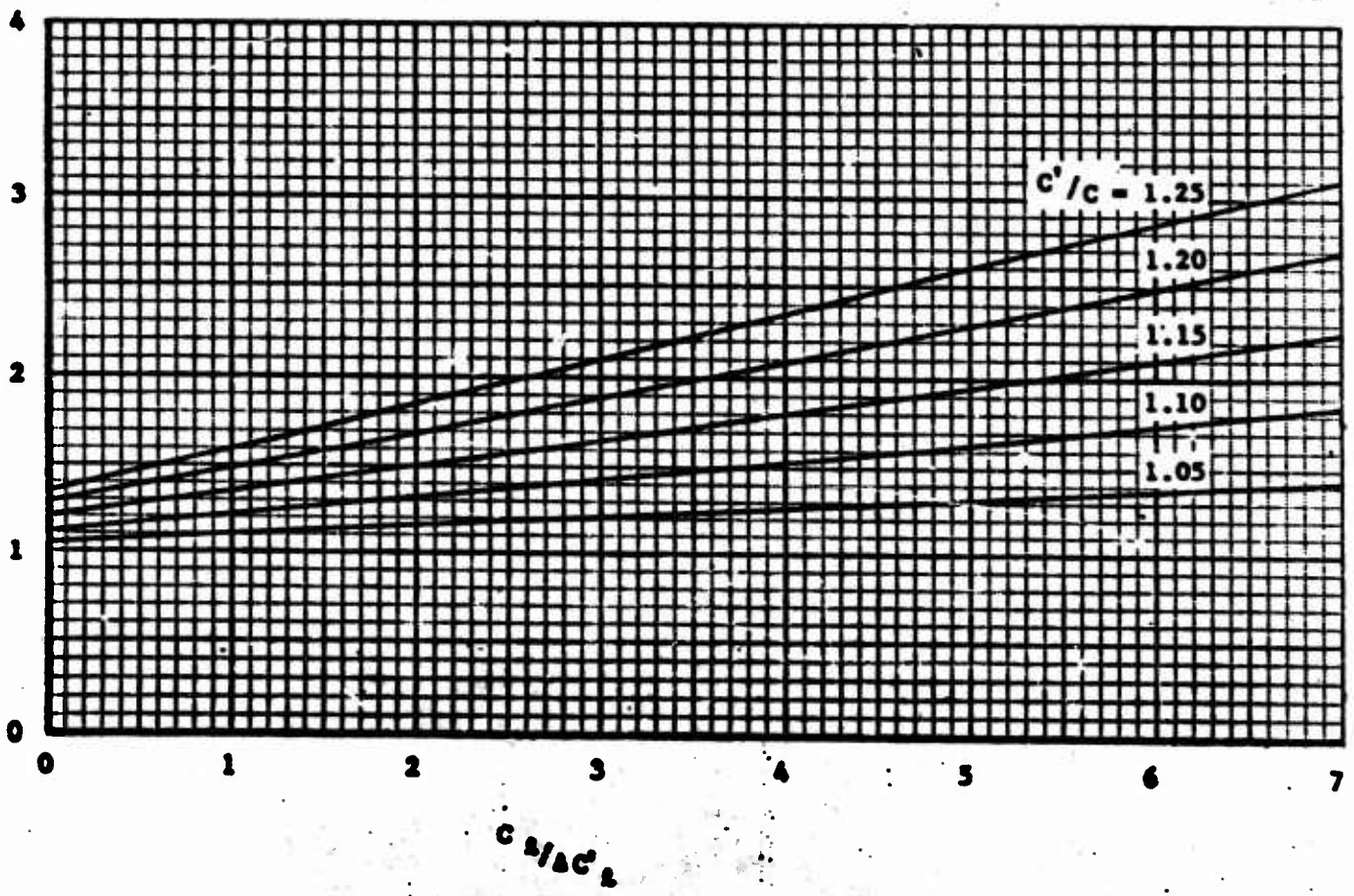

FIGURE 3-39 Lift Correction for Increased Airfoil Area Due to Flap Extension.

The details of this are described in the split flap section but is briefly repeated here

ΔC_{ℓ_δ} is computed above.

$\left(\frac{C_{L_\alpha}}{C_{\ell_\alpha}}\right)$ - ratio of the wing to section lift curve slope.

$\left[\frac{(\alpha_\delta)_{C_L}}{(\alpha_\delta)_{C_{L_\alpha}}}\right]$ From Figure 3-32.

K_b From Figure 3-33.

c. C_{L_α} - For any type of flap where a translation of the flap chord occurs the lift curve slope can be obtained from

$$C_{L_\alpha} = (C_{L_\alpha})_\delta = \left[\left(\frac{C'}{C} - 1\right)\frac{S_F}{S_{REF}} + 1\right](C_{L_\alpha})_{\delta = 0}. \qquad \text{(III-22)}$$

d. $\Delta\alpha_0$ The change in angle-of-attack at zero-lift is obtained from

$$\Delta\alpha_0 = \frac{\Delta C_L}{C_{L_\alpha}}\frac{C'}{C}(C_1) \qquad \text{(III-23)}$$

where $C_1 = 1.$ for $AR > 4$

$C_1 = 1.2$ for $AR < 4$

C'/C is the deflected to undeflected wing chord ratio.

e. $\Delta C_{\ell_{max}}$ is the increase in the section maximum lift coefficient and was described previously.

$\Delta C_{\ell_{max}} = k_1 k_2 k_3 (\Delta C_{\ell_{max\ base}})$

$(\Delta C_{\ell_{max\ base}})$ Figure 3-27

k_1 Figure 3-28

k_2 Figure 3-29

k_3 is an angle correction factor obtained from Figure 3-35.

f. The total wing increment in lift can be computed from

$$\Delta C_{L_{MAX}} = \Delta C_{\ell_{max}} \frac{S_F}{S_{REF}} (1 - .08 \cos^2 \Lambda_{C/4}) \cos^{3/4} \Lambda_{C/4} \quad \text{(III-24)}$$

where $\Delta C_{\ell_{max}}$ comes from part e.

S_F is the wing area affected by the flap.

S_{REF} is the wing reference area.

$$\Lambda_{C/4} = \text{Tan}^{-1} \left[\text{Tan} \Lambda_{LE} - \frac{(1 - TR)}{(1 + TR)AR} \right].$$

g. $\Delta\alpha_{C_{L_{MAX}}}$ - The change in the angle-of-attack for maximum lift can be obtained as follows:

for $AR < 4 \quad \Delta\alpha_{C_{L_{MAX}}} = -.5 \left(\frac{\Delta C_{L_{MAX}}}{C_{L_\alpha}} \right)$

$AR > 4 \quad \Delta\alpha_{C_{L_{MAX}}} = 0.$

F. STEP 6. HIGH LIFT DEVICES - LEADING EDGE

The effects of two types of leading edge devices on the lift characteristics are discussed in this section. The types are:

1. Flaps
2. Slats

The nomenclature is the same as for the trailing edge flaps. The procedure used for calculating both types of devices is the same. The difference is in the reference geometry.

1. Leading Edge Flaps

The section characteristics can be obtained from

a. $\Delta C_\ell = C_{\ell_\alpha} \left(\frac{\Delta\alpha}{\delta}\right) \delta$

where C_{ℓ_α} is the clean section lift curve slope from Step 2.

$\left(\frac{\Delta\alpha}{\delta}\right)$ = f $(C_{d/C})$ from Figure 3-40.

δ is the deflection in degrees.

b. ΔC_L the wing lift increment is

$$\Delta C_L = \Delta C_\ell \left(\frac{C_{L_\alpha}}{C_{\ell_\alpha}}\right) \left[\frac{(\alpha_\delta)_{C_L}}{(\alpha_\delta)_{C_\ell}}\right] K_b \qquad \text{(III-25)}$$

The details of this are described in the split flap section 3, but is briefly repeated here

ΔC_ℓ is computed above.

$\left(\frac{C_{L_\alpha}}{C_{\ell_\alpha}}\right)$ ratio of the wing to section lift curve slope.

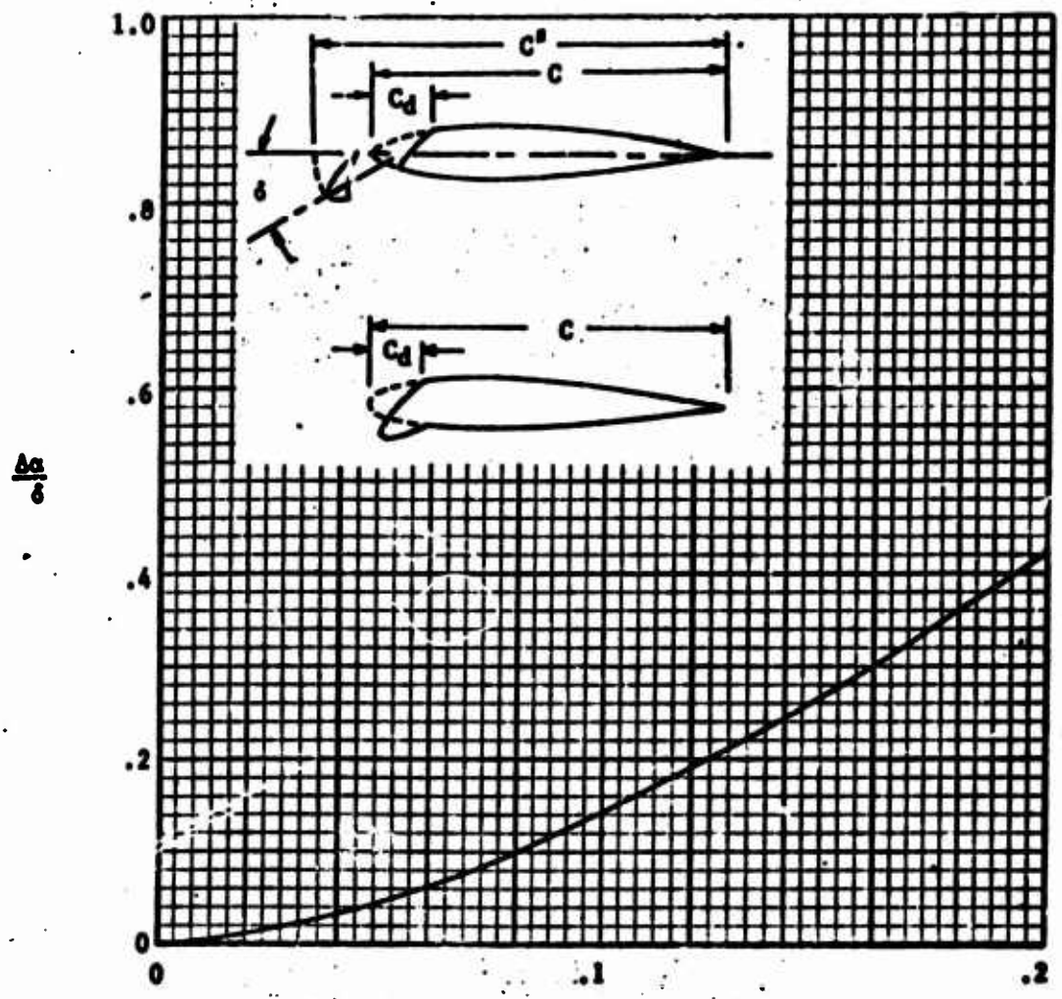

FIGURE 3-40 Leading-Edge-Flap Effectiveness - Low Speeds.

$\left[\frac{(\alpha_\delta)_{C_L}}{(\alpha_\delta)_{C_\ell}}\right]$ from Figure 3-32

K_b from Figure 3-33.

c. C_{L_α} for the flap deflected is the same as for the clean wing lift curve slope.

d. $\Delta\alpha_o = \frac{\Delta C_L}{C_{L_\alpha}}(.2)$ (III-26)

e. $\Delta C_{\ell_{max}}$ is the increase in the section maximum lift coefficient and is obtained from

$$\Delta C_{\ell_{max}} = \left(\frac{\Delta C_{\ell_{max}}}{\delta}\right)\delta$$

where $\left(\frac{\Delta C_{\ell_{max}}}{\delta}\right)$ is obtained from Figure 3-41.

and δ is the deflection (See Figure 3-40).

f. The total wing increment in maximum lift can be computed from:

$$\Delta C_{L_{MAX}} = \Delta C_{\ell_{max}} \frac{S_d}{S_{REF}} (1 - .08 \cos^2 \Lambda_{C/4}) \cos^{3/4} \Lambda_{C/4} \quad \text{(III-27)}$$

where $\Delta C_{\ell_{max}}$ is computed above.

S_d is the wing area affected by the device

S_{REF} is the wing reference area

$$\Lambda_{C/4} = \tan^{-1}\left[\tan \Lambda_{LE} - \frac{(1 - TR)}{(1 + TR)AR}\right]$$

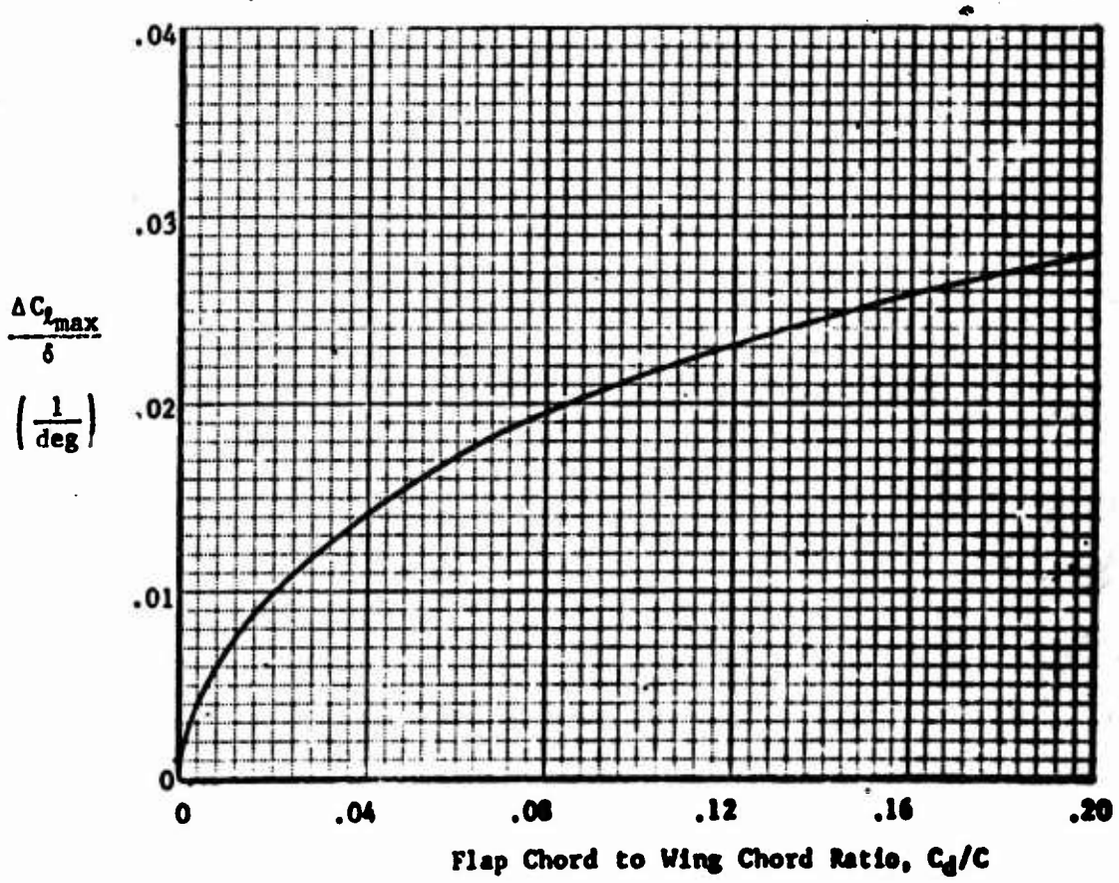

FIGURE 3-41 Effect of Leading-Edge Flaps on $\Delta C_{\ell_{max}}$

g. $\Delta_{\alpha}C_{L_{MAX}}$ - The change in the angle-of-attack for maximum lift is

$$\Delta_{\alpha}C_{L_{MAX}} = \frac{\Delta C_{L_{MAX}}}{C_{L_{\alpha}}} \qquad \text{(III-28)}$$

2. Leading Edge Slats

For the section characteristics

a. $\Delta C_{\ell} = \frac{C''}{C} C_{\ell_{\alpha}} \left(\frac{\Delta\alpha}{\delta}\right) \delta$

where C"/C is the ratio of the wing chord with the slat extended to the clean wing chord (See Figure 3- 4e).

$C_{\ell_{\alpha}}$ is the clean section lift curve slope from Step 2.

$\left(\frac{\Delta\alpha}{\delta}\right)$ = f $(C_{d/C''})$ from Figure 3-40

b. ΔC_L the wing lift increment is $\Delta C_{\ell} \left(\frac{C_{L_{\alpha}}}{C_{\ell_{\alpha}}}\right) \left[\frac{(\alpha_{\delta})_{C_L}}{(\alpha_{\delta})_{C_{\ell}}}\right] K_b$ (III-29)

The details of this are described in the split flap section 3, but is briefly repeated here

ΔC_{ℓ} is from part a.

$\left(\frac{C_{L_{\alpha}}}{C_{\ell_{\alpha}}}\right)$ ratio of the wing to section lift curve slope.

$\left[\frac{(\alpha_{\delta})_{C_L}}{(\alpha_{\delta})_{C_{\ell}}}\right]$ from Figure 3-32

K_b from Figure 3-33

c. C_{L_α} - For any type of flap where a translation of the flap chord occurs the lift curve slope can be obtained from

$$C_{L_\alpha} = \left(C_{L_\alpha}\right)_\delta = \left[\left(\frac{C'}{C} - 1\right)\frac{S_d}{S_{TOT}} + 1\right](C_{L_\alpha})_{\delta = 0} \quad \text{(III-30)}$$

d. $\Delta\alpha_o$ The change in angle-of-attack at zero-lift is obtained from

$$\Delta\alpha_o = \frac{\Delta C_l}{C_{L_\alpha}}\frac{C'}{C}\ (.2) \quad \text{(III-31)}$$

e. $\Delta C_{l_{max}}$ is the increase in the section maximum lift coefficient and is obtained from

$$\Delta C_{l_{max}} = \left(\frac{\Delta C_{l_{max}}}{\delta}\right)\delta$$

where $\left(\frac{\Delta C_{l_{max}}}{\delta}\right)$ is obtained from Figure 3-41.

and δ is the deflection (See Figure 3-40).

f. The total wing increment in maximum lift can be computed from

$$\Delta C_{L_{MAX}} = \Delta C_{l_{max}}\frac{S_d}{S_{REF}}\left(1 - .08\ \mathrm{Cos}^2\ \Lambda_{C/4}\right)\mathrm{Cos}^{3/4}\Lambda_{C/4} \quad \text{(III-32)}$$

where $\Delta C_{l_{max}}$ is computed above.

S_d is the wing area affected by the flap

S_{REF} is the wing reference area

$$\Lambda_{C/4} = \mathrm{Tan}^{-1}\left[\mathrm{Tan}\ \Lambda_{LE} - \frac{(1 - TR)}{(1 + TR)AR}\right]$$

g. $\Delta\alpha_{C_{L_{MAX}}}$ - The change in the angle-of-attack for maximum lift is

$$\Delta\alpha_{C_{L_{MAX}}} = \frac{\Delta C_{L_{MAX}}}{C_{L_\alpha}} \qquad \text{(III-33)}$$

6. STEP 7. LANDING LIFT CHARACTERISTICS

The landing lift characteristics of modern aircraft are a function of C_{L_α}, the lift curve slope, α_o, the zero lift angle-of-attack, and α_g, the angle-of-attack at touchdown.

The values of C_{L_α} and α_o are available from the previous steps.

α_g, the angle-of-attack at touchdown, may be limited by one of the following:

1. Ground clearance angle
2. Pilot's visibility
3. Rate of sink at touchdown
4. Flare technique (some aircraft use a flare maneuver and some do not).
5. Control effectiveness.

The landing lift coefficient $C_{L_{TD}}$, then becomes:

$$C_{L_{TD}} = C_{L_\alpha} (\alpha_g - \alpha_o) \qquad \text{(III-34)}$$

where C_{L_α} is the lift curve slope

α_o is the zero lift angle-of-attack with high lift devices deflected.

NOTE: If $\alpha_g \geq \alpha_{C_{L_{MAX}}}$ then $C_{L_{TD}} = C_{L_{MAX}}$

H. STEP 8. - TOUCHDOWN SPEED

The aircraft's touchdown speed can now be computed from:

$$V_{TD.} = \left[\frac{W - F_N \sin(\alpha_g - \gamma)}{.00119\, C_{L_{TD}}\, S_{REF}}\right]^{1/2} \quad \text{Ft/Sec} \qquad \text{(III-35)}$$

Where W is the aircraft weight in pounds.

S_{REF} is the aircraft reference area in ft^2

F_N is the net thrust of aircraft at touchdown in lbs.

α_g is the aircraft angle-of-attack at touchdown in degrees.

γ is the flight path angle at touchdown in degrees.

$C_{L_{TD}}$ is the lift coefficient at touchdown and was calculated above.

I. STEP 9. AIRCRAFT MINIMUM DRAG (NO HIGH LIFT DEVICE)

This step will describe the procedure to be used in obtaining an aircraft's minimum drag. This is the drag of the aircraft with no lift, landing gear extended.

1. Landing Gear Drag

No adequate method for estimating landing gear drag was found during the literature search. The following empirical method was found to give reasonable results.

a. For aircraft whose wing area is more than 1,000 ft^2 a value of $\Delta C_{D_{LG}} = .02$ is reasonable. These are normally bomber or transport type aircraft.

b. For aircraft whose wing area is less than 1,000 ft^2 (fighter type) the following empirical method was used based on the data shown in Figure 3-42.

$$\Delta C_{D_{LG}} = \Delta f_e / S_{TOT} = \left[.275 \left(\frac{W_E}{S_{REF}}\right) - 6.\right] \left(\frac{1}{S_{REF}}\right) \qquad \text{(III-36)}$$

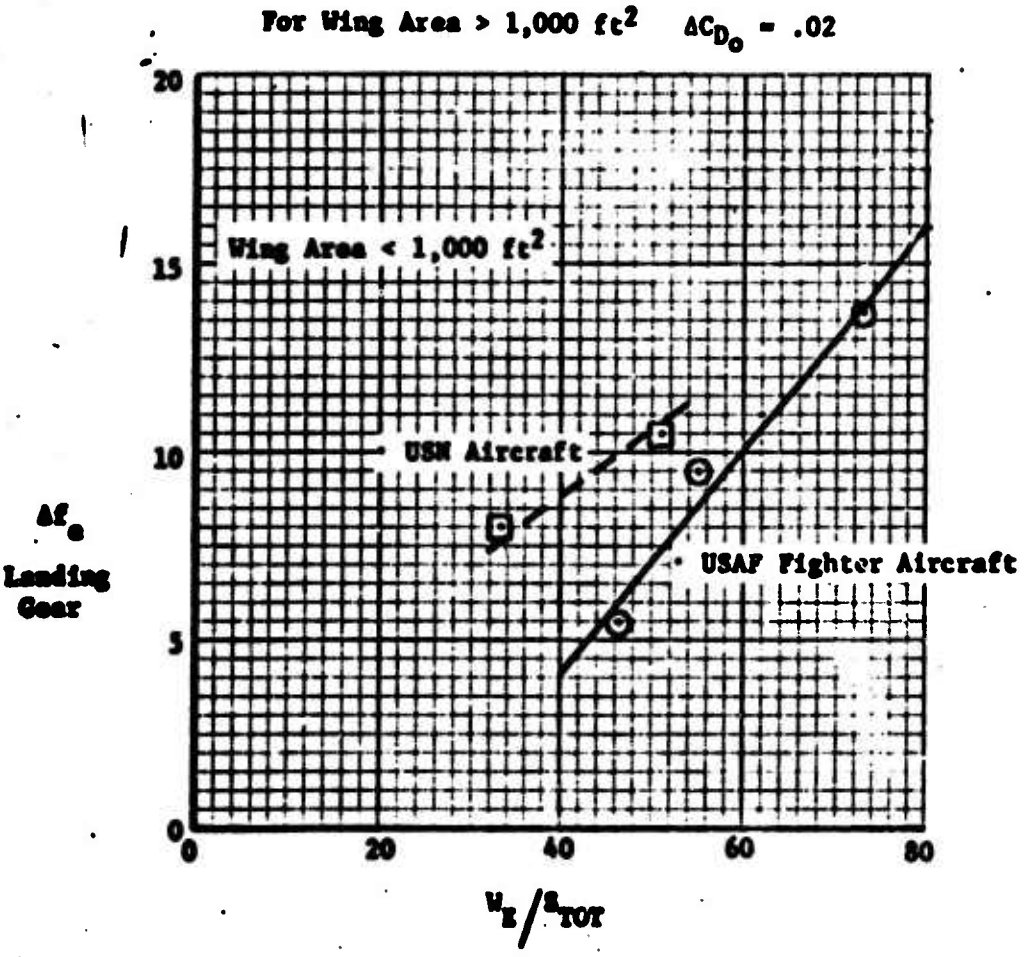

FIGURE 3-42: Landing Gear Drag

For the purposes of computing the aircraft minimum drag coefficient the velocity of the aircraft is considered to be the touchdown speed (V_{TD}) from Step 8.

Once V_{TD} is known then the drag coefficient computation can proceed.

2. Reynold's Numbers

The Reynolds Number of the wing (based on sea level standard conditions)

a. $RN_{wing} = .00636\ (V_{TD})\ (MAC) \times 10^5$ (III-37)

where MAC is the wing mean aerodynamic chord - ft.

For the fuselage

b. $RN_{fuselage} = .00636\ (V_{TD})\ (\ell_{fuselage}) \times 10^5$ (III-38)

where $\ell_{fuselage}$ is the fuselage length - ft.

3. Minimum Drag - Wing and Tails

$$\Delta C_{D_{Min.\ Wing}} = [2\ C_f\ (1 + 2\ t/c + 100\ (t/c)^4]\ 1.4 \quad \text{(III-39)}$$

(the factor 1.4 accounts for the tail surfaces.)

Where C_f is obtained from Figure 3-43, where the RN is computed in (a) and the ratio ℓ/k is a surface finish factor. For a wing, ℓ = MAC (inches).

For aircraft the following k values can be used:

	k
Natural Sheet Metal	$.16 \times 10^{-3}$
Smooth Paint	$.25 \times 10^{-3}$
Careful Camouflage Paint	$.40 \times 10^{-3}$
Production Camouflage	1.2×10^{-3}

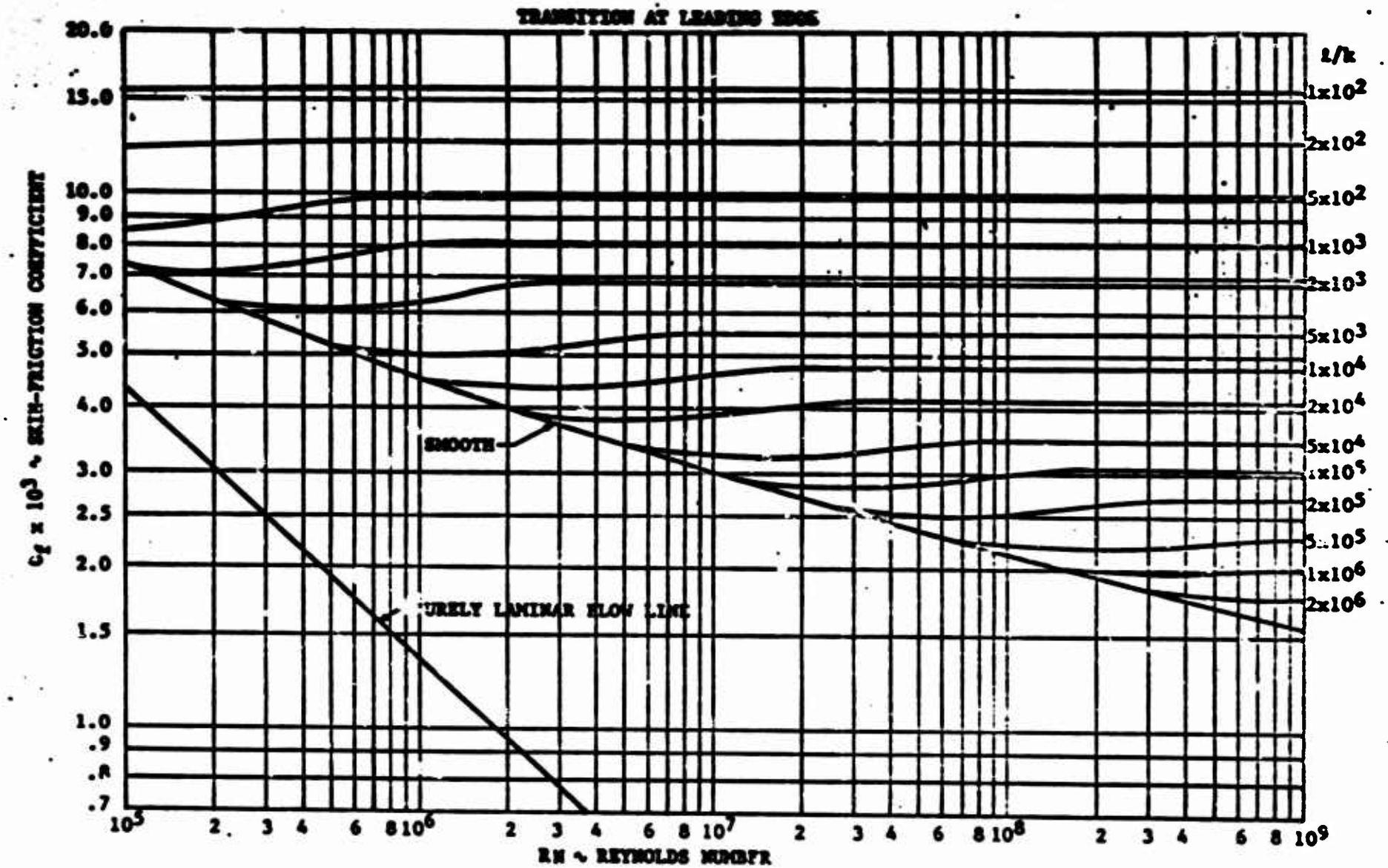

FIGURE 3-43 Incompressible Skin-Friction Coefficient.

4. Minimum Fuselage Drag

$$\Delta C_{D_{\substack{Min \\ Fuselage}}} = 1.02\, C_f \left[1 + \frac{1.5}{(b/d)^{1.5}} + \frac{7}{(b/d)^3} \right] \frac{S_{Wet}}{S_{REF}} \qquad \text{(III-40)}$$

C_f here is obtained from Figure 3-43 where RN is computed in (b) above for the fuselage and ℓ/k again is a surface finish factor. k is the same as above and $\ell = \ell_b$, in inches.

5. Total Minimum Drag Coefficient

The total minimum drag coefficient is therefore

$$C_{D_{Min}} = \Delta C_{D_{\substack{Min \\ Wing}}} + \Delta C_{D_{\substack{Min \\ Fuselage}}} + \Delta C_{D_{LG}} \qquad \text{(III-41)}$$

J. STEP 10. DRAG-DUE-TO-LIFT - CLEAN WING

The drag-due-to-lift may be obtained from the following expression

$$\Delta C_{D_i} = \frac{C_{L_{D_i}}^2}{(AR)} (1 + A_1 A_2) + K_D A_3 \qquad \text{(III-42)}$$

where $C_{L_{D_i}}$ is the lift coefficient to be used for determining the drag due-to-lift,

$$C_{L_{D_i}} = C_{L_{TD}} - C_{L_{DES}}$$

where $C_{L_{TD}}$ is the lift coefficient at touchdown

$C_{L_{DES}}$ is the wing design lift coefficient

AR is the wing aspect ratio

$A_1 = f$ (AR, TR) for $\Lambda_{C/4} = 0$ See Figure 3-44

$A_2 = f$ ($\Lambda_{C/4}$, AR) See Figure 3-45

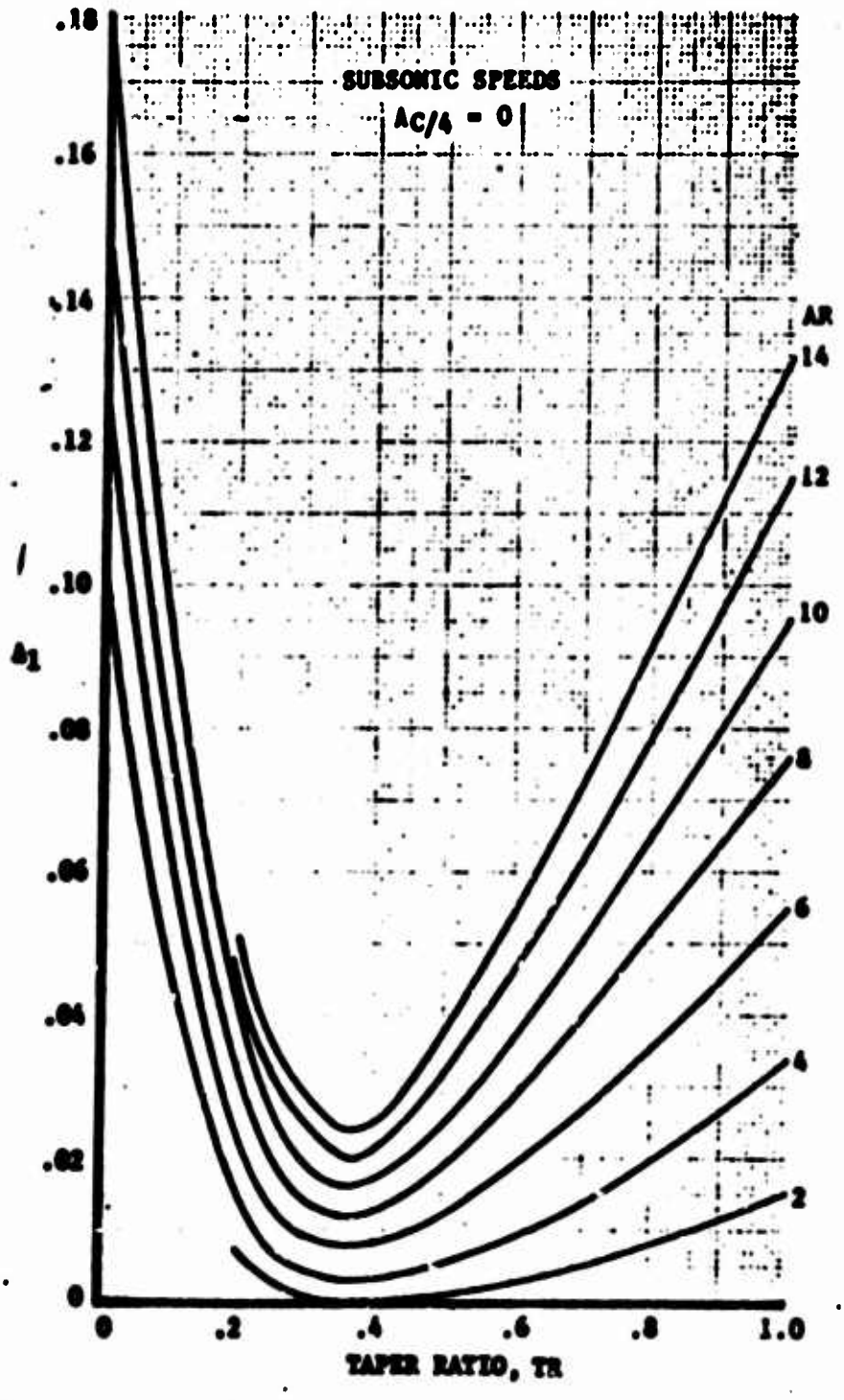

FIGURE 3-44 Taper Ratio Correction Factor, A_1

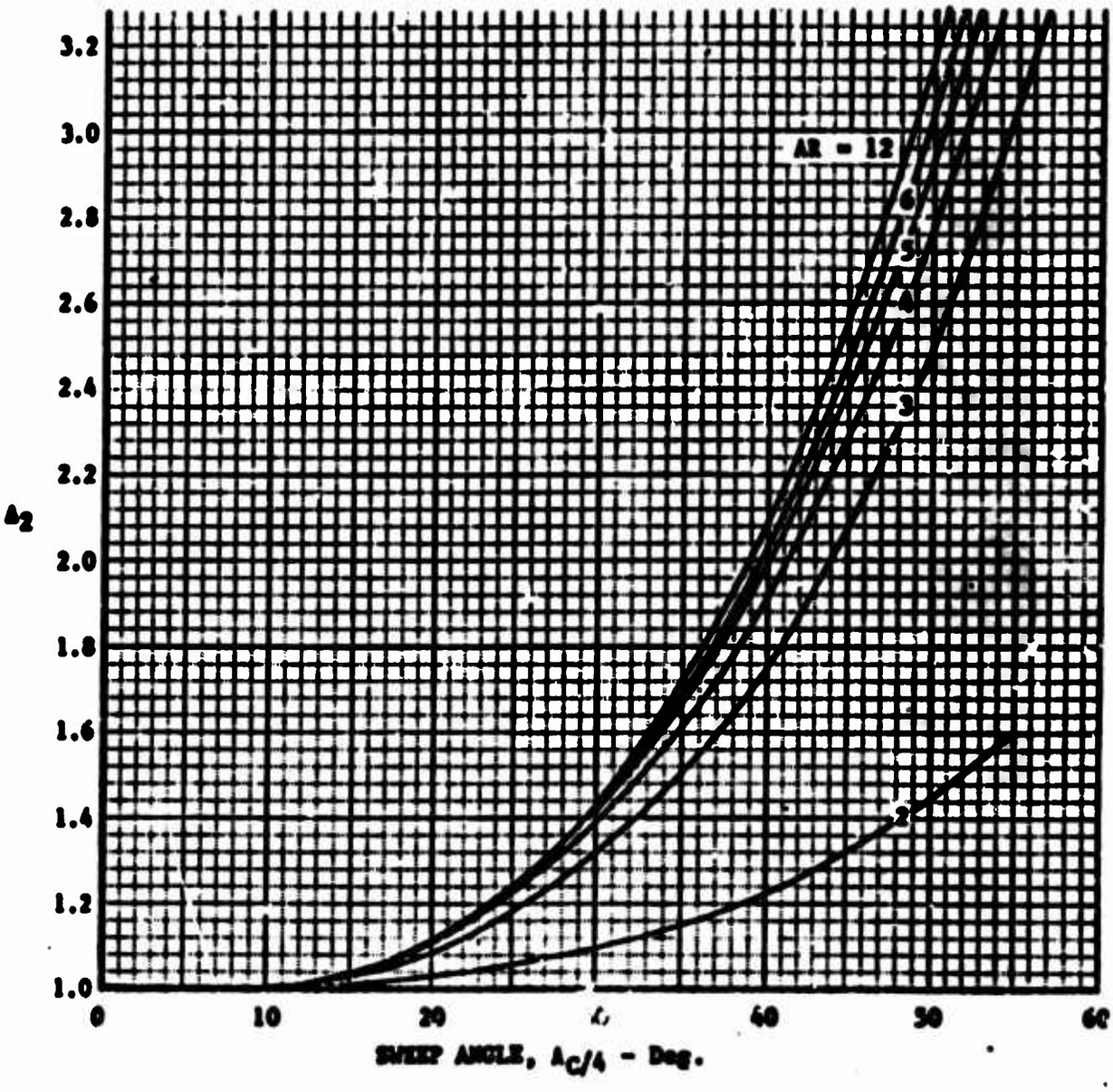

FIGURE 3-45 Sweep Angle Correction Factor, Δ_2

Δ_3 an empirical correction, f(J, α_g, $\alpha_{C_{L_{MAX}}}$) See Figure 3-46a or 3-46b.

K_D is an empirical correction, f(A_{LE}, J) See Figure 3-47

where

$$J = .3\,(C_1 + 1)\,AR\,\cos A_{LE}\left\{(C_1 + 1)\,(C_2 + 1) - \left[\frac{(C_2 + 1)\,AR\,\tan A_{LE}}{7}\right]^2\right\} \qquad \text{(III-43)}$$

where C_1 is obtained from Figure 3-12

C_2 is obtained from Figure 3-16

and α_g is the angle-of-attack at touchdown.

K. STEP 11. DRAG OF HIGH LIFT DEVICES

1. Trailing Edge Flaps

Methods available for computing trailing edge flap drag are very limited.

For purposes of this study, flaps were considered to be of 2 types:

Non-Slotted	Slotted
Plain	Single
Split	Double
	Fowler

a. Minimum Drag

The minimum drag of a flap is then obtained from

$$\Delta C_{D_{\substack{\text{Min}\\\text{Flap}}}} = \Delta C_{d_{\text{Flap}}}\, K_b\, I_F$$

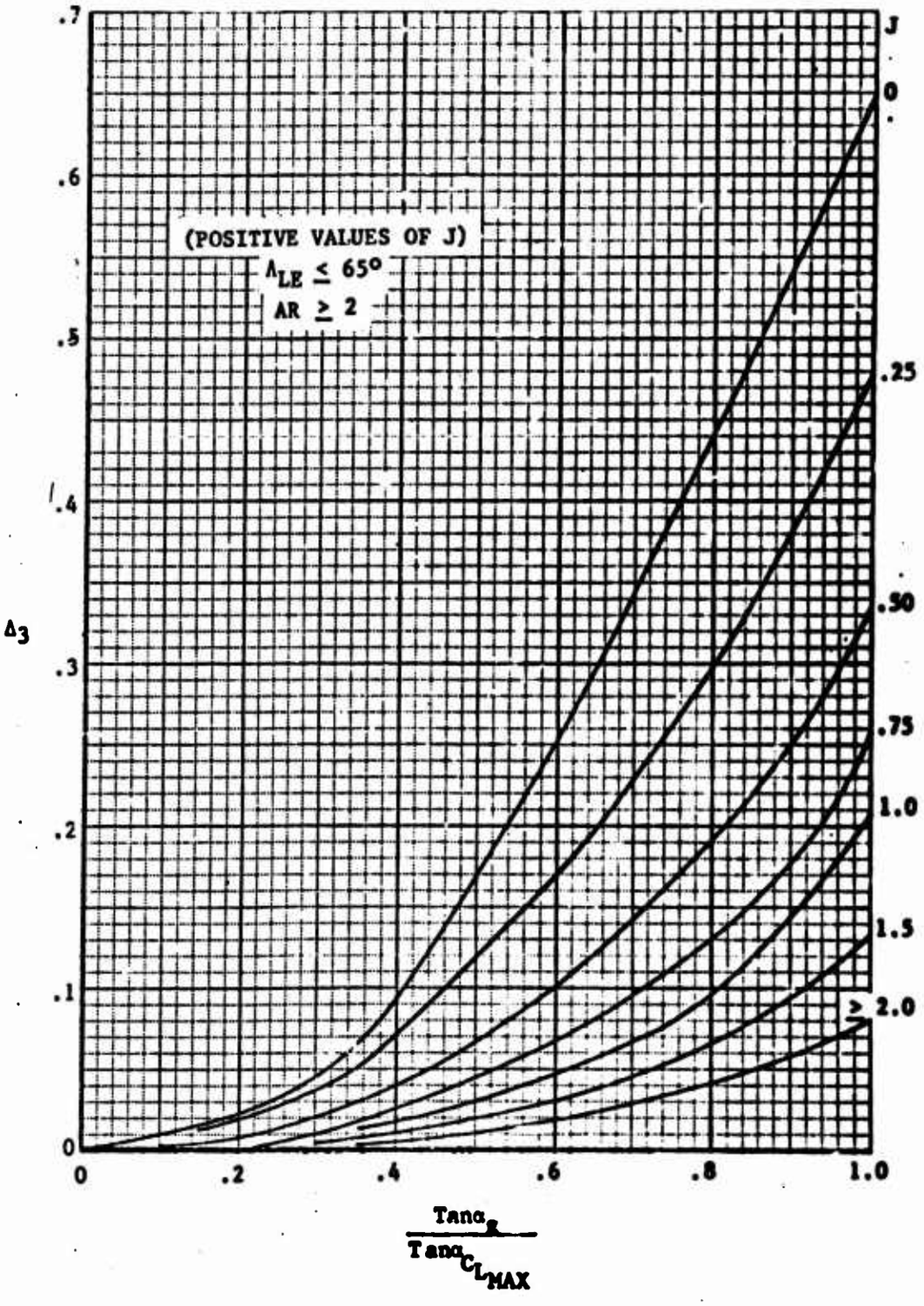

FIGURE 3-46a Variation with Angle of Attack of Drag Increment Due to Wing Shape, $\Delta_3(+J)$.

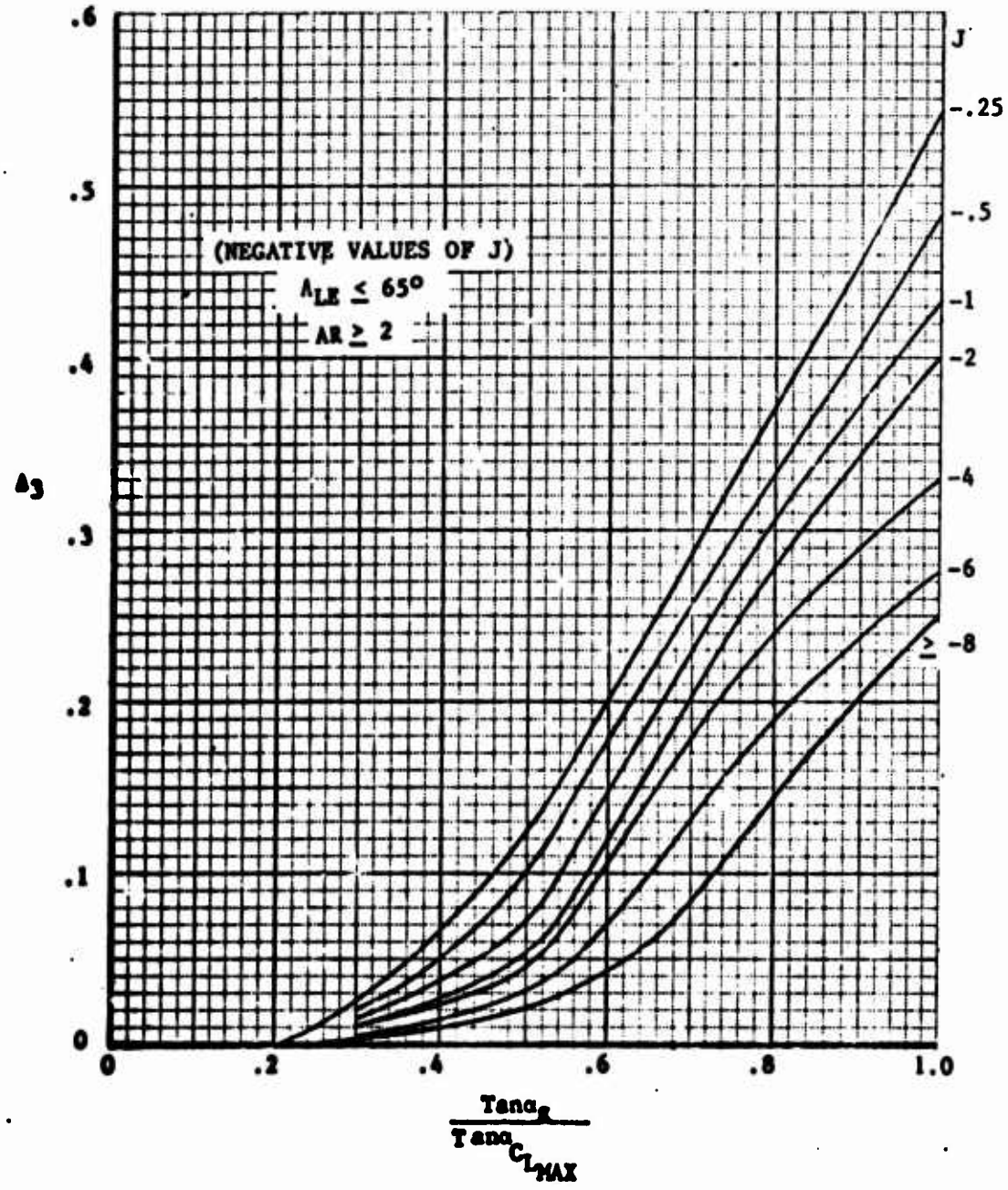

FIGURE 3-46b Variation With Angle of Attack of Drag Increment Due to Wing Shape, $\Delta_3(-J)$.

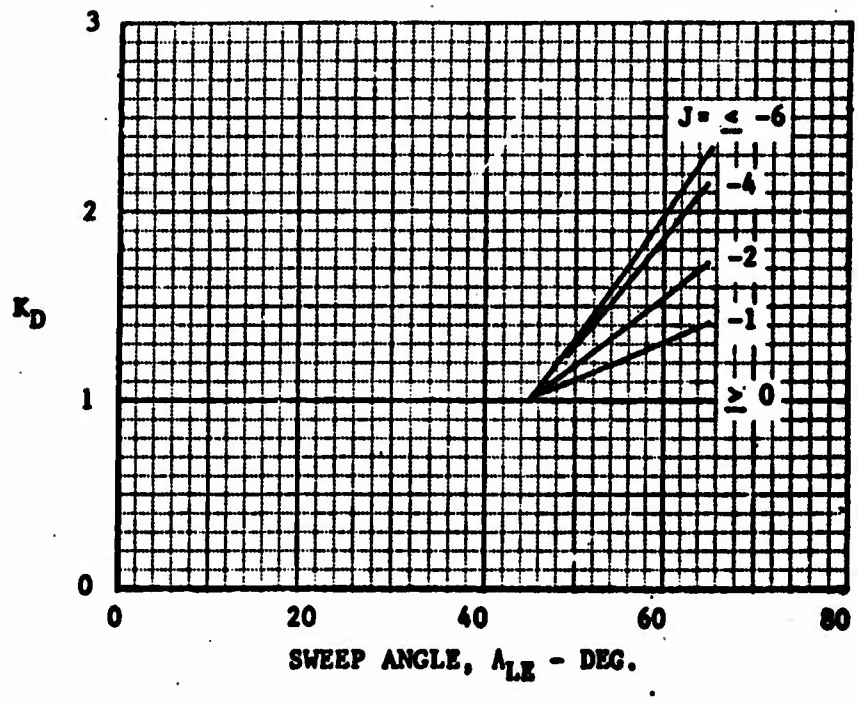

FIGURE 3-47 Sweep Angle Correction Factor, K_D.

where $\Delta C_{d_{Flap}} = f\left(\frac{C_F}{C}, \delta_F\right)$ is obtained from either Figure 3-48a or 3-48b depending on the type flap.

K_b is from Figure 3-33 and is a flap span factor correction. (Again direct use is recommended)

I_F is an interference factor and for

$AR > 4$ let $I_F = 1.$

$AR < 4$ let $I_F = (1 + .006676_F)$ where

δ_F is the flap deflection in degrees

b. Drag-Due-To-Lift

The drag-due-to-lift of a flap is

$$\Delta C_{D_{i_{Flap}}} = K' \frac{(\Delta C_L)^2}{\pi\, AR}$$

where K' is a flap span factor available from Figures 3-49a to 3-49c. Interpolation may be necessary (as an example (overall flap span/wing span) = .7 for an AR = 6 wing and if the flap begins at .2 of the span (cut-out = .2) then K' = .8 from Figure 3-49b.

ΔC_L is the increment in wing lift due to flap deflection and was calculated previously.

The total flap drag is then

$$\Delta C_{D_{Total\ Flap}} = \Delta C_{D_{Min\ Flap}} + \Delta C_{D_{i_{Flap}}}$$

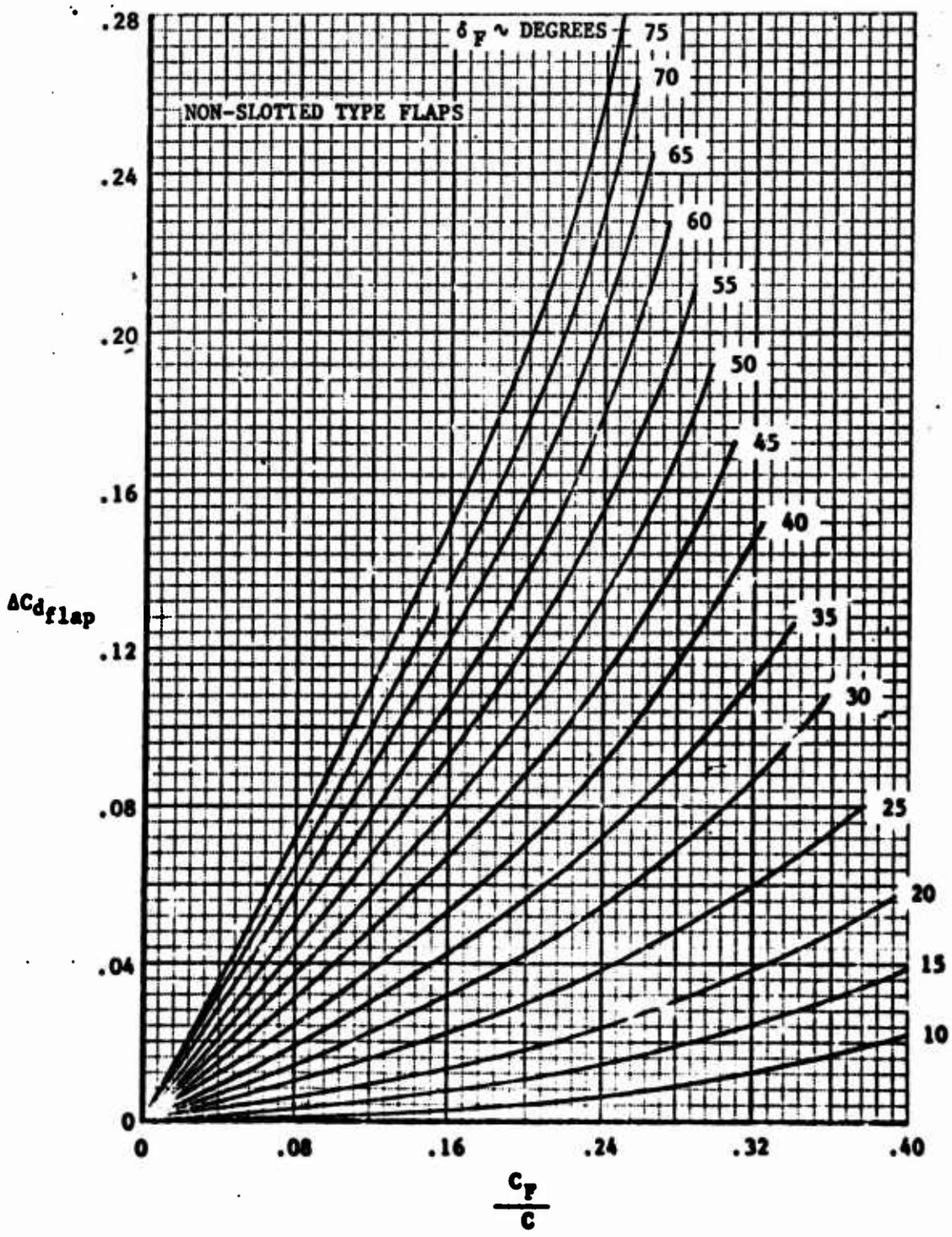

FIGURE 3-48a Two-Dimensional Drag Increment Due to Flaps; (Non-Slotted Type Flaps).

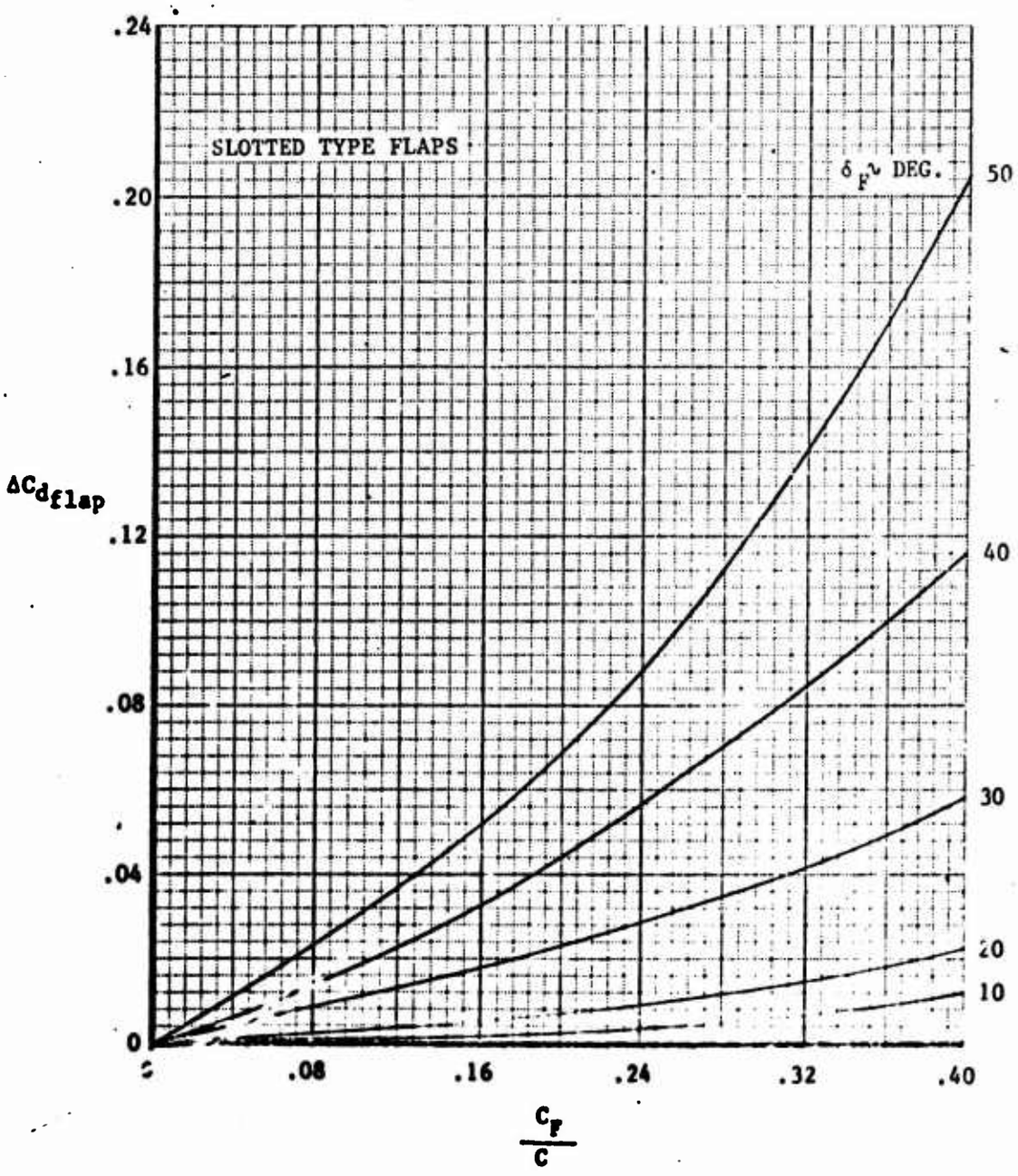

FIGURE 3-48b Two-Dimensional Drag Increment Due to Flaps; (Slotted Type Flaps).

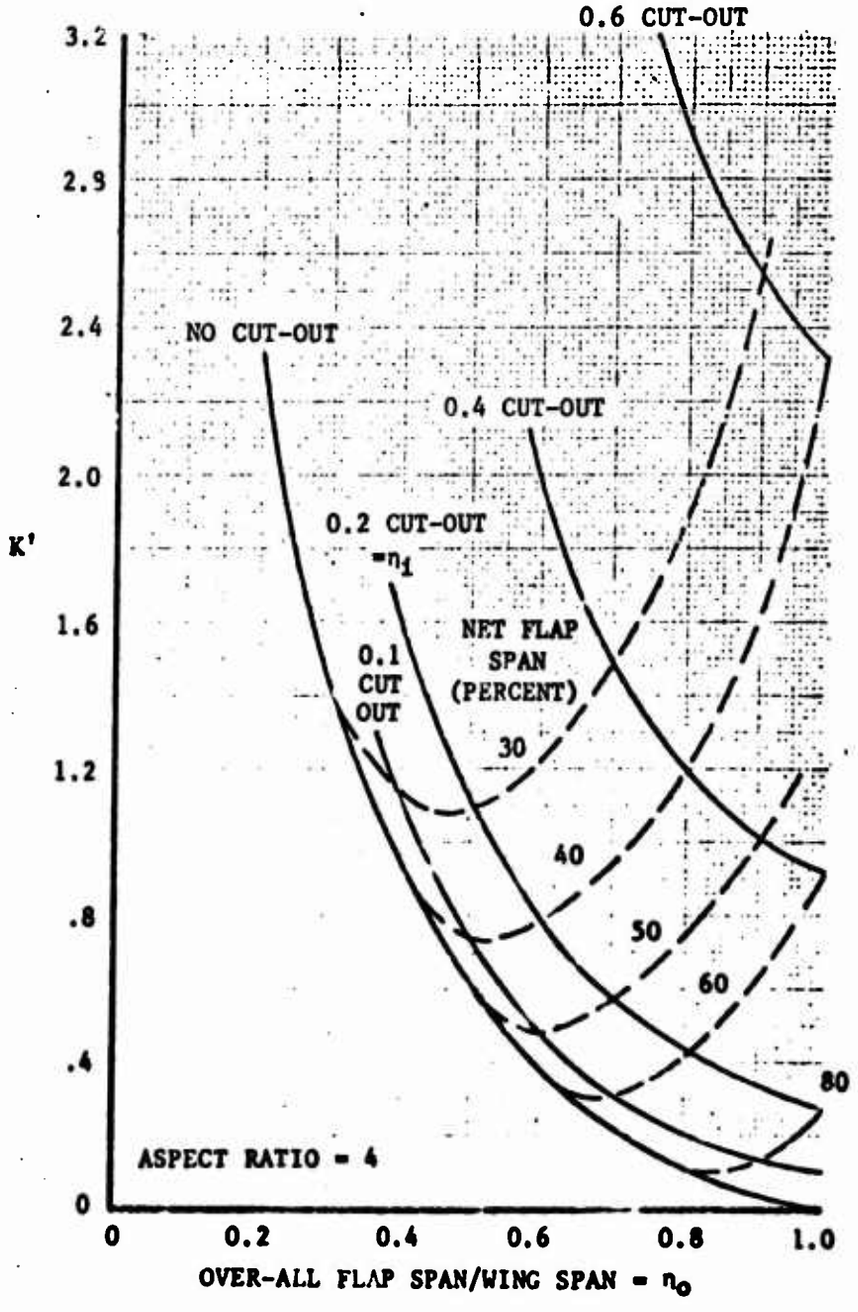

FIGURE 3-49a Factor K' for Calculating Induced Drag of an Elliptic Wing With Part-Span Flaps and Cut-Out, AR = 4.

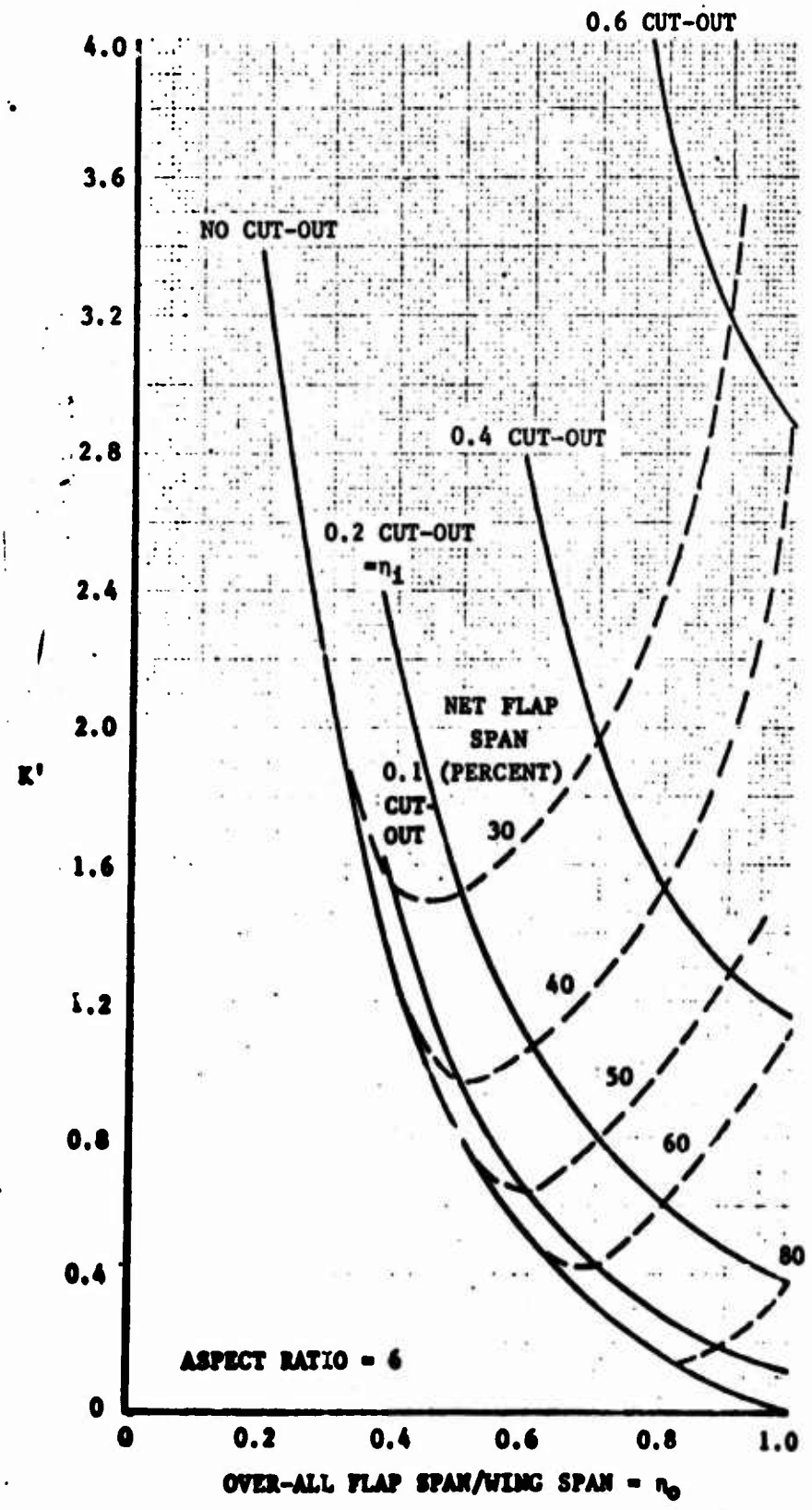

FIGURE 3-49b Factor K' For Calculating Induced Drag of an Elliptic Wing With Part-Span Flaps and Cut-Out, AR=6.

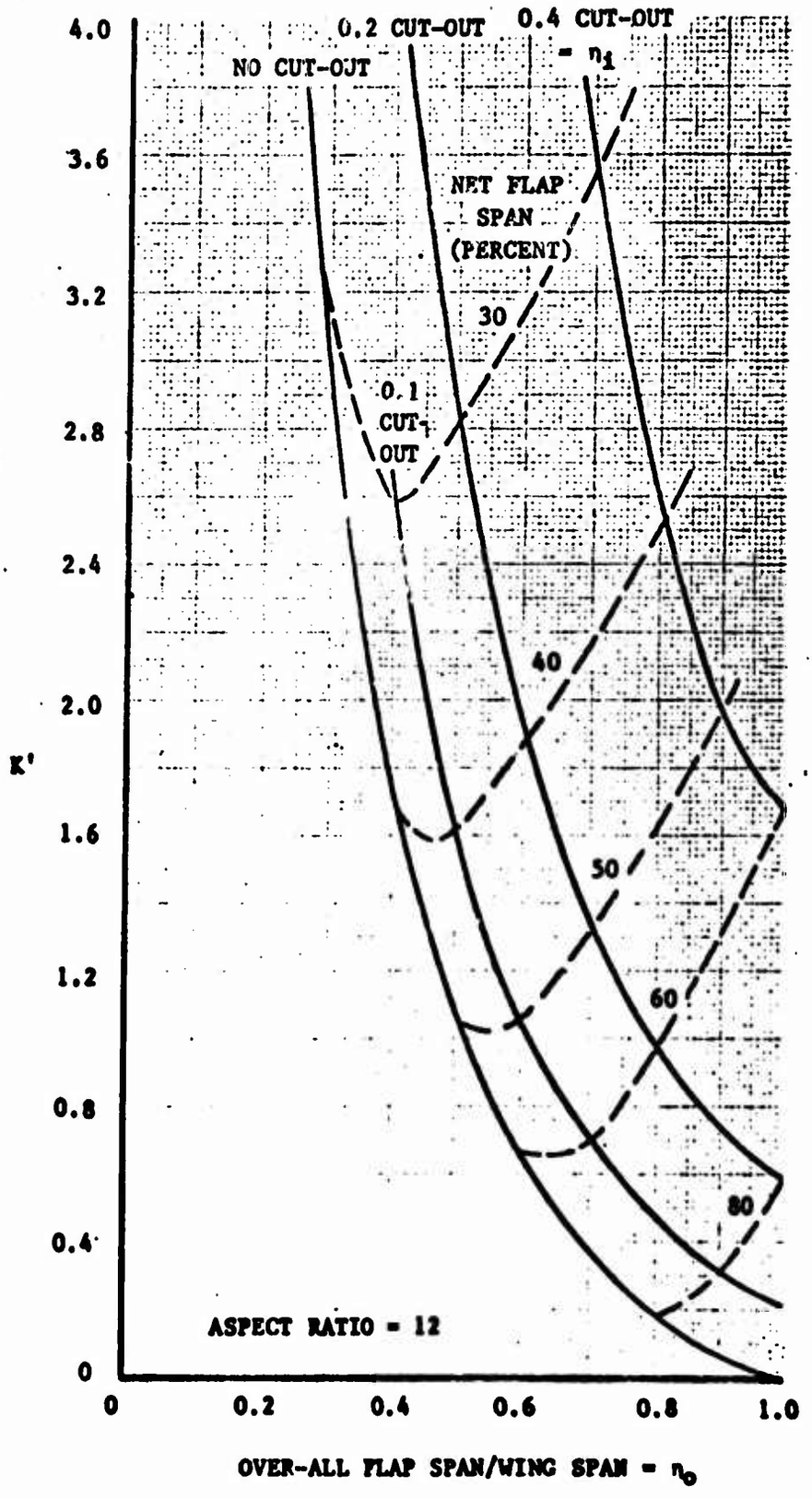

FIGURE 3-49c Factor K' For Calculating Induced Drag of an Elliptic Wing With Part-Span Flaps and Cut-Out, AR=12.

2. Leading-Edge Devices

An approximation of the minimum drag coefficient due to deflection of leading edge devices is as follows:

a. Flap

$$\Delta C_{D_{Min}} = (1 - \cos\delta) \frac{b_d}{b} \frac{C_d}{C} \frac{S_d}{S_{REF}} \qquad \text{(III-47)}$$

where the geometry is defined in Step 1.

b. Slats

$$\Delta C_{D_{Min}} = 0$$

c. Since the leading edge devices normally extended the useable angle-of-attack range and prevent leading edge stall the drag-due-to-lift was assumed to be zero.

L. STEP 12. DRAG OF DRAG DEVICES

1. Spoilers

The methods presented below are for spoilers used to destroy wing lift. Spoilers used for lateral control are not considered.

The loss in lift is:

$$\Delta C_{L_{SP}} = -\frac{\Delta\alpha_{SP}}{57.3 C_{L_\alpha}} \sin\delta_{SP} \frac{S_{SP}}{S_{REF}} \qquad \text{(III-48)}$$

where $\Delta\alpha_{SP}$ comes from Figure 3-50.

C_{L_α} is the aircraft lift curve slope.

δ_{SP} is the deflection of the spoiler from the wing surface in degrees ($45° \leq \delta_{SP} \leq 90°$)

S_{SP} is the wing area affected by the spoiler

S_{REF} is the aircraft reference area.

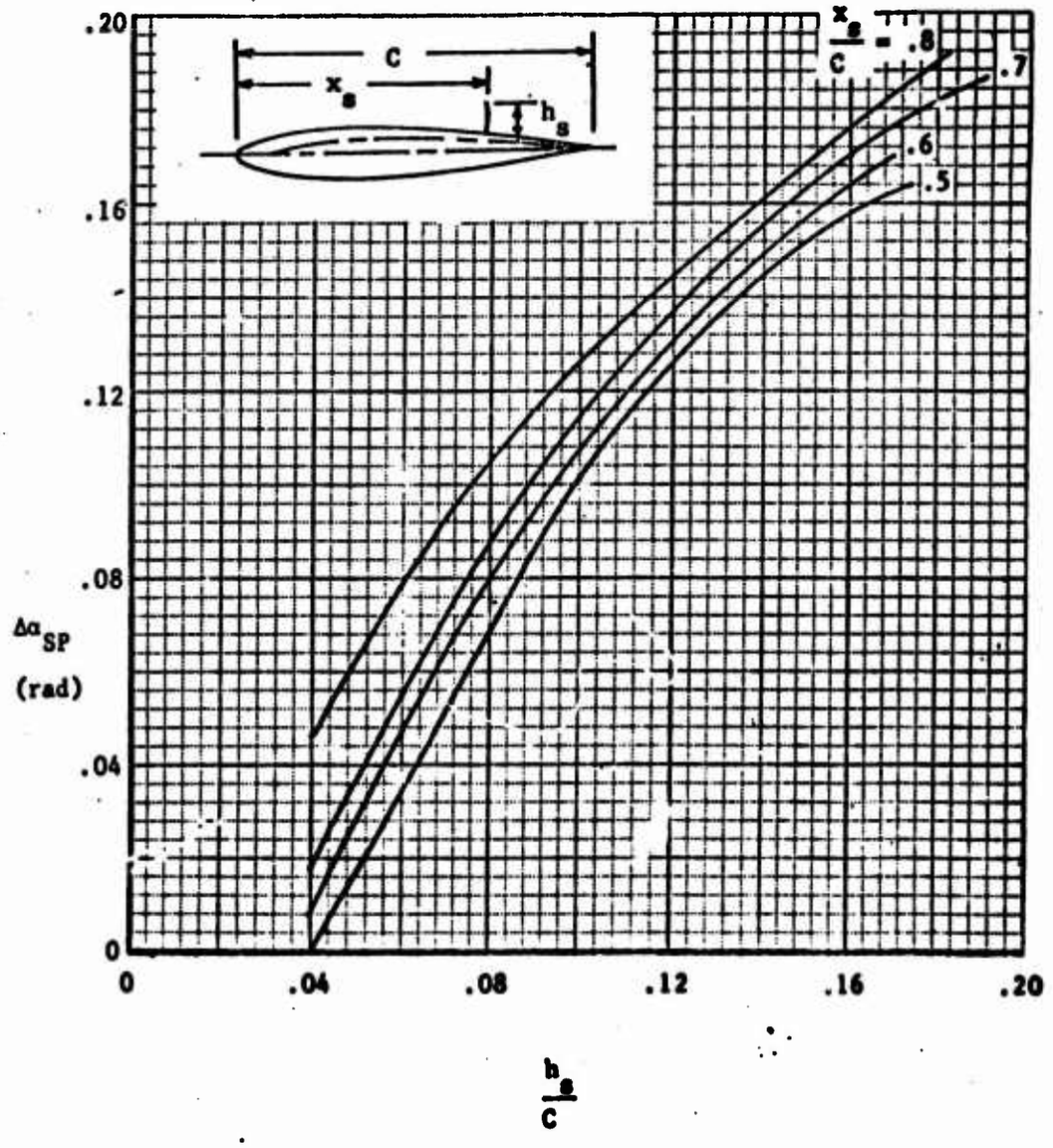

FIGURE 3-50: Spoiler Lift Effectiveness - Low Speeds.

The increase in drag is:

$$\Delta C_{D_{SP}} = (-.1 + .011\delta_{SP}) \frac{S_{SP}}{S_{REF}} \qquad \text{(III-49)}$$

valid for $45° \leq \delta_{SP} \leq 90°$

2. Speed Brake

For low speed flight, or during ground roll, the incremental drag due to speed brake reduces, for all practical purposes, to one equation. This conclusion is based on the data presented by the various aircraft manufacturers.

$$\Delta C_{D_{SB}} = 1.13 \text{ Sin } \delta_{SB} \frac{A_{SB}}{S_{TOT}} \qquad \text{(III-50)}$$

where S_{REF} is the aircraft reference area.

δ_{SB} is the speed brake deflection measured from the aircraft centerline.

A_{SB} is the speed brake panel area.

3. Drag Chutes

Landing drag chutes have been in operational use for approximately twenty years. No new method for estimating the drag chute C_D has been found during this study. Only four pertinent references were obtained. References 10 and 11 indicate that two types of aircraft drag chutes are used. Their characteristics for design purposes are described below.

	Reference 10 $\Delta C_{D_{o_c}}$ design	Reference 11 $\Delta C_{D_{o_c}}$ design	Reference 11 $\Delta C_{D_{o_c}}$ range
Ribbon	.45	.50	.45 to .55
Ring-Slot	.65	.55	.45 to .65

$\Delta C_{D_{o_c}}$ is based on a reference area of a circle of diameter equal to twice the distance from the canopy skirt to the center of the apex or vent (nominal canopy diameter).

References indicate that the above values are not absolute and may vary due to porosity and airflow behind aircraft.

Table III-3 shows which drag chutes that current aircraft are using and the associated $\Delta C_{D_{o_c}}$.

The drag force of the chute is:

$$\Delta D_{chute} = \Delta C_{D_{o_c}} q S_{chute}$$

Based on the aircraft reference area, the incremental drag coefficient is:

$$\Delta C_{D_{DC}} = \Delta C_{D_{o_c}} \frac{S_{chute}}{S_{REF}} \qquad \text{(III-51)}$$

Full deployment of the drag chutes from the time it is released by the pilot is usually less than 4 seconds.

4. Thrust Reverser Door Deployment

As explained in Section V, deployment of thrust reversers will affect the drag of aerodynamic surfaces such as flaps located in the vicinity of the reversed thrust plume. This effect is highly sensitive to reverser location and geometry of local aerodynamic surfaces and is not amenable to the generalized treatment required by the scope of this report. However, for purpose of generalized studies, it is suggested that the aerodynamic drag increment due to thrust reverser deployment be approximated by:

$$\Delta C_{D_{TR}} = 0.5 \frac{S_{TR}}{S_{REF}} \qquad \text{(III-52)}$$

which represents the aerodynamic drag due to suction

TABLE III - 3

AIRCRAFT DRAG CHUTE DATA SUMMARY

(Information obtained from References, Flight Manuals & Manufacturer's Reports)

Aircraft Designation	Type Chute	$\Delta C_{D_{o_c}}$ Based on Aircraft Referenced Area	Aircraft Reference Area (Wing Area) Ft^2	Chute Diameter and Area Ft/Ft^2	$\Delta C_{D_{o_c}}$ Based On Chute Area	Maximum Deployment Speed - Kts.
F-4C	R-S	.1875	530	16/201	.495	
F-5A	R-S	.572	170	15/176.5	.550	165
F-104	R-S		196	18/254		185
F-105	R-S	.449	385	20/314	.550	200
F-106	R-S	.1445	695	14.6/167.4	.600	220
B-47	Ribbon	.203	1428	32/804	.361	160
B-52H	Ribbon	.169	4000	44/1520	.444	170
B-58	R-S		1542	24/453		

NOTE: R-S Ring-Slot.

acting on the aft face of the thrust reverser doors. In this equation:

S_{TR} - Base area of the thrust reverser doors.

5. Total Drag of Drag Devices

The summation of the drag increments due to spoiler and speed brake deflection and drag chute and thrust reverser door deployment can be expressed as:

$$(\Delta C_{D_{\substack{Min \\ DD}}}) = \Delta C_{D_{SP}} + \Delta C_{D_{SB}} + \Delta C_{D_{DC}} + \Delta C_{D_{TR}} \qquad \text{(III-53)}$$

M. STEP 13: TOTAL DRAG COEFFICIENT

The total drag coefficient of the aircraft can be expressed as:

$$C_D = \underbrace{C_{D_{Min}}}_{\text{Step 9}} + \underbrace{\Delta C_{D_i}}_{\text{Step 10}} + \underbrace{(\Delta C_{D_{\substack{Min \\ Flap}}} + \Delta C_{D_{i_{Flap}}} + \Delta C_{D_{\substack{Min \\ Device}}})}_{\text{Step 11}}$$

$$+ \underbrace{(\Delta C_{D_{\substack{Min \\ DD}}})}_{\text{Step 12}} \qquad \text{(III-54)}$$

6. BOUNDARY LAYER CONTROLLED FLAP

The few companies employing boundary layer control in conjunction with leading and trailing edge high lift devices consider the pertinent data and installation details to be highly proprietary. As a result, empirical evaluation of effects of these devices is precluded at this time. However, during the past 30 years a number of tests have been conducted, mostly with two dimensional models. These are reported upon in numerous documents (see Bibliography).

The primary advantage of boundary layer control in conjunction with high lift devices is to prevent or to delay flow separation. In the case of the suction flap (suction at the nose of the flap) the low energy (tired) boundary layer is removed and a fresh boundary layer is initiated. This new boundary layer is able to withstand the effects of the steep adverse pressure gradient immediately aft of the flap nose. In the case of a blowing flap, a high energy sheet of air is blown over the nose of the flap. This jet sheet energizes the existing boundary layer to enable it to negotiate the turn about the flap radius with its associated adverse pressure gradient.

Prevention of flow separation makes it possible to achieve lift coefficients approximating values predicted by potential flow theory even at very large flap deflection angles.

An additional increase in lift coefficients results from what is termed "supercirculation". This is due to the sink effect resulting from suction at the flap nose or in the case of blowing flaps, results from momentum transfer from the jet sheet to the surrounding flow field.

Another term which some of the authors include in the blown flap lift coefficient is the lift component of the jet reaction force.

As is the case with mechanical trailing edge lift devices, full advantage cannot be taken of the lift capability unless measures are taken to prevent separation of flow at the wing leading edge. This is particularly true where the leading edge radius is small.

The effectiveness of blown flaps is very sensitive to flap and jet slot geometry. Of particular importance is the position of the flap upper surface relative to the jet stream as emitted from the slot.

A. EFFECT OF BLC FLAPS ON LIFT

Although sufficient airplane data is lacking to formulate an empirical method for evaluating BLC flap characteristics, the following method was developed for determining the lift characteristics based on the information presented in References 14 through 19 . This method assumes that proper measures are taken to avoid leading edge separation and in the case of a suction flap, entrance geometry is near ideal, and in the case of blown flaps, the slot and the flap geometry are matched properly.

1. Blowing Flap

The lift coefficient for blowing flaps is considered to consist of two increments, one due to circulation lift and the other representing the lift component of the jet reaction force, so that

$$C_\ell = C_{\ell_\Gamma} + C_{\ell_R} \qquad \text{(III-55)}$$

$$C_{\ell_R} = C_\mu \cdot \sin(\delta_F + \delta_J) \qquad \text{(III-56)}$$

$$C_{\ell_\Gamma} = \frac{C_{\ell_\alpha}}{2\pi} \cdot \left(\frac{\partial C_\ell}{\partial \beta}\right)_{E=1.0} \cdot \sin(\alpha - \alpha_o') + \left(\frac{\partial C_\ell}{\partial \beta}\right)_{E=C_F/C} \cdot \sin \delta_F + \left(\frac{\partial C_\ell}{\partial \beta}\right)_{E=0} \cdot \sin \delta_J \qquad \text{(III-57)}$$

where C_{ℓ_α} is the lift curve slope for the clean airfoil section. See subsection 5B.

$\alpha_o' \sim \alpha_o$ @ $\delta_F = C_\mu = 0.0$

$\delta_F \sim$ Flap deflection angle

δ_J - angle at which the jet is ejected into the stream, if $\alpha = \delta_F = 0$. In the case where the jet "blows" over the upper surface of the flap, δ_J is the angle included by the trailing edge of the flap upper surface and the reference chord line. See Figure 3-51.

$\frac{\partial C_\ell}{\partial \beta} = f(C_\mu)$ is presented in Figure 3-52.

This Figure duplicates Figure 1 of Reference 14 except that C_μ has been substituted for C_J. In References 15 (page 475) and 16, it is indicated that C_J is equivalent to C_μ.

E in this figure represents the ratio of the flap hinge station to airfoil reference chord length. E = 1.0 is the limit condition where flap hinge theoretically coincides with the airfoil leading edge so that $\delta_F = \alpha$. E = 0.0 is the limit condition where flap hinge coincides with the airfoil trailing edge such as where a pure jet flap (jet emitted at the trailing edge) is employed.

C_μ is the blowing momentum coefficient defined by

$$C_\mu = \dot{W}_J \cdot V_J \; / \; g \cdot q \cdot S_B \qquad \text{(III-58)}$$

S_B is the area of the wing influenced by the blowing flap ("affected" area) as illustrated by Figure 3-51.

Figures 3-53a, 3-53b and 3-53c present a comparison of lift coefficient predicted by equation (III-57) with test data presented in Reference 17. These results indicate good correlation above $C_\mu = 0.05$. Below this value, $C_{\mu_{Crit}}$, the boundary layer is not sufficiently energized to completely forestall flow separation. Thus, below $C_{\mu_{Crit}}$, the increase in lift with C_μ is due primarily to increased flow attachment. Above this value, the further increase in lift is primarily due to supercirculation. Supercirculation is the increased circulation associated with transfer of momentum of the jet sheet to the free stream and may be treated

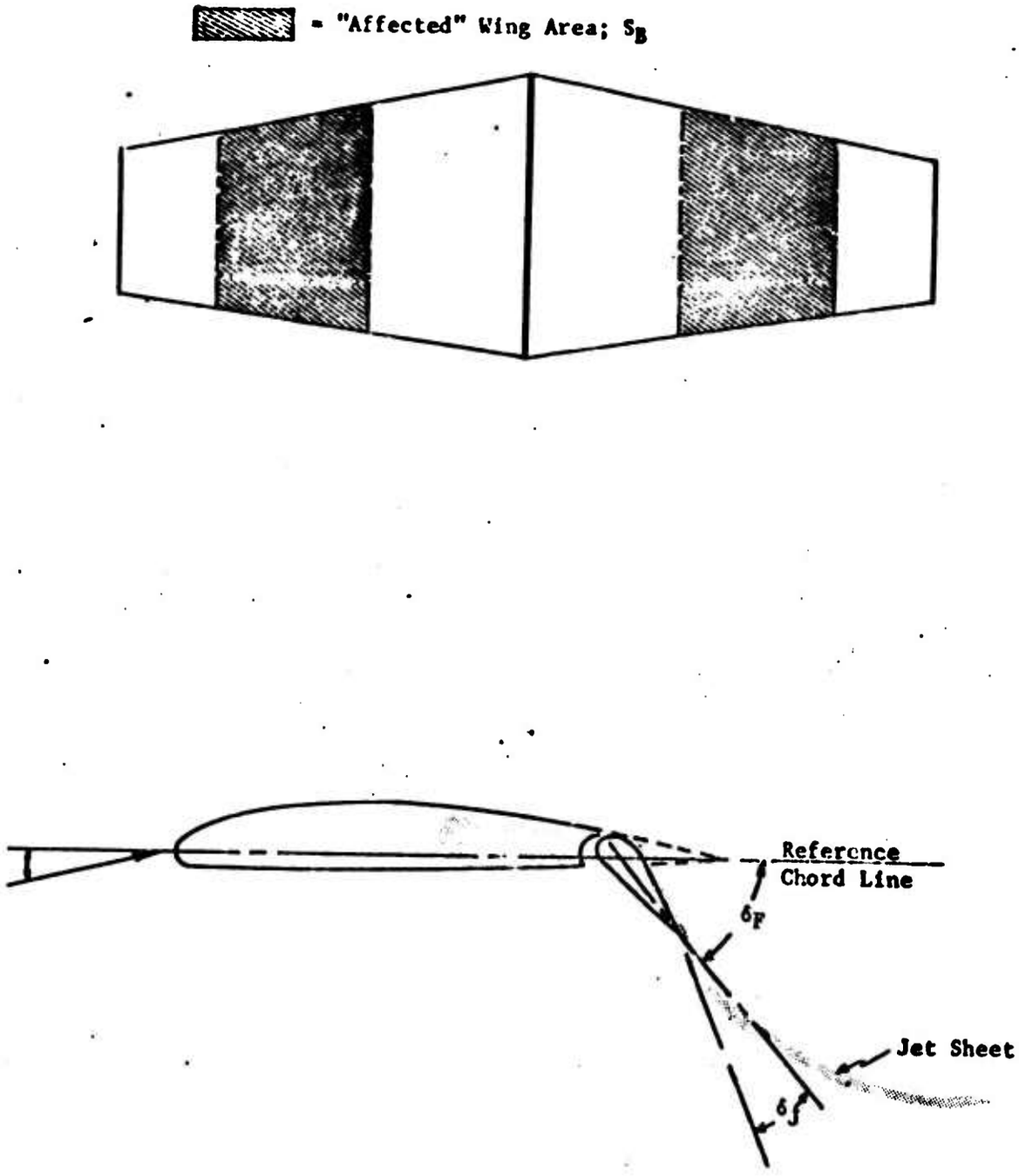

FIGURE 3-51: Blowing Flap Geometry

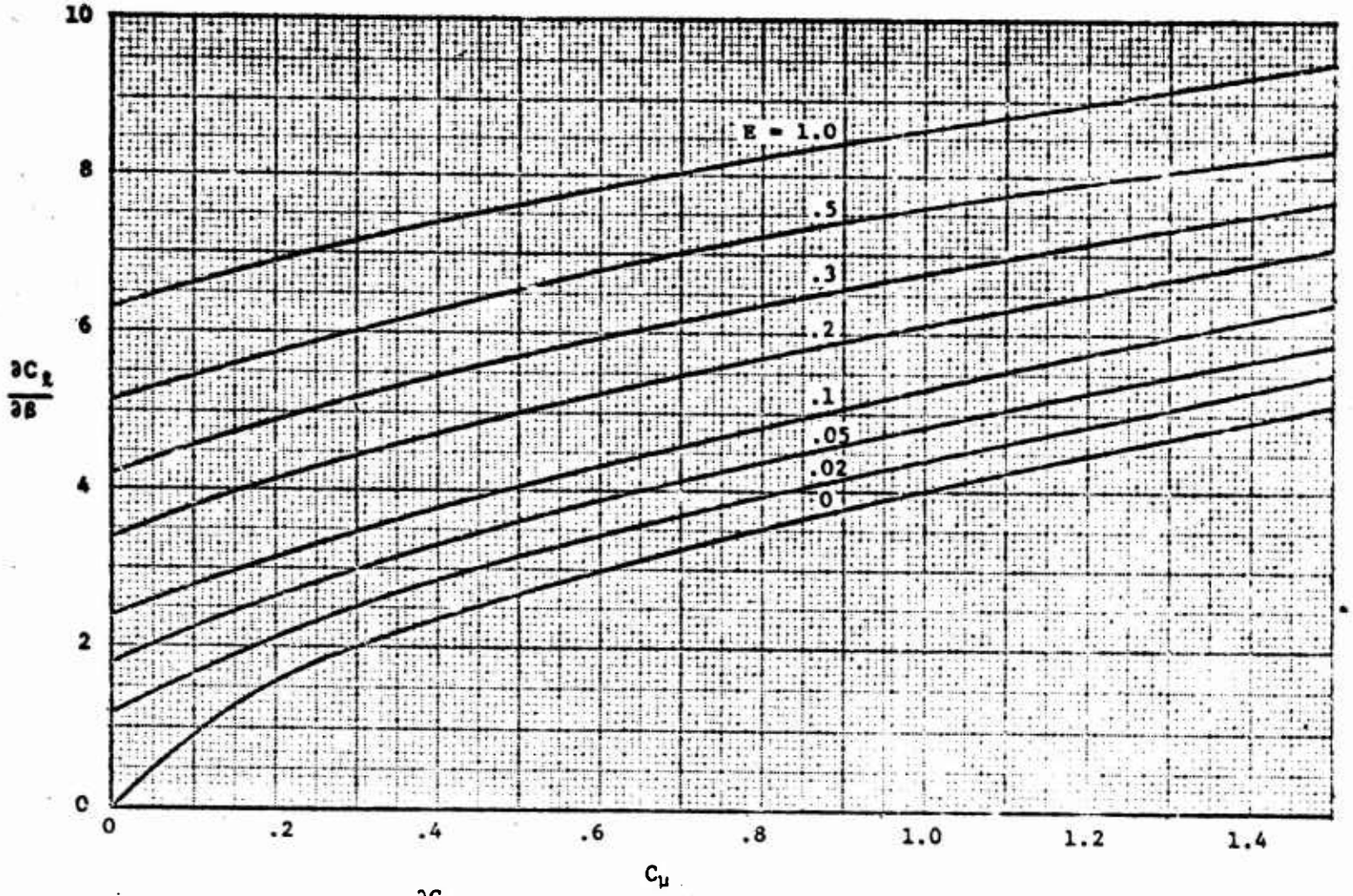

FIGURE 3-52: $\frac{\partial C_\ell}{\partial \beta}$ For Thin Wings With Blown Flaps

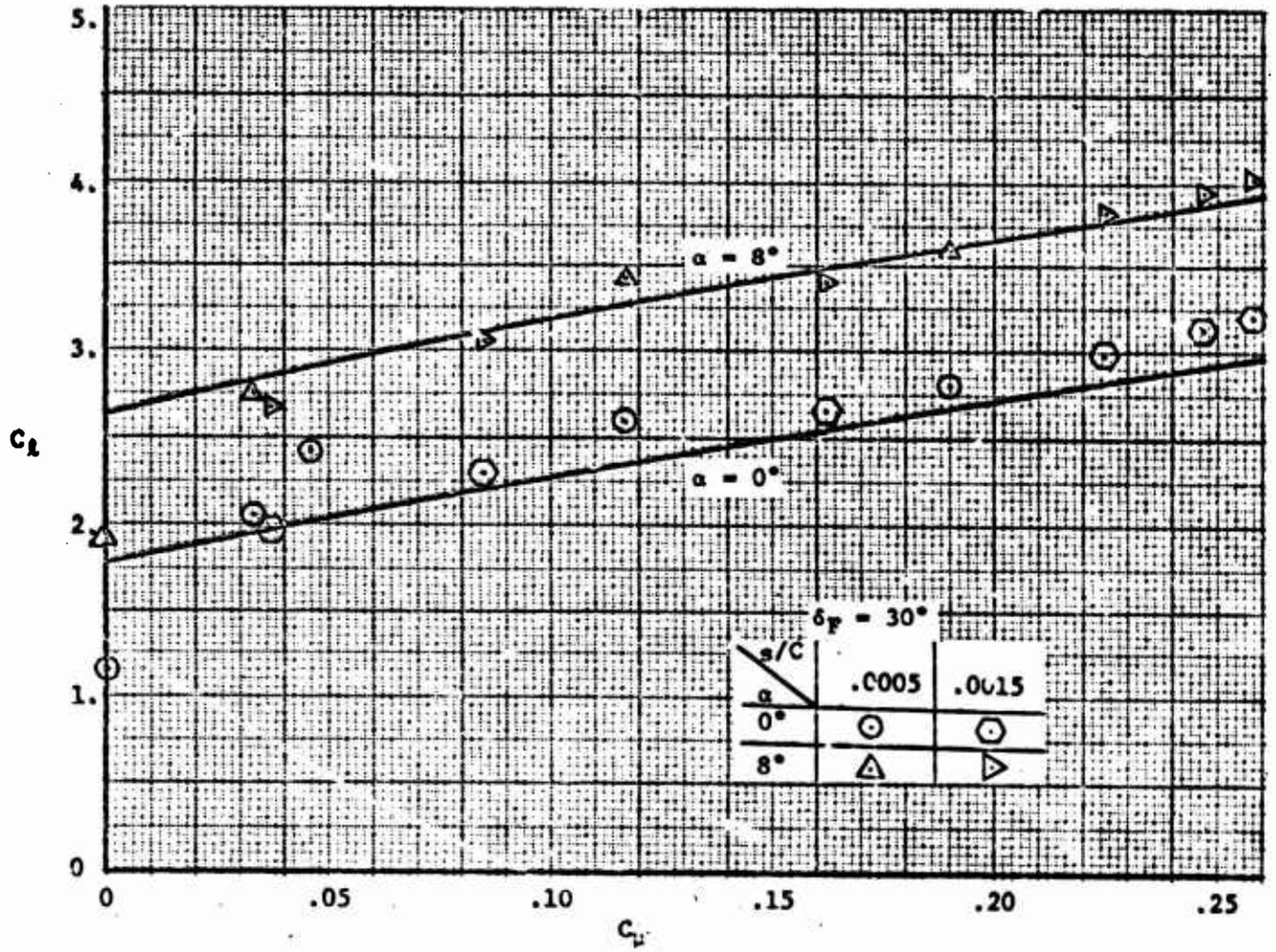

FIGURE 3-53a: Comparison of Lift Coefficient Predicted by Equation III - 57 with Test Data; $\delta_F = 30°$.

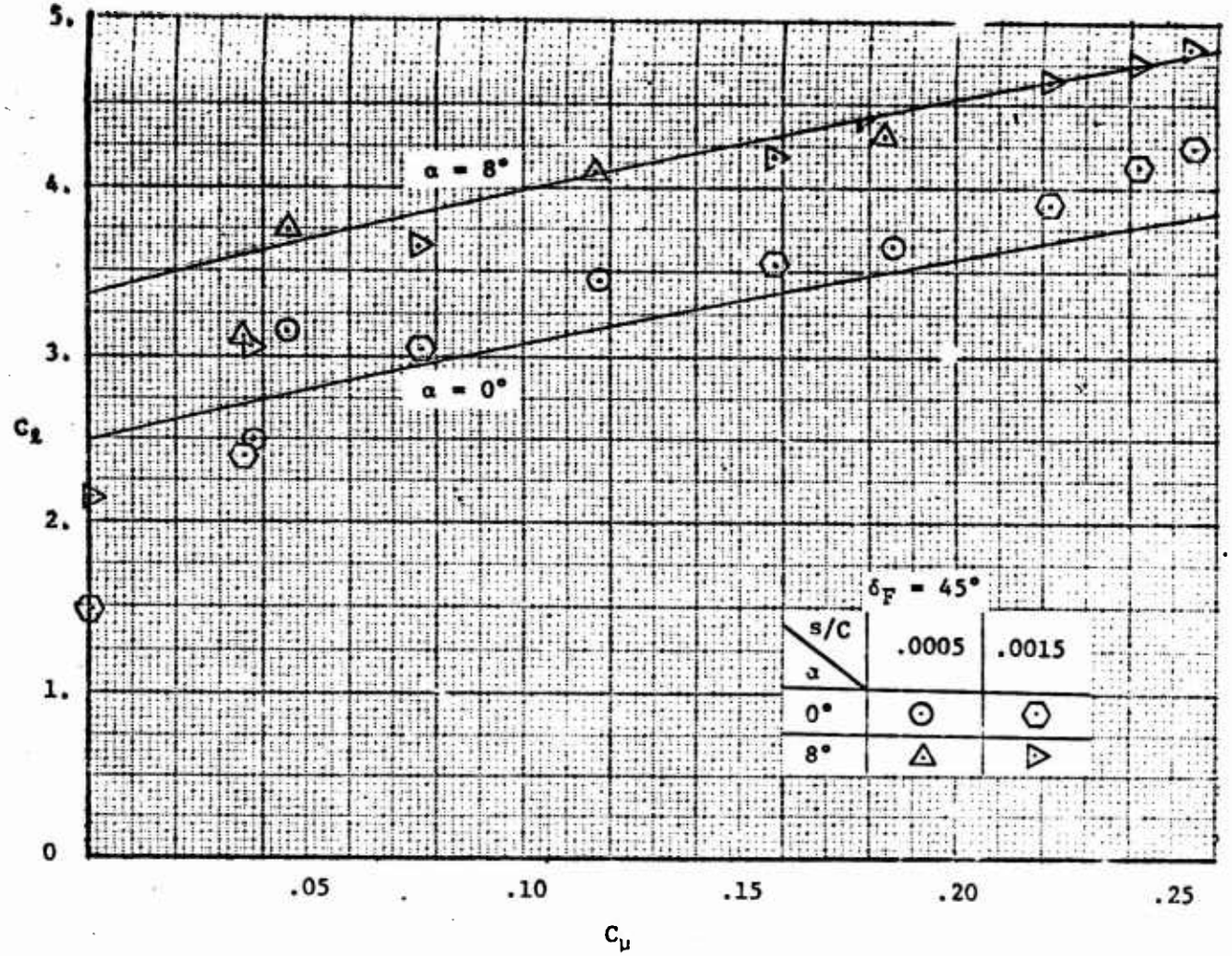

FIGURE 3-53b: Comparison of Lift Coefficient Predicted by Equation III-57 with Test Data ; $\delta_F = 45°$.

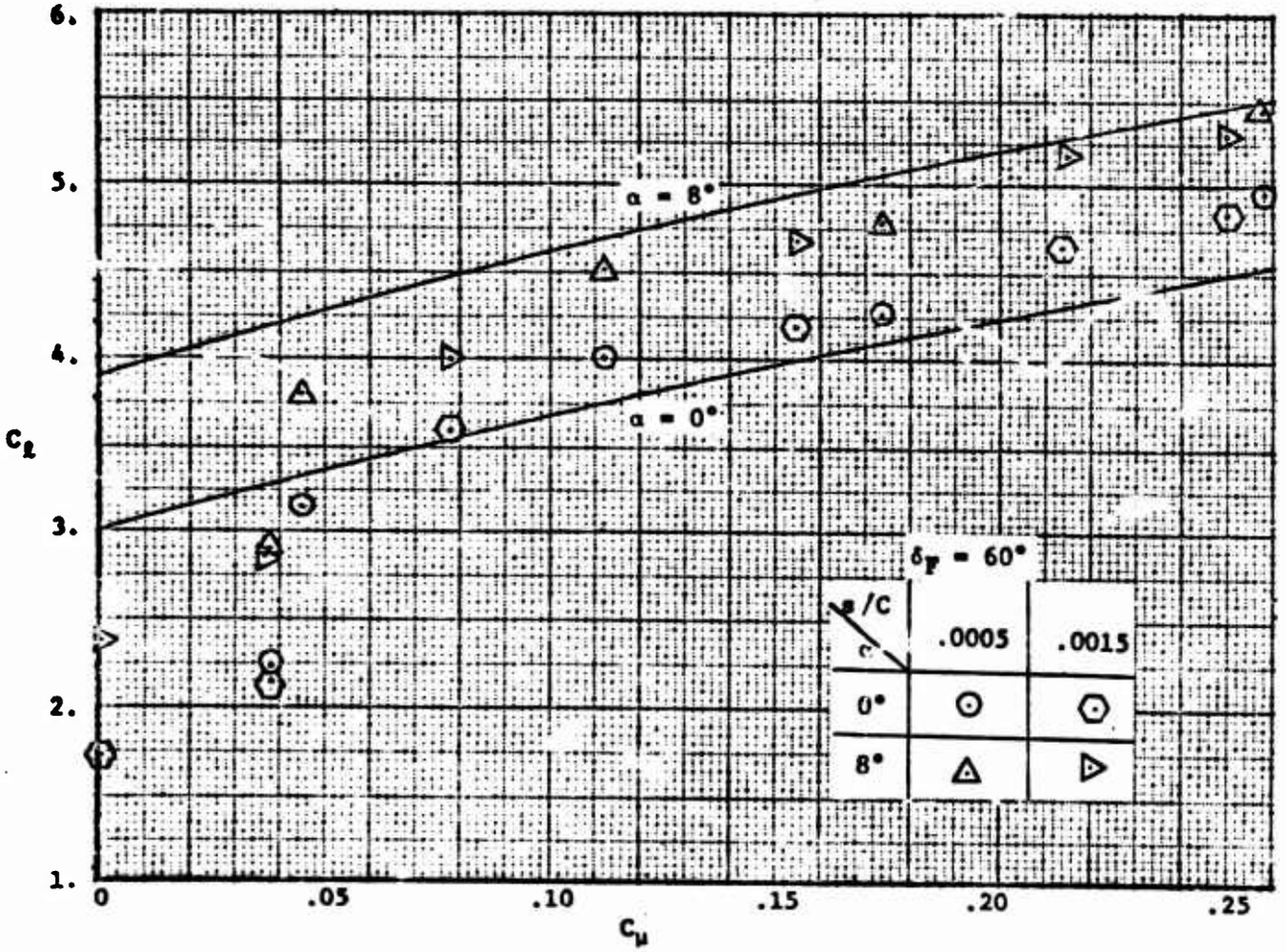

FIGURE 3-53c: Comparison of Lift Coefficient Predicted by Equation III-57 with Test Data; $\delta_F = 60°$.

analytically by a system of sinks coinciding with the profile of the jet sheet.

These regions of blowing flap effectiveness are illustrated by Figure 3-54 which duplicates Figure 6 of Reference 15. According to Reference 15, $C_{\mu_{Crit}}$ for a three dimensional wing may be estimated from the plot presented in Figure 3-55. In regard to this plot, Reference 15 (page 469) states:

> The relationship of $C_{\mu_{Crit}}$ is dependent upon wing aspect ratio, flap deflection and the "affected" area ratio, $[S_B/S]$. It can be appreciated that this is an over simplification of the many parameters involved; however, this plot due to Chaplin is considered to represent fairly consistent data for sweepback angles from 0° to 45°; flap chord ratios from 0.25 to 0.40; and angles of attack from 0° to 10° (but below the stall angle). Preliminary estimates of $C_{\mu_{Crit}}$ can therefore be obtained from Figure 3-55 for the conditions within these ranges, assuming a reasonably good nozzle flap orientation and flap geometry.

However, the 2-D data of Reference 17, presented in Figures 3-53a, 3-53b and 3-53c indicate that $C_{\mu_{Crit}}$ is not as sensitive to δ_F as indicated by Figure 3-55. These data indicate that $C_{\mu_{Crit}} = 0.05$ is applicable regardless of δ_F at least within the range $30° < \delta_F < 60°$.

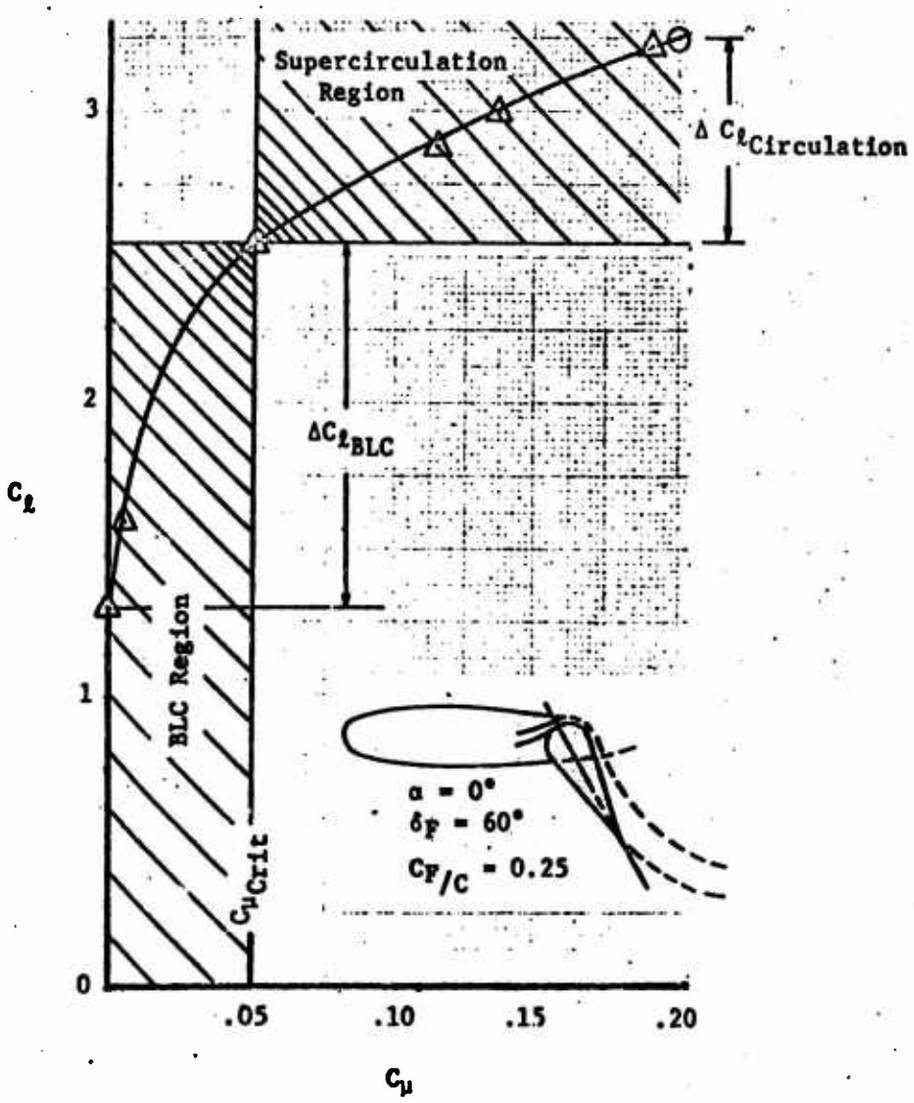

FIGURE 3-54: Definition of Boundary Layer Control and Supercirculation Regions.

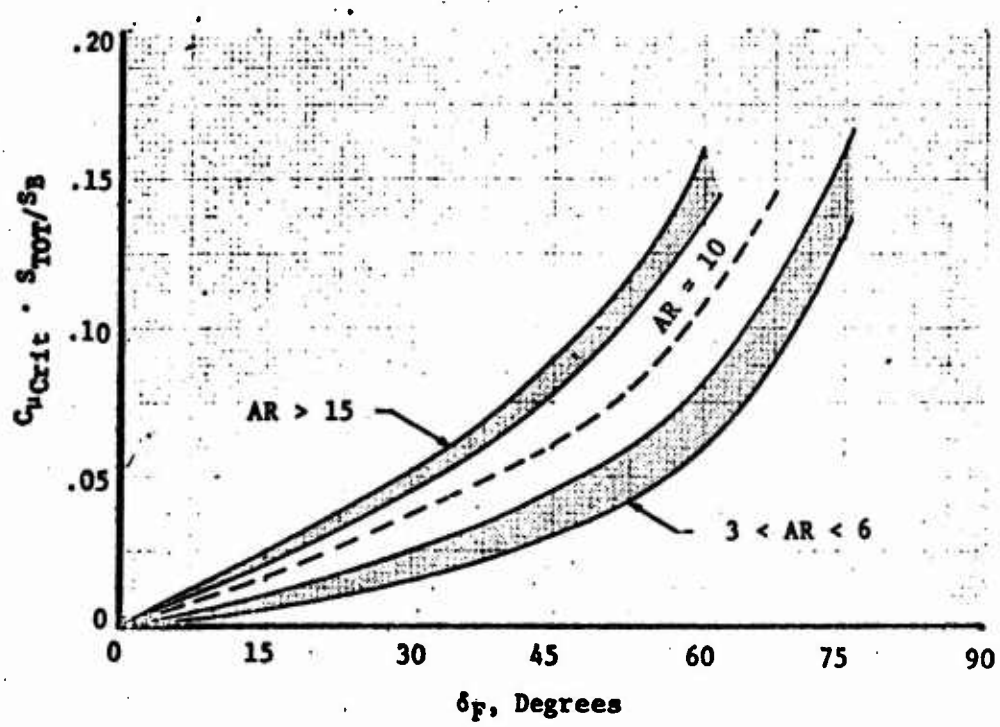

FIGURE 3-55: Critical C_μ for Attached Flow.

2. Procedure for Estimating Blowing Flap Lift

Based on the above discussion, the following procedure is suggested for estimation of wing lift when blowing flaps are employed.

a. Estimate the section lift curve slope, C_{ℓ_α}', (C_{ℓ_α} for the clean airfoil ($\delta_F = 0$, $C_\mu = 0$)) using the procedure given in Subsection 5B.

b. Estimate α_o' (α_o for clean airfoil) using the procedure given in Subsection 5B.

c. Compute C_ℓ' for $\delta_F = 0$, $C_\mu = 0$ where $C_\ell' = C_{\ell_\alpha}' (\alpha - \alpha_o')$.

d. Compute C_μ for given flight condition and blowing power setting where:

$$C_\mu = \dot{W}_J \cdot V_J / g \cdot q_o \cdot S_B$$

e. If $C_\mu > 0.05$

1. Obtain $\left(\frac{\partial C_\ell}{\partial \beta}\right)_{E=1}$; $\left(\frac{\partial C_\ell}{\partial \beta}\right)_{E=\frac{C_F}{C}}$ and $\left(\frac{\partial C_\ell}{\partial \beta}\right)_{E=0}$ from Figure 3-52.

2. Compute λ_B where

$$\lambda_B = \left[\left(\frac{\partial C_\ell}{\partial \beta}\right)_{E=1.0} \cdot \text{Sin}\,(\alpha - \alpha_o') + \left(\frac{\partial C_\ell}{\partial \beta}\right)_{E=\frac{C_F}{C}} \cdot \text{Sin}\,\delta_F + \left(\frac{\partial C_\ell}{\partial \beta}\right)_{E=0} \cdot \text{Sin}\,\delta_J \right]$$

3. Compute the sectional circulation lift coefficient as:

$$C_{\ell_\Gamma} = \frac{C_{\ell_\alpha}'}{2\pi} \cdot (\lambda_B)$$

f. If $C_\mu < 0.05$

1. Obtain $\left(\frac{\partial C_\ell}{\partial \beta}\right)_{E=C_F/C}$ for $C_\mu = 0.05$ from Figure 3-52.

2. Compute $\lambda_{B_{Crit}}$ where:

$$\lambda_{B_{Crit}} = \left[6.28 \text{ Sin } (\alpha - \alpha_o') + \left(\frac{\partial C_\ell}{\partial \beta}\right)_{E=C_F/C} \text{ Sin } \delta_F + 0.5 \text{ Sin } \delta_J\right]$$

3. Compute $C_{\ell_{\Gamma_{Crit}}}$ where:

$$C_{\ell_{\Gamma_{Crit}}} = \frac{C_{L_\alpha}'}{2\pi} (\lambda_{B_{Crit}})$$

4. Compute $(\Delta C_\ell)_\delta$ for $C_\mu = 0.0$ for plain flap using the procedure of Subsection 5E1.

5. Compute the sectional circulation lift coefficient as:

$$C_{\ell_\Gamma} = C_\ell' + (\Delta C_\ell)_\delta + \frac{C_\mu}{0.05}\left[\frac{C_{\ell_\alpha}}{2\pi} \cdot (\lambda_{B_{Crit}}) - C_\ell' - (\Delta C_\ell)_\delta\right]$$

g. Compute:

$$(\Delta C_{\ell_\Gamma})_{\delta_B} = C_{\ell_\Gamma} - C_\ell'$$

h. Compute:

$$(\Delta C_{L_\Gamma})_{\delta_B} = (\Delta C_{\ell_\Gamma})_{\delta_B}\left(\frac{C_{L_\alpha}}{C_{\ell_\alpha}}\right)\left(\frac{(\alpha_\delta)\ C_L}{(\alpha_\delta)\ C_\ell}\right) \cdot K_b$$

The details of this are described in the split flap Subsection 5E3, but is briefly repeated here

$\left(\frac{C_{L_\alpha}}{C_{\ell_\alpha}}\right)$ - ratio of the wing to section lift curve slope for clean wing ($\delta_F = 0$, $C_\mu = 0$)

$\left[\frac{(\alpha_\delta)_{C_L}}{(\alpha_\delta)_{C_\ell}}\right]$ From Figure 3-32

but where $(\alpha_\delta)_{C_\ell} = \dfrac{\left(\frac{\partial C_\ell}{\partial \beta}\right)_{E=C_{F/C}}}{\left(\frac{\partial C_\ell}{\partial \beta}\right)_{E=1}}$

and K_b is obtained from Figure 3-33.

i. Compute C_{L_α} in the same manner as suggested for a clean wing in Subsection 5C. That is:

$$C_{L_\alpha} = \frac{2\pi AR}{2 + \left\{\frac{4\pi^2 AR^2}{C_{\ell_\alpha}^2}\left(1 + (\text{Tan}\,\Lambda_{LE} - \frac{2}{AR}\frac{1-TR}{1+TR})^2\right) + 4\right\}^{1/2}}$$

where $C_{\ell_\alpha} = \dfrac{C_{\ell_\alpha}'}{2\pi} \cdot \left(\dfrac{\partial C_\ell}{\partial \beta}\right)_{E=1}$

j. Estimate the shift in α_o due to the deployment of blowing flap by:

$$\Delta\alpha_o = \frac{\left[(\Delta C_{\ell_\Gamma})_{\delta_B} \cdot \left(\frac{C_{L_\alpha}}{C_{\ell_\alpha}}\right) + C_\mu \text{ Sin } (\delta_F + \delta_J)\right]}{C_{L_\alpha}}$$

k. The increase in maximum section lift coefficient is:

$$\Delta C_{\ell_{max}} = k \cdot (\Delta C_{\ell_\Gamma})_{\delta_B} + C_\mu \sin(\delta_F + \delta_J)$$

where $0.5 < k < 1.0$, depending upon the tendency of the airfoil to incur leading edge separation. If leading edge separation occurs without flap deflection, $k = 0.5$ is applicable. However, if proper measurements are taken to preclude leading edge separation even at very high lift coefficient, then $k = 1.0$ is applicable.

1. $$\Delta C_{L_{MAX}} = \left[\Delta C_{L_R} + \Delta C_{\ell_{max}} (1 - .08 \cos^2 \Lambda_{C/4}) \cos^{3/4} \Lambda_{C/4}\right] \frac{S_B}{S_{REF}} \quad \text{(III-59)}$$

3. Suction Flaps

In references 18 and 19, it is shown that the increment of lift due to the sink effect of suction is $\Delta C_{\ell_S} = C_{Q_S} \cdot f(\delta_F, C_{F/C})$.

This relationship is presented by Figure 3-56 as:

$$K_S = \frac{\Delta C_\ell}{C_{Q_S}} = f(\delta_F, C_{F/C}).$$

$$C_{Q_S} = \frac{Q}{V \cdot S_S}$$

where Q - air flow quantity, $ft^3/sec.$
V - freestream velocity, ft/sec.
S_S - wing area affected by trailing edge suction flap, ft^2.

The circulation lift of a thin flat plate with a trailing edge flap with fully attached flow is given by potential flow theory to be:

$$(C_{\ell_\Gamma})_{PF} = 2\pi \cdot \text{Sin } \alpha + 2(\chi + \text{Sin } \chi) \cdot \text{Sin } \delta_F \qquad \text{(III-60)}$$

If sufficient suction is employed to preclude flow separation, the lift of the thin flapped plate with suction is estimated by

$$C_{\ell_{\Gamma_S, \text{ thin}}} = 2\pi \text{ Sin } \alpha + 2(\chi + \text{Sin } \chi) \cdot \text{Sin } \delta_F + K_S \cdot C_{Q_S} \qquad \text{(III-61)}$$

χ is defined in Reference 20 to be

$$\chi = \text{Cos}^{-1} \left(1 - 2 \frac{C_F}{C}\right).$$

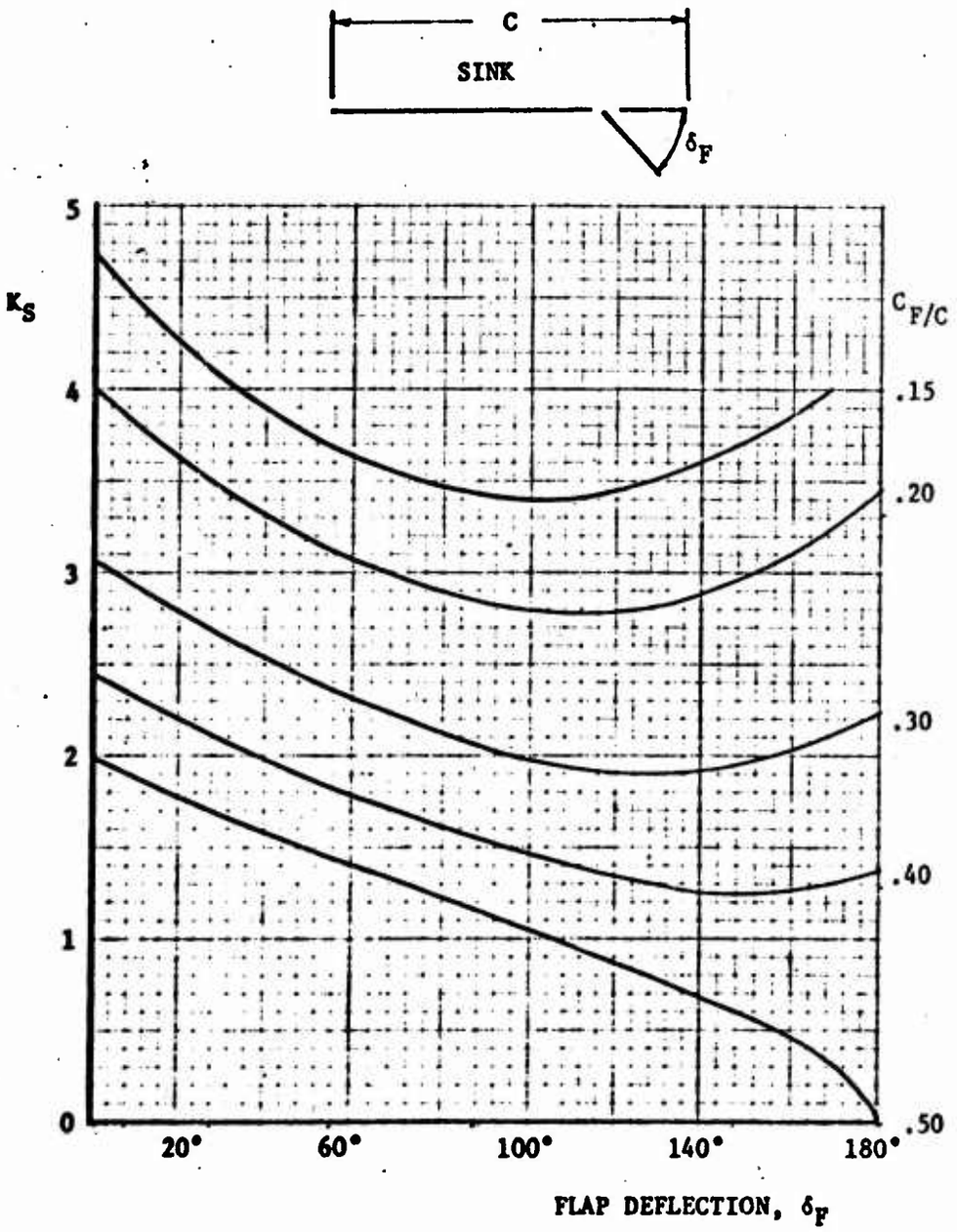

FIGURE 3-56: Sink Effect on Plain Flap Airfoils; t/C = 0

4. Procedure For Estimating Suction Flap Lift

Based on the above discussion and an assumption that sufficient suction is applied to assure flow attachment over the flap, the following procedure is suggested for estimation of wing lift when suction flaps are employed.

a. Estimate the section lift curve slope. C_{ℓ_α}', (C_{ℓ_α} for the clean airfoil ($\delta_F = 0$, $C_\mu = 0$)) using the procedure given in Subsection 5B.

b. Estimate α'_o (α_o for clean airfoil) using the procedure given in Subsection 5B.

c. Compute C_ℓ' for $\delta_F = 0$, $C_\mu = 0$ where

$$C_\ell' = C_{\ell_\alpha}' \ (\alpha - \alpha_o')$$

d. Obtain K_S from Figure 3-56.

e. Compute:

$$C_{Q_S} = \frac{Q}{V_o \cdot S_S}$$

f. Compute:

$$\chi = \cos^{-1}\left(1 - 2\frac{C_F}{C}\right)$$

g. Compute:

$$C_{\ell_\Gamma} = \frac{C_{\ell_\alpha}'}{2\pi}\left[2\pi \ \sin(\alpha - \alpha_o) + 2(\chi + \sin\chi) + K_S \cdot C_{Q_S}\right]$$

h. Compute:

$$(\Delta C_{\ell_\Gamma})_{\delta_S} = C_{\ell_\Gamma} - C_\ell'$$

i. Compute:

$$(\Delta C_{L_\Gamma})_{\delta_S} = (\Delta C_{\ell_\Gamma})_{\delta_S} \left(\frac{C_{L_\alpha}}{C_{\ell_\alpha}}\right) \left(\frac{(\alpha_\delta)C_L}{(\alpha_\delta)C_\ell}\right) \cdot K_b$$

The details of this are described in the split flap Subsection 5E3, but is briefly repeated here

$\left(\frac{C_{L_\alpha}}{C_{\ell_\alpha}}\right)$ - ratio of the wing section lift curve slope for clean wing ($\delta_F = 0$, $C_\mu = 0$)

$\left[\frac{(\alpha_\delta)C_L}{(\alpha_\delta)C_\ell}\right]$ From Figure 3-32

but where $(\alpha_\delta)_{C_\ell} = \frac{2(\chi + \sin\chi)}{2\pi}$

K_b is obtained from Figure 3-33.

j. C_{L_α} for the suction flap deflected is approximately the same as for the clean wing.

k. The change in angle of attack at zero-lift is obtained from:

$$\Delta\alpha_0 = -\frac{(\Delta C_{L_\Gamma})_{\delta_S}}{C_{L_\alpha}}$$

1. The increase in maximum section lift coefficient is:

$$\Delta C_{\ell_{max}} = k \cdot (\Delta C_{\ell_\Gamma})_{\delta_s}$$

where $0.5 < k < 1.0$ depending on the tendency of the airfoil to incur leading edge separation. See discussion on blowing flaps.

m. $$\Delta C_{L_{MAX}} = \Delta C_{\ell_{max}} \cdot \frac{S_s}{S_{REF}} \cdot (1 - .08 \cos^2 \Lambda_{C/4}) \cos^{3/4} \Lambda_{C/4} \qquad \text{(III-62)}$$

B. EFFECT OF BLC FLAPS ON DRAG

Data available, with regard to the effect of BLC flaps upon wing drag, are sparse and somewhat conflicting. Data given in Figure 33 of Reference 15 for the Grumman F9F-4 indicates that blowing reduces profile drag, whereas Figure 62 of the same Reference indicates that blowing increased the profile drag of the British aircraft "Submarine Scimitar". Seemingly, the effect of preventing flow separation over the flap surface would appreciably reduce profile drag at those flap deflection angles where the flow would be separated but for BLC. However, in cases where BLC flaps are employed, the profile drag is normally small compared with the induced drag. Thus, it would seem adequate for the type of analysis within the present scope of this handbook to assume that $\Delta C_{d_{Flap}}$ is the same as that given in Figure 3-48b for slotted flaps.

Procedure for Estimating Drag Due to BLC Flaps

1. Obtain $\Delta C_{D_{min_{flap}}}$ using Figure 3-48b and the procedure suggested in Subsection 5K for non-BLC flaps.

2. Determine $\Delta C_{D_{i_{flap}}}$ in the same manner as suggested in Subsection 5K for non-BLC flaps, that is:

$$\Delta C_{D_{i_{flap}}} = K' \frac{(\Delta C_L)^2}{\pi AR}$$

where K' is obtained from Figure 3-49a through 3-49c, and ΔC_L is the increment in wing lift due to BLC flap deflection.

3. The drag increment due to BLC flap deployment is:

$$\Delta C_{D_\delta} = \Delta C_{D_{min_{flap}}} + \Delta C_{D_{i_{flap}}} - C_\mu \cdot \frac{S_B}{S_{REF}} \cdot \cos(\delta_F + \delta_J) \qquad \text{(III-63)}$$

REFERENCES

1. Greiner, H., AIRDAT, Rohr Aircraft Report 24-2279, June 1968.
2. Ellison, D. E., USAF Stability and Control DATCOM, Contract AF 33(616)-6460, Douglas Aircraft Company, Inc., Revised November 1965.
3. Young, A. D., The Aerodynamic Characteristics of Flaps, ARC R & M 2622, 1953.
4. Gajdjis, S., Substantiation Report for F-105D, Standard Aircraft Characteristics Charts, Contract AF 33(600)-40838, December 1963.
5. Lewis, Perkins, Weutz, Substantiating Data Report B-52H Flight Manual and Standard Aircraft Characteristics Charts, Boeing Airplane Company Report D3-3211, January 19, 1961.
6. Douglas Aircraft Division, Douglas Skyhawks CA-4E and CA-4F, DAV Report 49773, March 1965.
7. White, W. C., F-5 Basic Aerodynamic Data, Volume I, Take-Off and Landing Configurations, Northrop Corporation Report NOR-64-2, January 1964.
8. U. S. Air Force, F-5A/B Aircraft Flight Manual, USAF T.O. 1F-5A-1, Contract AF33(657)136, December 1965.
9. U. S. Air Force, F-105D and F-105F Aircraft Flight Manual, USAF T.O.1F-105D-1, Contract AF33(600)34752, March 1965.
10. Reuter, J. D., Letter and Data to Rohr from Pioneer Parachute Company, 1999-Eng. '67, September 1967.
11. American Power Jet Co., Performance of and Design Criteria for Deployable Aerodynamic Decelerators, ASD-TR-61-579, (DDC-AD 429 971), December 1963.
12. Swenson, W. A., A Study of Parachutes and Systems for Aircraft Deceleration, WADC-TR-57-128 (ASTIA #233 185), January 1959.
13. Jennings & Peterson, Study & Development of Parachutes and Systems for In-Flight and Landing Deceleration of Aircraft, WADC-TR-57-566, Part I (ASTIA #234 008), January 1959.

14. Spence, D. A., The Lift on a Thin Airfoil with a Blown Flap, RAE TN Aero 2450, May 1956.

15. Lachmann, G. V., editor, Boundary Layer and Flow Control, (Two Volumes), Pergamon Press, 1961.

16. Helmbold, H. B., Theory of the Finite-Span Blowing Wing, Journal of the Aeronautical Sciences, Volume 24, No. 5, May 1957.

17. Wallace & Stalter, Systematic Two-Dimensional Test of an NACA 23015 Airfoil Section with a Single-Slotted Flap and Circulation Control, University of Wichita Aero Report 120, August 1954.

18. Ringleb, F. O., Investigations of Suction Flaps, Princeton University, Report No. 304, 1955.

19. Ryan Aeronautical Company, Interim Report on Analytical Studies and Bench Tests of a High Lift Boundary Layer Control System, Contract DA 44-177-AMC-35(T), Ryan Aeronautical Company Report 64B053, April 1964.

20. Allen, H. J., Calculation of the Chordwise Load Distribution Over Airfoil Sections with Plain, Split, or Serially-Hinged Trailing Edge Flaps, NACA TR-634, 1938.

SECTION IV

WHEEL BRAKES

1. DISCUSSION

This section is intended to provide an analytical tool to estimate the force generated by an aircraft wheel braking system. An estimate can be made if the physical description of the wheel, tires and brakes and the condition of the runway surface are known.

During the evaluation of an aircraft's landing distance, there are two items that must be considered regarding the braking system:

a. The braking force,

b. The brake's limitation.

The braking force is defined, as is customary, in terms of the product of a coefficient and a force normal to the runway surface. The brake limitation is given in terms of an energy absorption limit.

2. BRAKING FORCE AND EQUATIONS OF MOTION

The present industry procedure for computing the ground roll distance is to solve the equation:

$$\frac{GW}{g}\dot{V} = T - D - (\text{Braking force})$$

where braking force $= \mu_B k_1 (GW-L) + \mu_R (1-k_1) (GW-L)$;

k_1 denotes the portion of (GW-L) supported by the main landing gear at zero air lift velocity.

With this procedure, the braking and rolling coefficients are assumed to be invariant during the ground roll. In addition, no account is

taken of variation in main landing gear loading due to deceleration and aerodynamically induced moments. Thus the above equation provides inaccurate results, particularly when braking is restricted to the main landing gear.

The following method provides a wheel braking estimate that accounts for redistribution of loading between the main gear and nose gear due to deceleration and aerodynamic moments. Procedures are included for taking into account the use or non-use of anti-skid devices, runway contamination and tire geometry. In addition, Subsection 5 presents an evaluation of brake energy limits.

The equations of motion which describe the forces and moments acting on the aircraft are as follows:

$$\Sigma \text{Forces Vertical} = 0 = GW - F_{mg} - F_{nw} - L \qquad \text{(IV-1)}$$

$$\Sigma \text{Forces Horizontal} = 0 = \frac{GW}{g} \cdot \dot{V} + T - D - \mu_B \cdot F_{mg} - \mu_R \cdot F_{nw} \qquad \text{(IV-2)}$$

$$\Sigma \text{Moments about the nose wheel} = 0 = \ell_{x_{c.g.}} \cdot (GW-L) + M_{aero} + D \cdot \ell_{z_{c.g.}} - T \cdot \ell_{z_{T.L.}} - F_{mg} \cdot \ell_{x_{mg}} - \frac{GW}{g} \cdot \dot{V} \cdot \ell_{z_{c.g.}} \qquad \text{(IV-3)}$$

$$\Sigma \text{Moments about the main wheels} = 0 = -(\ell_{x_{mg}} - \ell_{x_{c.g.}}) \cdot (GW-L) + M_{aero} + D \cdot \ell_{z_{c.g.}} - T \cdot \ell_{z_{T.L.}} + F_{nw} \cdot \ell_{x_{mg}} - \frac{GW}{g} \cdot \dot{V} \cdot \ell_{z_{c.g.}} \qquad \text{(IV-4)}$$

where the pertinent force and moment vectors are depicted in Figure 4-1.

Here it is assumed for simplicity that during ground roll, drag and lift act through the center of gravity parallel and perpendicular to the ground.

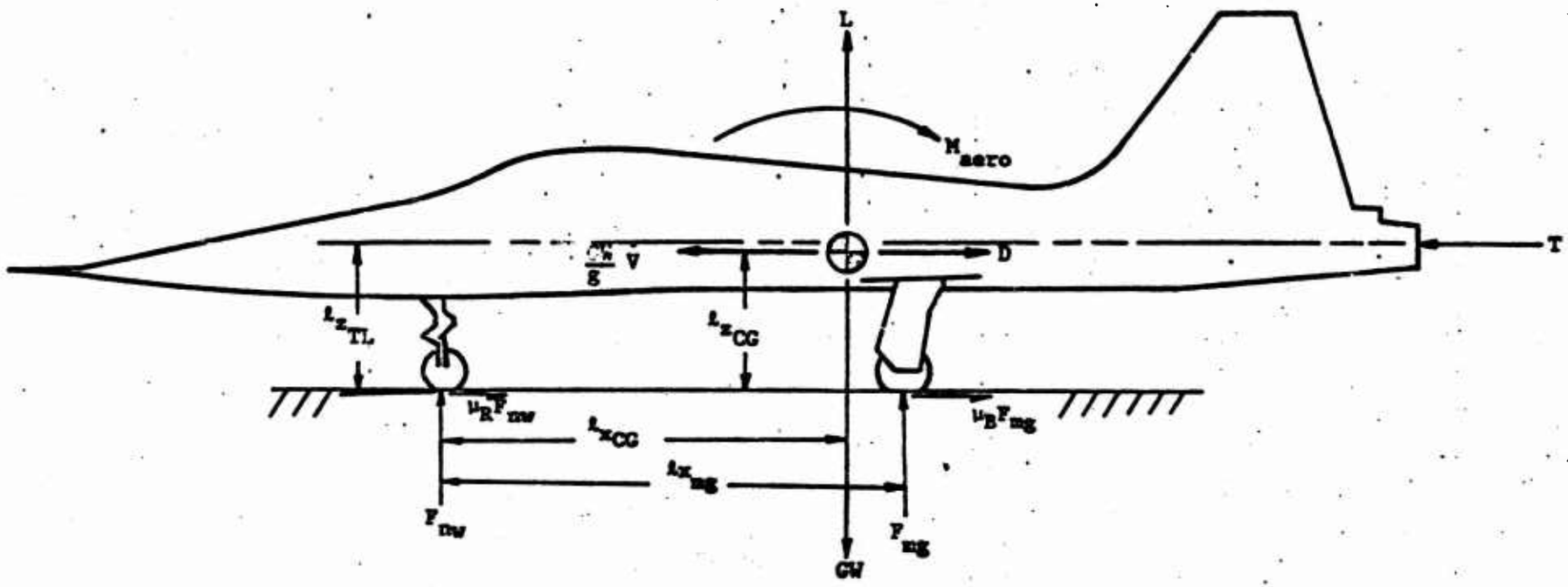

FIGURE 4-1: Force and Moment V :tor Diagram for Ground Roll Analysis.

Where braking is restricted to the main gear, the braking force is $(\mu_B \cdot F_{mg}) + (\mu_R \cdot F_{nw})$ Rewriting the moment equations (IV-3 and IV-4) as follows:

$$F_{mg} = \frac{1}{\ell x_{mg}} \left(M_{aero} + \ell x_{c.g.} \cdot (GW-L) + D \cdot \ell z_{c.g.} - T \cdot \ell z_{T\,L.} - \frac{GW}{g} \cdot \dot{V} \cdot \ell z_{c.g.} \right) \qquad \text{(IV-5)}$$

$$F_{nw} = \frac{-1}{\ell x_{mg}} \left(M_{aero} - (\ell x_{mg} - \ell x_{c.g.}) \cdot (GW-L) + D \cdot \ell z_{c.g.} - T \cdot \ell z_{T.L.} - \frac{GW}{g} \cdot \dot{V} \cdot \ell z_{c.g.} \right) \qquad \text{(IV-6)}$$

provides expressions for the wheel normal forces which accounts for deceleration thrust and aerodynamic moment and drag in addition to consideration traditionally given to weight and lift.

A perusal of References 1 and 2 indicates that an empirical expression for μ_B is:

$$\mu_B = f\,(\text{var.}) \left(C_1 - C_2 \frac{F_{mg}}{A_n} \right) \qquad \text{(IV-7)}$$

where f (var.) describes the runway condition, use of an anti-skid device, etc.

C_1 is the empirical nondimensional maximum braking coefficient

C_2 accounts for the tire geometry and has the units corresponding to(force) $^{-1}$.

F_{mg} is the vertical force exerted on the tires of the main gear.

A_n is the tire print area discussed in Subsection 7.

Methods for computing μ_B for anti-skid and non-anti-skid brakes with consideration given to runway contamination and tire geometry are presented by Subsections 3 and 4.

Rolling friction, denoted by the coefficient μ_R varies with aircraft velocity. The data of Reference 2 indicates that μ_R increases from approximately 0.02 at 40 knots to 0.05 at 120 knots. However, B-58 data presented in Reference 3 indicates much less of an increase, μ_R = 0.0116 at 0.0 knots to 0.0158 at 150 knots. The B-58 data tends to justify the standard practice of using a constant value of μ_R for the ground roll deceleration calculations. The T-38 computations of Reference 4 uses μ_R = 0.01. Reference 5 computations for the C-135 uses 0.015.

Equations IV-1 through IV-7 provide the force data required to evaluate ground roll deceleration of aircraft equipped with brakes applied through only the main landing gear. If, in addition, nose wheel braking is employed, equation IV-2 must be modified by replacing μ_R with a brake coefficient (μ_B) appropriate to the nose gear.

3. BRAKING COEFFICIENT FOR DRY CONCRETE RUNWAYS

This section provides a method for determining the brake coefficient, μ_B, corresponding to operation on dry concrete runways. Effect of runway contaminants are discussed in Subsection 4.

It has been determined experimentally that the braking for a given aircraft tire on a dry uncontaminated runway is affected by the various factors as follows:

Factor	Effect on μ_B
1. Vertical Load	Decreasing coefficient with increasing load
2. Velocity	None
3. Tread Design	None
4. Tread Composition	Very slight
5. Tire Inflation	Very slight decrease with increased pressure
6. Tire Temperature	Very slight decrease with increased temperature

A good discussion of these factors is given in Reference 1, 2, and 6. In Reference 6 it is stated that:

> "Most of the information on tire friction has, in the past, been obtained with fully skidding or locked wheels. Information for the fully skidding condition may be of value where a relatively small amount of kinetic energy is to be dissipated and tire wear is of little consequence. However, for aircraft operation involving enormous kinetic energies, deceleration with locked wheels would be disastrous. Tire wear, of course, varies with wheel slip - the lower the slipping velocity the lower the tire wear. Tire wear can be reduced appreciably by operating in the incipient skidding region which also provides the maximum available tire-to-ground friction coefficient and hence maximum aircraft deceleration. For these reasons, and the fact that anti-skid devices tend to operate in the region of incipient skid, information on $\mu_{a[\mu_{max}]}$ appears to be of considerably more interest and use in the aircraft operation than information on tire friction with wheels locked."

An expression for μ_{max} which accounts for the above factors is given by the equation.

$\mu_{max} = .93 - .0011p_n$ (Verification of this is given in Figure 4-2, which was originally presented in Reference 2.)

where p_n is the net bearing pressure which is $p_n = \frac{F_z}{A_n}$

where F_z is the vertical force and A_n is the tire net foot print area.

Although this equation was obtained from rolling speeds of 1 to 2 MPH, the data of Reference 2 verifies this equation up to 90 knots.

For an aircraft whose braking is obtained solely from the main landing gear tires:

$$\mu_{max} = .93 - .0011 \frac{F_{mg}}{A_n} \qquad \text{(IV-8)}$$

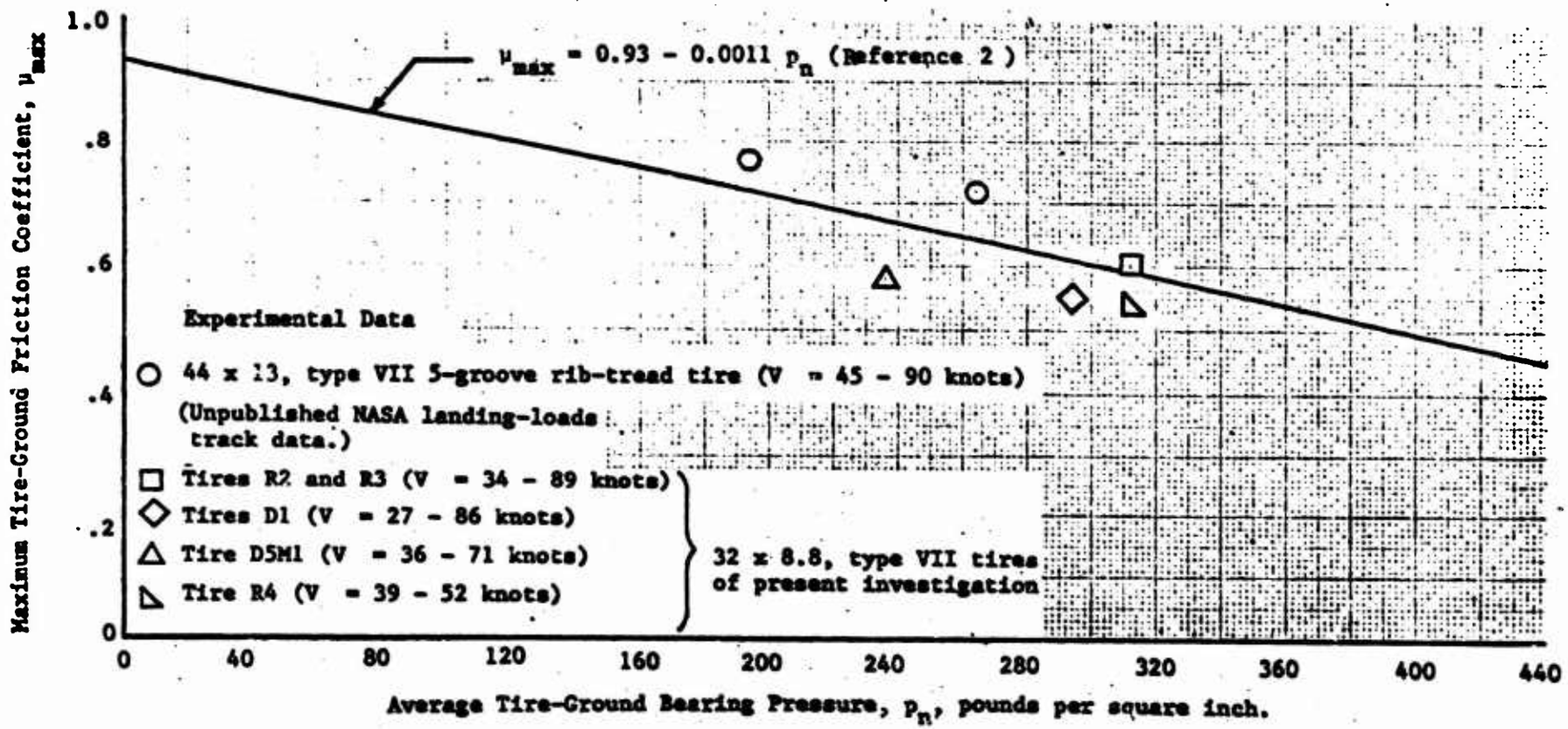

FIGURE 4-2: Variation of Maximum Tire-ground friction coefficient μ_{max} with Average Tire-Ground Bearing Pressure p_n for several different tires and tread designs on a dry concrete runway.

For any rolling tire that has a braking system the coefficient of friction is a function of the slip ratio. Slip ratio is defined in Reference 2, page 11, which states:

> "The difference between the peripheral velocity of the tire and the horizontal velocity of the wheel axle is defined as the relative skidding velocity occurring between the tire and the ground. The ratio of this relative skidding velocity to the horizontal velocity of the axle is defined as the slip ratio. Thus for a freely rolling wheel the slip ratio is effectively zero while for a completely braked wheel (full skid) the slip ratio equals 1. "

The variation of μ with slip ratio is shown in Figure 4-3. The shaded area in this figure represents the normal range of operations for anti-skid devices.

Horne (Reference 2) shows that for a braking system employing an anti-skid device, the effective μ is approximately $.9\mu_{max}$ (Figure 36 of Reference 2 shows verification of this statement), see Figure 4-4. Therefore, the equation for effective μ (or μ average) is,

$$\mu_{avg} = .837 - .00099 \cdot \frac{F_{mg}}{A_n}$$

where a method for determining tire print area (A_n) is presented in Subsection 7.

μ_{max} may then be considered the "best" braking coefficient that would be possible for an aircraft landing on a dry uncontaminated (no rubber or oil deposits) concrete runway, and using an anti-skid device.

Due to the sensitivity of the brakes and the desirability of avoiding skid to reduce tire wear and to maintain controllability, non-skid brakes are normally operated at low slip ratios, below 0.1. Thus it is doubtful that a braking system that does not employ an anti-skid device could obtain even the μ associated with a full skid (brakes locked). Figure 4.5 indicates μ for full skid in the velocity range above 40 knots to be:

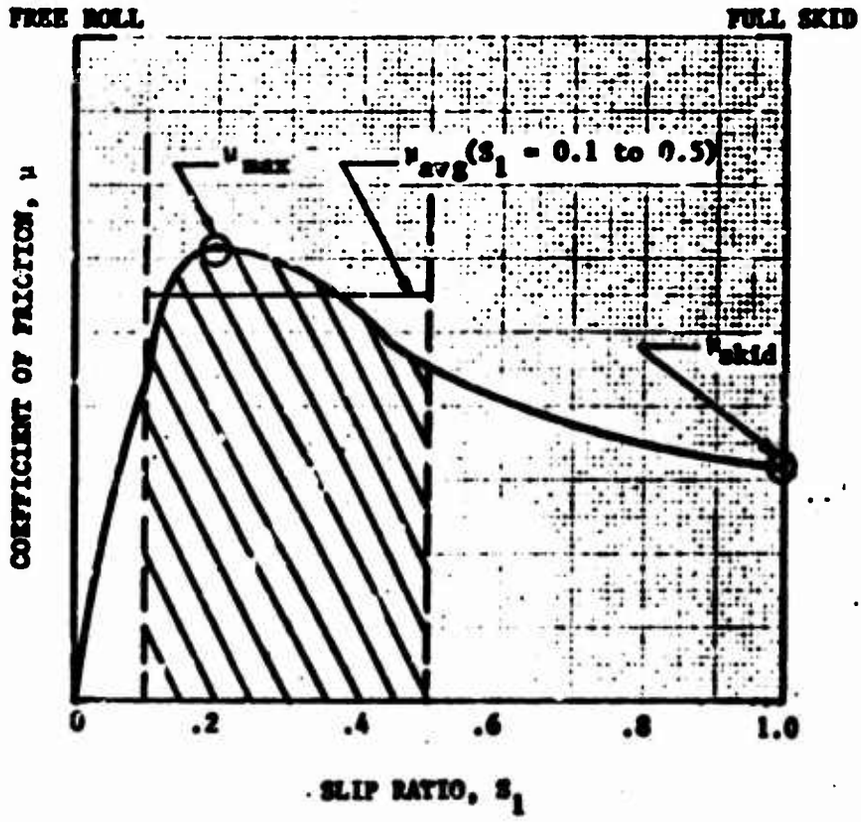

FIGURE 4-3: Determination of μ_{avg}

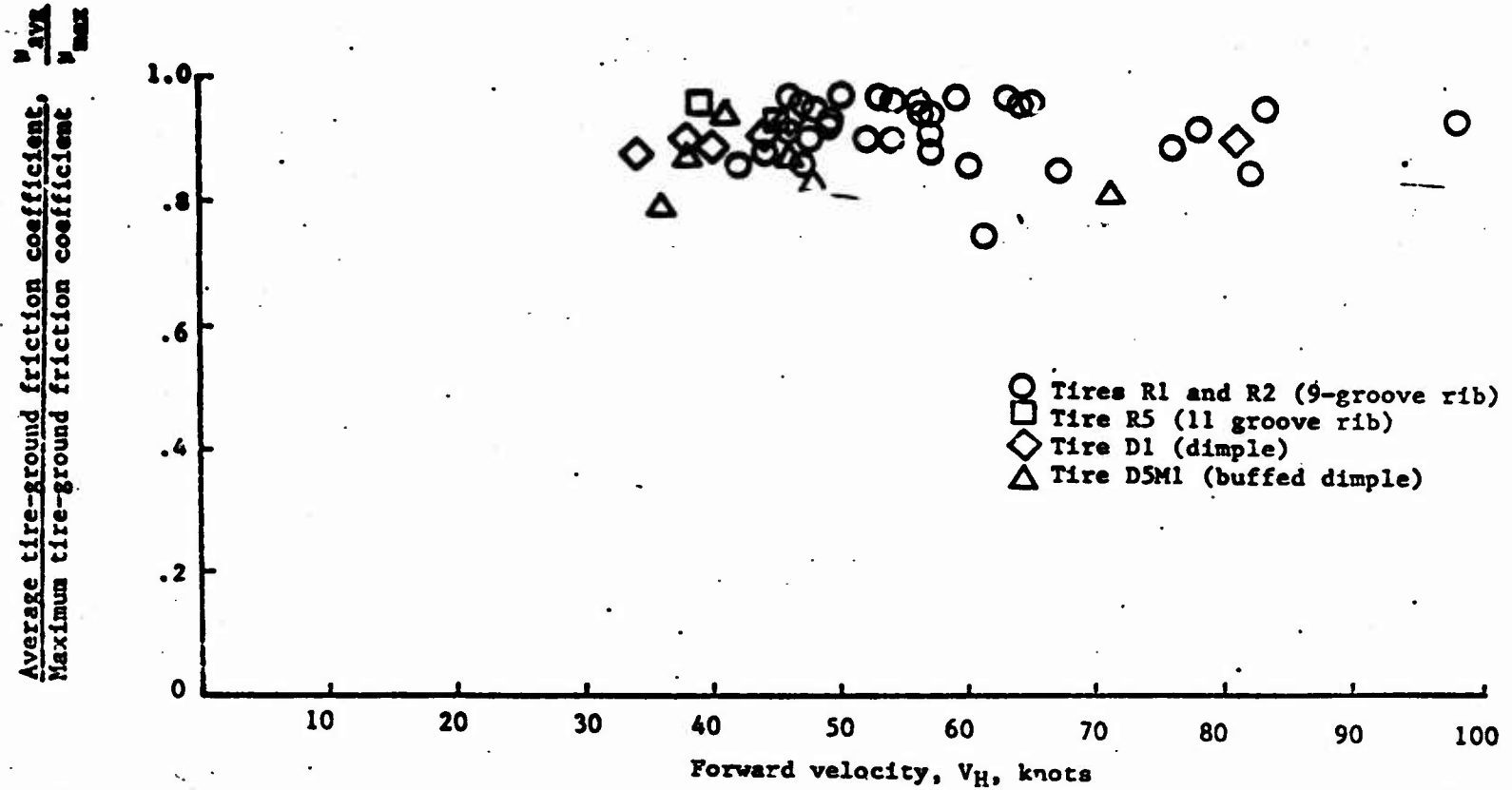

FIGURE 4-4: Variation of the Ratio of Tire-Ground Friction Coefficient $\frac{\mu_{avg}}{\mu_{max}}$ with Forward Velocity for Several Tires on a Dry Concrete Runway. $F_{mg} \approx 10{,}000$ lbs; p = 260 lb/sq.in.

○ Tire D5M1
□ Tire R4
◇ Tire R2
△ Tire D1

32 x 8.8 type VII; Present Investigation
p = 260 lb/in^2

▷ Tire 44 x 13, type VII, p = 200 lb/in^2
▯ Tire 44 x 13, type VII, p = 150 lb/in^2
◇ Tire 56 x 16, type VII, p = 168 lb/in^2
◇ Tire 26 x 6.6, type VII, p = 103 lb/in^2
◇ Tire 26 x 6.6, type VII, p = 230 lb/in^2
⬭ Tire 40 x 12, type VII, p = 124 lb/in^2

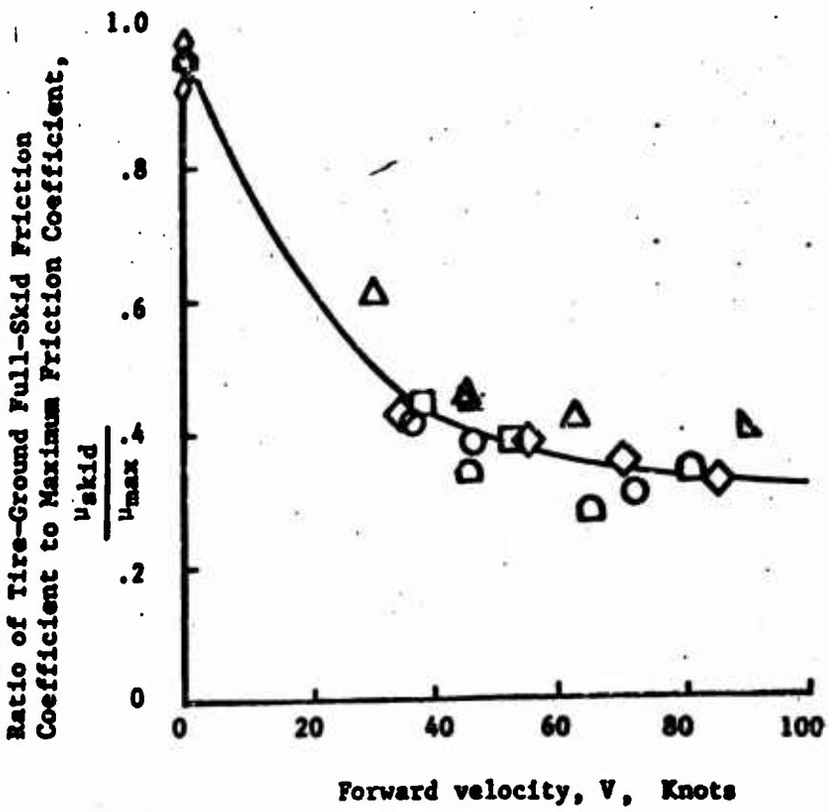

FIGURE 4-5: Effect of Forward Velocity on the Ratio of Tire-Ground Full-Skid Friction Coefficient to Maximum Friction Coefficient $\frac{\mu_{skid}}{\mu_{max}}$. Data Obtained on Dry Concrete Runways.

$$\mu_{skid} < 0.4\ \mu_{max}$$

It is suggested that for an aircraft that does not have an anti-skid system, the braking coefficient be estimated as follows:

1. Compute μ_{max} as for the anti-skid case
2. Modify μ_{max} with the curve shown in Figure 4-5 by assuming

$$\mu_{max} = \frac{\mu_{skid}}{\mu_{max}} \times (\mu_{max})_{\text{anti-skid}} \qquad \text{(IV-10)}$$

3. Use of .9 of the results to insure no skidding.

The curve in Figure 4-5 can be expressed as:

$$f(V) = C_1 + C_2V + C_3V^2 + C_4V^3 + C_5V^4 \qquad \text{(IV-11)}$$

where $C_1 = 1.0$

$C_2 = -.24492 \times 10^{-1}$

$C_3 = .3368 \times 10^{-3}$

$C_4 = -.20098 \times 10^{-5}$

$C_5 = .42539 \times 10^{-8}$

V = knots

and so the estimated effective μ for non-anti-skid systems is given by:

$$\mu_{avg} = f(V)\ (0.837 - 0.00099\ \frac{F_{mg}}{A_n}) \qquad \text{(IV-12)}$$

This again applies only for dry concrete runways.

For the purpose of landing ground roll evaluation calculations it should be assumed that:

$$\mu_R = \mu_{avg}$$

4. RUNWAY CONTAMINANTS

The current method for accounting for runway conditions other than dry concrete is to use a RCR measurement. RCR (Runway Condition Reading) is a measure of the deceleration capability of an aircraft as determined by driving an automobile type vehicle over a runway and then getting the vehicle into a skid. The deceleration measurement made during this skid (in ft/sec^2) is the RCR value.

Industry figures and descriptive runway conditions are usually considered as follows:

RCR	Runway Condition
23	Dry Uncontaminated Concrete
12 - 17	Wet
5	Ice

Various manufacturer's (See Table IV-1) have their own values of μ corresponding to dry, wet or icy runways.

As indicated in Subsection 3, methods such as the above which provide information only for the fully skidding case are inadequate for evaluation of aircraft braking systems employing anti-skid devices. In this case, μ_{max} is the pertinent coefficient rather than μ_{skid}.

The following material summarizes results of tests conducted to measure μ_{max} for various conditions of runway contamination, and in addition a method is suggested for analytically predicting the effects of climatic contamination upon the friction coefficient.

Runway contamination which induces tire wear is, of course, undesirable and therefore to the extent practical, is avoided. As a result, the nature and extent of the contamination is uncontrollable and usually non-uniform. In recent years a number of tests have been conducted to determine the effect of runway contaminants upon tire friction. The validity of the results of these tests is somewhat restricted to the special conditions under which the testing was conducted.

TABLE IV-1

AIRCRAFT MANUFACTURER'S BRAKING COEFFICIENTS (μ_B)

Manufacturer	Anti-Skid	Runway Condition RCR# (Concrete) Dry 23	Wet 17	Wet 14	Wet 12	Icy 5	Theory	Test
McDonnell F-4	Yes	.23	.20	.154		.026	X	
Northrop F-5	No	.30			.157	.065	X	
Northrop F-5	No	.20-.35						X
Grumman A-6A	Yes	.38					X	
Lockheed F-104*	Yes	.25		.15		.10	X	
Republic F-105**	No	.30/.20					X	
Boeing B-52	No	.30			.10-.15		X	
Boeing KC-135A†	Yes	.2-.4	.12-.14					X
Lockheed C-141	Yes	.4					X	
Gen. Dynamics F-111	Yes	.4					X	

NOTES:

* RCR unknown for these values.

** 1957/1960 values

† RCR 23-24 Dry, RCR 19.5-22 Wet

Because of their extreme non-uniformity and resultant unpredictability, the effects of contaminants such as fuel, oil, tire rubber deposits, etc. are considered to be beyond the scope of this report except to note that in Reference 2 certain test data indicate that μ_{avg} decreases from about 0.64 for the dry uncontaminated concrete surface to about 0.48 for the dry rubber-contaminated concrete surface under the conditions of the investigation.

Reference 6 reported on tests conducted with various climatic contaminants. These results are summarized by Table IV-2 and Figure 4-6. It was reported that for dry and ice or snow covered runways there appeared to be no variation of μ_{max} over the airplane speeds covered in the tests and within the scatter of the data. The large scatter in the data for wet runway and runways in light and heavy rain is attributed to the variation in the amount of water along the runway.

A. BRAKING COEFFICIENT FOR ICE AND SNOW COVERED RUNWAYS

If Table IV-1 contains values of μ_B that are appropriate for the aircraft and runway condition under consideration, these values may be used. However, if no appropriate values of μ_{avg} are listed therein, the following method for estimating μ_B is suggested.

1. Select an appropriate value of μ_{max} from Table IV-2.
2. Calculate μ_{avg} from μ_{max} in the same manner as was suggested in Subsection 3 for dry runways. That is

   a. If anti-skid devices are employed:

   $$\mu_{avg} = 0.9\ \mu_{max}$$

   b. If no anti-skid device is employed:

   $$\mu_{avg} = 0.9\ (\mu_{skid}/\mu_{max})\ (\mu_{max})_{\text{anti-skid}} \qquad \text{(IV-13)}$$

   where (μ_{skid}/μ_{max}) is given by Eq. IV-11 and Figure 4-5.

B. WET RUNWAYS

Several experimental programs (See References 2 and 6 through 15) have been completed in an effort to measure μ on a wet runway. Based on these programs, some insight has been obtained into the influencing factors on μ on a wet runway.

TABLE IV-2

SUMMARY OF TIRE FRICTION COEFFICIENTS

(a) Dry Runways

RUNWAY COVER	$\bar{\mu}_{max}$	σ	Speed range (knots)
Portland cement concrete (P.C.C.)	0.77	0.05	46-88
Bituminous concrete (B.C.)	.81	.06	49-108

(b) Snow Covered Runways

RUNWAY COVER	$\bar{\mu}_{max}$	σ	Speed range (knots)
1/4 in. of new, soft, moist snow over an icy and refrozen snow subsurface	0.28	0.05	20-60
1/4 to 1/2 in. of new, hard-packed, moist snow over bituminous pavement. Packed by recent ploughing	.35	.04	17-72
5 to 6 in. of new, soft, dry snow over ice-spotted bituminous pavement	.35	.05	11-65
1 to 2 in. of new, soft, dry snow over an icy, packed snow subsurface	.27	.03	16-103
1 to 4 in. of new, soft,moist snow over an icy, packed snow subsurface	.24	.03	39-115
5 in. of old, soft to hard, moist to wet snow left on frozen lake surface when top 7-in. layer was removed by ploughing	.26	.03	11-90
1 to 3 in. of new, soft, dry snow over 5 in. of old, hard, dry snow left on frozen lake by previous ploughing	.28	.02	32-86

TABLE IV-2 (cont.)

(c) Ice

RUNWAY COVER	$\bar{\mu}_{max}$	σ	Speed range (knots)
Frozen lake surface, with thin patchy snow residue left on ice from ploughing operation, surface temperature 32°F. No water film evident. Air temperature, 32°F.	0.18	0.02	17-78
Frozen lake surface, with thin patchy snow residue left on ice from ploughing operation, surface temperature 19°F. No water film evident. Air temperature, 0°F.	.18	.02	25-85

(d) Wet Runways

RUNWAY COVER	$\bar{\mu}_{max}$	σ	Speed range (knots)
Wet Portland cement concrete	0.36	0.13	53-94
	.42	.16	44-109
	.43	.12	33-93
Bituminous concrete in heavy rain	.20	.09	61-103
Bituminous concrete in light rain	.53	.07	48-98
Bituminous concrete in light rain with runway dotted with puddles from previous rain	.80	.10	69-91

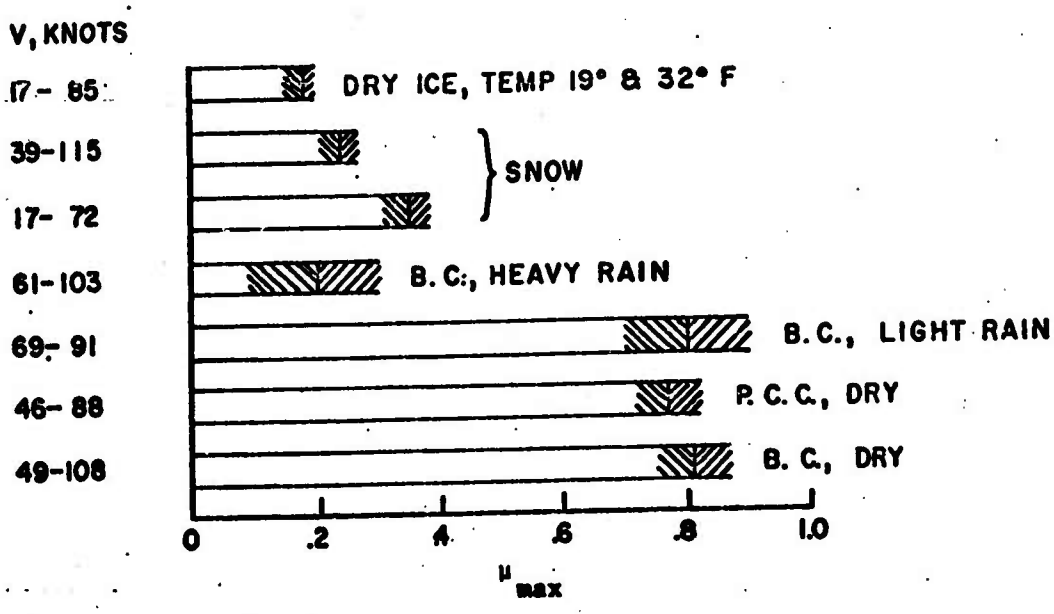

FIGURE 4-6: Mean values of Maximum Available Tire Friction Coefficient μ_{max} for Various Runway Surfaces.

Value of standard deviation shown as shaded area about the mean. Abbreviation B.C. refers to bituminous concrete and P.C.C. to portland cement concrete.

The results are summarized as follows:

Factor	Effect on
1. Vertical Load	Decreasing coefficient with increasing load.
2. Velocity	Decreasing coefficient with increasing velocity (See Figure 4-5)
3. Tread Design	Order of best braking (See Figure 4-7) 1. Circumferential Rib 2. Lateral Groove and Diamond 3. Smooth and Dimple
4. Tread Composition	Very slight
5. Tire Inflation Pressure	Slight decrease with increased pressure
6. Tire Temperature	Slight decrease with increased temperature

As was indicated above for ice and snow, if appropriate values of μ_B are available in Table IV-1, these should be utilized. If otherwise, the following method for estimating μ_B is suggested.

1. Compute μ_{avg} for dry runway using the appropriate method (for anti-skid or non-anti-skid) given in Subsection 3.

2. Compute:

$$f(\text{tread},V) = C_1 + C_2V + C_3V^2 + C_4V^3 + C_5V^4 \qquad \text{(IV-14)}$$

where the coefficients are defined by:

Tread Design	C_1	C_2	C_3	C_4	C_5
Smooth or Dimple	.9666	$-.21398\times10^{-1}$	$.24384\times10^{-3}$	$-.14359\times10^{-5}$	$.31745\times10^{-8}$
Diamond	.9748	$-.12863\times10^{-1}$	$.92995\times10^{-4}$	$.39654\times10^{-6}$	$.78224\times10^{-9}$
Ribs (4)	1.0	$-.11943\times10^{-1}$	$.75697\times10^{-4}$	$-.14953\times10^{-6}$	$-.590157\times10^{-10}$

Equation IV-14 is presented graphically by Figure 4-7.

3. $$\mu_{B_{wet}} = \mu_{avg} \cdot f(\text{tread},V) \qquad \text{(IV-15)}$$

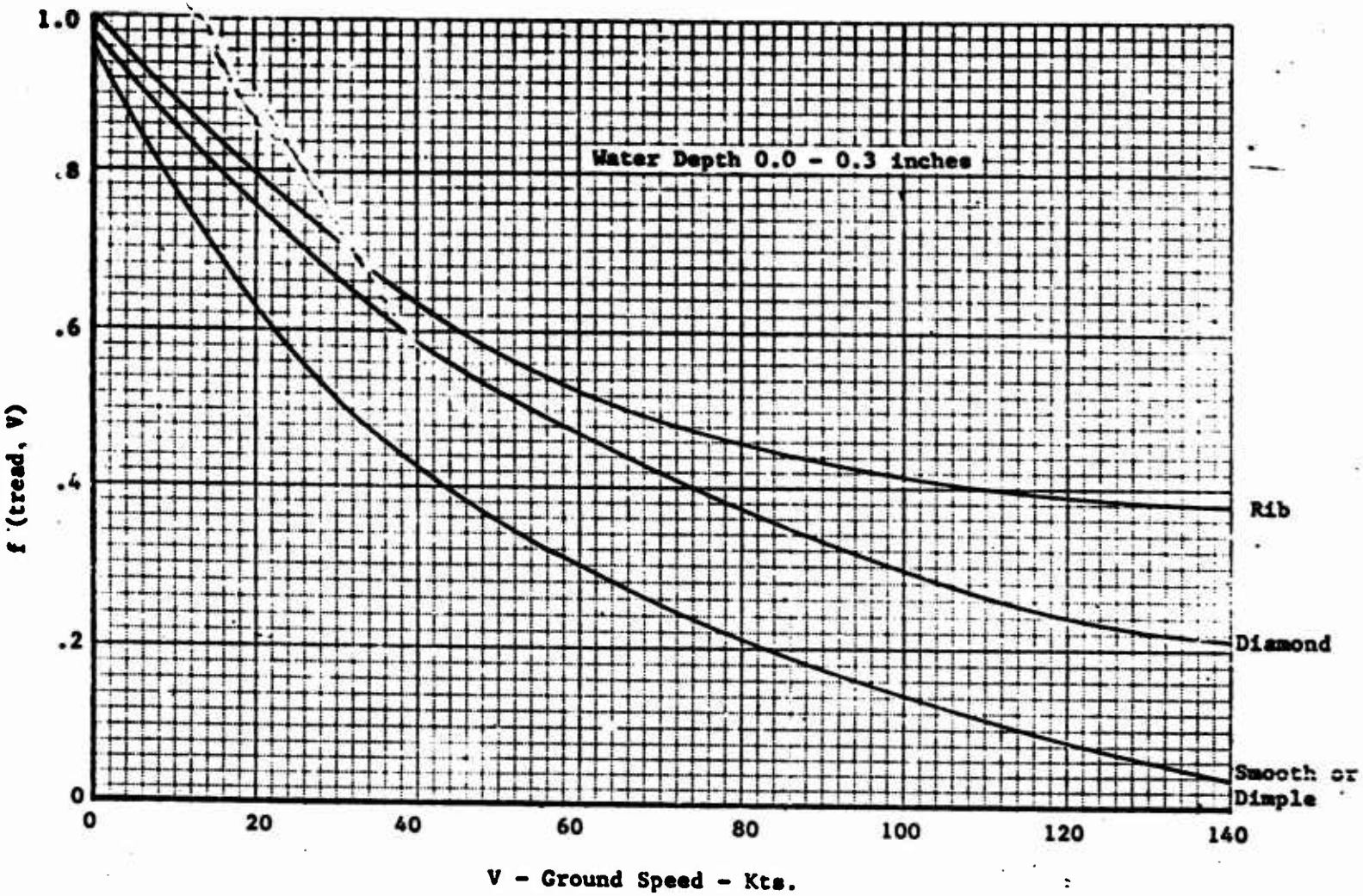

FIGURE 4-7: Effect of Tread Design and Velocity on Wet Runways.

5. BRAKE ENERGY LIMITATIONS

The brakes are limited by the amount of energy the brakes can absorb without causing damage to the brakes or causing a fire due to excess heat. This energy limit is empirically established by the brake manufacturer and is a function of the type and number of stops that are anticipated. For example, for the F-104G airplane, if 50 stops are anticipated without change of brake-lining, then a kinetic energy of 6×10^6 ft-lbs cannot be exceeded during each stop. If only one stop is to be made (maximum performance landing) without causing a fire or explosion, then the energy limit is raised to 10×10^6 ft-lbs. (See Table IV-3)

The kinetic energy that the aircraft brakes will absorb during a landing can be obtained by integration of the horizontal forces equation (equation VI-2) over the landing distance. Rewriting the equation:

$$\mu_B \cdot F_{mg} = \frac{GW}{g} \cdot \dot{V} + T - D - \mu_R \cdot F_{mw}$$

integrating along the ground roll distance

$$\int_{s_o}^{s_f} \mu_B \cdot F_{mg} \cdot ds = m \int_{s_o}^{s_f} \dot{V} \cdot ds + \int_{s_o}^{s_f} (T - D - \mu_R \cdot F_{mw}) \, ds$$

where s_o is the initial distance where the brakes are applied

s_f is the final distance where the brakes are released.

TABLE IV-3

BRAKE ENERGY LIMITS

A. From the aircraft flight manual

Normal - Normal operation use. Some time factors may be required for brake cooling when operating near the limit.

Caution - Possible fire. Brake damage may occur. Inspections are required.

Danger - Fire and explosions are imminent. Brake and tire inspections are required.

Aircraft	C-135	C-141	F-111	B-58
Description	Brake Energy Limits ($\times 10^{-6}$ ft-lbs)			
Normal	20	18	18	10
Caution	28	27	23	11.8
Danger	40	39.4	37.5	18

B. From Brake Manufacturer's data: (Bendix)

Aircraft	No. of Stops	Brake Energy Limit ($\times 10^{-6}$ ft-lbs)
F-102	1	11.25
	10	9.1
	*40	5.5
F-104G	1	10
	*50	6
F-106	1	15.9
	5	9.1
	*45	8.3
B-52	1	40.6
	5	30.2
	*45	16.8
DC-8	1	36.9
	5	19.5
	*100	11.2
DC-9	RTO(1)	26.5
	6	16.1
	*100	12.2
CV-880	1	24.5
	3	17.3
	*92	13.9
CV-990	1	31.6
	3	20.2
	*92	16.2
CL-44	1	17.7
	3	11.0
	*100	8.8

*To be completed without change of lining

Now $m \int_{s_o}^{s_f} V \, ds = 1/2 \, m \cdot V^2 \Big]_{s_o}^{s_f}$ the change in kinetic energy (ΔK.E.)

$$\text{Brake energy (B.E.)} = \int_{s_o}^{s_f} \mu_B \cdot F_{ng} \, ds$$

and so

$$\text{B.E.} = \Delta\text{K.E.} + \int_{s_o}^{s_f} (T - D - \mu_R \cdot F_{nw}) \, ds \qquad \text{(IV-16)}$$

It can be seen that the brake energy can be reduced by permitting a longer ground roll ($s_f - s_o$) so that ($T - D - \mu_R \cdot F_{nw}$) creates a larger negative number and thereby subtracting from the total ΔK.E.

Anti-skid systems permit brake operation near μ_{max}, which in turn is the condition where maximum heat is generated. The brake energy limit is also a direct function of this heat generation. Therefore, if an aircraft ground roll occurs during which the brakes are operated in the anti-skid mode for a long distance, there exists the possibility of exceeding the brake energy limit. All aircraft that employ anti-skid devices include brake energy limits in the -1 handbook.

It should be emphasized that to determine if a ground roll calculation is compatible with the braking system, a brake energy check must be made.

Table IV-3 shows brake energy limits for various aircraft. This information was obtained from either the manufacturer's T.O. ( )-1 Flight Manual or from Reference 16.

6. TIRE FOOTPRINTS

In order to obtain the net tire footprint, one of the following procedures should be used:

1. The best way to obtain a tire footprint is to obtain an impression and graphically obtain the actual contact area.
2. The next best method is to measure the tire deflection and then compute the footprint area as follows (From Reference 17) (See Figure 4-6 for definitions).
   a. Obtain:
      d - Tire Radial Deflection (difference between loaded and unloaded section heights)
      D_o - Tire outside diameter
      W - Tire section width
      D_f - Rim flange diameter
   b. Calculate dimensions of basic "Decap Area", which is the area of intersection of a horizontal plane through the tire at the radial deflection point (or depth) d:

      M = Major Axis of Decap = $2\sqrt{d(D_o - d)}$

      m = Minor Axis of Decap = $2\sqrt{d(W - d)}$

   c From the above values, approximate footprint dimensions may be calculated as follows:

      F = Major Axis of Footprint = .85 M

      f = Minor Axis of Footprint = $m \times \begin{cases} 1.00 \text{ for Type VII \& VIII Tires} \\ .93 \text{ for Type III Tires} \\ .84 \text{ for Type I Tires} \end{cases}$

      Footprint area = $.785 \cdot F \cdot f \times \begin{cases} .95 \text{ for Type III, VII \& VII Tires} \\ .85 \text{ for Type I Tires} \end{cases}$

3. If the tire deflection is unknown the following approximation can be used.

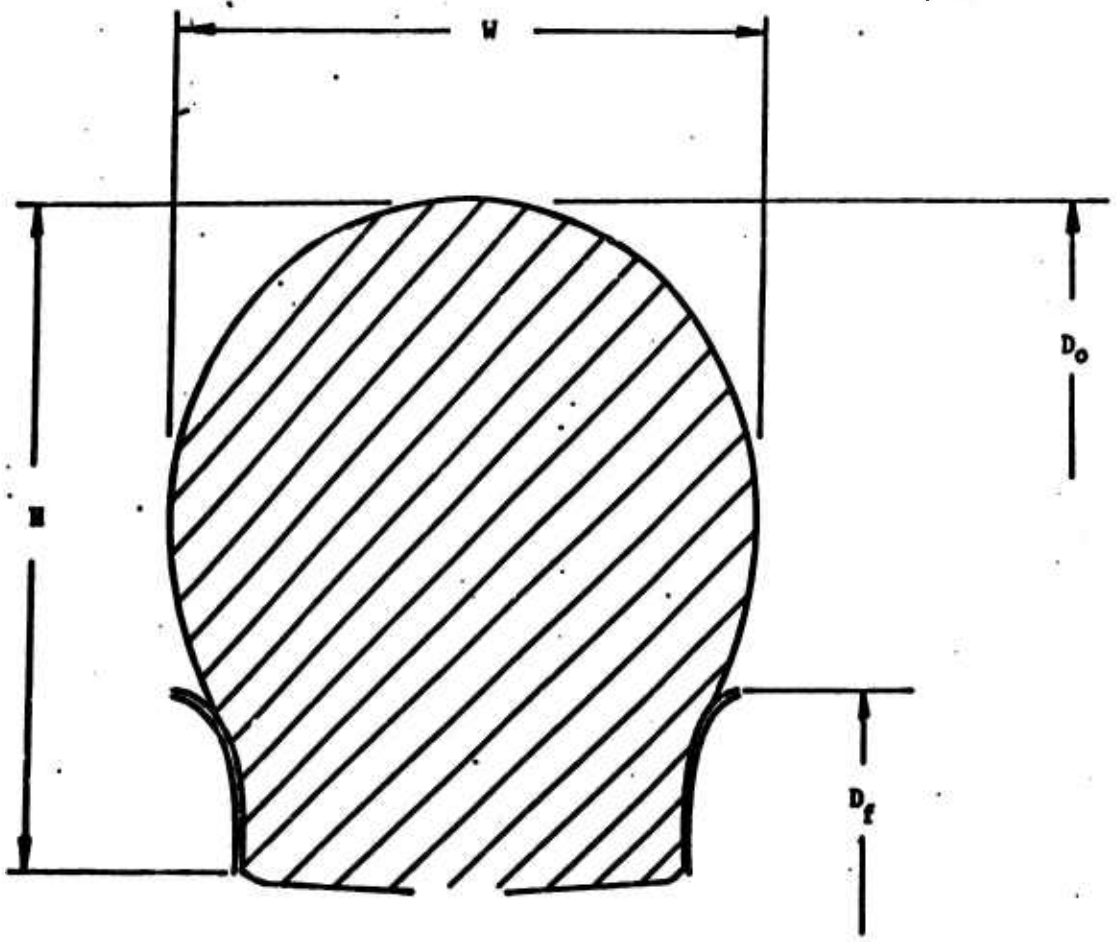

D_f = Flange Diameter
D_o = Tire Outside Diameter
H = Section Height
W = Section Width

FIGURE 4-8 Tire Geometry

$$d = \frac{B}{100} FH$$

where B = present deflection and

B = 35% for Type I, III, & VI

B = 32% for Type VII & VIII

FH = free height (unloaded section height above the top of the rim flange)

$$FH = \frac{D_o - D_f}{2}$$

For an analytical estimation of A_n (net footprint area), the above definitions can be reduced to the following:

Tire Type	Net Footprint Area
I	$A_n = .333(D_o - D_f)\sqrt{(D_o W) - .175(D_o - D_f)[(D_o + W) - .175(D_o - D_f)]}$ (IV-17)
III	$A_n = .412(D_o - D_f)\sqrt{(D_o W) - .175(D_o - D_f)[(D_o + W) - .175(D_o - D_f)]}$ (IV-18)
VII, VIII	$A_n = .404(D_o - D_f)\sqrt{(D_o W) - .16(D_o - D_f)[(D_o + W) - .16(D_o - D_f)]}$ (IV-19)

Table IV-4 (Abstracted from Reference 17) gives values of D_o, D_f, and W for numerous tires in use at this time.

TABLE IV-4

TIRE FOOTPRINT PARAMETERS

TYPE I

Size	D_o	W	D_f
27"	28.16	9.66	15.75
33"	33.06	11.30	18.125
36"	36.86	13.08	19.50
44"	44.94	15.76	24.125
47"	47.98	17.00	25.75
56"	56.62	19.92	29.75
65"	65.66	23.04	34.438
8.00	8.10	3.06	3.843
10.00	10.06	4.18	4.218
12.50	12.50	5.40	5.062
14.50	14.[illegible]	6.24	5.969
17.00	17.[illegible]	7.20	6.906
26.00	26.00	11.00	10.50

TYPE II

Size	D_o	W	D_f
26x6	25.75	6.65	15.5

TYPE III

Size	D_o	W	D_f
5.00-4	13.25	5.05	5.50
5.50-4	14.20	5.75	5.50
8.00-4	18.00	8.30	5.38
5.00-5	14.20	4.95	6.50
6.[illegible]-6	17.50	6.30	7.50
7.00-6	18.75	7.00	7.50
8.00-6	19.50	7.95	7.50
8.00-6	19.50	7.95	7.50
8.50-6	22.10	8.85	7.75
9.00-6	22.40	9.25	7.75

Type III continued on next page

TYPE III Continued

Size	D_o	W	D_f
10.00-7	25.45	10.25	9.50
6.50-8	19.85	6.95	9.63
7.00-8	20.85	7.30	9.63
6.50-10	22.10	6.65	11.63
7.50-10	24.15	7.65	11.63
8.50-10	25.65	8.70	11.63
8.50-10	25.65	8.70	11.63
29x11-10	29.00	11.00	12.00
15.00-10	34.80	15.00	12.00
11.00-12	32.20	11.20	14.00
8.90-12.50	27.70	9.00	14.25
7.50-14	27.75	7.65	15.63
9.50-16	33.35	9.70	18.00
12.50-16	38.45	12.75	18.00
13.50-16	39.80	14.00	19.25
15.00-15	42.40	15.30	18.75
14.00-16	45.05	17.40	18.75
17.00-16	45.05	17.40	18.75
15.50-20	45.25	16.00	23.25
17.00-20	48.75	17.25	23.50*
20.00-20	56.00	20.00	24.00
19.00-23	55.10	19.38	27.00
25.00-28	71.15	25.70	33.25

TYPE VI

Size	D_o	W	D_f
15x6.00-6	15.20	6.30	7.5
22x7.25-11.50	22.34	7.43	13.94

TYPE VII

Size	D_o	W	D_f
16x4.4	16.00	4.45	9.624
18x4.4	17.90	4.45	11.624
20x4.4	20.00	4.45	13.624
12-1/2x 4-1/2	12.60	4.45	5.75
18x5.5	17.90	5.70	9.75

continued on next page

TYPE VII continued

Size	D_o	W	D_f
20x5.5	20.15	5.70	11.75
22x5.5	22.15	5.70	13.75
22x5.5	22.15	5.70	13.75
24x5.5	24.15	5.70	15.75
25x6.0	25.00	6.16	15.75
22x6.6-10	21.75	6.80	12.0
26x6.6	25.75	6.65	16.0
30x6.6	30.12	6.50	22.0
32x6.6	32.00	6.50	22.0
25x6.75	25.50	6.85	16.0
24x7.7	24.15	7.65	11.812
28x7.7	27.40	7.85	16.0
29x7.7	28.40	7.83	17.0
30x7.7	29.40	7.85	18.0
30x8.8	30.40	8.90	17.25
32x8.8	31.00	8.90	18.25
46x9	45.50	8.70	33.0
34x9.9	33.40	10.20	18.50
34x11	33.40	11.30	17.0
34x11	33.40	11.30	17.0
36x11	35.10	11.50	18.75
38x11	37.10	11.50	20.75
40x12	39.40	12.35	21.0
39x13	38.25	13.00	18.75
42x13-18	41.25	13.50	21.25
44x13	43.55	13.50	23.75
40x14	39.80	14.00	19.25
40x14	39.80	14.00	19.25
44x16	43.25	16.00	21.25
46x16	45.25	16.00	23.50**
56x16	56.40	16.20	32.50
49x17	48.75	17.25	23.50
47x18-18	46.90	18.00	21.75

TYPE VIII

Size	D_o	W	D_g
14x4.5-8	14.00	4.50	9.624
18x6.5-8	18.00	6.50	9.75
27.5x7.5-16	27.75	7.50	18.0
22x7.7-12	22.35	7.70	14.0
26x8.0-14	26.00	8.00	16.25
22x8.5-11	22.00	8.50	12.75
30x11.50-14.50	20.25	11.50	17.00
31x11.50-16	31.00	11.50	18.50
32x11.50-15	32.00	11.50	17.50
41x15.0-18	41.00	15.00	21.25
40x17.50-18	40.50	17.50	21.50
50x20-20	50.00	20.00	23.75

BRITISH TYPE TIRES

Size	D_o	W	D_g
18x4.25-10	18.25	4.70	11.20
23x7.00-12	23.20	7.20	13.30
24x7.25-12	24.50	11.40	
26x7.75-13	26.20	7.90	14.40
35x0.00-17	34.80	9.40	19.20
36x10.75-16-1/2	35.90	10.70	18.80

Eight tire types have been established by the U.S. Aircraft Tire and Rim Industry.

TYPE	PRESSURE	USE	ACTIVE FOR NEW DESIGN
I	Low	Fixed Gear Aircraft	No
II	High	Retractable Gear Aircraft	No
III	Low	Same as I Small Aircraft and Helicopter	Yes
IV	Extra Low	Nearly Obsolete	No
V		Obsolete	
VI	Low	Nose Wheel - Old Aircraft	No
VII	Extra High	Military & Commercial Jets	Yes
VIII	Extra High	High Speed Take-off - Military	Yes

7. SAMPLE PROBLEM

GIVEN: **FIND:** μ_{avg}

1. F-104G
2. GW = 20,000 lbs.
3. Assume .9 GW on Main Gear
4. No Anti-skid System
5. V = 100 knots
6. Wet Runway
7. Tire: Type VIII 26 x 8.0 - 14 rib tread

SOLUTION:

From Table IV-4 $D_o = 26.00$

$W = 8.00$

$D_f = 16.25$

$A_n = 99\ in^2$ (2 Tires) (From Eq. IV-19, Tire Footprint Section)

$\mu_{avg} = .657$ (Anti-Skid) (Equation IV-9)

$\mu_{avg} = .22$ (No anti-skid) (Equation IV-11 and IV-12)

$\mu_{wet} = .09$ (Wet no anti-skid) (Equations IV-14 and IV-15)

REFERENCES

1. Smiley & Horne, Mechanical Properties of Pneumatic Tires with Special Reference to Modern Aircraft Tires, NASA TR R-64, 1960.

2. Horne & Leland, Influence of Tire Tread Pattern and Runway Surface Condition on Braking Friction and Rolling Resistance of A Modern Aircraft Tire , NASA TN D-1376, September 1962.

3. Ransone & Fulton, B-58A Heavy Weight Take-Off Refusals, AFFTC-TR-61-14, August 1961.

4. Polis & Adams, T-38A Aerodynamic Braking Refused Take-Off Tests, AFFTC-TR, April 1965.

5. Peterson and Cross, Evaluation of A 5-Rotor Brake and Modulated Anti-Skid System Installed on A KC-135A, AFFTC FTC-TR-64-43, March 1965.

6. Zalovcik, Ground Deceleration and Stopping of Large Aircraft, AGARD Report 231, October 1949.

7. Tomita, Friction Coefficients Between Tires and Pavement Surfaces, USN-CEL-TR-R303 (AD 602 930), USN Civil Engineering Lab, Port Hueneme, California, June 1964.

8. Sawyer & Kolnick, Tire-to-Surface Friction-Coefficient Measurements with A C-123B Airplane on Various Runway Surfaces, NASA TR R-20, 1959.

9. Harrin, Investigation of Tanden-Wheel & Air-Jet Arrangements for Improving Braking Friction on Wet Surfaces, NASA TND-405, June 1960.

10. Sawyer, Batterson & Harrin, Tire-to-Surface Friction Especially Under Wet Conditions, NASA Memo 2-23-59L.

11. Leland & Taylor, An Investigation of the Influence of Aircraft Tire and Tread Wear on Wet-Runway Braking, NASA TN D-2770, April 1965.

12. Keyes, A Review of the Problems of Aircraft Wheel Braking on Wet Surfaces and a Description of a Method of Artifically Wetting Runways for Test Purposes, ARC CP No. 592.

13. McCabe & Bement, B-58A Wet Runway Performance Evaluation, AFFTC-TR-64-34 (AS 456 750), February 1965.

14. Yancey & Cross, C-135B Category III Performance Tests, AFFTC-TDR-63-35, June 1964.

15. Horne, Skidding Accidents on Runways and Highways Can Be Reduced, AIAA Astronautics and Aeronautics, August 1967.

16. Bendix Corporation, Wheel and Brake Specification for Various Aircraft - Loose Sheets.

17. B. F. Goodrich Co., Aircraft Tires Engineering Data, Second Edition.

18. Bendix Corporation, Concepts for Advanced Aircraft Braking Methods, AP-290R (AD 468 065), Revised January 5, 1965.

SECTION V

THRUST

1. DISCUSSION

This section presents the two methods used to vary the thrust and thrust line of the engine other than throttle control that are in current use. These two methods are respectively, thrust reversing and thrust vectoring.

The methods of producing reverse thrust are presented as well as methods to determine the amount of reverse thrust and the flow phenomenon associated with it.

A generalized discussion is given at the end of this section on thrust vectoring. It is intended to present the methods and use of thrust vectoring along with a simplified mathematical approach for use in the generalized force balance equation. A detailed analysis is beyond the scope of this report.

2. THRUST REVERSERS, DESCRIPTION OF TYPES

Over the years numerous aerodynamic and mechanical devices for reversing the thrust of a jet engine have been designed and used. However, most of the present installations fall into two basic categories. These are: 1) internal blocker door and 2) target type reversers. These two basic types differ only in their location in the engine installation. The internal blocker door reverser is located forward of the exhaust gas exit plane (when deployed) while the target type is located aft of the exhaust gas exit plane (when deployed).

A. INTERNAL BLOCKER DOOR TYPE

The internal blocker door type can be divided into two categories: 1) cascade and 2) deflector. These are shown schematically in Figure 5-1. Most "fan air" reversers on present day aircraft utilize the cascade type. The only U.S. aircraft utilizing the

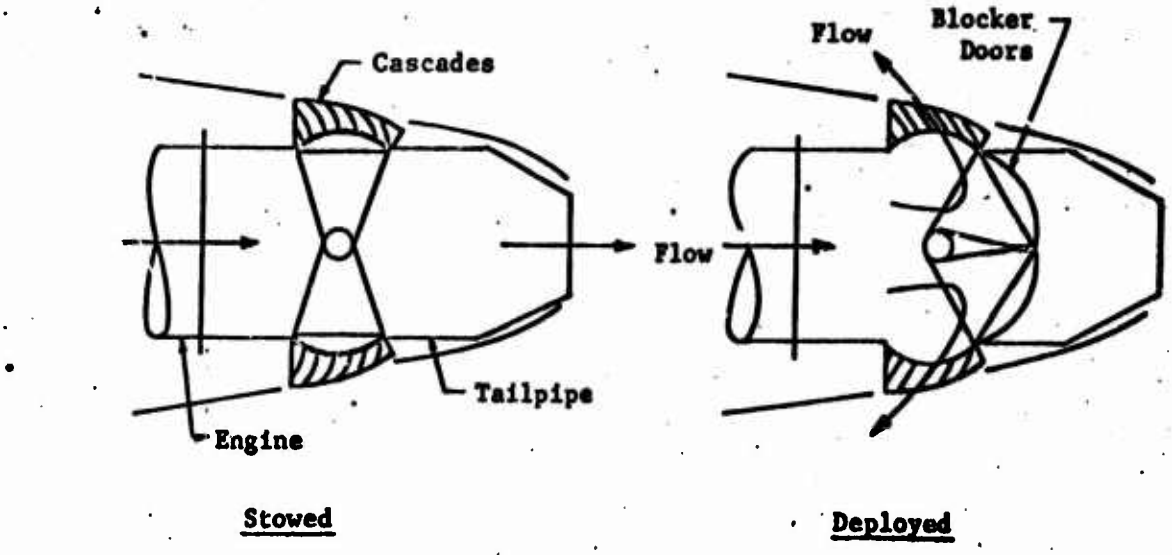

Stowed

Deployed

Cascade Type

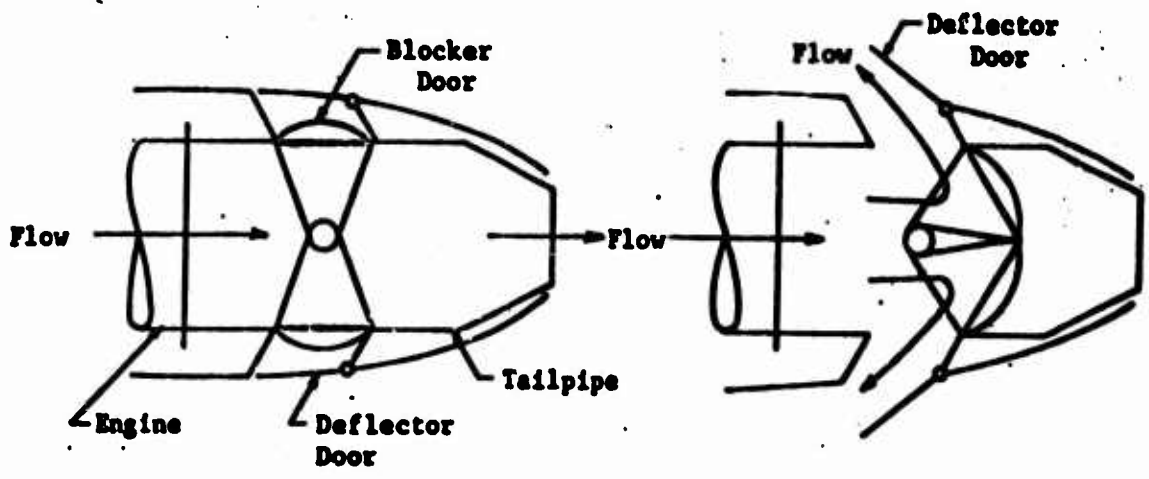

Stowed

Deployed

Deflector Type

FIGURE 5-1 : Internal Blocker Door Thrust Reversers.

internal blocker door on the primary exhaust are the Boeing 707, 727 and the Convair 880 and 990 series aircraft.

B. TARGET TYPE

The target type reverser can also be divided into two categories: 1) stang mounted and 2) barrel mounted. These are shown schematically in Figure 5-2. The "stang mounted" are currently used on the DC-9, C-140, C-141, 737, Gulfstream II, and the Sabreliner. The "barrel mounted" are currently used on the DC-8 and the Swedish Viggen. The barrel mounted is usually employed when the aircraft uses a primary ejector for thrust augmentation or engine bay cooling. This latter type has been proposed for use on military aircraft.

C. GROUND ROLL REVERSERS

This type of reverser is a two position device that is either stowed or fully deployed. The reverser is normally deployed at touchdown and remains deployed until a ground speed is reached called the "cut-off speed". This is discussed in Subsection 6. One aircraft, however, uses the inboard reversers on occasion during approach. This is the DC-8. All aircraft equipped with reversers today have ground roll type reversers.

D. IN-FLIGHT REVERSERS

This type of reverser is used to increase the aircraft's maneuvering ability by enabling virtually instantaneous thrust changes from full forward to full reverse. The reverser doors modulate manually or automatically providing rapid deceleration and instant power control. In use, the engine is kept at a high power setting while modulating the thrust, thereby enabling the pilot to obtain maximum thrust within one or two seconds. This type of reverser (usually referred to as a thrust diverter) is proposed for military aircraft to improve their combat performance, and it will usually be used during ground roll.

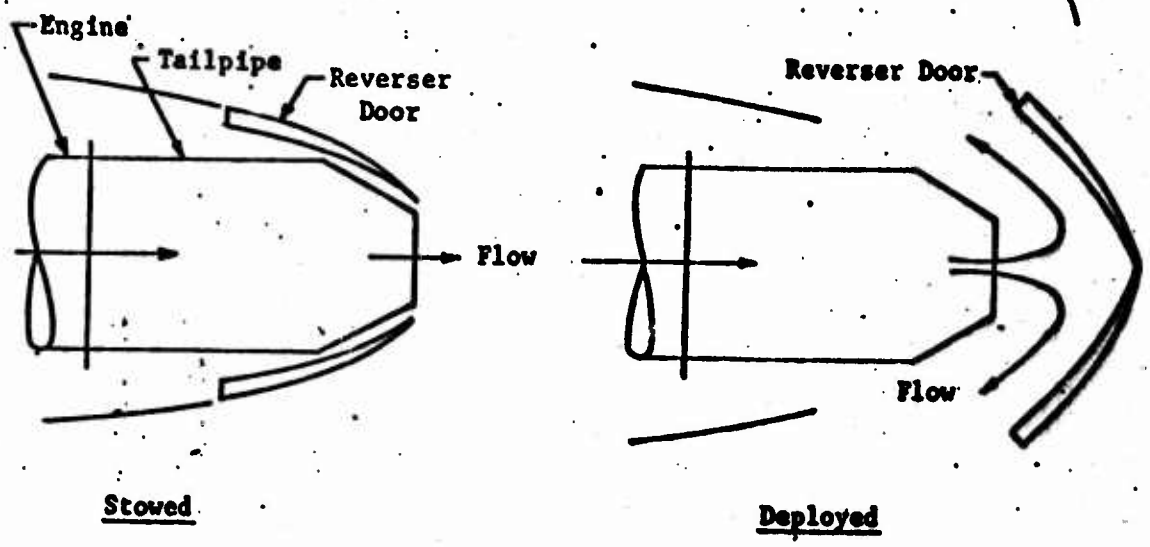

Stang Mounted

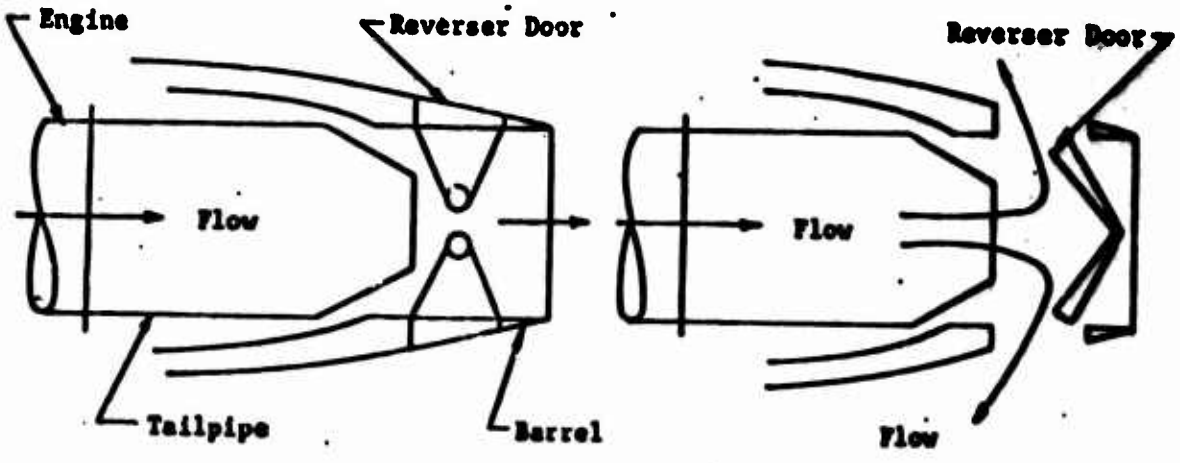

Barrel Mounted

FIGURE 5-2 : Target Type Thrust Reversers.

1. DECELERATION FORCE ATTRIBUTABLE TO REVERSER DEPLOYMENT

Although there is a vast variety of possible reverser configurations, the deceleration force attributable to reverser deployment can, regardless of configuration, generally be represented by the equation:

$$\Delta F = \eta F_G - (\Delta Drag)_{TR} - \text{Ram Drag} \qquad \text{(V-1)}$$

where the thrust vector η is +1 for 100% forward thrust and -1 for 100% reversed thrust. Practical limitations on the value of η are discussed in Subsection 4.

$(\Delta Drag)_{TR}$ for an isolated thrust reverser in compressible flow is essentially base drag. The appropriate base area is the frontal area of the reverser and base areas forward of the reverser exposed by deployment of the reverser doors as shown in Figure 5-3. The base drag acting on the aft side of the reverser doors increases with increasing engine nozzle pressure ratio (NPR). This latter phenomenon is probably due to strengthening of vortices formed behind the door during reversed thrust modes. These vortices were readily observable in the flow visualization test of Reference 1.

Test data indicates that at an NPR of 1.0, the base pressure coefficient is approximately $C_p = -0.$. The variation of base pressure with NPR is dependent upon reverser configuration. Tests with target reversers have indicated the increase in the absolute value of C_p can be as much as 0.25 (i.e. $C_p = -0.75$) at NPR = 1.5.

In addition to the base drag, reversed thrust further influences airplane drag by influencing the aerodynamic characteristics of lifting surfaces and other aircraft components in the near vicinity of the exhaust plume profile. This effect plays a prominent roll in the design of reversers for wing mounted engines. In the instance of thrust reversers located forward of the wing flaps with the exhaust plume directed spanwise, there occurs at certain

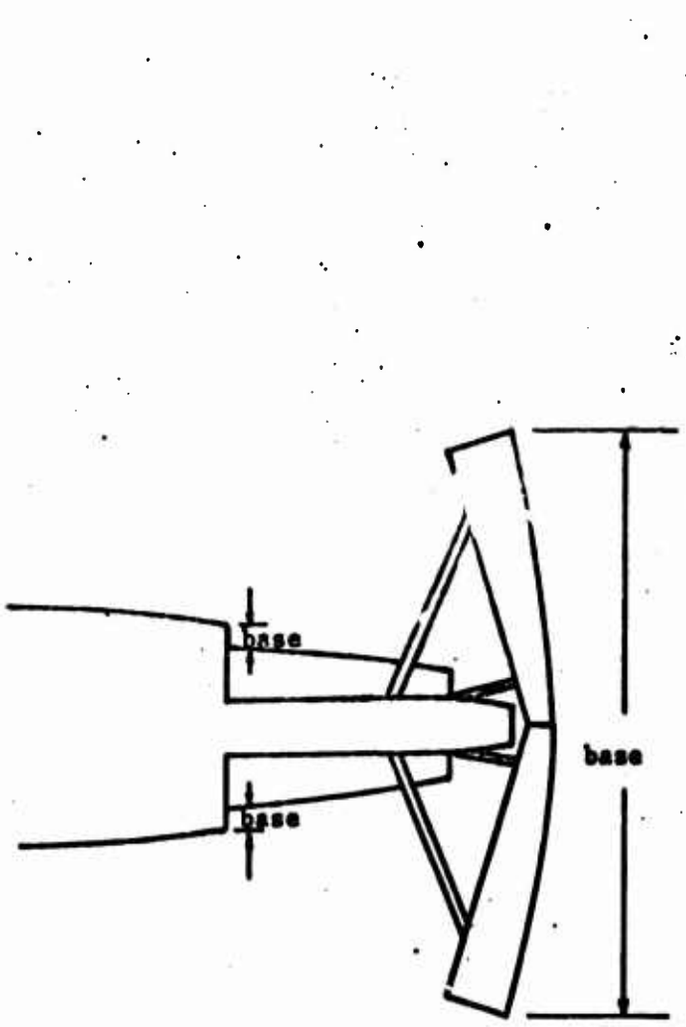

FIGURE 5-3: Base Areas with Reversers Deployed.

aircraft velocities a reduction of pressure acting on the forward face of the flap. The resulting negative drag (thrust component) acting on the flap can be of sufficient magnitude so as to null the net effectiveness of thrust reversal as a deceleration device. Judicious and/or fortuitous location of the reverser and exhaust plume will minimize adverse aerodynamic effects and in some instances create positive increments of drag (e.g. where reverser deployment increases the suction on the leeward side of the flaps). A method for predicting plume profile as a function of flight dynamic pressure and engine nozzle pressure ratio is presented in Subsection 7.

Although ram drag is present anytime the aircraft has forward motion with air passing through the engine, it generally cannot be used to advantage in decelerative modes. It is only of significant magnitude when engine airflow is high in which case gross thrust is also large. Without thrust spoiling or reversal devices it is necessary to "throttle back" to effectively decelerate the aircraft. Thus in determining the increase in aircraft deceleration force increment due to reverser application account should be made of the increase in ram drag available through operation of the engine at high power settings. The adverse forward thrust that exists during conventional idle thrust deceleration should also be taken into account in evaluating the increase in decelerative force due to reverser application.

Thus in comparing ground roll with thrust reverser against ground rolls made at idle thrust without thrust reversal, the net increase in deceleration force due to reverser deployment is given by:

$$(\Delta DF)_{Net} = -nF_G + (\Delta Drag)_{TR} + \text{Ram Drag} + (F_N)_{Idle} \qquad (V\text{-}2)$$

When comparing cases involving emergency landing conditions, it should probably be assumed that the ground roll performed without thrust reverser is executed with the engine switched off. In

which case:

$$(\Delta DF)_{Net} = -\eta Fg + (\Delta Drag)_{TR} + Ram\ Drag - (Ram\ Drag)_{Power\ Off} \quad (V-3)$$

4. REVERSER EFFECTIVENESS

The reverser effectiveness is the ratio of revetser thrust to forward thrust T_R/F_G and is related to the thrust factor employed in equation (V-1) by $-\eta = T_R/F_G$.

Theoretically, reverser effectiveness up to 1.0 is possible. Values in excess of 0.8 have been obtained with both target and cascade type reversers. However, high values of reverser effectiveness at low forward flight speeds tend to cause impingement and/or attachment of the exhaust gases on engine cowling and/or fuselage. This combination also results in re-ingestion of exhaust gases into the engine inlet. The primary adverse effect of re-ingestion is engine surge resulting from non-uniform temperatures of the inlet air. The primary adverse effect of flow impingement and attachment is excessive heating of affected aircraft components. In addition, flow attachment sometimes results in re-ingestion. Re-ingestion is discussed further in Subsection 5. Thus for those aircraft where exhaust attachment and/or re-ingestion are critical, a trade off must be made between reverser effectiveness and cut-off speed (the minimum speed at which reverse thrust will be employed). For the higher reverse thrust effectiveness a larger deceleration force is available but is available only during the initial phase of the landing. A lower reverser effectiveness applied over a larger portion of the landing ground roll may result in an overall shorter landing distance. In addition, a less effective thrust reverser will have lower loads which allows for more forgiving design criteria.

A. COMMERCIAL AIRCRAFT

Ground roll reversers for use with turbojet commercial airliners are usually designed with effectiveness ranging from 0.3 to 0.5 with the majority at 0.4. However, if fanjet engines are employed, a higher reverser effectiveness can be utilized. Fan reversers can tolerate some re-ingestion and attachment because

of the relatively low (100 to 200°F) fan air temperature. Reversed thrust ratios of 0.6 can be used on fan reversers in commercial applications.

B. MILITARY AIRCRAFT

If the thrust reverser is to be deployed strictly for ground roll deceleration, the design criteria is much the same as that stated above for present day commercial airliners.

Most of the fighter aircraft have the engine mounted in the aft fuselage with inlets far forward so that the probability of re-ingestion during landing is reduced or at least delayed until the aircraft has decelerated to low velocities. These factors weigh the compromise towards higher reverser effectiveness. Values in the order of 0.6 are reasonable.

There are present plans to equip several of the military aircraft with in-flight thrust reversers for use in conjunction with high speed maneuvers. For these aircraft the emphasis is on high values of reverser effectiveness. If, on ground roll, re-ingestion, impingement or re-attachment are problems, it may be necessary to either tolerate a rather high cut-off velocity, reduce the power setting, or modulate the reversers during ground roll. However, in an emergency situation it is likely that full reverser would be used throughout the ground roll.

Although thrust reverser effectiveness varies grossly from installation to installation as dependent upon various specific design criteria, it is often necessary for generalized studies to use some representative value. For the purpose of such generalized studies, the following values are recommended.

Type Aircraft	T/R Effectiveness
Commercial Turbine Jet	.4
Commercial Fan Jet	.6
Military Aft Fuselage Jet	.6

5. RE-INGESTION

There are basically three types of re-ingestion: cross ingestion, reflective ingestion and self ingestion. Each of these is discussed below and illustrated in Figure 5-4. The associated discussion of cut-off speed and plume shape are presented in Sections 6 and 7 respectively.

Cross ingestion is illustrated by the flow from nacelle 2 to the inlet of nacelle 1 in Figure 5-4. This is a major problem when multiple engines are mounted on a wing section and the exhaust from the engines are diverted with spanwise components. Re-ingestion of this type can occur at fairly high ground roll speeds especially when the wing is significantly swept back in which case exhaust from the inboard engines is ingested by the outboard engines. The spanwise component of flow is conducive of temperature gradients which cause engine surge. Engine surge is evidenced by a belch of fire out of the inlet or the tailpipe accompanied by a loud bang.

If the reversed flow is directed in a vertical rather than a spanwise direction there is a tendency for flow to bounce off the ground and up into the engine inlet causing reflecting ingestion. This is illustrated by nacelle 4 in Figure 5-4. In addition to engine surge this may cause stones and other foreign objects to be ingested by the engine.

The third type (self ingestion) illustrated by nacelle 3 in Figure 5-4, usually occurs at a relatively low aircraft velocity. Self ingestion is usually coincident with flow attachment in which case the flow adheres to the outer wall of the nacelle, flows forward and into the inlet. This type of ingestion is detrimental only in

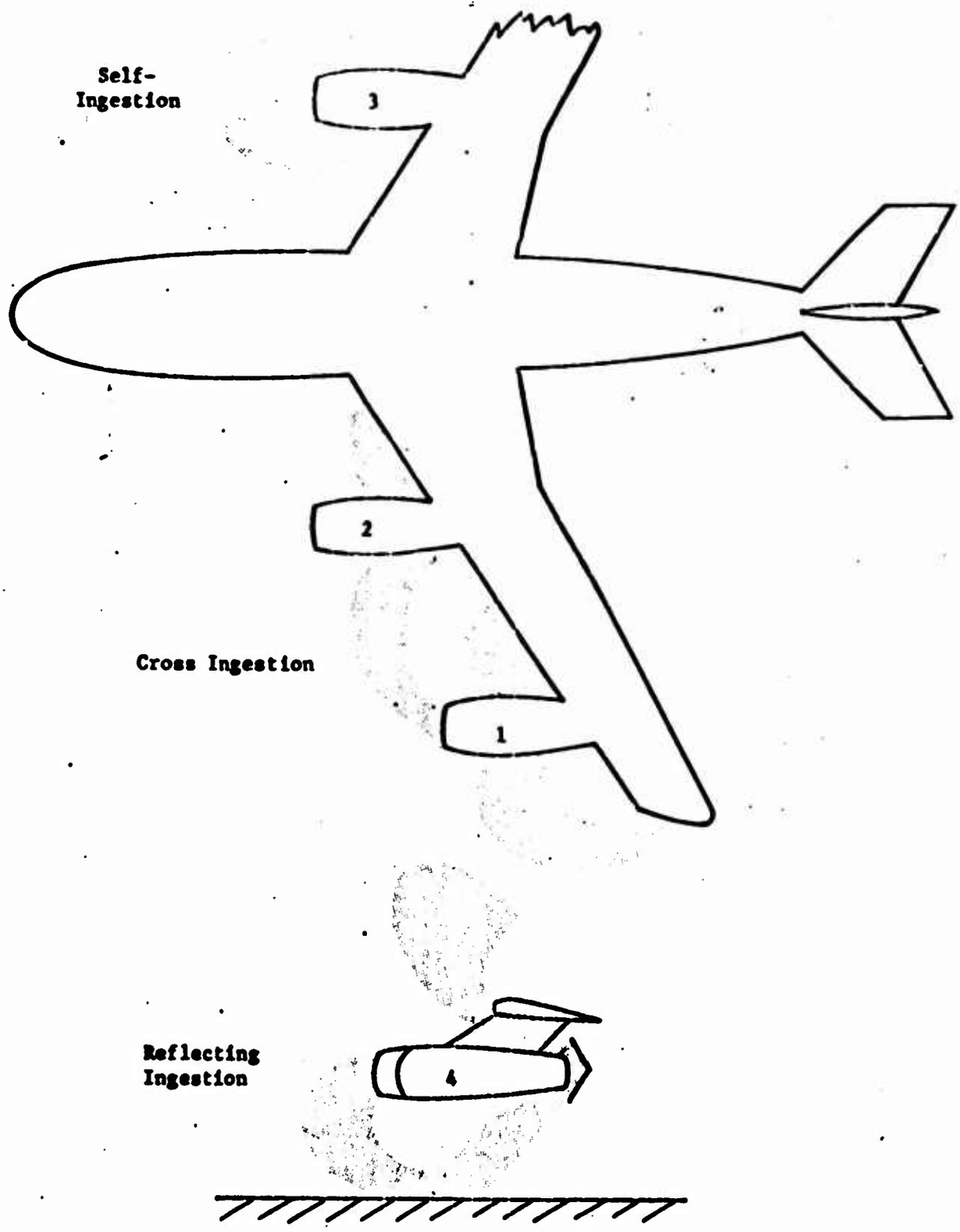

FIGURE 5-4: Description of Re-ingestion Types

the velocity range when the exhaust flow is just strong enough relative to free stream to make its way to the inlet. When the aircraft is at somewhat lower velocities the exhaust plume progresses forward of the inlet and then carried aft to the engine inlet. If the forward progress is sufficient, the flow in its regress to the inlet is mixed sufficiently with free stream that temperature becomes fairly uniform, and engine surge is no longer a problem. When self ingestion is prevalent it is necessary to cut power in the velocity range when engine surge is likely to occur but at lower velocities maximum engine power may be resumed without detremental effects.

6. CUT-OFF SPEED

As indicated above, the minimum speed at which full advantage may be taken of thrust reversal is limited primarily by the occurence of reingestion. This cut-off speed is usually established by taxi tests. However, preliminary estimates are sometimes made by plume analysis such as that presented in Subsection 7.

A typical test evaluation utilizes ansol dust (sodium bicarbonate) or chalk on the runway. Movies are made while the airplane passes over a stretch of the runway that is covered with pieces of chalk. Test runs conducted at various speeds determine when or if the chalk is ingested into the engine.

Factors which affect reingestion are discussed in Subsection 5. As indicated in that section, the speed at which reingestion occurs is strongly affected by airplane configuration, reverser configuration and thrust setting. A well designed commercial jet installation with proper consideration given to reingestion can be expected to be operated in full reversed thrust at speeds down to 30 knots. Military aircraft,especially those incorporating aft fuselage installations,should be operative with significant reverse thrust to speeds somewhat below 30 knots.

For the purpose of generalized studies where specific data is not available for estimation of cut-off speed, it is recommended that the following values be used.

Type Aircraft	Cut-Off Speed, Kts.
Commercial Turbine Jet	50
Commercial Fan Jet	20
Military Aft Fuselage Jet	20

In emergency conditions, it should be assumed that thrust reversers are deployed to V = 0 knots.

7. PLUME SHAPE

Plume shape varies with reverser geometry, engine nozzle pressure ratio (NPR) and aircraft forward velocity. Flow visualization wind tunnel tests have been conducted with target reversers with approximately .55 reverser effectiveness. These tests indicate that plume shapes vary in a predictable manner with variation of the term C_{PR}, defined as $C_{PR} = 100\ (NPR-1)/q$. This is illustrated by Figure 5-5 which presents the variation X - Y coordinates of the position of the points of maximum forward projection of the jet plume. These values of X and Y were obtained from measurements made over a wide range of NPR, and 'q' combinations. The values of X and Y are related to barrel diameters so that they may be used with any barrel. A given value of C_{PR} applies to a number of flight conditions as illustrated by Figure 5-6.

Approximate Method for Predicting Plume Shape

The foregoing discussion is useful in determining an envelope of flight conditions that correspond to a given plume shape. Based on the same data as that mentioned above, a method has been formulated for predicting the shape of the plume profile for given NPR and 'q' values. This method is presented graphically by Figure 5-7. In using this approximation, it should be kept in mind that the method is based on tests involving only two thrust reverser configurations, both of which were target reversers with a design effectiveness of approximately 0.55.

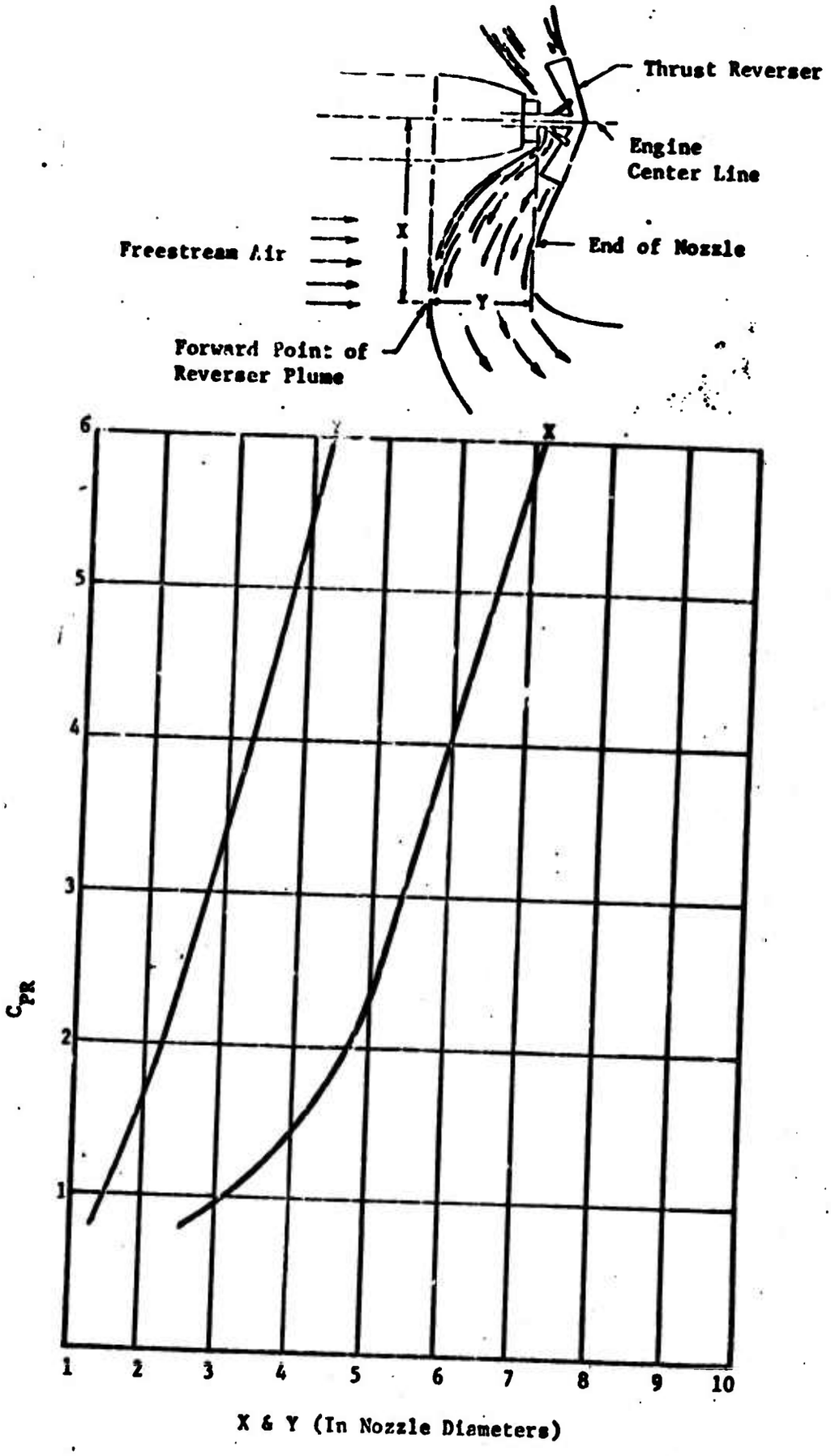

FIGURE 5-5: Variation of X and Y with C_{PR}

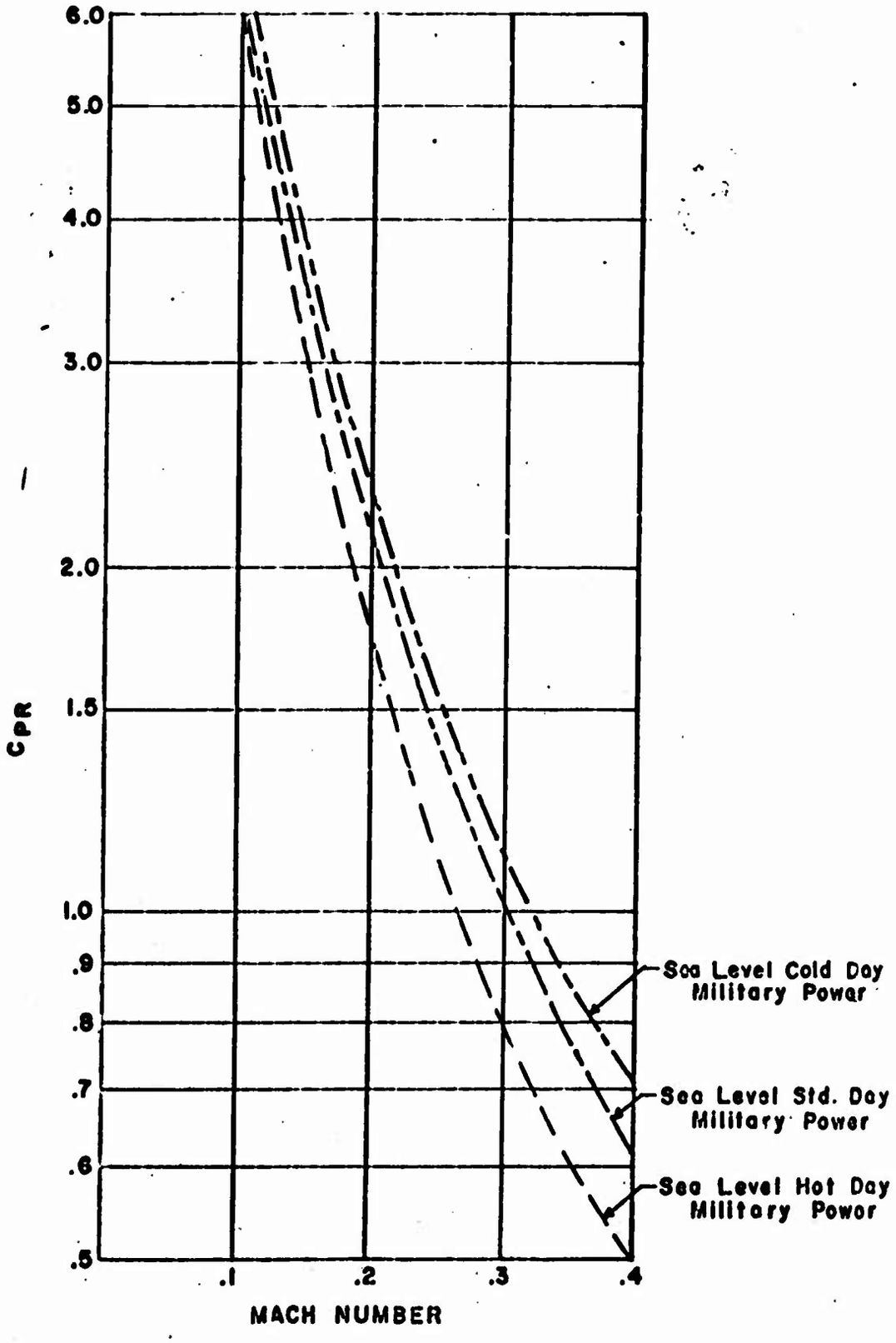

FIGURE 5-6: C_{PR} Versus Mach Number for an Aircraft at Various Altitudes

It is likely that exhaust plumes emanating from reversers with lower design reverser efficiency will be blown back sooner than indicated by this method.

Figure 5-7 is a chart which will yield the three major dimensions of the outer profile of a reverse plume. It gives, in the axis of symmetry of the reverser, the distance the plume travels forward from the nozzle exit plane (Y), the perpendicular distance from the nozzle centerline to this forward most point (X), and the distance from the engine centerline to the outer surface of the plume after it has completely turned and is travelling with the free-stream air (W).

For simplicity, the chart will be explained with the following example:

The nozzle pressure ratio for reverser operation = 2.16.
Nozzle diameter = 12 inches.
Consider the plume shape at 100 knots;
From Figure 7 for NPR = 2.16 and 100 knots EAS, obtain a horizontal line to intersect the W, X and Y lines. Carry the three lines downward to intersect the line corresponding to the nozzle diameter (12 inches in this example).

This gives Y $\geq$ 32 inches (approx.)
X = 58 inches (approx.)
W = 124 inches (approx.)
Where Y, X and W are as identified in Figure 5-7.

8. THRUST VECTORING

Thrust vectoring in this section refers to vectoring systems designed primarily to produce vertical components of force as opposed to thrust reversal. The intent is to assist lift to enable the aircraft to maintain reasonable flight paths on landing approach at lower speeds than possible with lift alone.

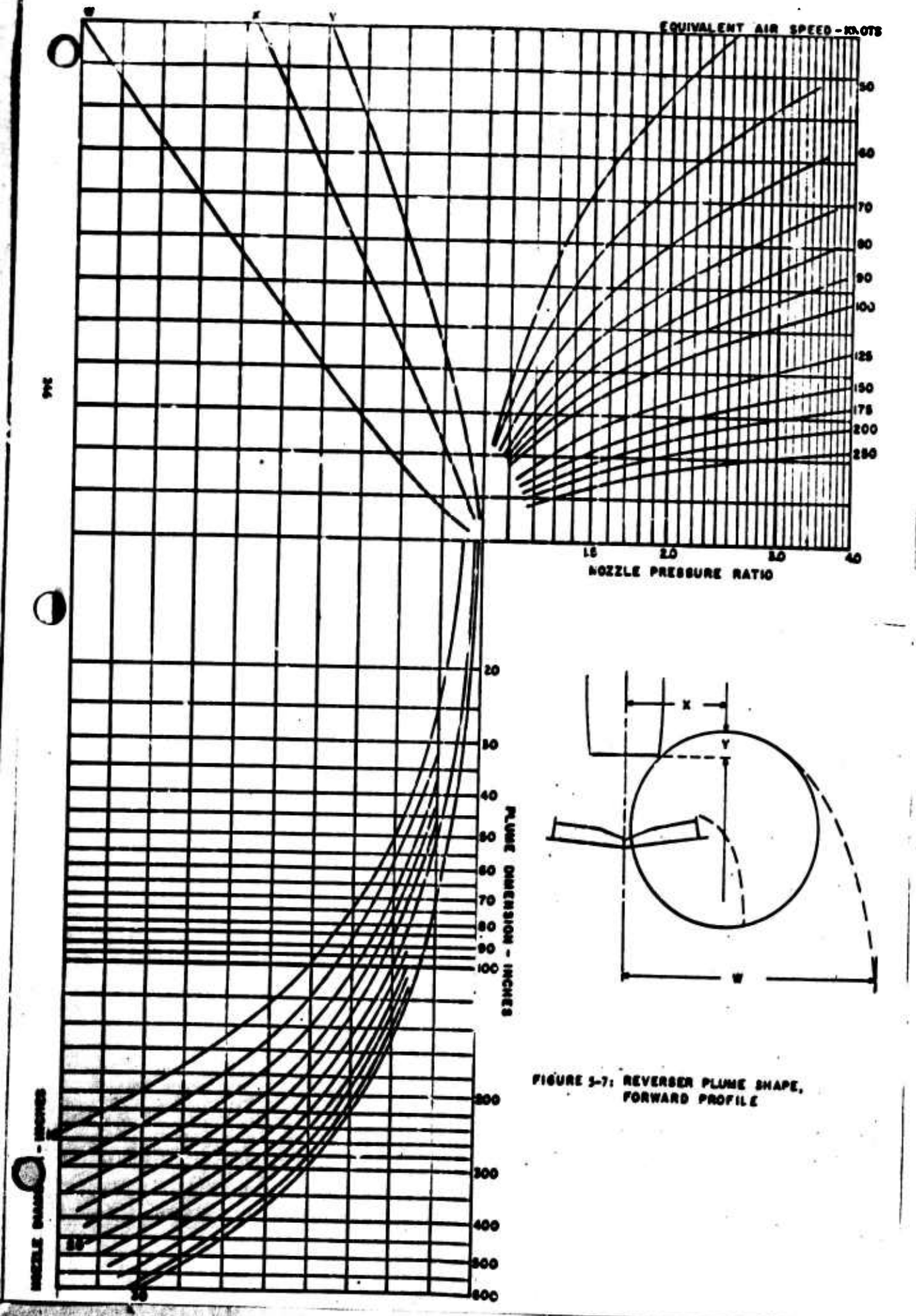

FIGURE 5-7: REVERSER PLUME SHAPE, FORWARD PROFILE

Numerous schemes have been employed to obtain vertical thrust for VTOL and STOL performance. For VTOL operation it is usually necessary to size the aircraft power plants for the VTOL mode at appreciable sacrifice in conventional flight performance. Where reduction of landing touchdown speed is the primary consideration, it is possible to make significant improvements using power plants sized for optimum performance during conventional flight modes.

A recent study was made of effectiveness and possibility of modifying four existing fighter aircraft to incorporate thrust vectoring capability (Reference 2). In this study it was concluded that thrust vectoring of engine sized for conventional flight requirements is a feasible means of reducing landing speeds. In addition, modulative thrust vectoring can be used effectively to improve glide path control and wave-off capability. However, retrofitting certain existing aircraft may be prohibitive because of structural modification or system weight required.

Assuming that the thrust vector is nullified after touchdown so as not to effect wheel brake effectiveness, the primary effect of thrust vectoring upon ground roll is to reduce the touchdown velocity. For this purpose, an adequate evaluation can be made by considering the forces acting on the aircraft in static equilibrium during approach. These forces include consideration of the aircraft's inertia characteristics, earth's gravity, propulsive forces generated by the engine, and the aerodynamic forces and moments due to the aircraft's motion through the air.

The evaluation can be made by simultaneous solution of the following equations:

LIFT

$$\left[C_{L_\alpha}(\alpha - \alpha_o) + C_{L_{\delta_e}}.\delta_e + C_{L_{i_H}}.i_H + C_{L_{\delta_F}}.\delta_F\right] qS + F_G.\sin(\alpha + \delta_T) +$$

$$R.\cos\alpha.W.\cos\gamma = 0.$$

DRAG

$$-\left\{C_{D_o} + \frac{C_D}{2} C_{L_\alpha}\left[(C_{L_\alpha}(\alpha - \alpha_o) + C_{L_{\delta_e}}.\delta_e + C_{L_{i_H}}.i_H + C_{L_{\delta_F}}.\delta_F - C_{L_K}\right]^2\right\} qS$$

$$+ F_G\cos(\alpha + \delta_T) - \text{Ram Drag} + W\sin\gamma - R\sin\alpha = 0.$$

PITCHING MOMENT

$$\left\{C_{m_o} + C_{m_{C_L}}\left[C_{L_\alpha}(\alpha - \alpha_o) + C_{L_{\delta_e}}.\delta_e + C_{L_{i_H}}.i_H + C_{L_{\delta_F}}.\delta_F\right] + C_{m_{i_H}}.i_H + C_{m_{\delta_e}}.\delta_e + C_{m_{\delta_F}}.\delta_F\right\} \bar{C}.q.S + R(\Delta x_R) -$$

$$F_G(\Delta x_T \sin\delta_T + \Delta Z_{CG}\cos\delta_T) = 0.$$

The aircraft's axis system is established as indicated in Figure 5-8. The X-axis is the aircraft longitudinal axis and the Z-axis is perpendicular to it in the plane of symmetry. The major aerodynamic and inertia forces, lift, drag, pitching moment and weight are considered as acting through and about the center of gravity as shown. These aerodynamic forces are composed of the various component forces contributed by the wing, flaps and horizontal control surfaces.

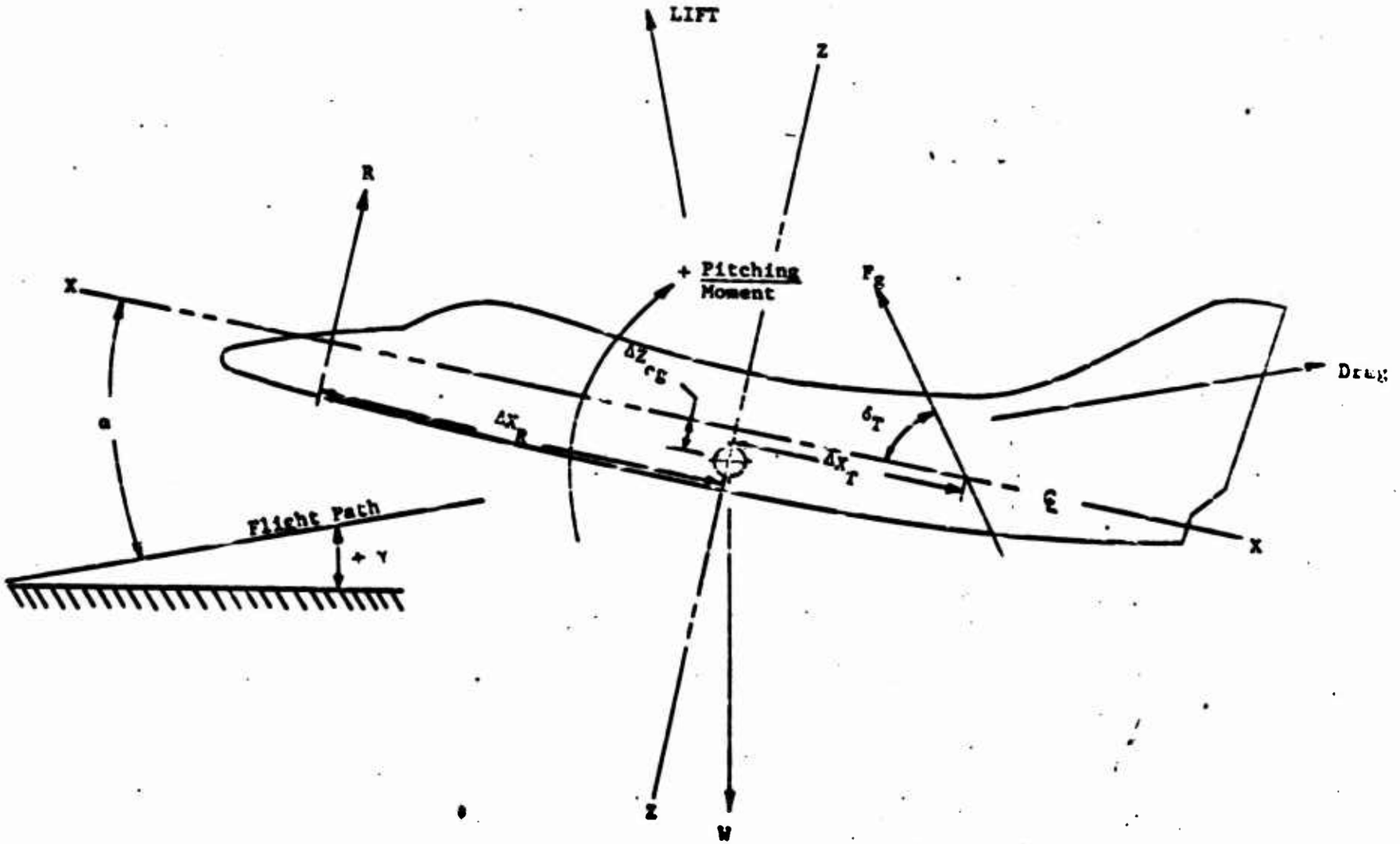

FIGURE 3-8: Axis System and Resolution of Forces for Consideration of Vectored Thrust.

The propulsive force due to deflected main engine thrust has components in the lift and drag directions as well as contributing a counter-moment to the aerodynamic moment (when the main force vector is offset from the c.g.). The pitch control reaction force is integrated into the equations when necessary to balance the moment about the c.g. for equilibrium.

REFERENCES

1. Eschenburg, R., Scale Model Thrust Reverser Wind Tunnel Test Program, Rohr 24-5008, January 1967.

2. Kuczwara & Eschenburg, Reduction of Landing Speed of Carrier Based Aircraft by Thrust Vectoring, Rohr Report 24-2273, January 1968.

SECTION VI

WEIGHT PENALTY-EVALUATION

1. DISCUSSION

This section presents a method for comparing the weight penalty for the various deceleration devices available for design of airplanes and considered by this study.

The weight penalty concept described herein will predict the total weight increment to the aircraft resulting from the installation of the device. This will include but not be limited to the peripheral structure removed, the basic structure added or supplemented, and the means of operating and controlling the device. Special design considerations are noted in the description of each device that follows.

In all cases the unknown value or variable of the parameters considered is a number which can be defined by performance requirements.

Attention has been directed toward the solution of these problems utilizing as much data as could be collected. These data include much of the referenced information as well as other actual measurements of existing aircraft and have been plotted on the appropriate graph to illustrate the effectiveness of the formulae.

Careful attention has been paid to the aircraft's existing systems, in particular those hydraulic or pneumatic lines which have been expanded to include the added deceleration device requirement.

For each device, series of equations were established to derive the weight penalty formulae. No one solution would satisfy every case; therefore, the one formula yielding the narrowest band was used which provided the best obtainable confidence level.

2. TRAILING EDGE FLAP

Flaps are auxiliary surfaces making up a rear portion of the wing. When they are lowered, they alter the camber of the wing. The result is an increase in lift and drag, and the zero lift angle changes to a more negative value. As a result of these changes, the aircraft can: (1) land at a lower speed, (2) glide at a steeper angle over obstacles, or (3) use more power during the approach and thus minimize engine acceleration time in case of a go around. The four basic types of flaps are: plain, split, slot, and Fowler.

The plain flap is a simple hinged portion of the trailing edge.

The split flap consists of a flat surface which is hinged to the bottom of the wing. This type generates a slightly greater change in maximum lift than the plain flap and because of the greater turbulent wake that it causes, a much higher drag is produced.

The slotted flap is similar to the plain flap except that the gap between the wing section and the leading edge of the flap has a special contour.

The Fowler flap resembles the slotted flap except that the deflected flap segment is moved aft along a set of tracks. When extended, it increases the chord and produces an increase in wing area. The Fowler flap is characterized by large increases in maximum lift with minimum changes in drag.

Variations of these four basic types are considered under two formulae where the unknown variable "S", is the flap planform area. The first,

$$W = 5.17 \quad (S)^{.94} \qquad \text{(VI-1)}$$

includes single slot, hinged and split flaps. The second,

$$W = 6.98 \quad (S)^{.86} \qquad \text{(VI-2)}$$

includes Fowler, double slotted, and triple slotted.

The weight penalty for all types of trailing edge flaps is illustrated on Figure 6-1. This figure and the formulae were established by evaluating the weight of the required trailing edge device, including the associated mechanical requirements, as compared to the weight of a wing trailing edge structure of minimum gage properly stiffened with the necessary ribs and closures to prevent wrinkling. The wing structure reinforcement required by the additional loads for a trailing edge flap installation was also considered in the evaluation.

3. LEADING EDGE SLAT

High-lift devices on the leading edge of a wing, such as slats, flaps, and other auxiliary airfoils, can also be used to change the camber of the wing.

The fixed slot conducts a flow of high-energy air into the boundary layer on the upper surface of the wing, thereby delaying air flow separation.

The automatic slot (slat), which consists of a segment of the leading edge, is free to move on tracks. At low angles of attack it is held flush against the leading edge by the high positive local pressures, and in this position it is referred to as a slat. When the wing section is at high angles of attack, the high local suction pressures at the leading edge create a forward chordwise force to actuate the slat, lifting it away from the wing to form a slot. This allows the wing section to continue at a higher angle of attack and produce a $C_{L_{MAX}}$ greater than that of the remaining wing section.

The weight penalty for the leading edge slats includes the evaluation of the structure removed from the leading edge of the wing, in addition to any mechanism or system required to operate the leading edge slats. Also the wing structure reinforcement necessary to accommodate the increased loads for a leading edge installation was considered in the evaluation. Figure 6-2 presents a graph which shows the weight

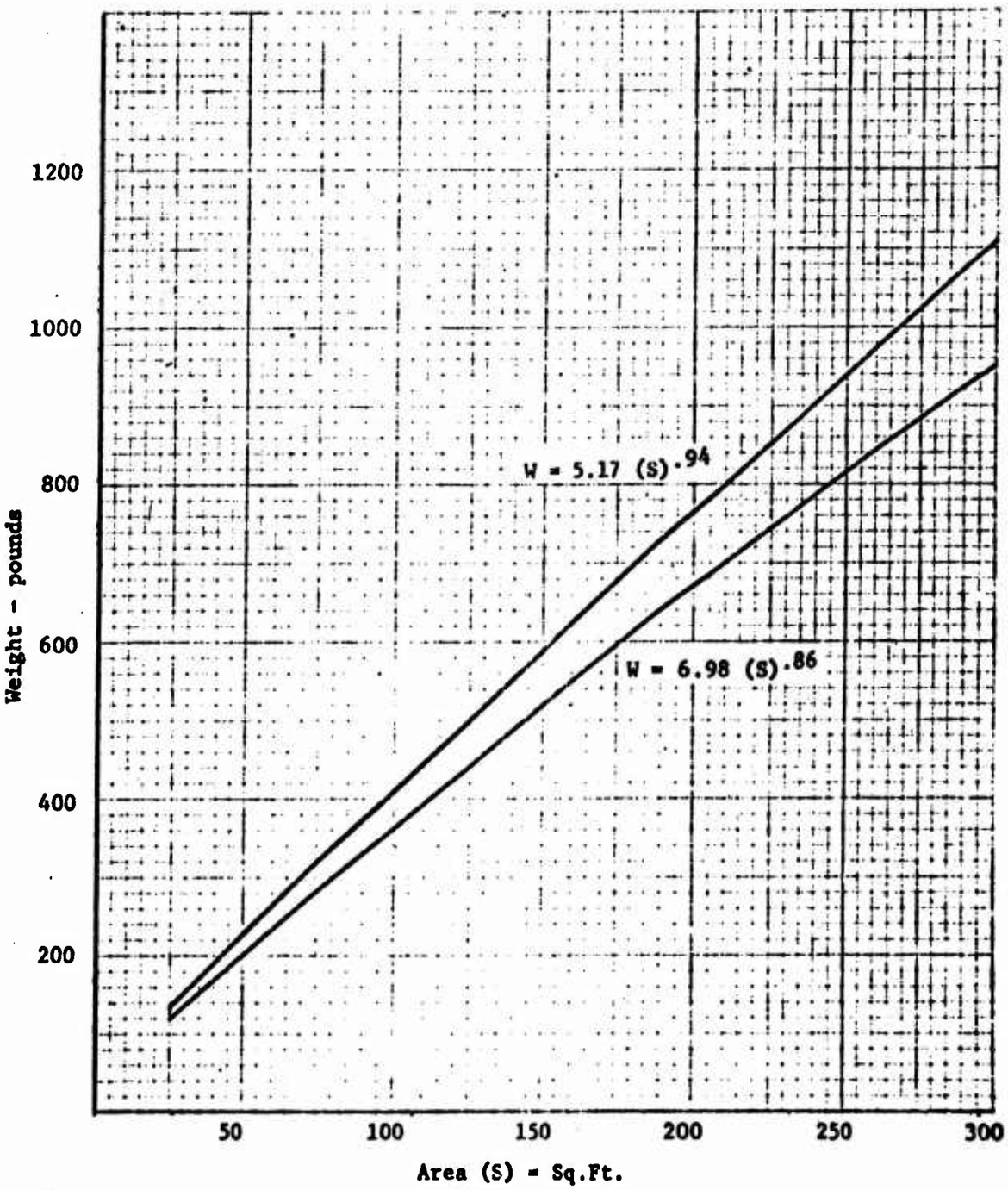

FIGURE 6-1 : Trailing Edge Flaps; Weight vs. Area

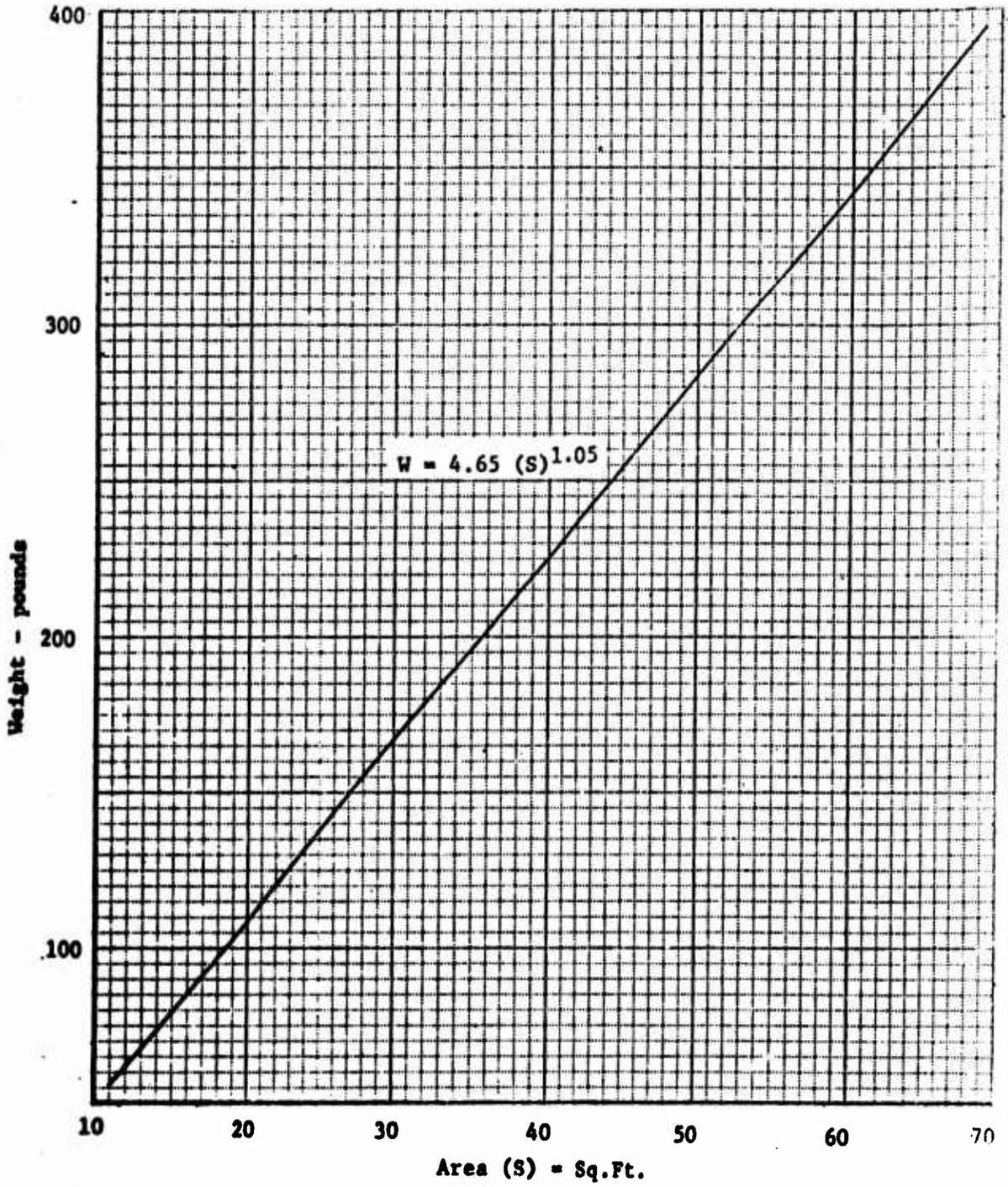

FIGURE 6-2 : Leading Edge Slats; Weight vs. Area

penalty for a defined slat planform area and the formula is expressed as

$$W = 4.65 \quad (S)^{1.05} \qquad \text{(VI-3)}$$

4. BOUNDARY LAYER CONTROL

There were no available weight and geometrical data available for BLC devices; therefore no weight increments could be established.

5. SPOILER

These small auxiliary surfaces have eliminated ailerons on some aircraft, and are operated in conjunction with the aileron for primary roll control on others. The wing on which the spoiler acts loses some of its lift when the spoiler is extended into the airflow above the wing, causing turbulence, and the aircraft turns and a banking movement is established.

The weight penalty formula for spoilers is

$$W = 5.95 \quad (S)^{1.04} \qquad \text{(VI-4)}$$

where S = the surface area of the spoiler.

The weight increment derived from the formula on the graph shown on Figure 6-3 accounts for hinge mechanisms, spars, pressure switches, and other systems.

6. DRAG CHUTE

Conventional ribbon drogues and ringslot parachutes are most commonly used in aircraft deceleration applications.

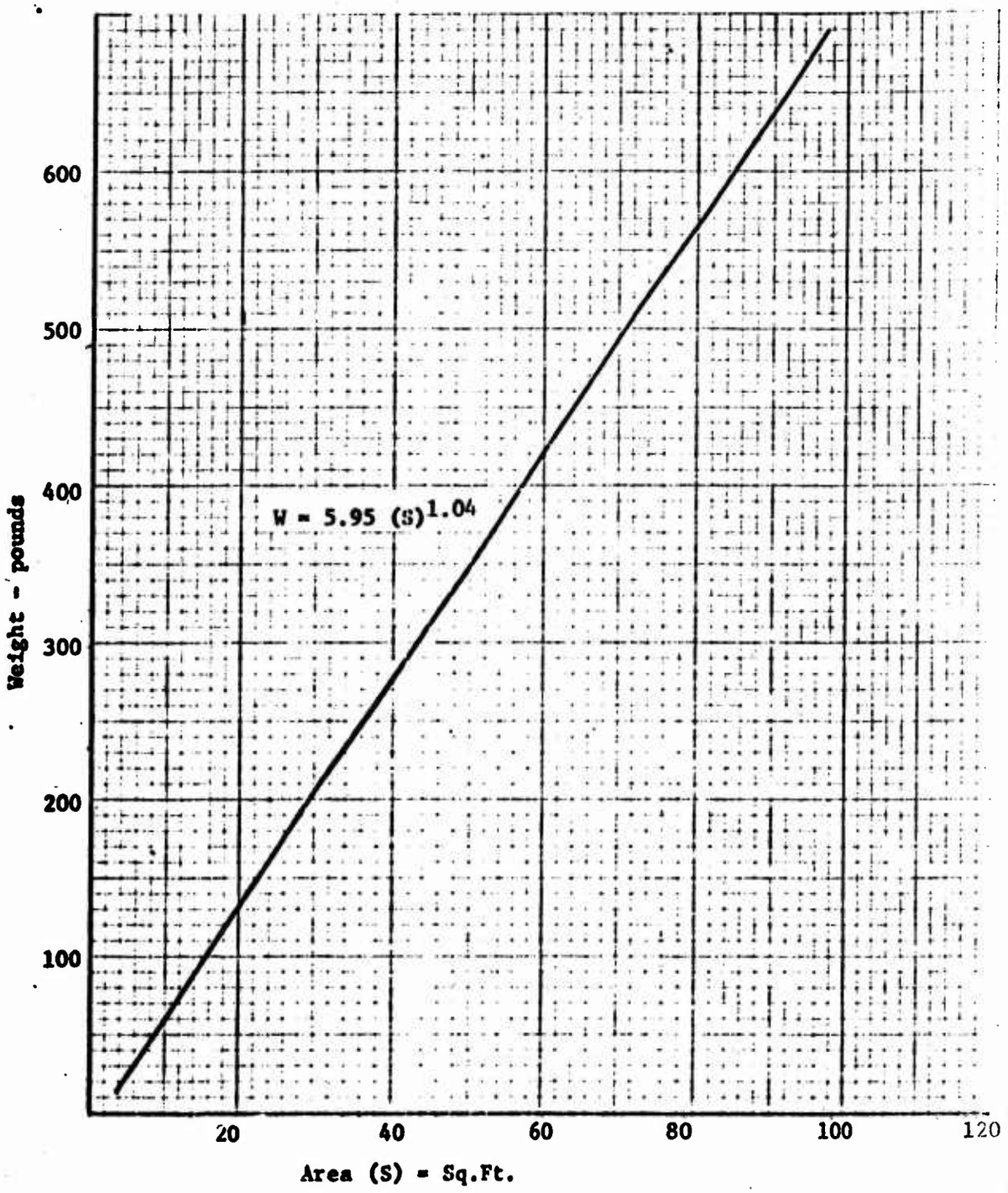

FIGURE 6-3 : Spoilers; Weight vs. Area

The ribbon drogue is made up of a series of circumferential ribbons separated by open spaces, or slots. Ribbon drogues are capable of sustaining high loads, and resist damage due to contact with the ground or runway and repeated usage.

The ringslot parachute is made up of circumferential rings of conventional parachute cloth separated by open spaces, or slots. They are slightly lighter when compared to a ribbon drogue of equivalent drag.

The weight penalty for Drag Chutes are expressed in the following formulae and the graph shown on Figure 6-4 includes the weight of the chute assembly, canister, release mechanism, controls, and fuselage reinforcement required to resist the chute induced loads. The ribbon drogue weight penalty formula is

$$W_{RIB} = 1.95 \quad (D_C)^{1.43} \qquad \text{(VI-5)}$$

and the ringslot parachute weight penalty formula is

$$W_{RING} = 1.15 \quad (D_C)^{1.43} \qquad \text{(VI-6)}$$

where (D_C) is the canopy diameter.

7. WHEEL BRAKE

In order to slow or stop an airplane, the kinetic energy (energy of motion) of the airplane must be absorbed by rolling friction, aerodynamic drag, and braking action. The relative effect of these factors depends upon the length of the landing roll and the touchdown speed.

Four factors limit the ability of the brakes to stop an airplane. These factors are: braking friction available between the tire and the runway, torque capability of the brake, kinetic energy limits of the brake and pilot technique for brake usage.

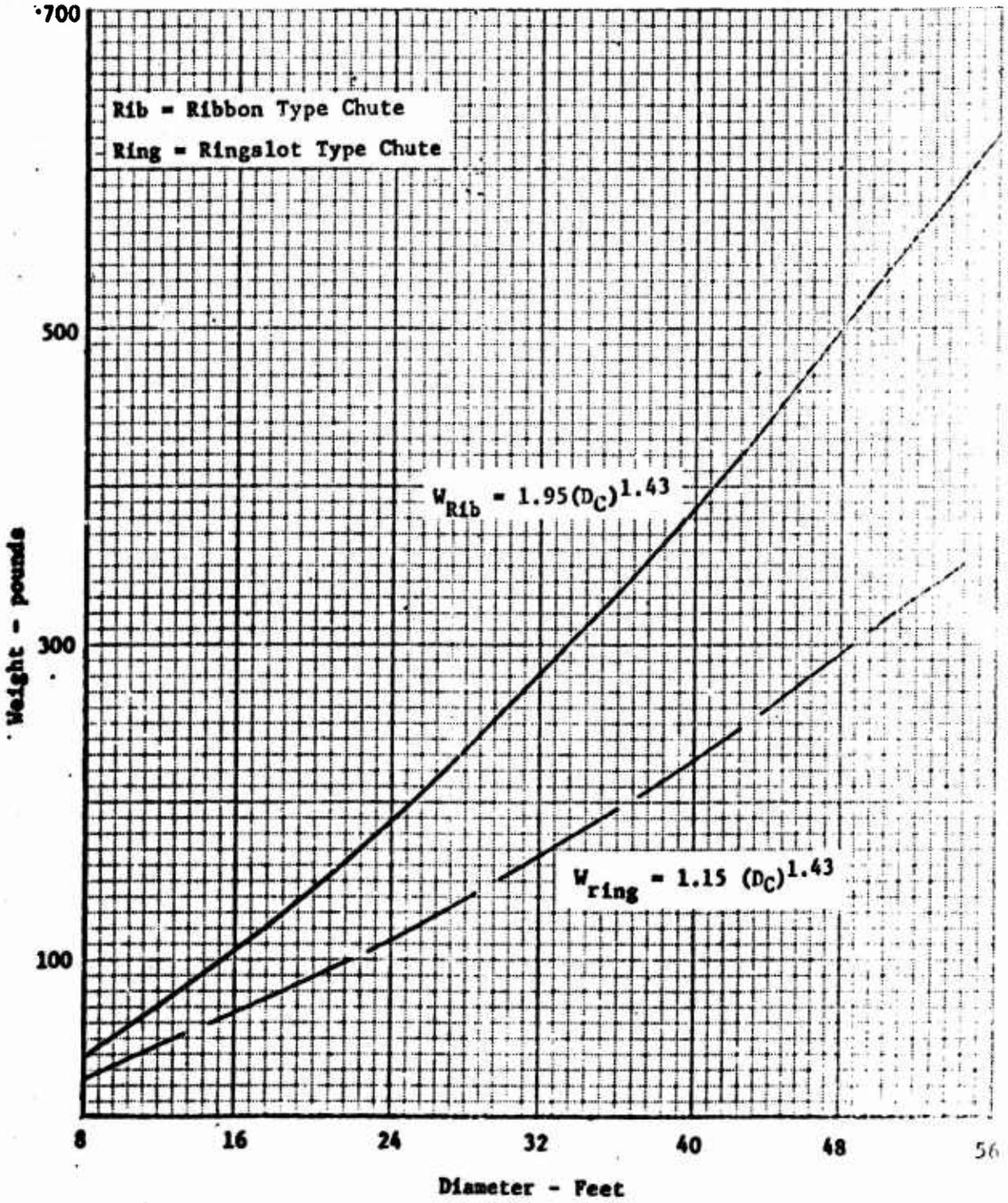

FIGURE 6-4 : Drag Chutes; Weight vs. Diameter

The kinetic energy is limited by design and is a measure of the energy to be absorbed by the brakes. This energy appears in the form of heat, and the absorption capability of the brakes is a function of the brakes mass and material.

The weight penalty graph is shown on Figure 6-5 and the weight penalty formula for wheel brakes and associated systems is

$$W_{BS} = N\,(2.2\,[3.80 \times 10^{-4}\ (K.E.)^{3/4}]^{1/2} + [3.80 \times 10^{-4}\ (K.E.)^{3/4}]) \quad \text{(VI-7)}$$

where N = number of tires with brakes
and K.E. = kinetic energy design factor.

THRUST REVERSER

Since power is available from the engines during the landing condition in jet aircraft, this power may be utilized in generating reverse thrust to help retard the landing roll. This is accomplished simply by turning the exhaust gases from the jet engine in such a manner that they issue in a forward direction rather than aft, resulting in a reverse thrust force.

There are two basic types of thrust reversers: the cascade and the target. Both of these are currently used on our modern jet aircraft and have withstood the test of time.

The weight penalty of a landing roll target-type thrust reverser configuration which deflects only the engine primary-exhaust gases is

$$W = .15\ L\ D_{EF} \quad \text{(VI-8)}$$

and the weight penalty of a landing roll target-type thrust reverser configuration which deflects both the engine primary-exhaust gases and the ducted fan air is

$$W = .11\ L \cdot D_{EF} \quad \text{(VI-9)}$$

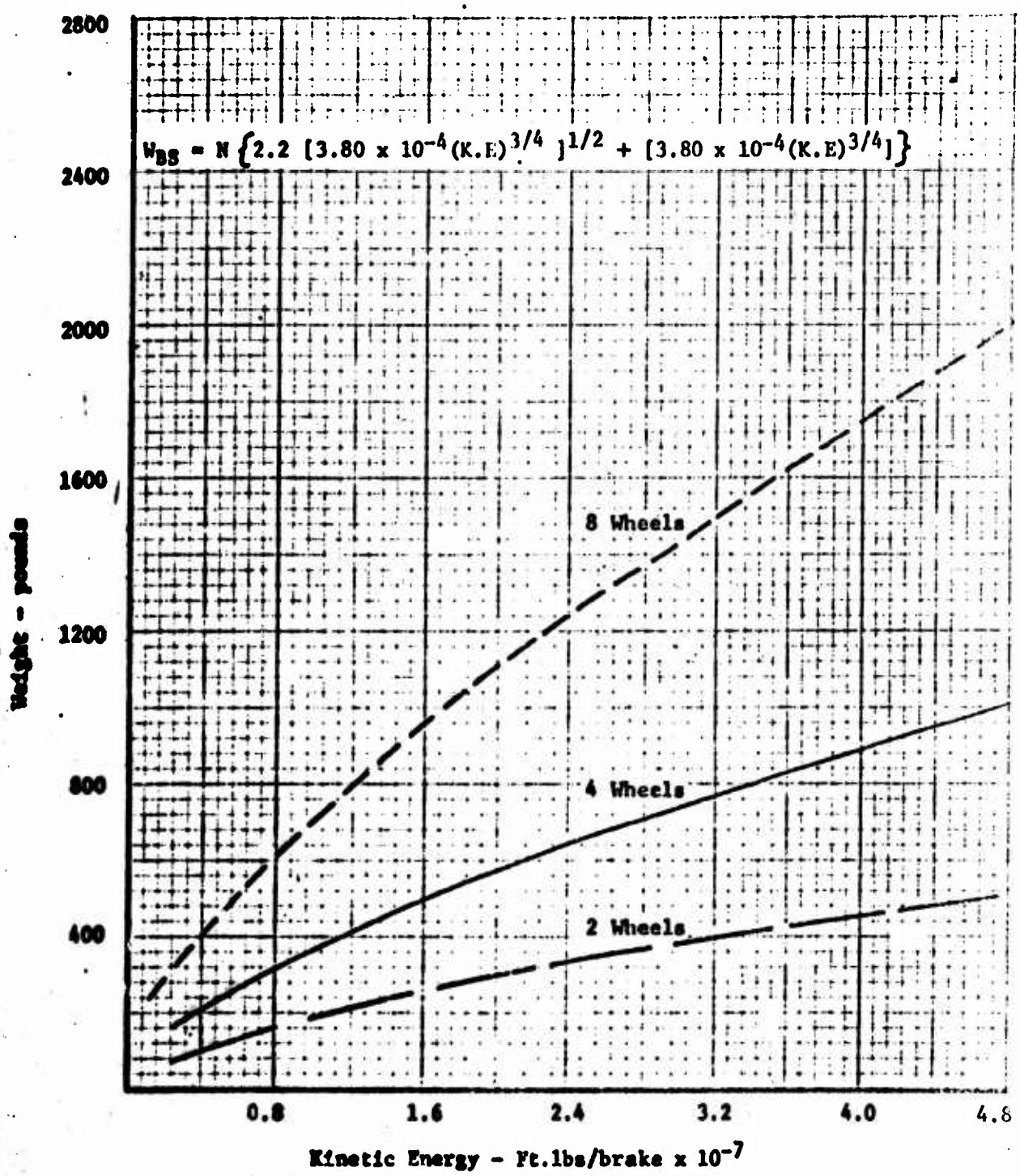

FIGURE 6-5 : Wheel Brake Installation; Weight vs. Kinetic Energy.

where D_{EF} = overall diameter at engine flange,

and L = overall length (do not consider extended fairup in length).

These formulae and the graphs shown on Figures 6-6 and 6-7 are limited to an engine-mounted thrust reverser installation and include the necessary structure and system modification. It is assumed that adequate operational systems are included in the aircraft design.

The weight penalty of an in-flight target type thrust reverser configuration which deflects only the engine primary-exhaust gases can be determined on Figure 6-8. This graph was prepared using estimated weights of target-type nacelle-mounted thrust reversers proposed for a limited number of aircraft. Both a landing roll configuration and an in-flight configuration for a maximum velocity of Mach 1.2 were included for each. An estimated weight penalty can be obtained for a given engine thrust with an associated velocity. There are insufficient data available to establish a method to evaluate the weight penalty for an in-flight target-type thrust reverser configuration which deflects both the engine primary exhaust gases and the ducted fan air.

9. SPEED BRAKE

These small auxiliary surfaces are usually mounted to the fuselage and operated in flight and/or during landing to reduce speed rapidly.

Their operation is quite often limited to a speed far below the maximum speed of the aircraft. For this reason two formulae have been constructed; one for subsonic and one for supersonic deployment.

The weight penalty formula for speed brakes operated below 600 KIAS is:

$$W = 1.85\ (10^{-2})\ (S)\ (KIAS) \qquad \text{(VI-10)}$$

and for speed brakes operated above 600 KIAS is:

$$W = 2.35\ (10^{-2})\ (S)\ (KIAS) \qquad \text{(VI-11)}$$

where S = Speed Brake surface area and KIAS = Knots indicated air speed.

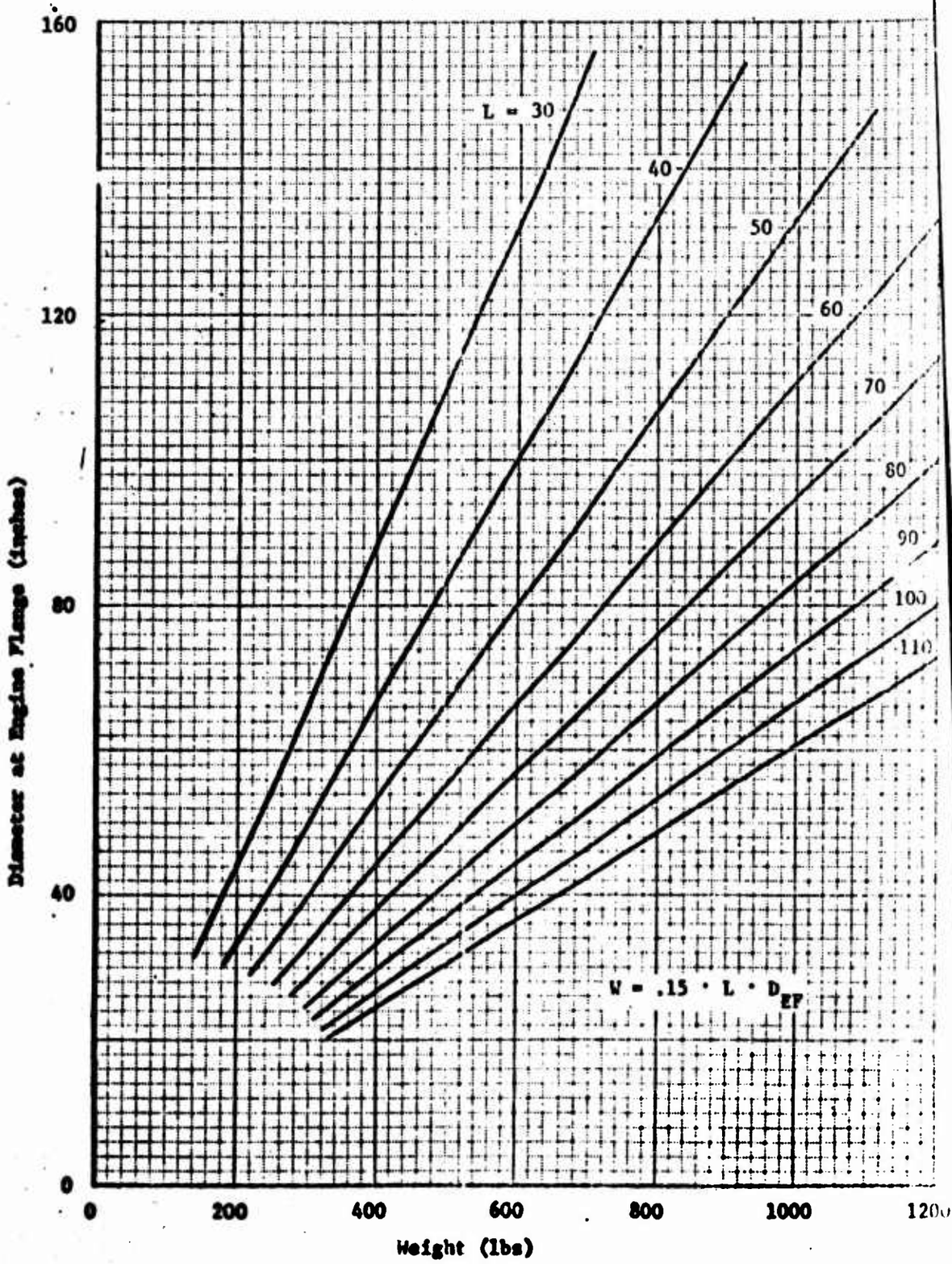

FIGURE 6-6 : Target Type Thrust Reverser Deflecting Engine Thrust Only-Landing Roll Configuration; Weight vs. Diameter.

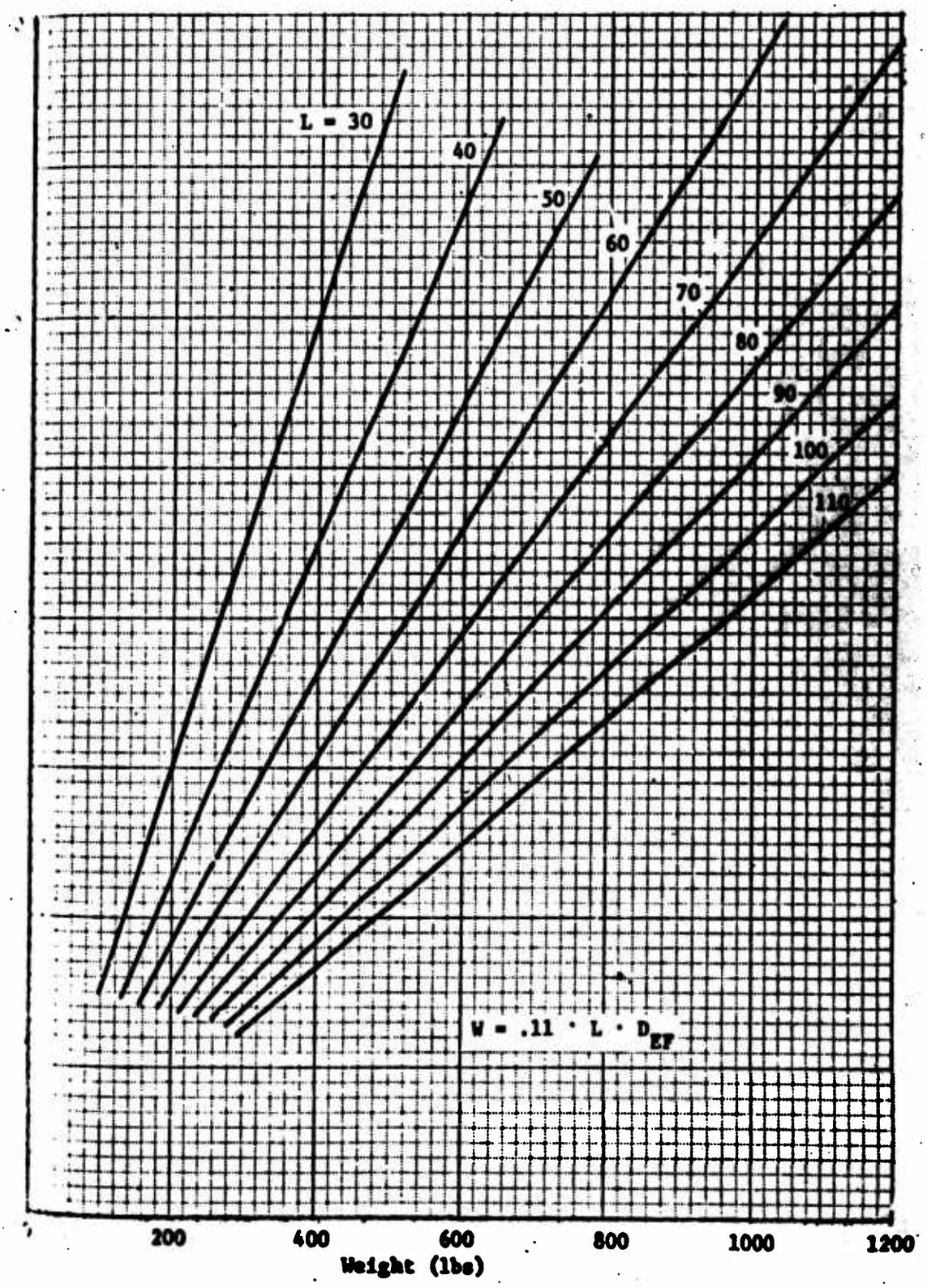

Fig. 6-7 : Target Type Thrust Reverser Deflecting Engine Thrust and Ducted Fan Air - Landing Roll Configuration; Weight vs. Diameter.

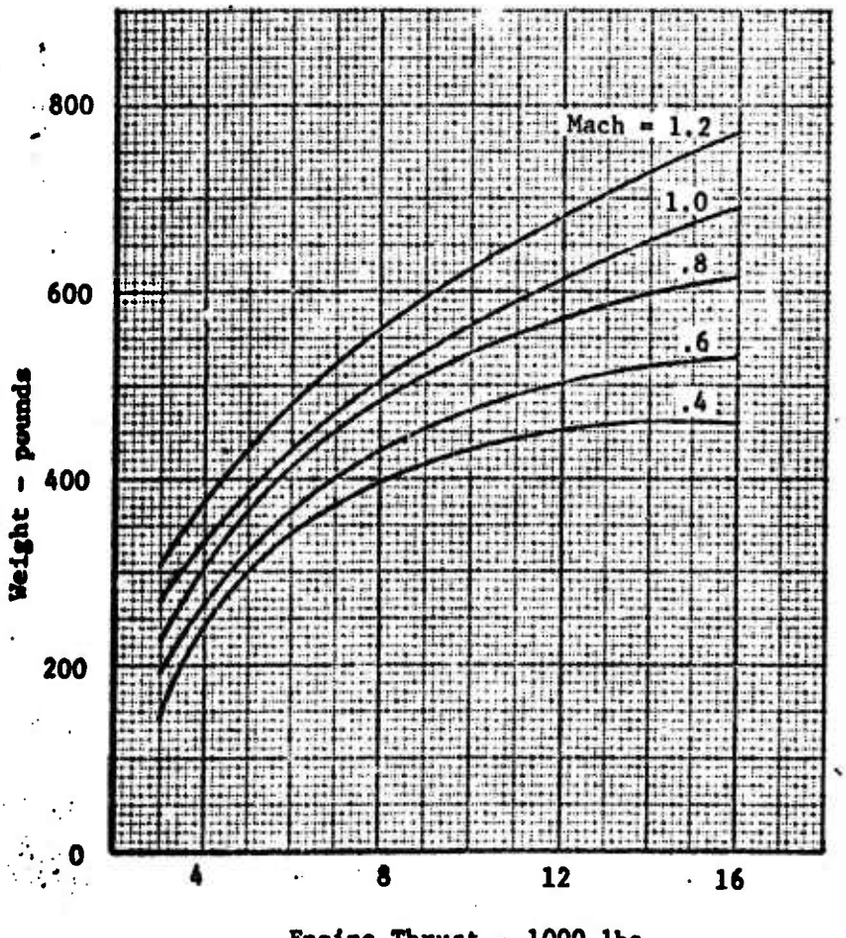

FIGURE 6-8 : Target Type Thrust Reverser Engine Thrust Only - In-Flight Configuration; Weight vs. Engine Thrust.

The weight value obtained from these formulae or the graphs shown on Figures 6-9 and 6-10 includes the weight of the pedal, hinge mechanism, systems and fuselage reinforcement.

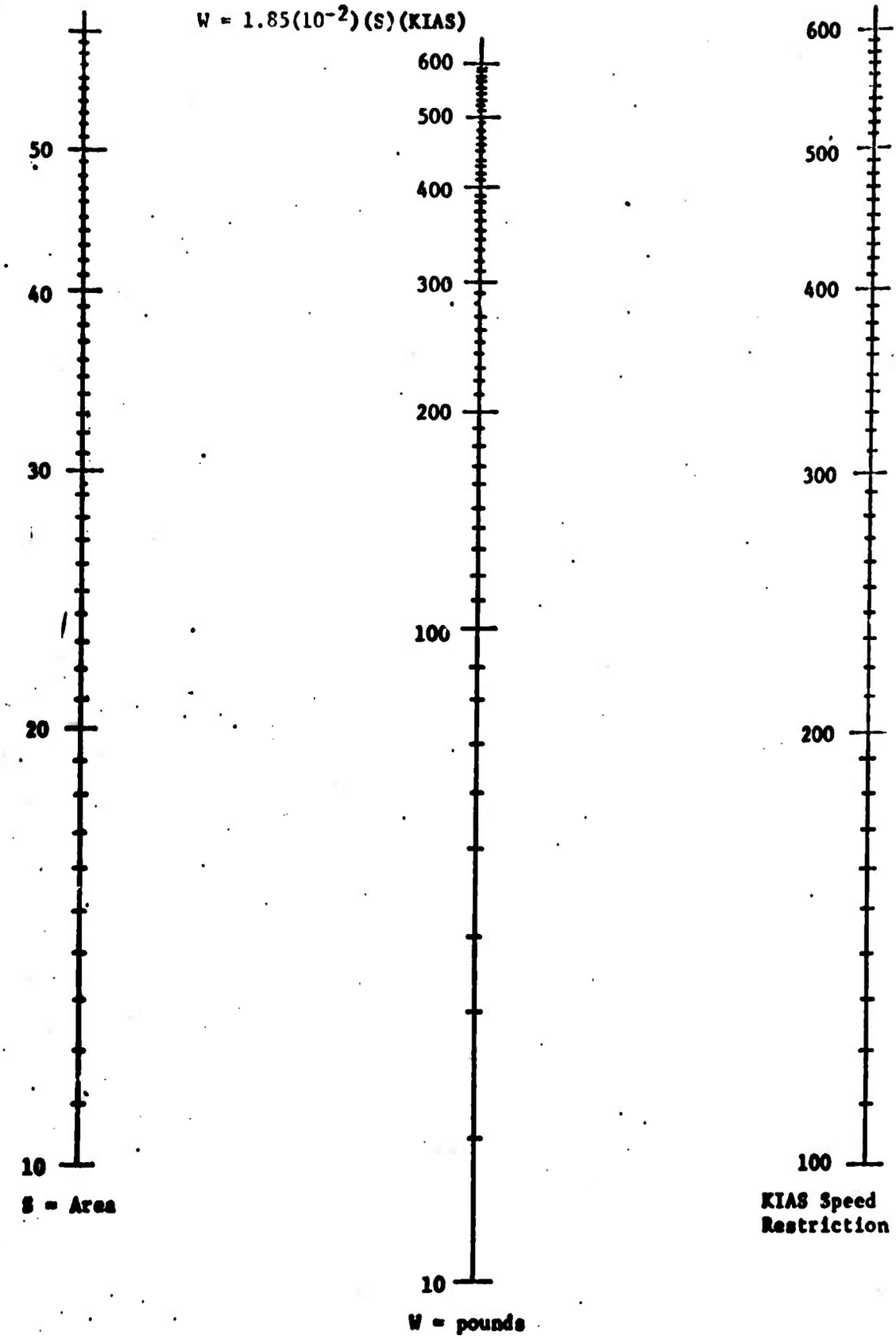

FIGURE 6-9 : Speed Brakes - Fuselage Mounted; KIAS < 600
Weight vs. Area and Limit Speed.

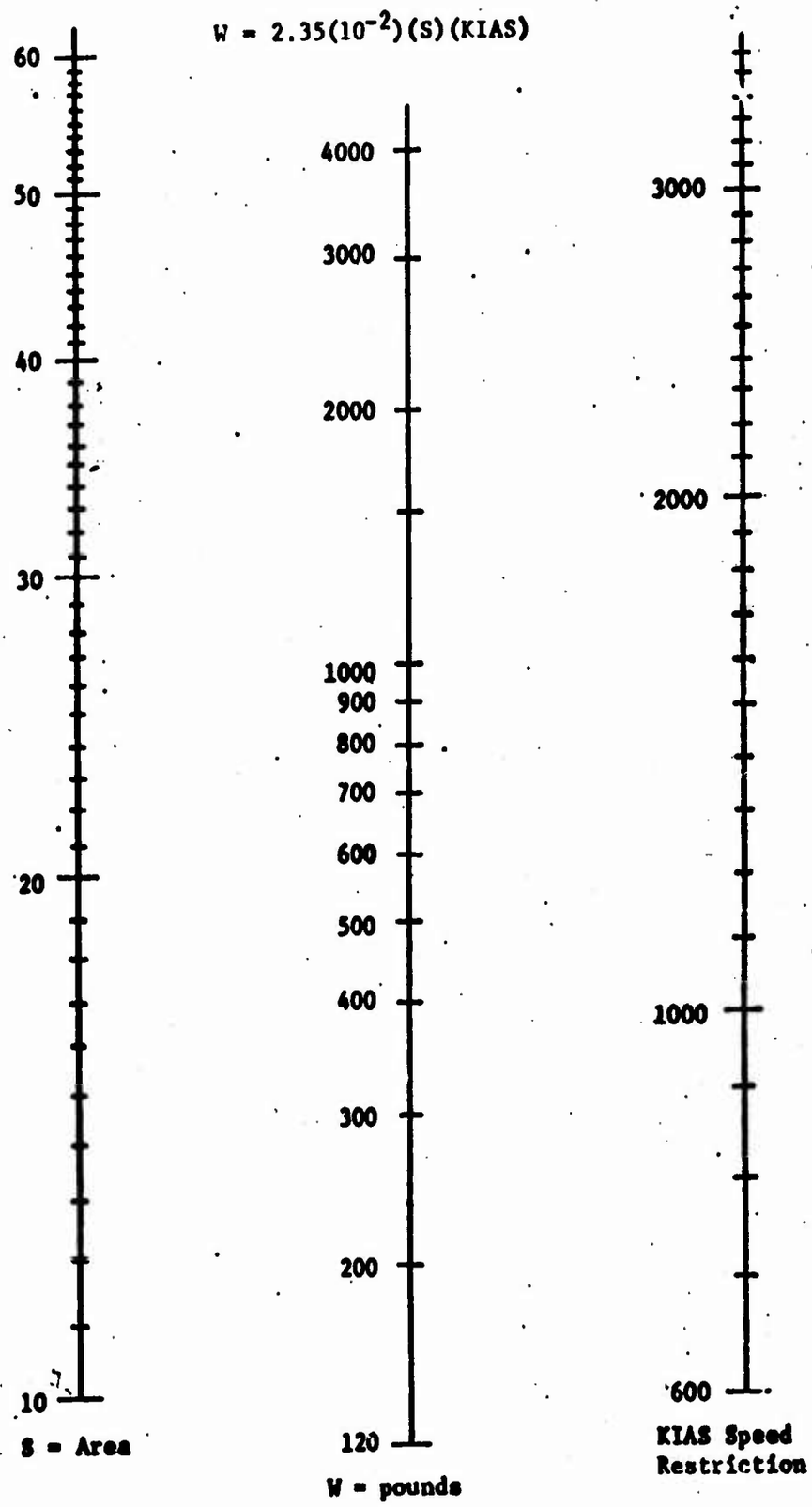

FIGURE 6-10: Speed Brakes - Fuselage Mounted; KIAS > 600
Weight vs. Area and Limit Speed

SECTION VII

CONCLUSIONS AND RECOMMENDATIONS

1. CONCLUSIONS

a. A sensitivity study indicates that touchdown velocity and thrust reverser effectiveness are the factors that have the strongest influences on ground roll distance. Following these are wheel braking, drag and lift. However, it should be noted that lift is a pertinent factor in establishing touchdown velocity.

b. The computation of landing stopping distance is improved by using three equations-of-motion rather than one, as is standard practice. The three equations required solve for forces in the vertical and horizontal direction and for moments created by these forces. These solutions permit inclusion of the effects of deceleration and pitching moments on the unloading of the main landing gear and the resulting effect on the braking force.

c. The procedure used for computing ground roll distance should account for non-linear variations of braking coefficient with changes in velocity. These variations can be readily obtained by using the equations presented by Section IV of this handbook.

d. Lift and drag coefficients and the associated touchdown speed can be precisely determined from the methods described if accurate detailed geometry is available. This is an essential requirement, since the touchdown speed is the most important factor in determining the landing distance.

Another significant factor in determination of the landing speed is the landing technique (Flare or no-flare) and its direct effect on the touchdown angle-of-attack. Factors such as rate-of-sink at landing; pilot's visibility restrictions due to angle-of-attack; aircraft geometry limitations; and control requirements will all effect the touchdown angle-of-attack.

2. RECOMMENDATIONS

a. Calculations of landing stopping distance should use three equations-of-motion rather than the standard practice of one equation;

b. Calculations of landing stopping distance should account for non-linear variations of braking coefficient with changes in velocity;

c. Further studies should be conducted on reverser geometry and reverser maximum useable effectiveness to permit thrust reversers to be used to their maximum potential (i.e. to a ground speed of zero knots with maximum reverse thrust available for ground roll and in-flight useage).

SECTION VIII

BIBLIOGRAPHY

SECTION III: COMPUTATION OF THE LIFT, DRAG, AND TOUCHDOWN VELOCITY FOR AN AIRCRAFT IN THE LANDING CONFIGURATION

Allen, H. J., Calculation of the Chordwise Load Distribution Over Airfoil Sections with Plain, Split, or Serially-Hinged Trailing Edge Flaps, NACA TR-634, 1938.

American Power Jet Co., Performance of and Design Criteria for Deployable Aerodynamic Decelerators, ASD-TR-61-579, (DDC-AD 429 971), December 1963.

Douglas Aircraft Division, Douglas Skyhawks CA-4E and CA-4F, DAV Report 49773, March 1965.

Ellison, D. E., USAF Stability and Control DATCOM, Contract AF 33(616)-6460, Douglas Aircraft Company, Inc., Revised November 1965.

Gajdjis, S., Substantiation Report for F-105D, Standard Aircraft Characteristics Charts, Contract AF 33(600)-40838, December 1963.

Griffin, Holzhauser and Weiberg, Large-Scale Wind Tunnel Tests of an Airplane Model with an Unswept, Aspect-Ratio-10 Wing, Two Propellers, and Blowing Flaps, NASA Memo. 12-3-58A.

Helmbold, H. B., Theory of the Finite-Span Blowing Wing, Journal of the Aeronautical Sciences, Vol. 24, No. 5, May 1957.

Helmbold, H. B., Analysis of the Power Requirement of a Blowing Airfoil with Slotted Flap, Fairchild Aircraft Engineering Report No. R246A-002, April 1958.

Helmbold, H. B., Power Requirements of a Blowing Wing With Sealed and Slotted Trailing-Edge Flaps, Fairchild Aircraft Engineering Report No. R246A-004, March 1959.

James and Hunton, Estimation of Incremental Pitching Moments Due to Trailing-Edge Flaps on Swept and Triangular Wings, NACA RM A55D07, June 1955.

Jennings & Peterson, Study & Development of Parachutes and Systems for In-Flight and Landing Deceleration of Aircraft, WADC-TR-57-566, Part I (ASTIA #234 008), January 1959.

Lachmann, G. V., editor, Boundary Layer and Flow Control, (Two Volumes), Pergamon Press, 1961.

Lewis, Perkins, Weutz, Substantiating Data Report B-52H Flight Manual and Standard Aircraft Characteristics Charts, Boeing Airplane Company Report D3-3211, January 19, 1961.

Royal Aeronautical Society, R. A. E. Data Sheets, Fifteenth Issue, August 1964.

Reuter, J. D., Letter and Data to Rohr from Pioneer Parachute Company, 1999-Eng. '67, September 1967.

Ringleb, F. O., Investigations of Suction Flaps, Princeton University, Report No. 304, 1955.

Ryan Aeronautical Company, Interim Report on Analytical Studies and Bench Tests of a High Lift Boundary Layer Control System, Contract DA 44-177-AMC-35(T), Ryan Aeronautical Company Report 64B053, April 1964.

Schwier, W., Lift Increase Produced By Blowing A Wing of a Profile Thickness of 9% Equipped with a Slat and a Slotted Flap, Translation, Headquarters Air Material Command, Report No. F-TS-645-RE, August 22, 1946.

Spence, D. A., The Lift on a Thin Airfoil with a Blown Flap, RAE TN Aero 2450, May 1956.

Stone, H. N., Use of Boundary Layer Control with Rocket Induction Pumps, AF Technical Report No. 6288, August 1950.

Swenson, W. A., A Study of Parachutes and Systems for Aircraft Deceleration, WADC-TR-57-128 (ASTIA #233 185), January 1959.

Tancredi, S. A., Parachute Technology, A Report Bibliography, (AD 427014), January 1964.

U. S. Air Force, F-5A/B Aircraft Flight Manual, USAF T.O. 1F-5A-1, Contract AF33(657)136, December 1965.

U. S. Air Force, F-105D Aircraft Flight Manual, USAF T.O.1F-105D-1, Contract AF33(600)34752, March 1965.

Wallace & Stalter, Systematic Two-Dimensional Test of an NACA 23015 Airfoil Section with a Single-Slotted Flap and Circulation Control, University of Wichita Aero Report 120, August 1954.

Weiberg, Griffin and Florman. Large-Scale Wind Tunnel Tests of an Airplane Model with an Unswept, Aspect Ratio-10 Wing, Two Propellers, and Area-Suction Flaps, NACA TN 4365.

White, W. C., F-5 Basic Aerodynamic Data, Volume I, Take-Off and Landing Configurations, Northrop Corporation Report NOR-64-2, January 1964.

Young, A. D., The Aerodynamic Characteristics of Flaps, ARC R & M 2622, 1953.

SECTION IV: WHEEL BRAKES

Bendix Corporation, Wheel and Brake Specification for Various Aircraft-- Loose Sheets.

Bendix Corporation, Concepts for Advanced Aircraft Braking Methods, AP-290R (AD 468 065), Revised January 5, 1965.

B. F. Goodrich Co., Aircraft Tires Engineering Data, Second Edition.

Harrin, Investigation of Tanden-Wheel & Air-Jet Arrangements for Improving Braking Friction on Wet Surfaces, NASA TND-405, June 1960.

Horne, Skidding Accidents on Runways and Highways Can Be Reduced, AIAA Astronautics and Aeronautics, August 1967.

Horne & Leland, Influence of Tire Pattern and Runway Surface Condition on Braking Friction and Rolling Resistance of a Modern Aircraft Tire, NASA TN D-1376, September 1962.

Keyes, A Review of the Problems of Aircraft Wheel Braking on Wet Surfaces and a Description of a Method of Artifically Wetting Runways for Test Purposes, ARC CP No. 592.

Leland & Taylor, An Investigation of the Influence of Aircraft Tire and Tread Wear on Wet-Runway Braking, NASA TN D-2770, April 1965.

McCabe & Bement, B-58A Wet Runway Performance Evaluation, AFFTC-TR-64-34 (AS 456 750), February 1965.

Peterson and Cross, Evaluation of a 5-Rotor Brake and Modulated Anti-Skid System Installed on a KC-135A, AFFTC FTC-TR-64-43, March 1965.

Polis & Adams, T-38A Aerodynamic Braking Refused Take-Off Tests, AFFTC-TR, April 1965.

Ramsone & Fulton, B-58A Heavy Weight Take-Off Refusals, AFFTC-TR-61-14, August 1961.

Sawyer, Batterson & Harrin, Tire-to-Surface Friction Especially Under Wet Conditions, NASA Memo 2-23-59L.

Sawyer & Kolnick, Tire-to-Surface Friction-Coefficient Measurements with a C-123B Airplane on Various Runway Surfaces, NASA TR R-20, 1959.

Tomita, Friction Coefficients Between Tires and Pavement Surfaces, USN-CEL-TR-R303 (AD 602 930), USN Civil Engineering Lab, Port Hueneme, California, June 1964.

Yancey & Cross, C-135B Category III Performance Tests, AFFTC-TDR-63-35, June 1964.

Zalovcik, Ground Deceleration and Stopping of Large Aircraft, AGARD Report 231, October 1949.

SECTION V: THRUST

Anderson, Cooper and Faye, Flight Measurements of the Effect of a Controllable Thrust Reverser on the Flight Characteristics of a Single-Engine Jet Airplane, NASA Memo 4-26-59A, May 1959.

Angel and Stimler, Thrust Reversers for Braking and Directional Control of Jet Aircraft During Landing, GER 8203, May 1957.

Brownson, Jack J. and Sutton, F. B., The Effects of Thrust Reversal at Mach Numbers Up to 0.86 and the Longitudinal and Buffeting Characteristics of a Typical Jet-Transport Airplane Configuration, NASA TND-786, March 1960.

Eschenburg, R., Scale Model Thrust Reverser Wind Tunnel Test Program, Rohr 24-5008, January 1967.

Greif, Richard K., Kelly, Mark W., and Tolhurst, William H., Jr., Full-Scale Wind-Tunnel Investigation of the Effects of a Target-Type Thrust Reverser on the Low-Speed Aerodynamic Characteristics of a Single-Engine Jet Airplane, NASA TND-72, September 1959.

Greif, Richard K., Kelly, Mark W., and Tolhurst, William H. Jr., Full-Scale Wind-Tunnel Tests of a Swept-Wing Airplane with a Cascade-Type Thrust Reverser, NASA TND-311, April 1960.

Hawk, G. W., Summary of the Development of Mechanical Type Thrust Reversers, WADC TR 57-17, May 1957.

Hickey, Tolhurst and Aoyagi, Investigation of the Longitudinal Characteristics of a Large-Scale Jet Transport Model Equipped with Controllable Thrust Reversers, NASA TN D-786.

Hilbig, J. H., Inflight Thrust Reversers for Tactical Fighter Application, WADC AFAPL-TR-66-118, January 1967.

Kuczwara & Eschenburg, Reduction of Landing Speed of Carrier Based Aircraft By Thrust Vectoring, Rohr Report 24-2273, January 1968.

McCormick and Koepcke, Capabilities of In-Flight Thrust Reversing on Tactical Aircraft, AFFDL-TR-67-120, October 1967.

McDermott Jr., Summary of the Development of Aerodynamic Type Thrust Reversers, WADC TR 57-18, May 1957.

Newell, Fred, Feasibility Study of Thrust Reversers for L/D Control on a T-38 Airplane, FDM No. 312, September 1960.

Tolhurst, Kelly and Greif, Full-Scale Wind-Tunnel Investigation of the Effects of a Target-Type Thrust Reverser on the Low-Speed Aerodynamic Characteristics of a Single Engine Jet Airplane, NASA TN D-72, September 1959.

SECTION VI: WEIGHT

General Dynamics, Weight and Balance Status Report Model F-111B, Report No. Ft.W-12-1020-1, Fort Worth Division.

Hammitt, R. L., Structural Weight Estimation By the Weight Penalty Concept for Preliminary Design, Paper No. 141, Society of Aeronatical Weight Engineers, Inc., 1956.

Hilbig, J. H., In-Flight Thrust Reversers for Tactical Fighter Applications, Technical Report AFAPL-TR-66-118, Aero Propulsion Laboratory, January 1967.

Hinds, C. M., Design Data For a Target Type Thrust Reverser Report No. 24-2268, Rohr Corporation, April 1967.

Liebermann, C. R., Rolling Type Alighting Gear Weight Estimation, Paper No. 210, Society of Aeronautical Weight Engineers, Inc. 1959.

Pioneer Parachute Company, Aircraft Deceleration Drague Parachutes, Report No. 1999-Eng., 1967.

Republic Aviation Corporation, Actual Weight and Balance Report F 105 31RE, Report No. EW97-211.

Shanley, F. R., Weight Strength Analysis of Aircraft Structures, Dover Publications, Inc., 1960.

UNCLASSIFIED
Security Classification

DOCUMENT CONTROL DATA - R & D

(Security classification of title, body of abstract and indexing annotation must be entered when the overall report is classified)

1. ORIGINATING ACTIVITY (Corporate author)
ROHR CORPORATION
CHULA VISTA, CALIFORNIA

2a. REPORT SECURITY CLASSIFICATION
UNCLASSIFIED

2b. GROUP

3. REPORT TITLE
METHOD FOR EVALUATING THE EFFECTIVENESS AND WEIGHT OF AIRCRAFT DECELERATION DEVICES

4. DESCRIPTIVE NOTES (Type of report and inclusive dates)
Final Report - June 1967, June 1968

5. AUTHOR(S) (First name, middle initial, last name)
Greiner, Herbert
Hilbig, Jack H.

6. REPORT DATE	7a. TOTAL NO. OF PAGES	7b. NO. OF REFS
June 1968	276	40

8a. CONTRACT OR GRANT NO.	9a. ORIGINATOR'S REPORT NUMBER(S)
F33615-67-C-1558	None
8b. PROJECT NO. 5101-63	
8c.	9b. OTHER REPORT NO(S) (Any other numbers that may be assigned this report)
8d.	None

10. DISTRIBUTION STATEMENT
Foreign Announcement and Dissemination of this Report by DDC Not Authorized.

11. SUPPLEMENTARY NOTES	12. SPONSORING MILITARY ACTIVITY
	Deputy for Development Planning Wright-Patterson Air Force Base, Ohio

13. ABSTRACT

This program was established in order to develop a standard and expedient method for estimating the performance and weights of deceleration devices used to decrease the landing ground roll of an aircraft. The method of approach to the problem was to obtain all data available both from flight test and theory; and to compile a step-by-step procedure for determining the weight penalties and the force increments affecting aircraft landing performance. Specifically, procedures are provided for determining airplane lift and drag, and decelerative force increments and weight penalties due to high lift devices, spoilers, wheel brakes, speed brakes, drag chutes and thrust reversers. In addition, a cursory study was made to evaluate the effectiveness of various factors affecting landing distance of three current military aircraft. The study showed that the ground roll distance was strongly influenced by touchdown speed; also that, of all the decelerating devices studied, the thrust reverser was the one most effective in reducing stopping distance. It is therefore recommended that further studies be conducted to optimize thrust reversers and devices such as deflected thrust, which reduce touchdown velocity.

DD FORM 1 NOV 68 1473

UNCLASSIFIED
Security Classification

Security Classification

14. KEY WORDS	LINK A		LINK B		LINK C	
	ROLE	WT	ROLE	WT	ROLE	WT
Deceleration Devices, Aircraft						
Ground Roll						
Thrust reverser						
Handbook						
Wheel brakes						
Speed brakes						
Spoilers						
Drag chutes						
Lift devices						

UNCLASSIFIED

Security Classification